UNIVERSITÉ DE STRASBOURG

ÉCOLE DOCTORALE DES SCIENCES CHIMIQUES
Institut de Chimie de Strasbourg, UMR 7177

THÈSE présentée par :

Morane LOINTIER

soutenue le : **11 décembre 2020**

pour obtenir le grade de : **Docteur de l'université de Strasbourg**

Discipline/Spécialité : Chimie-Biologie

Structural and functional investigations of designed histidine-rich peptides

with potent antimicrobial, transfection, and lentiviral transduction activities

THÈSE dirigée par :
  M. BECHINGER Burkhard   Pr, UMR 7177, Université de Strasbourg

  RAPPORTEURS :
  M. GUICHARD Gilles   DR, UMR 5248, Université de Bordeaux
  Mme. SIZUN Christina   Dr, ICSN-CNRS, Université de Paris-Saclay

AUTRES MEMBRES DU JURY :
  M. KICHLER Antoine   Dr, UMR7199, Université de Strasbourg
  Mme. PATERNOSTRE Maïté   DR, CEA-Saclay

Recherches structurales et fonctionnelles sur les peptides riches en histidine

présentant des activités élevées antimicrobienne, de transfection et de transduction lentivirale

Structural and functional investigations of designed histidine-rich peptides

with potent antimicrobial, transfection, and lentiviral transduction activities

Morane Lointier

Université de Strasbourg,

Institut de Chimie de Strasbourg, UMR 7177,

Laboratoire de RMN et biophysique des membranes.

Thesis

December 2020

À Nana, Lalous et Gillou

"Ils ne savaient pas que c'était impossible, alors ils l'ont fait."

Mark Twain

Contents

List of abbreviations

List of abbreviations

aa	amino acid	*v.s.*	*vide supre*
AMP	AntiMicrobial Peptides	WAXS	Wide Angle X-ray Scattering
CD	Circular Dichroism		
Cf	final Concentration		
CP	Cross Polarisation		
CPP	Cell Penetrating Peptide		
Cter	C-terminal		
CT-	ConTrol negative		
CT+	ConTrol positive		
DARR	Dipolar Assisted Rotational Resonance		
DNA	DeoxyriboNucleic Acid		
DSS	2,2-Dimethyl-2-Sila-pentane-5-Sulphonic acid		
E.coli	*Escherichia coli*		
EDTA	EthyleneDiamineTetraacetic Acid		
FTIR	Fourier Transform InfraRed		
GFP	Green Fluorescence Protein		
hCD34+	human Cluster Differentiation		
HPLC	High Performance Liquid Chromatography		
HSQC	Heteronuclear Single Quantum Coherence		
LUV	Large Unilamellar Vesicle		
LV	LentiVirus		
MALDI-TOF	Matrix Assisted Laser Desorption Ionization-Time Of Flight		
Mag2	Magainin 2		
MAS	Magic Angle Spinning		
MH	Mueller-Hinton		
MIC	Minimum Inhibitory Concentration		
NMR	Nuclear Magnetic Resonance		
NOESY	Nuclear Overhauser SpectroscopY		
Nter	N-terminal		
OD	Optical Density		
PGLa	Peptide starting with a Glycine and ending with a Leucine amide		
POPC	1-Palmitoyl-2-Oleoyl-sn-glycero-3-PhosphoCholine		
POPE	1-Palmitoyl-2-Oleoyl-sn-glycero-3-PhosphoEthanolamine		
POPG	1-Palmitoyl-2-Oleoyl-sn-glycero-3-PhosphoGlycerol		
POPS	1-Palmitoyl-2-Oleoyl-sn-glycero-3-Phospho-L-Serine		
RNA	RiboNucleic Acid		
SAXS	Small Angle X-ray Scattering		
SWAWS	Small-, Wide-Angles X-ray Scattering		
ssNMR	solid-state Nuclear Magnetic Resonance		
SUV	Small Unilamellar Vesicle		
TEM	Transmission Electron Microscopy		
TFE	TriFluoroEthanol		
TMS	TetraMethySilane		
TOCSY	Totally Correlated SpectroscopY		
Tris	2-amino-2-(hydroxymethyl)-1,3-propanediol		
v.i.	*vide infra*		

I. Introduction

We are facing the emergence of recent multidrug-resistant pathogens and microorganisms. Bacteria adapt and become more resistant thus existing treatments becoming ineffective. Therefore, there is an urgent need to develop alternative treatments and/or biomaterials [1]. In this context it is of major interest that during the last 30 years, new active compounds have been discovered in the animal and plant kingdom, capable of defending the host against attacks from microorganisms [2]. These are small proteins produced naturally by organisms: antimicrobial peptides (AMPs) [3].

Antimicrobial peptides have an extensive activity spectrum that covers most bacterial, yeast and fungal species [4]. Lately, they are also developed and used in biomedical applications for their cellular penetration, transfection and transduction activities [5]. In addition, these peptides have a great deal of structural diversity: the secondary structure (α-helical or β-sheet) [6], and the tertiary structure (self-assembly) may have an impact on their functionality.

Whereas many antibiotic peptides have been studied, their interaction with membrane are still challenging to analyse. Understanding the structure-function relationship of these peptides would allow the design of new, more effective antibiotics.

I.1 LAH4 structural properties

Our laboratory designed the histidine-rich peptide LAH4 as a model antimicrobial peptide specifically to study the interactions that determine membrane topology of α-helical peptides[7]. It is composed of 26 amino acids, but only four different types: two lysines (magenta) at each ends ensure a good solubility in water (**Figure 1**). The sequence core is composed of the hydrophobic residues leucine and alanine, interrupted by four histidines (blue) (**Figure 1**). The peptide therefore has a global charge of + 9 at acidic pH and of + 5 at neutral pH[8].

In solution, at acidic pH (<6), the histidines of the peptide are protonated and the peptide adopts a random coil conformation. When the pH increases above the pKa of the histidines at 6, the histidines become neutral, and the peptide adopts an α-helical conformation[8][9] (**Figure 1**).

LAH4   KKALL ALALH HLAHL ALHLA LALKK A

Figure 1: LAH4 pH-dependent conformation in solution. At pH 5 peptide is in a random coil conformation. A pH increase leads the peptide to adopt an α-helical conformation.

Histidine protonation states gives the peptide a pH-dependent hydrophobicity. The peptide is amphipathic when adopting an α-helical conformation and it presents two sides: one hydrophobic constituted of alanines and leucines, the other hydrophilic with histidine being a polar/cationic amino acid (**Figure 1**)[9].

LAH4 peptides in solutions adopt a random coil conformation at acidic pH, but with membrane environments, the LAH4 adopt an amphipathic α-helical conformation[9].

The peptide orientation in membranes depends on the histidines protonation state [10]. Indeed, at pH 5, LAH4 adopts an orientation parallel to the membrane surface (in-planar) [7][11]. At pH 6.1 (i.e., around the histidines pKa values of 5.8, 5.4, 5.7 and 6.0 for H10, H11, H14 and H18, respectively), there is a break in the α-helix between L9 and H14 [12]. At neutral pH, the histidines are deprotonated and the peptide changes from an in planar to a transmembrane orientation. The membrane orientation can be determined by oriented solid-state nuclear magnetic resonance (NMR). The backbone ^{15}N nitrogen chemical shift [13], is below one hundred ppm for in planar orientations or around two hundred ppm for transmembrane orientations (**Figure 2**) [7].
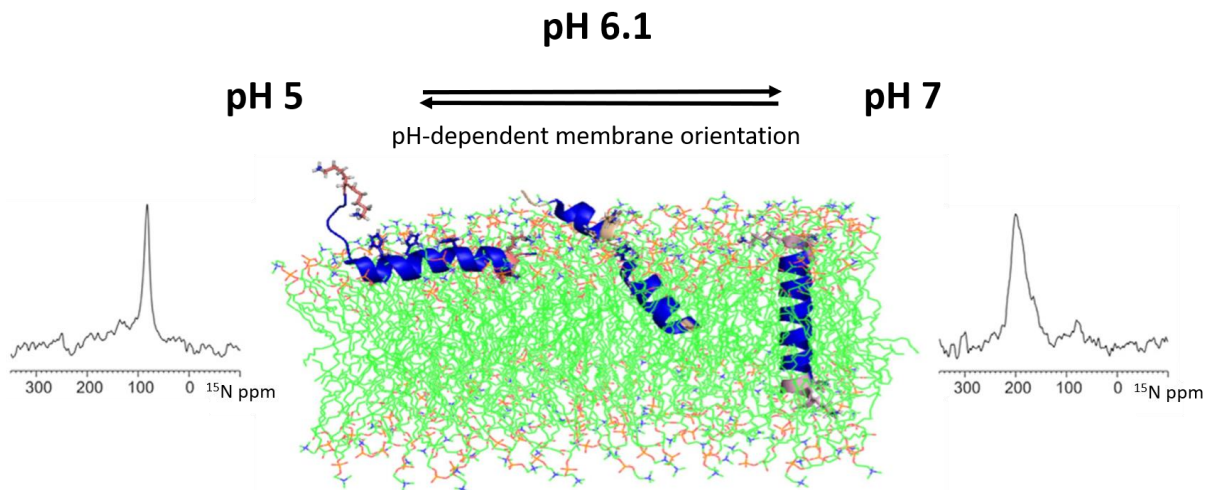

Figure 2: LAH4 orientation in the presence of membranes. The peptide adopts in planar orientations at pH 5 whereas at pH around 7 it adopts a transmembrane alignment. ^{15}N NMR spectra corresponding to these two conformations are also shown (adapted from [7][14]).

Notably, the mode of action is also dependent on the pH [15]. Vesicle disruption studies by calcein release show that LAH4 is more active at pH 5 than at pH 7 [8]. The membrane disruption at acidic pH, when the peptide is oriented parallel to the membrane should be more efficient [7][8]. However, the lipid composition and in particular the nature of the head group (charge density, heard group structure) or lipid acyl chain (length and saturation) can modulate this effectiveness [16].

Thereby, the LAH4 physical-chemical properties are responsible for its biological activities. Indeed, its pore-forming capacities allow it to kill microorganisms by permeabilizing their membrane.

I.2 Cell penetrating peptide

Besides these structural properties, LAH4 also presents interesting biological activities [17]. The LAH4 peptide exhibits pore forming activities in membranes and antimicrobial activities at both neutral and acidic pH even if more efficient at acid pH [9][18]. In order to increase these activities, LAH4 derivatives were designed (see **chapter I.3**) constituting the LAH4 family. More recently, peptides from the LAH4 family have also demonstrated powerful deoxyribonucleic acid (DNA) and ribonucleic acid (RNA) transfection activities [19]. Thereby the LAH4 family belongs to cell penetrating peptide (CPPs) category, relatively short peptides that are characterized by their ability to interact with the cellular plasma membrane and gain access to the cell interior by means of different mechanisms [20][21][22].

Penetrating peptides are used essentially to deliver different cargoes such as nucleic acids, polymers, liposomes, nanoparticles, and other molecules in the cell [23]. Complexes between CPPs and cargoes can be formed through covalent bonds (disulfide bond, amide bond, or other specific linkers) or noncovalently (electrostatic interaction, hydrophobic interactions). As it has been shown for LAH4, positively charged residues (lysines) interact with the negatively charged nucleic acids (small interfering RNA, plasmidic DNA, etc.) [24].

The CPPs internalization properties depend on the peptides' secondary structures [25][26]. The cargo penetration into the cells can be achieved in two different ways: via direct penetration or via endocytosis [27][23]. These two cargo internalization mechanisms are completely different: the first is based on the eukaryotic membrane permeabilization whereas the second is characterized by the interaction with the eukaryotic membrane followed by the absorption into an endosomal vesicle. The endosomal release allows the cargoes delivery into the cell [28]. LAH4 peptides have shown efficiency to enhance cellular uptake for a wide variety of cargo which can be divided into two types: viral or non-viral [29][30]. The delivery process of non-viral system is called transfection (**Figure 3**) while that of a viral vector is called transduction (**Figure 4**). LAH4 CPPs can be utilized to increase both transfection [31][32] and transduction efficiencies [33][34].

The transfection involves the transfer of nucleic acid materials to the cell interior via a non-viral vector [29], which is in our case the role played by LAH4 [19] (**Figure 3**). The first step is the complex formation between the nucleic acid and the LAH4 peptide [35] driven by the electrostatic interaction between LAH4 lysines residues and the DNA phosphate groups [36]. Then, this complex interacts with the cell membrane and is subsequently internalized into endosomes [18]. Thereafter, the endosome acidification leads to histidine protonation and thus to complex dissociation. Finally, the freed LAH4 peptide disrupts the endosomal membrane to release nucleic acid cargo [19].
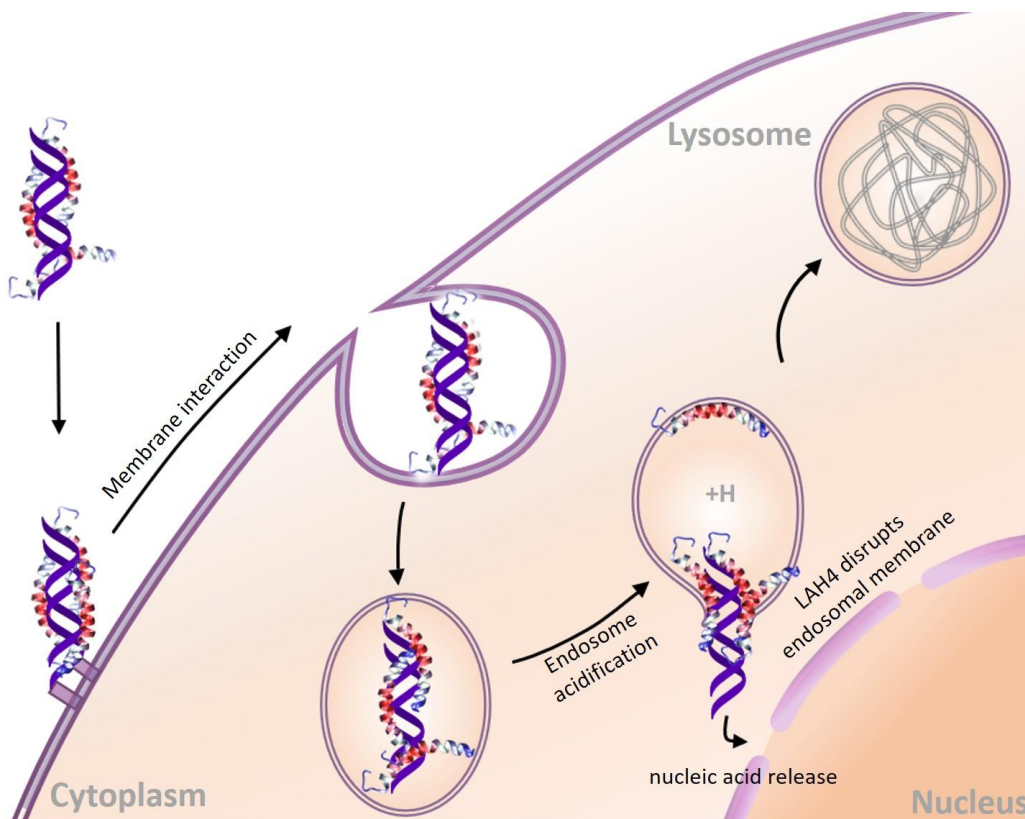

Figure 3: Schematic representation of transfection mechanism (adapted from [19] and [37]).

Transduction involves the nucleic acid material transfer into cells via a viral vector fusing its membrane with the cell membrane (**Figure 4**) [38]. The lentiviral vector particles are obtained from the assembly of the expression products from different plasmids including one plasmid encoding for envelope glycoprotein (responsible for the cell type specificity) and another displaying the gene coding for the green fluorescence protein GFP (to follow the transduction efficiency). The hypothetical transduction mechanism is that peptides form a complex with viral vectors and then interact with the cell membrane lipids. Once the complex adheres to the membrane, the peptides can disrupt the eukaryotic membrane, thus assist the lentiviral vectors entry into target cells [39].

Recently, LAH4-A4, a peptide derived from LAH4, was developed to be a new transduction enhancer [40] and thereby also called vectofusin-1 for its membrane fusion improved capacities.
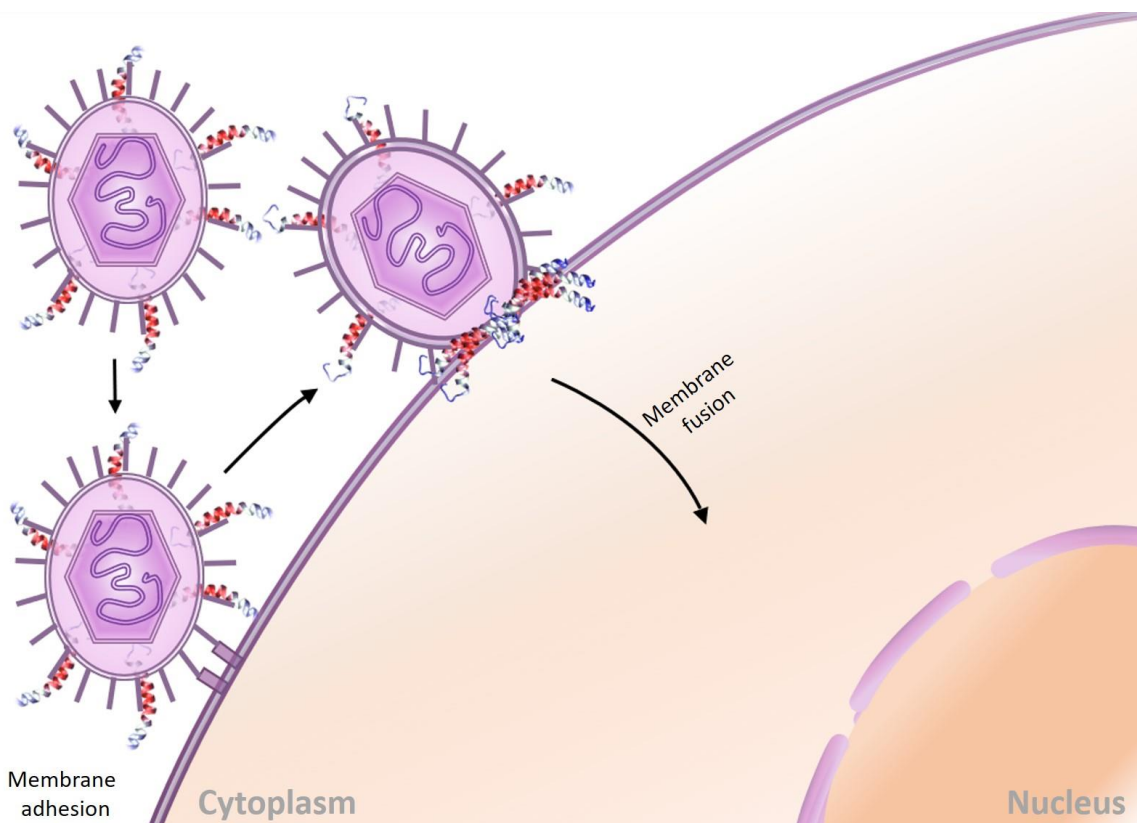

Figure 4: Schematic representation of transduction mechanism (extracted from [19] and [37]).

In this manuscript, investigation of LAH4 family peptides as cell penetrating peptides will be presented. CPPs provide a very promising strategy for intracellular drug delivery. To improve LAH4 properties and to better understand the action mechanism, different modifications were introduced into the sequence.

I.3 LAH4 derivatives

Peptides of the LAH4 family have shown good potential for gene transfer and for gene therapy applications. Since the discovery of LAH4 many derivatives have been synthesized to improve their performances in various applications [35]. The LAH4 primary sequence has been modified to increase its properties. At first, deletions of one or two amino acids at the N-terminal (Nter) or C-terminal (Cter) respectively were made (**Table 1**). The shortened peptides showed lower transfection activities [35]. The Cter amidation did not alter the transfection activity and the D-LAH4 isomer did not show activity [35].

Name	Sequences	Transfection efficiency (%)	Cell line	Ref
LAH4	KKALLALALHHLAHLALHLALALKKA	100	HepG2	[35]
LAH4-ΔN	KK_LLALALHHLAHLALHLALALKKA	4.3	HepG2	[35]
LAH4-ΔC	KKALLALALHHLAHLALHLALA_KK_	11	HepG2	[35]
D-LAH4	*KKALLALALHHLAHLALHLALALKKA*	3.2	HepG2	[35*]

*Table 1: LAH4 derivatives, Cter or Nter modification (_: deleted amino acid) of the sequence with their corresponding transfection activity percentage compared to LAH4 (100%) (extracted from [35] or *: luciferase activity (light units/10 s/well)).*

To improve the transfection efficiency, LAH4 derivatives with modified lysine positions have been synthesized (**Table 2**). Lysine is a key element for the peptide/DNA complex formation. The lysines in LAH4 must be free because they allow interaction with the DNAs phosphate groups. LAH4 peptides enriched or depleted in lysines residues were also less efficient. The results indicate that a fine balance between the various interactions is responsible for the high transfection activity by LAH4 [35].

Name	Sequences	Transfection efficiency (%)	Cell line	Ref
LAH4	KKALLALALHHLAHLALHLALALKKA	100	HepG2	17 35
LAH4-2Lys	KALLALALHHLAHLALHLALALKA	23.5	MRC5-V2	x
LAH4-6Lys	KKKALLALALHHLAHLALHLALALKKK	31.3	MRC5-V2	x
K2-LAH4-K2	KKKKALLALALHHLAHLALHLALALKK	12.4	HepG2	35*
LAK4	KKLAKALAKALAKALKLALALAKK	≤0.1	HepG2	17

Table 2: 4 derivatives, lysine and histidine modifications of the sequence with their corresponding transfection activity compared to LAH4 (100%) (adapted from [17] and [35] or *: luciferase activity (light units/10 s/well)); x: unpublished.

The role of histidines for transfection was also analysed. An LAK4 mimic is composed only of leucines, alanines and lysines (**Table 2**). In the absence of histidines, peptides lose their pH-dependent character and show lower transfection efficiencies [17,41], indicating the importance of histidine residues for transfection. The peptide charges are pH dependent (e.g., +9 at pH 5 vs +5 at pH 7.4), leading to a change in membrane topologies of the peptides which promote membrane disruption [8]. The histidines number and their position in the sequence are also crucial parameters for the transfection capacity [9]. One study carried out a series of transfection experiments on LAH by varying the histidine number in the sequence (**Table 3**) [17].

Name	Sequences	Transfection efficiency (%)	Cell line	Ref
LAH1	KKLALALALALHALALALALKKA	1.3	HepG2	17*
LAH2	KKLAHLALALALGLALAHLAKKA	0.2	HepG2	17*
LAH3	KKALALGLHLAHLALHLALALKKA	0.2	HepG2	17*
LAH4	KKALLALALHHLAHLALHLALALKKA	100	HepG2	17 35
LAH5	KKALLALALHHLAHLAHHLALALKKA	50	HepG2	17*
LAH4-H15	KKALLALALHHLAHHLALHLALALKKA	1.3	HepG2	35*
LAH4-P15	KKALLALALHHLAHPLALHLALALKKA	0.6	HepG2	35*
H4-LAK4	HHALLALALKKLAKLALKLALALHHA	2	HepG2	17

*Table 3: LAH4 derivatives, histidine modifications of the sequence with their corresponding transfection activity percentage compared to LAH4 (100%) (adapted from [17] and [35] or *: luciferase activity (light units/10 s/well)).*

The results showed that the most efficient peptides were those containing four and five histidine residues. LAH1-LAH3 are at least 38 times less efficient than LAH4 or LAH5 [17]. In the next step, the same sequence length and amino acids as LAH4 are kept, but the histidine and lysines are switched (H4-LAK4) (**Table 3**). The H4-LAK4 is less active in gene transfer so the lysines and histidine positions affect the transfection efficiency. The polarity effects of the extremity charges are investigated by the peptide sequence LAH4-K2-E2 and LAH4-K4-E4 (**Figure SI 1**). The positively charged lysines with pKa at 10.5 is substituted by negatively charged glutamic acid with pKa at 4.25. There is a drop-in transfection activity. In summary, the four histidines should be present in the peptide core and two lysines at each extremity.

Proline insertion at position 15 removes the peptide's ability to adopt an uninterrupted helical conformation [35]. This factor is also important for transfection efficiency since this latter is significantly inferior for LAH4-P15 than the original LAH4.

Similarly, the histidines' positioning in the sequence is very important. Indeed, when peptides are represented through a helical wheel projection, the amphipathic character appears clearly. The hydrophilic face is framed by the histidines residues, the angle thus defined is called hydrophilic angle (**Figure 5**) and varies according to the histidines positioning.
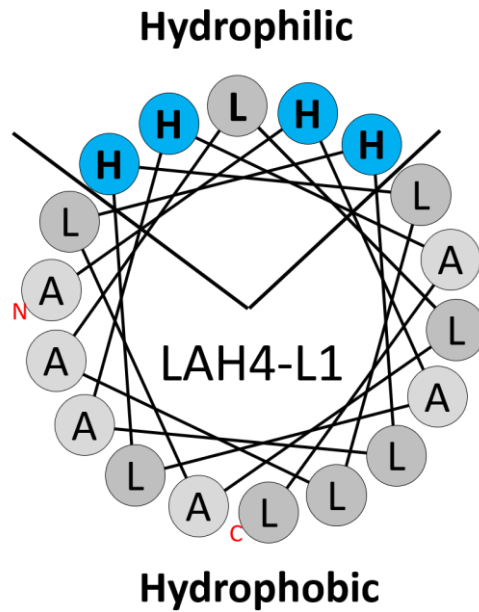
Figure 5: LAH4-L1 helical wheel projection with the hydrophilic face (bold) is framed by the histidines residues (blue) who defined the hydrophilic angle and the hydrophobic face composed of leucines and alanines.

In like manner, peptides are named "-Ln" or "-An" by following the number of leucine or alanine residues present between two pairs of adjacent histidine residues (**Figure SI 3**) [33]. For example, LAH4-L1 shows one leucine between the two histidine pairs in the helical wheel projection (this part is more detailed in **chapter III**).

We can see that the hydrophilic angle (**Table 4**) alters the transfection activity.

Name	Sequences	Transfection efficiency	Cell line	Hydrophilic angle	Ref
LAH4	KKALLALALHHLAHLALHLALALKKA	100	HepG2	100	[10 17]
LAH4-AL6	KKALLHLALALLALHAHALALHLKKA	1.4	HepG2	180	[10]
LAH4-L0	KKALLAHALAHLALLALHLALHLKKA	0.8	HepG2	60	[10]
LAH4-L1	KKALLALALHHLAHLALHLALALKKA	≥100	HepG2	80	[10]
LAH4-L2	KKALLALALHHLALLALHLAHALKKA	83	HepG2	100	[10]
LAH4-L3	KKALLALALHHLALLAHHLALALKKA	115	HepG2	120	[17]
LAH4-L4	KKALLALALHHLALLAHLLALHLKKA	51	HepG2	140	[17]

Table 4: LAH4 derivatives, histidine position modification on the sequence with their corresponding transfection activity percentage compared to LAH4 (100%) (adapted from [10] and [17]).

Compared to LAH4 (100%), transfection activity decrease when the angle is around 60° (LAH4-L0) but increase for an 80° angle with LAH4-L1 [10] (**Table 4**). Modifications on LAH4-L1 have also been carried out in the laboratory (**Figure SI 2**) but none allowed a better transfection activity. However, LAH4-L1 has also been tested for other activities [42].

Indeed, these amphipathic cationic peptides could improve the efficiency of target cell transduction by lentiviral vectors (LVs). Peptide modifications were initially designed to increase the transduction efficiency and results were published in the paper of Saliha Majdoul et al. [33].

LAH4-A4 derivatives with lysines at different positions have been analysed for their transduction efficiencies (**Table 5**).

Name	Sequences	Transduction efficiency (%)	LVs	Ref
LAH4-A4	KKALLHAALAHLLALAHHLLALLKKA	100	GALVTR	[33]
LAH4-A4-dKn	___ALLHAALAHLLALAHHLLALLKKA	2	GALVTR	[33]
LAH4-A4-K1n	_KALLHAALAHLLALAHHLLALLKKA	60	GALVTR	[33]
LAH4-A4-K3n	KKKLLHAALAHLLALAHHLLALLKKA	98	GALVTR	[33]
LAH4-A4-dKc	KKALLHAALAHLLALAHHLLALL___A	61	GALVTR	[33]

Table 5: LAH4-A4 derivatives, lysines mutations (_: deleted amino acid) in the sequence extremities with their corresponding transduction activity compared to LAH4-A4 (100%) (extracted from [33]).

Deletion of the lysines at the Nter or Cter of the sequence decreases the transduction efficiency compared to LAH4-A4 (**Table 5**). Indeed, complete lysines deletion at the Nter (LAH4-A4-dKn) decreases the transduction efficiency to 2%. Transduction efficiency increases when lysines are reintroduced at the Nter: 60% (-K1n) to 98% (-K3n) (**Table 5**). The full lysines deletion in Cter decreases the transduction efficiency to 61% which has less impact than in Nter.

In addition, the amino acid deletion in the LAH4-A4 sequence shortening the α-helix tends to decrease lentiviral transduction (**Table 6**).

Name	Sequences	Transduction efficiency (%)	LVs	Ref
LAH4-A4	KKALLHAALAHLLALAHHLLALLKKA	100	GALVTR	[33]
LAH4-A4-d1aa	KKALLHAALAHLLALAHHLLALLKK_	82	GALVTR	[33]
LAH4-A4-d2aa	KK_LLHAALAHLLALAHHLLALLKK_	30	GALVTR	[33]
LAH4-A4-d2Caa	KKALLHAALAHLLALAHHLLAL_KK_	8	GALVTR	[33]
LAH4-A4-d3aa	KK___LHAALAHLLALAHHLLALLKK_	3.5	GALVTR	[33]
LAH4-A4-d5aa	KK___LHAALAHLLALAHHLLA__KK_	15	GALVTR	[33]

Table 6: LAH4-A4 derivatives, modification (_: deleted amino acid) of the sequence length with their corresponding transduction activity compared to LAH4-A4 (100%) (extracted from [33]).

The K2-L10-A12-K2 is the peptide where all histidines have been replaced by alanines (**Table 7**).

Name	Sequences	Transduction efficiency (%)	LVs	Ref
LAH4-A4	KKALLHAALAHLLALAHHLLALLKKA	100	GALVTR	[33]
LAH2-A4	KKALLAAALAALLALAHHLLALLKKA	1.4	GALVTR	[33]
LAH2-A6	KKALLHAALAHLLALAAALLALLKKA	103	GALVTR	[33]
K2-L10-A12-K2	KKALLAAALAALLALAAALLALLKKA	17	GALVTR	[33]

Table 7: LAH4-A4 derivatives, histidine to alanine mutations in the sequence with their corresponding transduction activity percentage compared to LAH4-A4 (100%) (extracted from [33]).

There is a decrease in transduction activity only when mutating the histidine residues at positions 6 and 11 for alanines in the sequence: 17% and 1.4% for K2-L10-A12-K2 and LAH2-A4, respectively. Mutation of histidines H17 and H18 does not affect the transduction (103% for LAH4-A6). The histidines position in the primary sequence determines their spatial distribution along the α-helix and are therefore important for transfection activity.

Moreover, from LAH4-L1 sequence, new variants of histidine-rich peptides named HALO or HALK have been designed by mutating some residues next to the histidine in ornithines or lysines respectively. The tested HALO peptides all demonstrated antiplasmodial activity at low concentration (µM range) [43].

These studies show high variety of different activities for histidines rich peptides. However, these mechanisms remain unclear, a better knowledge is of particular interest as it could enable the design of new compounds.

I.4 Outline of the chapters content

All the peptides belonging to the LAH4 peptide family share some characteristics: they are all composed of 4 different types of amino acids: two lysines at each extremity ensure good solubility in the aqueous environment, the hydrophobic core built of alanines and leucines and interrupted by four histidines which modulate the charge state of the peptide according to the pH. In solution, LAH4 family peptides adopt an α-helical structure at neutral pH and a random coil conformation at acidic pH [9]. In membrane environments, the LAH4 α-helix adopts an in-plan orientation along the membrane surface at acidic conditions whereas at neutral pH the peptide is transmembrane [12]. Moreover, the histidines repartition confers an amphipathic character of the peptide when structured as an α-helix with a well-defined hydrophilic angle [33].

The LAH4 peptide family exhibits antimicrobial [9][18], cellular penetration [8], transfection [10][31][44], and transduction [33][40] activities. Studying the relationship between sequence similarity and the biological activities variety presented by the LAH4 family peptides is of high interest. Indeed, understanding the mechanism of these activities based on fine changes in their sequence would help to the design of more active peptides.

Another way to improve the peptide efficiency is to consider the structure as a modulator of the activity. The peptide self-assembly allows new functions or increase in their biological activities [45]. Indeed, for certain peptides supramolecular assembly like fibrils formation has been shown to be important for lentiviral transduction [34].

Hence, the manuscript is structured in three main chapters. First, we review the role of the hydrophobic angle on the peptide activities then we focus on three LAH4 peptides family members and their fibrillation abilities and biological activities to finally address the structure of the fibrils for the LAH4-A4 member. Each chapter is shortly summarized below, a more detailed introduction will precede each part.

In the first chapter of this thesis, to better understand the role of the hydrophilic angle, LAH4 family isomers that differ in this angle formed by histidine residues when the peptide is in α-helical conformation were studied. These isomers were obtained by mutating into histidines four amino acids of the LAH4 sequence, at different position to get a variety of hydrophilic angles ranging from 60° to 180°. Two peptide series LAH4-Ln and LAH4-An were thus designed that present varying numbers of leucine or alanines in between the histidines when represented in helical wheel projection. Some biophysical studies were first conducted on these peptides. Circular dichroism was used to determine the secondary structure pH dependency of the peptides in solution and their mode of action on model membranes by titration with vesicles of different lipid composition. Furthermore, calcein release assays were performed in parallel. Then, different biological activities: antimicrobial, transfection and transduction were analysed. This study will let us know if the hydrophilic angle influences these peptides' activities.

Indeed, small changes could greatly increase the activities. Each member of the family exhibits distinct biological activities relative to small changes in the amino acid sequence [10] [17] [44] [46]. We will focus our studies on the three members LAH4, LAH4-L1 and LAH4-A4 based on their specific biological activity: LAH4 exerts predominantly antimicrobial activities [9] [18], LAH4-L1 is an excellent nucleic acid transfection agent [10] [31] [44] or LAH4-A4 is a viral transducer without transfection activity [33] [40] (**Figure 6**). Their amino acid composition is identical but their histidine location differs (**Figure 6**). When the peptide is considered in an α-helix wheel representation [33], the histidine offers different hydrophobic angles. LAH4 has on its hydrophilic side a distribution of histidines forming a 100° angle while for LAH4-L1 and LAH4-A4 their histidines are pairwise aligned spanning a certain angle filled with the indicated amino acid. LAH4-L1 has one leucine between its two pairs of histidine forming an 80° angle and LAH4-A4 four alanines for a 140° hydrophilic angle (**Figure 6**).

LAH4

KKALLALALHH**LA**H**LAL**H**LALALKKA**

Transfection and
Antimicrobial activity

LAH4-L1

KKALLAHAL**H**LLALLAL**H**LA**HALKKA**

Transfection

LAH4-A4

KKALLHAALA**H**LLALA**HH**LLALLKKA**

Lentiviral transduction
enhancement

Figure 6: The sequence and helical wheel projection of the three peptides LAH4, LAH4-L1 and LAH4-A4 with their corresponding activity.

After considering the hydrophilic angle, **in the second chapter** we look at the modifications in lateral chains distributions of amino acids, and how they can lead to different supramolecular assemblies resulting in large shift in function. We will focus on three LAH4 family peptides (LAH4, LAH4-L1 and LAH4-A4): how the sequence of amino acids is transposed into supramolecular structure and how the latter determines biological function. The fibrillation conditions for these three peptides and the stability of these fibrils according to their environments have been investigated [47]. It can be adjusted simply by changing the buffer composition (pH, salt, ions) or by modest changes in their sequence [47]. In addition, the secondary structure of the peptides in the fibril was studied by chemical shifts variation of the solid-state MAS NMR spectroscopy and Fourier Transform InfraRed. And finally, antimicrobial and transfection activities were tested on peptides: in solution, self-assembly and a mixed of both.

In the third chapter, we are going deeper into structural details by investigating the LAH4-A4 self-assembly by liquid and solid-state NMR spectroscopy. The study of the peptide structure is essential for understanding their mechanism of fibrillation and their functionality. Assigning solid-state NMR spectra of LAH4-A4 is particularly difficult due to the similar chemical shifts related to repetitions of same amino acids. The strategy used to determine the LAH4-A4 fibrils structure was incorporated a few consecutive amino acids fully labelled with ^{15}N and ^{13}C in different regions of the peptides at a time. We used liquid and solid-state NMR spectroscopy to compare peptide and fibril signatures respectively in order to determine changes related to the peptide self-assembly and then to acquire a better structural understanding of these fibrils. The part of solid-state NMR work to obtain structural models of these fibrils already started but is still in progress. Besides, to get more information about the self-organization of these fibrils small-angle X-ray scattering (SAXS) and wide-angle X-ray scattering (WAXS) experiments were carried out.

In the last chapter, we conclude by summarizing all this information to get an overview as well as define the next steps and future perspectives for this work.

II. Techniques

II.1 Biophysical chemistry investigation

II.1.1 Circular dichroism

To determine the secondary structure of the peptides in solution, circular dichroism (CD) in the wavelengths ranges 190-250 nm is used. Shape and intensity of the CD spectrum depend on the secondary structure of the molecules [48]. During this study, the circular dichroism spectra will allow us to see the peptides' structural modifications from random coils to α-helix depending on the pH or their insertions into the membrane [49]. Indeed, circular dichroism spectroscopy can detect changes of peptides secondary structure upon inserting into the model membrane [49]. Many LAH4 like peptides are random coils in the acetate buffer at pH 5 and adopt an α-helical conformation when binding to the membranes of small unilamellar vesicles (SUVs). In this case α-helical content allows us to assess the amount of membrane-associated peptide as a function of lipid concentration (binding isotherm).

The CD spectrum has characteristic wavelengths depending on the peptides structure. The spectrum of random coil conformation has one minimum at about 195 nm, when the peptide adopts a β-sheet structure the minimum is at 217 nm, while the α-helical spectrum presents two minima at 208 nm and 222 nm (**Figure 7**).
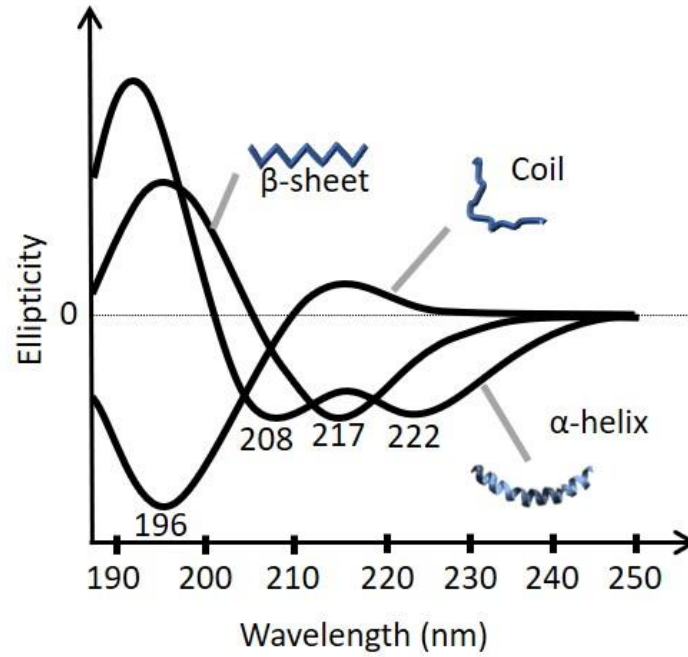
Figure 7: Circular dichroism spectra depend on the peptide secondary structure (extracted from [50]).

The CD spectra are converted to per residue molar ellipticity [θ] in deg cm ^{2} dmol^{-1} by the form [48]:

$$[\theta] = \frac{\dfrac{M \times \theta\lambda}{(Naa - 1)}}{(10 \times l \times [C])}$$

θ_λ is ellipticity (in milli-degrees) at wavelength λ, M is the peptide molar mass (in Da= g/mol),
Naa is the number of amino acid residues in the sequence, [C] is the concentration (in g/l),
l is the pathlength (in cm).

The secondary structure elements were estimated using the DICROPROT [51] software with (SELCON3) or CDpro [52] software with (CONTINLL) a self-consistent method for the fit.

II.1.2 Calcein release

The calcein loaded vesicles are used to study the interaction between peptide and lipid vesicles. The calcein is encapsulated in the liposomes at a high (local) concentration inducing self-quenching of calcein. When peptide-lipid interaction leads to membrane disruption, calcein is released from the liposome, diluted in the buffer and generates a strong fluorescence signal (**Figure 8**) [53].
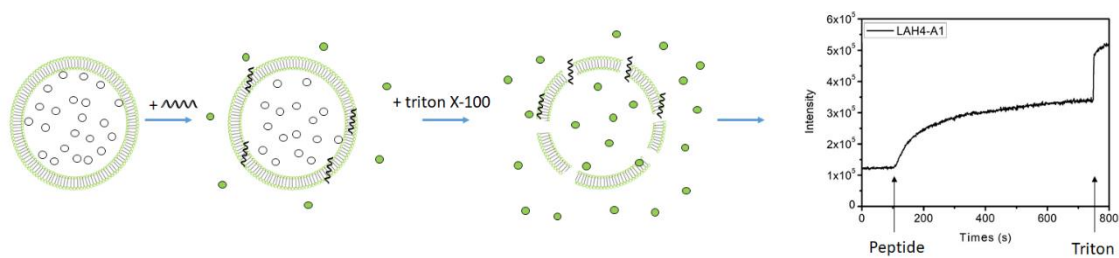
19

Figure 8: Calcein release experiments.

The calcein release percentage of the vesicles (*I%*) was calculated according to:

$$I\% \ = \ 100 * (I - Io) / (Imax - Io)$$

Where *Io* is the basal intensity of fluorescence before adding the peptide to the solution (0 to 100 seconds), and *Imax* is the maximum intensity observed after fully disrupting the vesicles with the addition of 10% Triton X-100.

II.2 Peptide structure investigation

Various techniques commonly used for peptide or protein structure determination were applied, including Fourier transform infrared and liquid and MAS solid-state NMR spectroscopy.

II.2.1 Fourier Transform InfraRed

Fourier transform infrared (FTIR) is a technique that is used to obtain molecular information of solids, liquids, and gases. The infrared absorption wavenumber range is between 400-4000 cm^{-1} [54] and absorption bands are characteristic for different functional groups in their wavelengths, and intensities [55].

The infrared spectra of peptides provide information about the secondary structure. Indeed, the amide I band (1600-1700 cm^{-1}) associate with stretching vibrations C=O and the amide II band (1480-1580 cm^{-1}) relate to N-H groups and the peptide bond. The amide I and II bands are very sensitive to the secondary structure variation of peptide [56]. The wavenumber of the amide I and II bands characteristic for secondary structure present in peptides are summarized in **Table 8**.

Secondary structural	Amide I wavenumber (cm^{-1}) range	Amide II wavenumber (cm^{-1}) range
Random coil	1645-1655	1520-1545
β-sheet	1620-1640 1670-1695	1525-1530
α-helix	1650-1658	1540-1545
β-turns	1660-1690 1635-1645	

Table 8: The wavenumber (cm^{-1}) of the amide I and II bands characteristic for secondary structure of peptides (extracted from [56]).

II.2.2 Nuclear Magnetic Resonance spectroscopy

As part of my thesis, NMR was used to obtain structural information [57] for peptide of the LAH4 family. In this study we used liquid/solid-state NMR to compare the structure of the peptide in its monomeric form in solution or in self-assembled fibrils. Isotopic labelling with ^{15}N and ^{13}C were used for signal intensity enhancement and to allow for easy assignments [58].

Solution-state Nuclear Magnetic Resonance spectroscopy

Solution state NMR allows us to precisely assign each proton, carbon and nitrogen for almost all amino acid in the sequence. For that purpose, we have used sequential assignment [59]. Two-dimensional spectra, namely Totally Correlated SpectroscopY (TOCSY) and Nuclear Overhauser SpectroscopY (NOESY) have been acquired. TOCSY spectra correlate all protons belonging to the same spin system [60]. NOESY connect protons through spatial proximity, in particular strong correlation are observed between the Hα and Hβ of a residue (i) with the NH proton of the next residue (i+1) [61] allowing for sequential walk along the amino acid backbone. NMR can allow to determine the secondary structure of proteins but also to precisely locate this structure within the peptide sequence. The NOE effects will be measured with the NH of the i+1 and i-1 residues. NOE effects are observed between amide protons neighbouring residues for α-helical structure. For the α-helix structures, we also have connectivity between Hα and NH of the residues i and i-3, i-4. For the β-sheet structures, the NOE effects will be measured between Hα and the NH of the residues. The NOE effects observed in the different secondary structures are shown in **Figure 9**.

As peptide of the LAH4 family are composed with only four different amino acid the assignment is not always straightforward. To facilitate assignment, 2D experiments were carried out with selectively labelled samples. HSQC-NOESY and HSQC-TOCSY simplifies the NOESY and TOCSY plans by editing them through the nitrogen dimension. Combination of these experiments allowed for complete assignment of the peptide sequences.
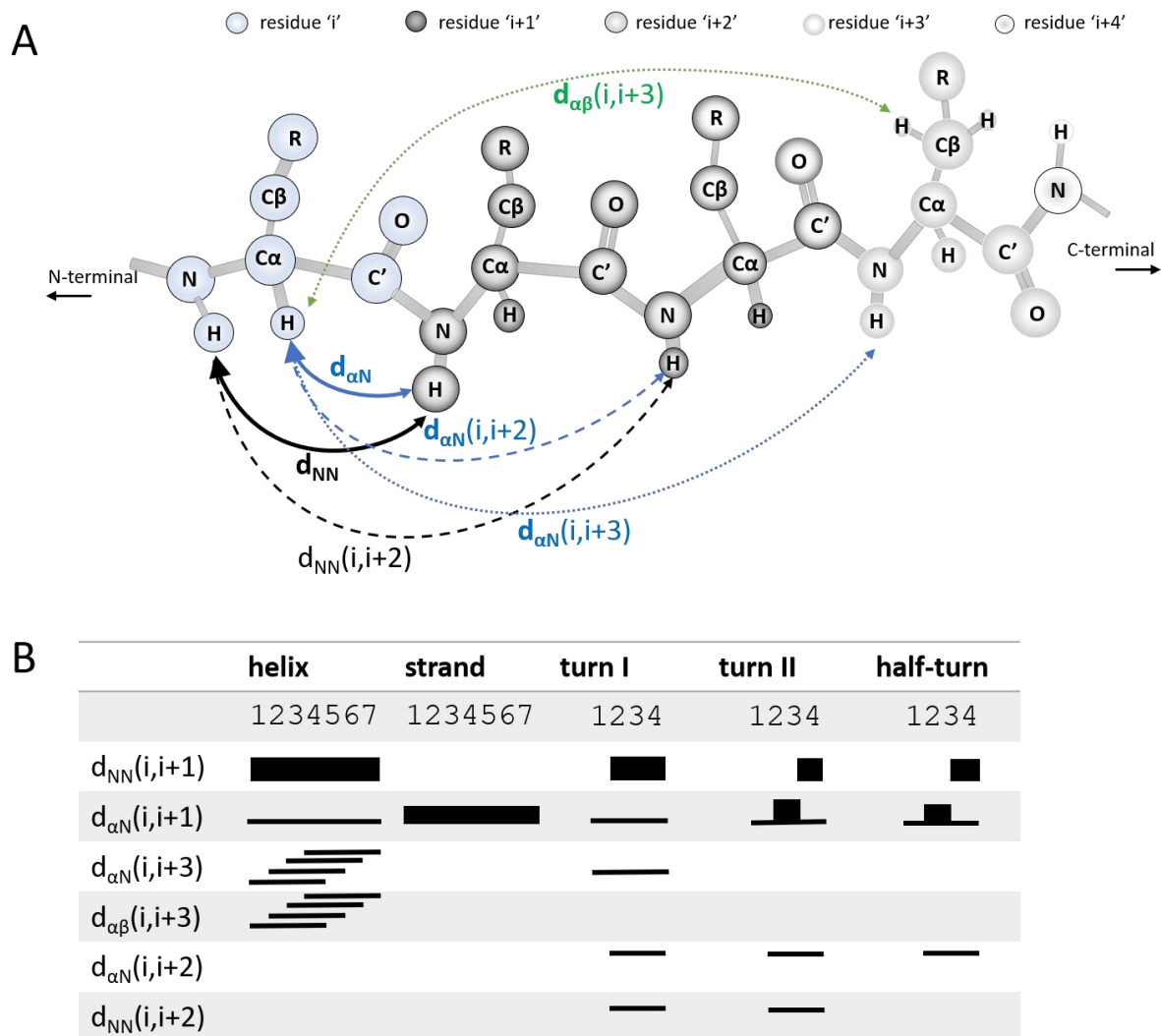

Figure 9: A- Peptide segment showing 1H-1H connectivity within a protein, B- NOE contacts in proteins based on their secondary structure.

Solid-state Nuclear Magnetic Resonance spectroscopy

Similarly to the liquid-state case, a wide range of structural and dynamic information can be accessed with solid-state NMR [62]. Solid-state NMR (ssNMR) allows us to study macromolecular systems such as fibrils. However, the molecules of a solid are static and then no Brownian averaging of anisotropic NMR interactions may take place. The solid-state NMR spectra for static sample are therefore broad and poorly resolved rendering signals difficult to interpret due to the dependence of dipolar and CSA interactions on different molecular orientations (anisotropy). In order to obtain a liquid-like resolution Magic Angle Spinning (MAS) technique had been used to determine the fibrils structure [63].

Magic angle spinning (MAS) [64]

Fast sample spinning at the magic angle (**MAS**) $\theta= 54.7°$ with respect to the main magnetic field (B_0), averages the anisotropic interactions, allowing much better resolved NMR spectra (**Figure 10**) [13]. MAS is used to eliminate the chemical shift anisotropy as well as the dipolar coupling and therefore to obtain high resolution spectra. For example, **Figure 10** compares the liquid crystalline phospholipid membranes ^1H spectrum with the same sample spectrum, but this time spinning at the magic angle ($\theta= 54.7°$) with a sample spinning frequency of 14 kHz.
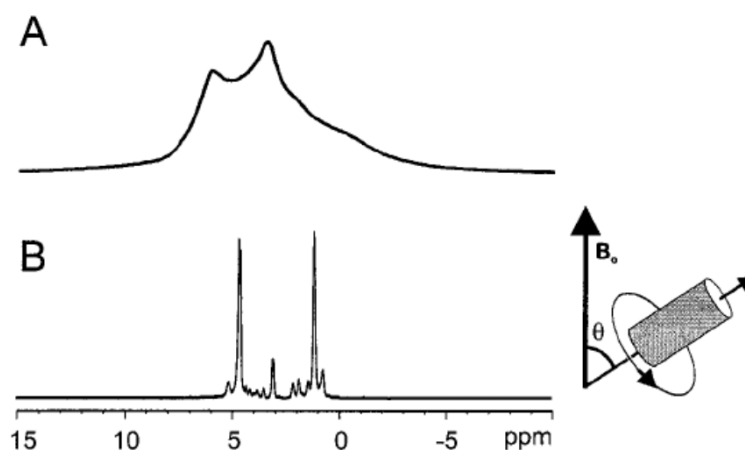

Figure 10: The liquid crystalline phospholipid membranes ^1H spectrum with the same sample spectrum, but this time spinning at the magic angle ($\vartheta= 54.7°$) with a sample spinning frequency of 14 kHz (extracted from [13]).

Cross polarization (CP) [62] allows the magnetization transfer from abundant nuclei ^{1}H to low sensitivity nuclei X like ^{13}C and ^{15}N (**Figure 11**). The 90° pulse in the ^{1}H channel is followed by the CP spinlock and the acquisition is measured on the X channel, during which time ^{1}H is decoupled. This technique is widely used in ssNMR because it allows to increase the signal/noise and faster recycling.
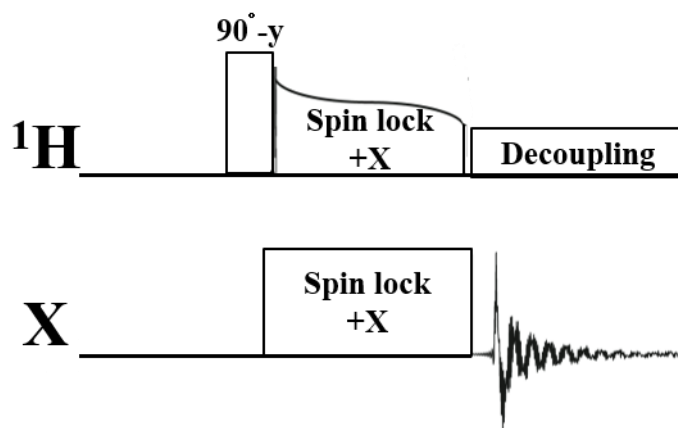

Figure 11: Sequence of cross polarization: the different pulses are indicated for the ^{1}H or X channels. The X channel corresponding to insensitive nuclei like ^{13}C or ^{15}N (adapted from [62]).

Dipolar Assisted Rotational Resonance (DARR) [65]**:** the magnetization is transferred from ^{1}H to ^{13}C nuclei by CP then transferred to other ^{13}C nuclei which are close in space. The 2D spectrum shows cross peaks from ^{13}C that are close to each other's. The intensity of the cross peak is modulated by the DARR mixing time: at short mixing time cross peak appear only for nearby ^{13}C, and when the mixing time is increased then longer contacts appear.

hNCO and hNCα spectra are acquired using a double CP experiment [66]. Magnetizations transfers involved here are also based on the dipolar interaction as the recoupling technique between ^{13}C and ^{15}N is CP. Contact times for the second polarization step (from ^{15}N to ^{13}C) are then chosen for direct neighbouring detection only (**Figure 12**). hNCO allows us to correlate the chemical shift of the carbonyl of a preceding amino acid (i-1) with the nitrogen of the next amino acid (i) (**Figure 12 A** arrow purple). hNCα allows to correlate the chemical shift of the α-carbon (Cα) with the nitrogen from the same amino acid (i) (**Figure 12 A** arrow green).
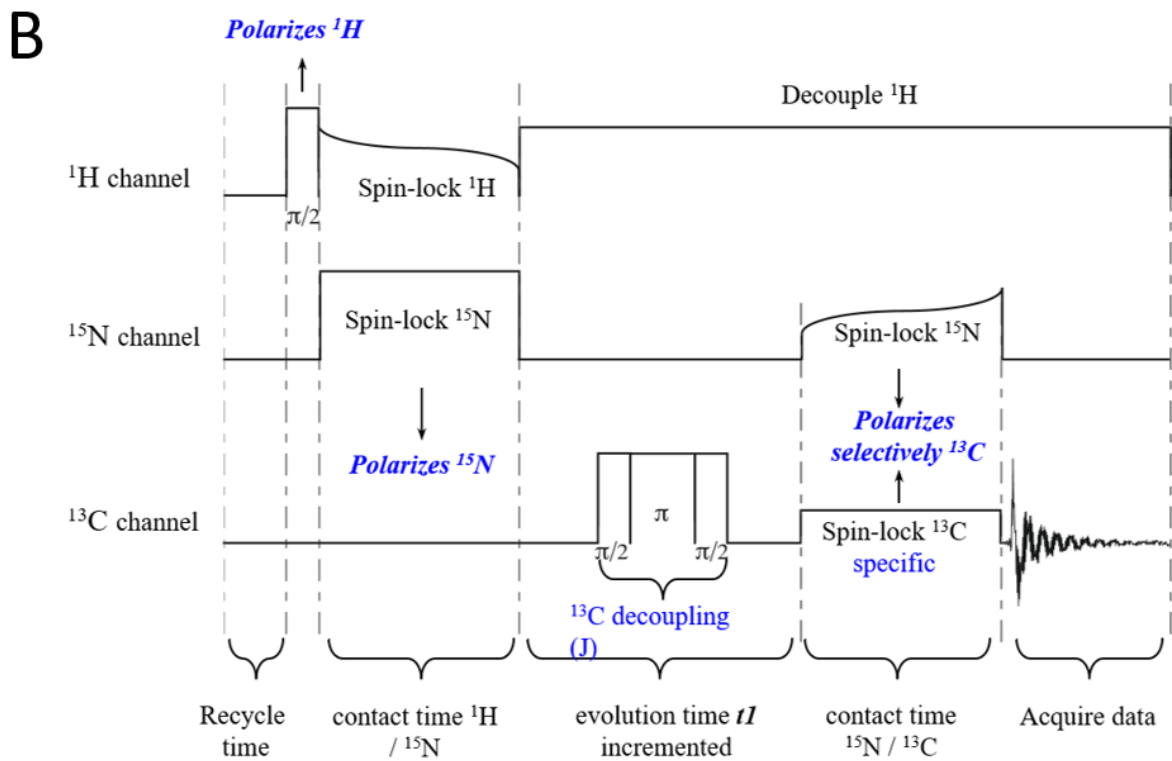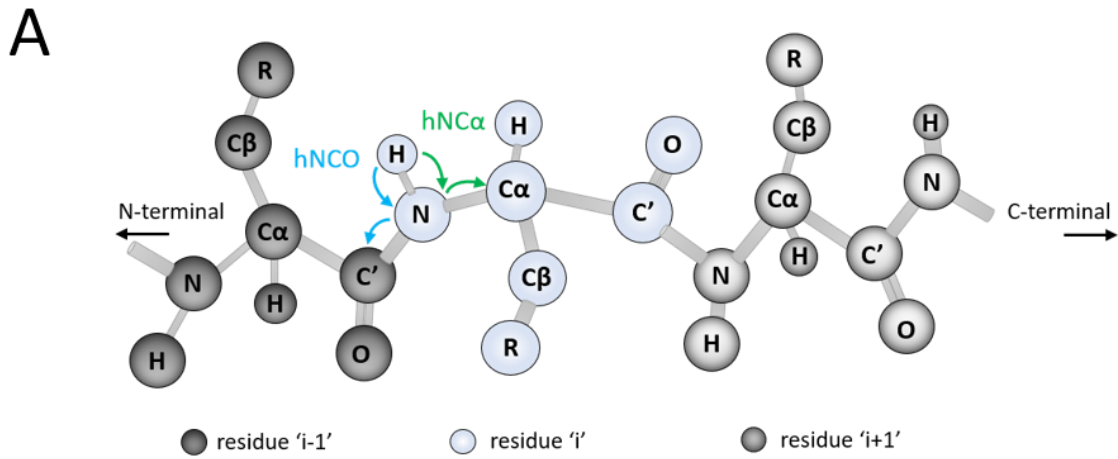
A

hNCO

hNCα

N-terminal

C-terminal

- residue 'i-1'
- residue 'i'
- residue 'i+1'

B

Polarizes ^1H

Decouple ^1H

^1H channel

Spin-lock ^1H

π/2

^{15}N channel

Spin-lock ^{15}N

Spin-lock ^{15}N

Polarizes ^{15}N

Polarizes selectively ^{13}C

^{13}C channel

π

π/2   π/2

Spin-lock ^{13}C
specific

^{13}C decoupling (J)

Recycle time

contact time ^1H / ^{15}N

evolution time *t1* incremented

contact time ^{15}N / ^{13}C

Acquire data

Figure 12: hNCO and hNCα experimentations. Schema of magnetizations pathways (A) for hNCO (arrow purple) and hNCα (arrow green) and the experimental NMR pulse scheme (B).

II.2.3 TALOS+

TALOS+ [67] software allows to determine the torsion angles of the peptide from the chemical shift values of the backbone and Cβ [68]. The software will predict the values of the φ/ψ dihedral angles and from the chemical shift values of the residue: (^{1}H, ^{13}C and ^{15}N). For each residue TALOS+ consider the environment with the chemical shifts of its two neighbours. Based on this tripeptide, the chemical shift values will be compared to the database composed of proteins with known structure. The database is composed of 200 proteins originally taken from the Biological Magnetic Resonance Data Bank (BMRB). TALOS+ identifies the approximate region of the Ramachandran diagram of residue as a function of the chemical shifts, the type of residue and immediate neighbours. The NMR chemical shifts are compared to the tri-peptide in the database to predict the location of the angles φ and ψ space, or the secondary structure (**Figure 13**) [69].
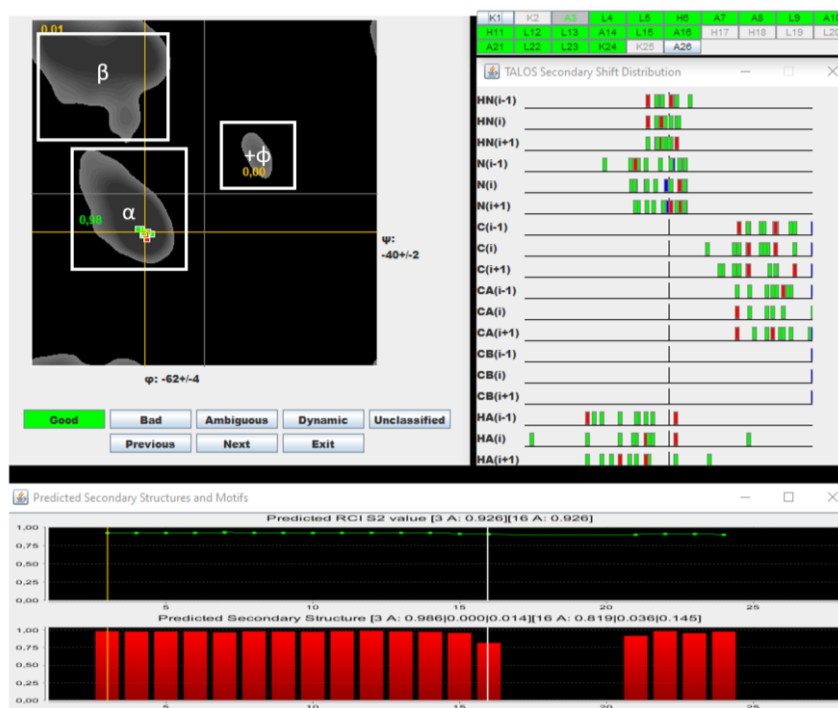

Figure 13: φ/ψ distribution of the LAH4-A4 at pH 7.4 with TALOS+. The Ramachandran maps with regions of backbone dihedral angles ψ against φ (left). The peptide sequence (top right) and the secondary shift distribution for the tripeptide (i, i+1, i-1) (bottom right). The prediction of secondary structures and motifs (bottom).

II.2.4 Small-Angle X-rays Scattering and Wide-Angle X-rays Scattering

Small angles X-rays scattering (SAXS), or wide-angle X-ray scattering (WAXS) allow the structural study of nanometric materials by the obtention of repeating lamellar distances. The X-ray can provide information on polymers, fibrils, lipids, membranes, biological tissues, liquid crystal and various particles [70]. X-ray diffraction pattern contain various pertinent information on the secondary, tertiary, and quaternary structure of peptides and proteins. The diffraction pattern make it possible to study the materials structural properties on a scale ranging from 1 to 100 nm with SAXS and <1 nm with WAXS [70]. SAXS and WAXS are differentiated by the distance between the sample and the detector (**Figure 14**). X-rays are sent to the samples and detected as a function of the scattering angle θ. If the sample has isotropy, the beams are scattered in all directions leading to a spherical pattern. On the other hand, if the atoms are ordered, the diffraction will be visible in well-defined directions: equatorial or meridian according to fibrils orientation in our case. The intensity variation of the deflected beam depending on the scattering angle 2θ will depend on the global and the molecule internal structure but also on supramolecular structures. The scattering angle 2θ allow to define a length between the sample and detector expressed by: $D = 2\pi/q$

modulated by the scattering vector with $q = 4\pi \sin(\theta)/\lambda$, with $\lambda = 0.154$ nm (Kα of copper Cu) X-ray source in our case.
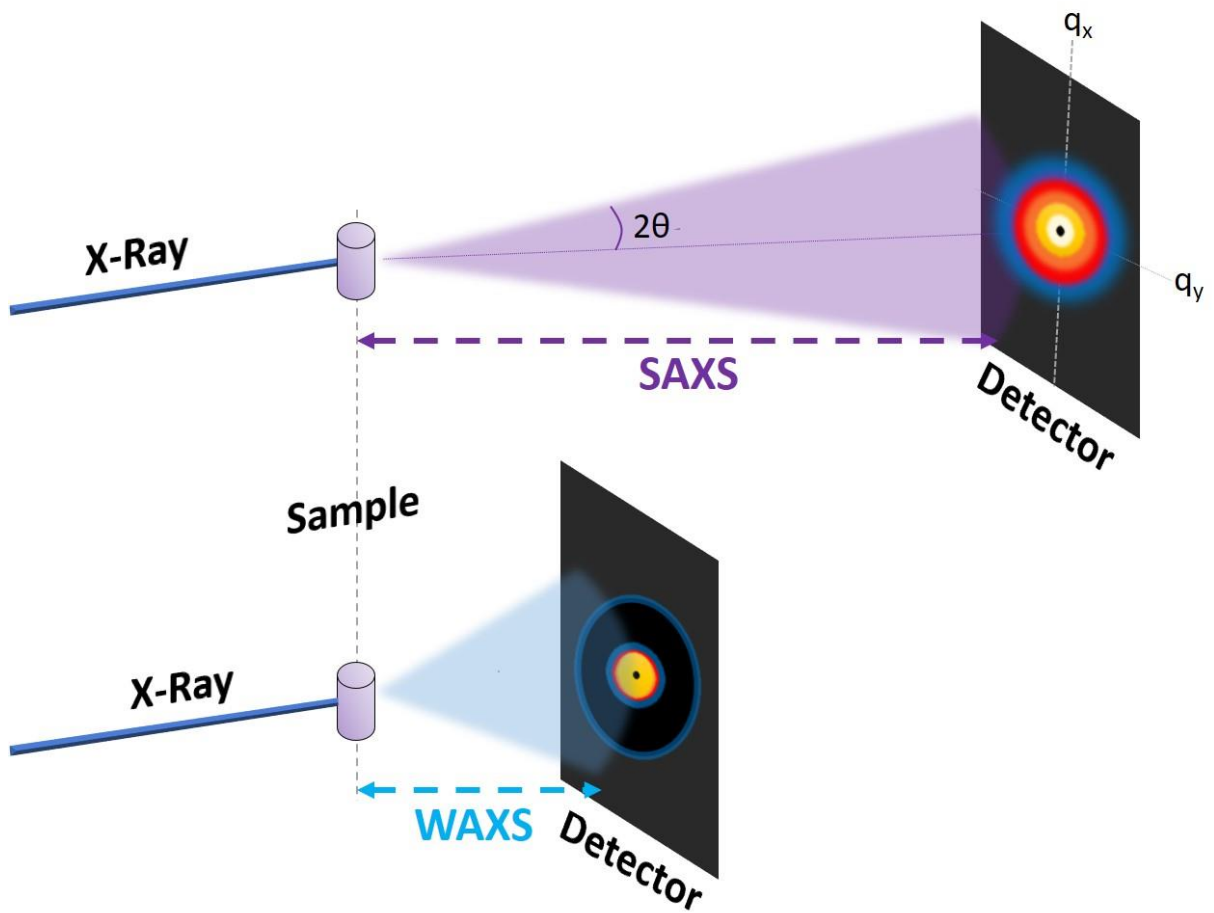
Figure 14: Small-angle X-ray scattering (SAXS) and wide-angle X-ray scattering (WAXS) schema (adapted from [71]).

III.   The effect of hydrophilic angle within histidine rich amphipathic peptides

III.1 Introduction

Since the design of LAH4 and the discovery of its biophysical and biological activities, two other peptides LAH4-L1 and LAH4-A4 have revealed great interest for their transduction and transfection enhancement, respectively. To better understand their mechanism and biophysical properties, several variants have been investigated [33]. Among them, two series of peptides, all isomers of LAH4 were designed. Thus, they are composed of the same 26 amino acids: two lysines at both termini and a central core of eight alanines, ten leucines and four histidines to form amphipathic helix. These isomers differ only by their hydrophilic angle and the numbers of leucines or alanines located between the histidines when represented as Schiffer-Edmundson helical wheel (**Figure 15** and **Figure SI 3**) [72]. The peptides of these series were thereby named "LAH4-Ln" and "LAH4-An" where n refers to the leucine or alanine number, respectively (**Figure 15**). For example, **Figure 15** LAH4-A4 (also named Vectofusin-1) [33] presents four alanine residues between the histidine pairs. **Table 9** shows the different sequences with leucines (green) and alanine (magenta) involved in the hydrophilic angle separated by histidines (blue). The amino acid modifications from the original LAH4 sequence resulted in hydrophilic angles ranging from 60° to 180°.
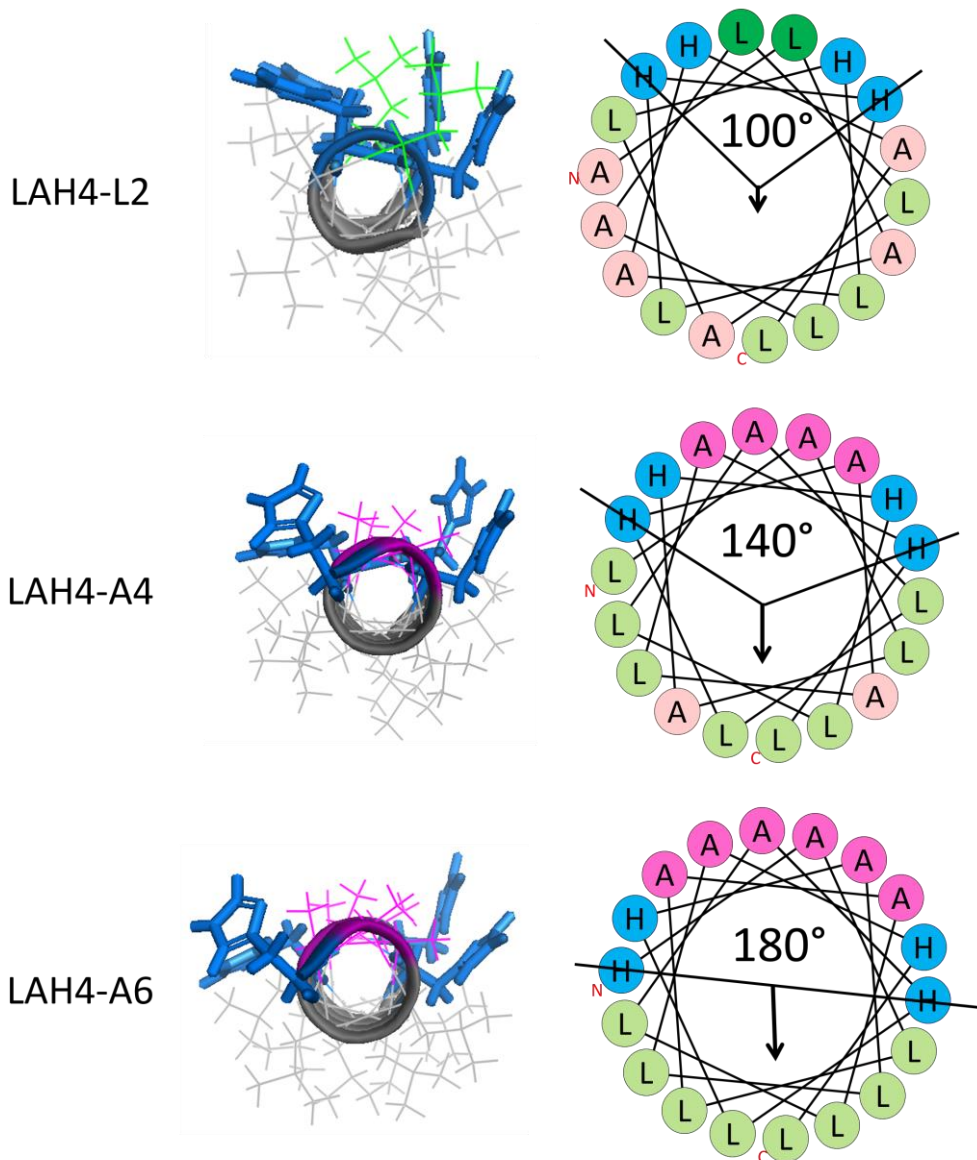
LAH4-L2

LAH4-A4

LAH4-A6

Figure 15: Helical representations of the core region (residues 6-23) for some of the LAH4-An and LAH4-Ln peptides. This figure shows LAH4-L2 (100°), LAH4-A4 (140°) and LAH4-A6 (180°) with their hydrophilic angle. PyMol representation of the perfect α-helical peptide with the distribution of histidine on the hydrophilic face (on the left) Schiffer-Edmundson helical wheel representations drawn with using the Heliquest software [73] to determine the hydrophilic angle and hydrophobic moment. Histidines (blue) delineate the hydrophilic angle, the amino acids present in the angle: leucine (dark green) and alanine (magenta). Figure SI 3 represents all peptides of the LAH4-Ln and LAH4-An series created using the Heliquest software [73]. The black arrow represents the hydrophobic moment.

Name	Sequences	Hydrophilic angle
LAH4-L0	NH₂-KKALLAHALAHLALLALHLALHLKKA-Amide	60°
LAH4-L1	NH₂-KKALLAHALHLLALLALHLAHALKKA-Amide	80°
LAH4-L2	NH₂-KKALLALAHHLALLALHLAHALKKA-Amide	100°
LAH4-L3	NH₂-KKALLALAHHLALLAHHLALALKKA-Amide	120°
LAH4-L4	NH₂-KKALLHLALLHAALLAHHLALALKKA-Amide	140°
LAH4-L5	NH₂-KKALLHLALLHAALLAHLAALHLKKA-Amide	160°
LAH4-L6	NH₂-KKALLHLALLLAALHAHLAALHLKKA-Amide	180°

Name	Sequences	Hydrophilic angle
LAH4-A1	NH₂-KKALLAHALHLLAALALHLAHLLKKA-Amide	80°
LAH4-A2	NH₂-KKALLLAALHHLAALALHLAHLLKKA-Amide	100°
LAH4-A3	NH₂-KKALLLAALHHLLALAHHLAALLKKA-Amide	120°
LAH4-A4	NH₂-KKALLHAALAHLLALAHHLLALLKKA-Amide	140°
LAH4-A5	NH₂-KKALLHALLAHLAALLHALLAHLKKA-Amide	160°
LAH4-A6	NH₂-KKALLHALLAALLAHLHALLAHLKKA-Amide	180°

Table 9: Peptide sequences from the LAH4-Ln and LAH4-An series investigated in this study and the corresponding hydrophilic angles when the peptide is represented as Schiffer-Edmundson helical wheel projection (v.s. Figure 15 and v.i. Figure SI 3). Histidines (cyan) delineates the hydrophilic angle, the amino acids present between the histidines within the hydrophilic face: leucine (green) and alanine (magenta).

In their article [33], Madjoul and collaborators investigated the different activities of the isomers but did not examine the correlation between activity and hydrophilic angle. This thesis chapter puts into perspective diverse biophysical studies and activity assays with respect to this angle. This work lead to a better understanding of the mechanism and differences within the peptide series, and has been published [74].

The physical characteristics and activities of all members of the LAH4-Ln and LAH4-An series from LAH4 family have been studied and compared. Circular Dichroism spectroscopy (CD) was used to determine the degree of helical structuration of the peptide systems according to pH and to assess the peptide secondary structure when inserted into the model membranes. The pore-forming activity of each peptide was characterized by fluorescence spectroscopy on two different model of lipid membrane vesicles: POPC/POPS (3/1) as a model for eukaryotic

plasma membrane and POPE/POPG (3/1) as model of bacterial membrane. Finally, the different biological activities: antimicrobial, transfection and transduction were analysed. This study will allow us to see if the hydrophilic angle and the repartition of alanines and leucines play a role on the insertion or activity of LAH4 isomers.

III.2 Materials and Methods

The LAH4 isomers peptides were purchased from Pepceuticals (Leicestershire, UK). To exchange the trifluoroacetic counterions the peptides were solubilized in 2 mM hydrochloric acid and lyophilized three times. The peptides were aliquoted in fractions of approximately 1 mg.

Circular Dichroism spectroscopy

We used circular dichroism spectroscopy to evaluate the secondary structure of the 13 peptides (*v.s.* **Table 9**) at two different pH. For this, the sample solutions were prepared as follows: each peptide was dissolved to reach a concentration of 0.1 mg/ml (36 µM), in either 10 mM phosphate buffer or in 10 mM acetate buffer at pH 7.4 and 5, respectively. These concentrations were chosen to ensure a good signal-to-noise ratio when working with cuvettes of 1 mm pathlength, while the absorption coming from the buffer being negligible. The measurements were performed on the Jasco J-810 spectropolarimeter (Tokyo, Japan) belonging to the "Service d'Analyses et de Mesures physiques" from our institute. Measurements were performed close to room temperature (T= 25 °C) and standard values for the acquisition parameters were used (1 nm in resolution, 50 nm/min of scanning speed and 1 second for the detector integration time). The data were recorded from λ= 260 nm down to 190 nm and 7 acquisitions were accumulated for each spectrum. Note that the values of the residual molar ellipticity was often underestimated due to error in the weighing of the samples, because of the presence of water molecules, salt, or counter ions.

Membrane partitioning by Circular Dichroism spectroscopy

Circular dichroism has also been used to determine the structural changes of peptides from a random coil in solution to an α-helix conformation when inserted into the vesicle membrane. For this purpose, small unilamellar vesicles (SUVs) composed of POPC/POPS at the ratio 9/1 mol/mol were prepared as follows. First, unilamellar vesicles (UV) were prepared by dissolving POPC and POPS lipids in chloroform/methanol 3/1 (v/v). The solution was evaporated under a stream of nitrogen gas and dried under vacuum of a lyophilizer for at least 24 hours. The lipid film was rehydrated at ambient temperature in 1 ml of 10 mM acetate buffer at pH 5 to yield a 13 mM lipid suspension. The suspension was then tip sonicated (Sonoplus H200, Bandelin, Berlin, Germany) 3 times for 15 seconds to obtain SUVs of approximately 50 nm diameter to reduce the light scattering during the measurements. Stock solutions of 36 μM peptide were prepared in the same 10 mM acetate buffer at pH 5. Each sample was prepared 3 times independently at the following lipid-to-peptide molar ratios: 0/1, 2/1, 5/1, 10/1, 20/1, 30/1, 50/1, 60/1, 70/1 and 80/1.

Measurements were performed close to room temperature (T= 25 °C) and standard values for the acquisition parameters were used. The data were recorded from λ= 260 nm down to 190 nm. The secondary structure composition was estimated [75][76] using the DICROPROT software [51] using the algorithms SELCON3 or CDpro software using the algorithms CONTINLL [52].

Calcein release experiments

Calcein release experiments make it possible to analyse membrane pore formation by the peptide. Large unilamellar vesicles (LUVs) of POPC/POPS or POPE/POPG, both at the molar ratio 3/1 were used. The POPC/POPS lipid mixture was commonly used as a simple model of the inner lipid leaflet of a eukaryotic membrane [77] and POPE/POPG are the main lipid components of inner bacterial membrane [78]. By studying these two vesicle models, we can study the LAH4 peptide interaction with eukaryotic and bacterial membranes and their disruption. The lipids were hydrated with 50 mM phosphate (pH≈ 7) or 50 mM acetate buffer (pH≈ 5) containing 50 mM calcein disodium salt. The mixtures were agitated for an hour before undergoing several freeze-thaw cycles and extruded 21 times through membranes with pores of 400 nm (Whatman, Maidstone, UK). The dye outside the calcein-loaded vesicles was removed by gel filtration through a Sephadex G-50 column (2.5 × 3.5 cm) equilibrated with the corresponding buffer (50 mM) and supplemented with 50 mM NaCl to compensate for the osmotic pressure induced by the calcein presence and its sodium counter ion. The vesicle concentration eluted from the column was estimated by light scattering measurement. Typical lipid concentrations of vesicles used in the calcein release experiments ranged from 1 to 3 µM. Fluorescence measurements were performed on the spectrofluorometer Fluorolog-3.22 (HORIBA Scientific, Kyoto, Japan) belonging to the "Service d'Analyses et de Mesures physiques" from our institute. For the experiment, 10 µl of LUVs suspension (concentration from 1 µM to 3 µM) were added to 1.5 ml of salt buffer supplemented with 1 mM EDTA in a quartz cuvette at room temperature. An aliquot of the peptide solution at 1 mg/ml was injected at t= 100 seconds into the cuvette to obtain a final peptide-to-lipid molar ratio of 1/50. The sample was continuously excited at $\lambda_{ex.}$= 485 nm, and the fluorescence intensity (I) was recorded at λ_{em}= 515 nm with 1.5 nm resolution.

Antimicrobial activity assays

A broth microdilution assay was used to determine the minimum inhibitory concentration (MIC) i.e., the lowest peptide concentration able to inhibit bacterial growth for each peptide. A peptide aliquot of 1 mg was solubilized in 50% EtOH (10 mM). A vortex cycle was carried out followed by a treatment in a sonication bath for 5 minutes. The peptide was diluted in H_2O

and a new vortex cycle and sonication bath for 5 minutes was then carried out to finally have a peptide stock solution of 300 μM.

For all the activity tests, *E. coli* bacteria (ATCC® 25,922™, Thermo Fisher Scientific, Courtaboeuf, France) were spread on Mueller-Hinton agar plates (MH) and incubated at 37 °C overnight. Some colonies were resuspended in 1 ml of Mueller-Hinton broth at pH 7.4. This suspension was used to seed a preculture (10 ml of MH broth pH 7.4) at the $OD_{550}= 0.005$. This preculture was incubated for about 6 hours at 37 °C ($OD_{550}= 1-2$) and then used to inoculate a culture with a starting $OD_{550}= 0.2$ in 10 ml of MH pH 5. The culture was incubated at 37 °C until an $OD_{550}= 1$ to 2 was reached (2-3 hours). According to the Mac Farland standard, $OD_{550}= 0.125$ to 0.25 should correspond to $1-2*10^8$ CFU/ml. Therefore, from the culture, a standard bacterial suspension was prepared at $OD_{550}= 0.2$ which was subsequently diluted a thousand-fold to prepare the final bacterial working solution of $OD_{550}= 0.0002$ that should correspond to $1-2*10^5$ CFU/ml.

The antimicrobial analyses were carried out in 96-well microplates (sterile polystyrene untreated with F-bottom, Thermo Scientific Nunc A/S, Roskilde, Denmark). The first column of the plate contains the highest final concentration (Cf) of peptide to test (Cf 100 μM or 30 μM). 100 μl of peptide stock solution at three times the desired highest final peptide concentration were added to 50 μl of MH3X at pH 5. After pipetting up and down, serial dilution by a factor of 1.5 was successively carried out by transferring 100 μl of peptide solution from one column to the next previously loaded with 50 μl MH1X at pH 5 (from columns 1 to 11). Column 12 was used for control conditions: bacteria without peptide (CT+) or broth without bacteria (CT-). The bacterial working suspension was distributed (50 μl) in each well, except those for CT-. The final volume was 100 μl/well and the range of peptide concentration tested was from 100 μM to 1.75 μM for the first experiment and from 30 μM to 0.52 μM for the second experiment. The microplates were incubated at 37 °C for 12 hours bacterial growth was assessed by the OD_{600} measurement.

To check the bacterial density for each experiment, the working bacterial suspension was diluted 1/100 and 1/500 in MH1X, pH 5 and 100 μl were spread on MH agar plates. After overnight incubation at 37 °C, the CFU were counted and the CFU/ml were determined.

Cell culture and preparation of peptide/DNA complexes for transfection [74]

The Roswell park memorial institute medium (RPMI) was supplemented with 100 units/ml penicillin, 100 µg/ml streptomycin and 10% of fetal calf serum for the culture of the human glioblastoma cell line U87. A total of 55,000 U87 cells were plated in 48 well plates one day before the experiment was performed. The cells were transfected using the following protocol: a fixed quantity of the plasmid DNA (1.5 µg of the 7.6 kb p-Luc plasmid which is an expression plasmid encoding the firefly luciferase gene under the control of the human cytomegalovirus (CMV) immediate-early promoter mixed to increasing amount of peptide.

Peptide and DNA solutions were each diluted into 25 µl of 50 mM acetate buffer with 50 mM NaCl at pH 5 and gently mixed at room temperature for 20 minutes. DNA complexes were generated using increasing peptide/DNA w/w ratios. These mixtures were then diluted with culture medium to obtain a final volume of 0.5 ml. For transfection, serum-free culture medium containing the DNA complexes were deposited in duplicate with 0.25 ml/well and were incubated for 2.5 hours at 37 °C. Then, medium was replaced with fresh one containing serum.

Cells were harvested 1 day after transfection, and the luciferase activity was measured. For luciferase activity, cells were harvested in 100 µl of lysis buffer (8 mM MgCl2, 1 mM DTT, 1 mM EDTA, 0.6% Triton X-100, 15% glycerol, and 25 mM Tris-phosphate buffer at pH 7.8). The cell lysate was centrifuged for 7 minutes at 10,000 g to pellet debris. Supernatants (2 µl) were transferred into 96-well plates to measure the luciferase activity with a Centro LB luminometer (Berthold. Technologies GmbH & Co. KG, Bad Wildbad, Germany). The measurement was done over 1 s after automatic injection of 50 µl assay buffer (lysis buffer without Triton X-100 but supplemented with 2 mM adenosine triphosphate (ATP)) and 50 µl of a luciferin solution (167 µM in water) to the supernatants. Luciferase background was subtracted from each value and the protein content of the transfected cells was measured by Bradford dye-binding using the BioRad protein assay (Bio-Rad, Marnes-la-Coquette, France). The transfection efficiency was expressed as light units/1s/mg protein (light units measured over a period of 1 s and the values were then normalized after measurement with respect to the amount of protein present in each well). Reported values are the mean of duplicates and error bars represent the standard deviation of the mean.

III.3 The secondary structure of histidine-rich peptides

The peptide secondary structure is one of the parameters, which can influence the lipid membranes disrupt [8]. Previous studies showed that LAH4 family peptides adopt an α-helical conformation at neutral pH and are unstructured when the pH is below 6.2 and thus the histidines are charged [7] [43]. These peptides exhibit properties that are strongly pH-dependent, and it is interesting to investigate their activities and secondary structure as a function of pH [79]. To investigate the structure of the LAH4 isomers, circular dichroism spectra were acquired at pH≈ 5 and 7.4. The data were converted to the common unit per residue molar ellipticity [deg*cm ^{2}/dmol] and the secondary structure content was analysed (**Figure 16**).
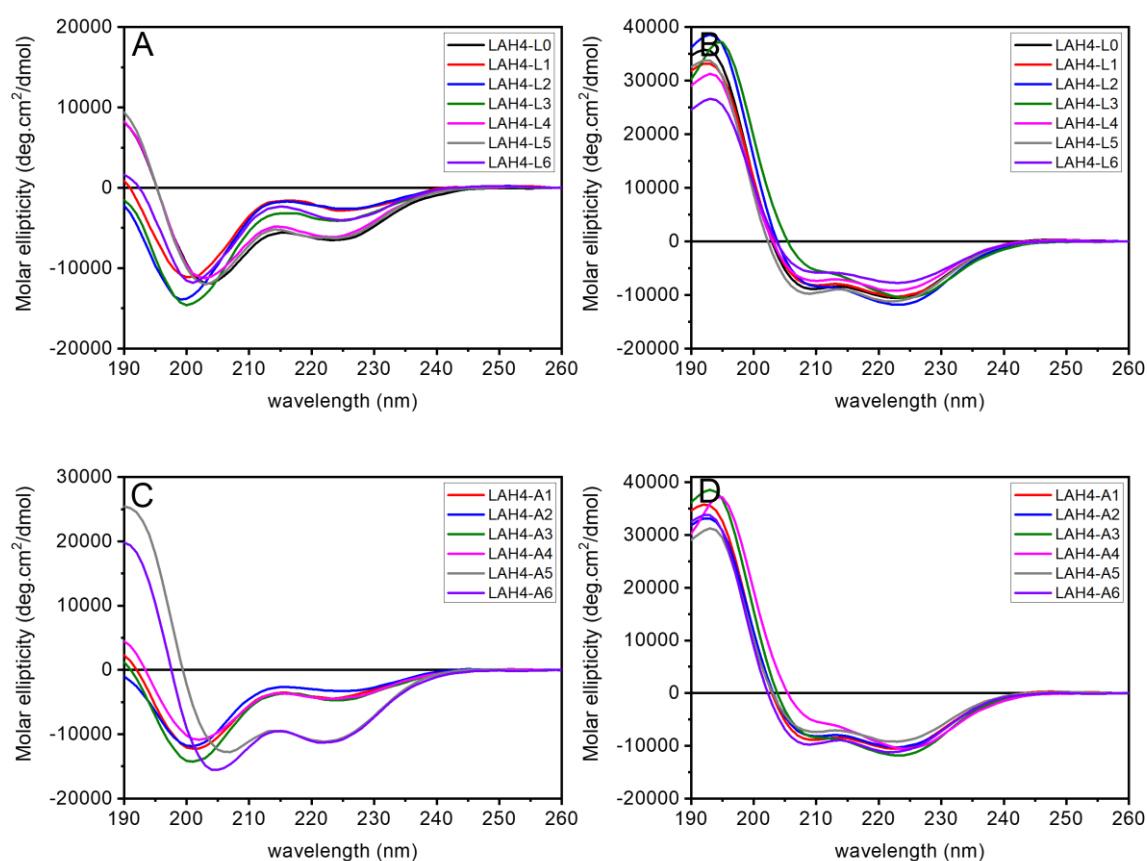

Figure 16: Circular dichroism spectra of the LAH4-Ln (A, B) and LAH4-An (C, D) series at pH 5 (A, C) and pH 7.4 (B, D).

Within the LAH4-Ln series, circular dichroism spectra show ellipticity shifts characteristic of peptide structure modification. In **Figure 16 A** for the LAH4-Ln peptides at pH 5 one minima at 200 nm characteristic of random coil conformation is observed whereas at pH 7.4 (**Figure 16 B**), two minima at 208 nm and 222 nm signature of an α-helix structure are present. This series adopts a random coil conformation at pH 5 and change to an α-helix structure at pH 7.4 (**Figure 16 A, B**). In **Figure 16 C** for the LAH4-An series at pH 5, similar observations are made for the members LAH4-A1 to LAH4-A4, but not for the LAH4-A5 and LAH4-A6 that present two minima at 208 nm and 222 nm signature of an α-helix structure already at pH 5. All this series peptides adopt an α-helix structure at pH 7.4 (**Figure 16 D**). The degree of helicity was also estimated using the CDpro software with (CONTINLL) self-consistent method fitted [80]. The resulting secondary structures estimates are given in **Table 10**.

	pH	LAH4-A1	LAH4-A2	LAH4-A3	LAH4-A4	LAH4-A5	LAH4-A6
ALPHA-HELIX	5	20	17	21	22	53	53
BETA		14	14	14	14	10	8
RANDOM COIL		38	38	38	35	26	30
OTHER		27	31	27	29	11	9
ALPHA-HELIX	7.4	89	69	92	69	56	72
BETA		3	7	4	8	11	7
RANDOM COIL		6	14	4	17	26	17
OTHER		2	9	1	5	7	5
	pH	LAH4-L0	LAH4-L1	LAH4-L2	LAH4-L3	LAH4-L4	LAH4-L5	LAH4-L6
ALPHA-HELIX	5	22	23	17	19	19	24	31
BETA		14	15	15	13	13	13	12
RANDOM COIL		38	36	34	39	39	36	38
OTHER		27	25	31	29	28	26	19
ALPHA-HELIX	7.4	77	65	57	91	81	56	69
BETA		7	8	10	4	6	10	9
RANDOM COIL		10	19	25	4	10	26	17
OTHER		6	8	9	1	3	8	6

Table 10: The secondary structure composition recorded in solution at pH 5 or pH 7.4. The data shown were averaged from three independent measurements for the LAH4-An and LAH4-Ln peptides from the CD spectra (7 scans).

For the LAH4-Ln series, the peptides are mainly unstructured at pH 5, with minor α-helix (ca 20%) and β-sheet content. However, the helicity approaches 70% at pH 7.4 (**Table 10**). For the LAH4-An series, at both pH 5 and 7 similar observations are made for the LAH4-A1 to LAH4-A4 members. The secondary structures of these peptides are strongly pH-dependent. However, much higher helicities are observed for the LAH4-A5 and LAH4-A6 already at pH 5 when compared to the corresponding LAH4-Ln peptides (**Table 10**). The LAH4-A5 and LAH4-A6 have circular dichroism spectra corresponding to α-helical structures, even at pH 5 (**Figure 16 C**) which is confirmed by the fitting values with a helicity estimation of 53% (**Table 10**). The LAH4-A5 and LAH4-A6 with a hydrophilic angle between 160° and 180° do not present pH dependent secondary structure change contrary to the peptides with hydrophilic angles between 80° and 140°. These latter assume random coil conformations at pH 5 and adopt an α-helical structure at pH 7.

III.4 Interactions of histidine-rich peptides with model membranes

The goal of the study is the assessment of the LAH4-An and LAH4-Ln series peptide secondary structure when interacting with model membranes, as it has already been performed for other members of the LAH4 family [81]. The changes in the peptide structure, like from a random coil in solution to an α-helix conformation when inserted into the vesicle membrane, are determined by CD spectroscopy. Therefore, circular dichroism spectra of the peptides were recorded for the molecular systems in solution and during the titration with small unilamellar vesicles (SUVs) of POPC/POPS (9/1; mole/mole) (**Figure 17**, **Figure SI 4** and **Figure SI 5**). The data were converted to the common unit deg*cm^2/dmol and the secondary structure content were estimated using the CDpro software with (CONTINLL) self-consistent method fit [80] (**Figure SI 6**). In order to generate an adsorption isotherm, the α-helical content was normalized: the helical content in absence of lipids corresponds by definition to 0% bound peptide whereas the maximal α-helical fraction observed for lipid-peptide titration was assigned to 100% bound peptide.
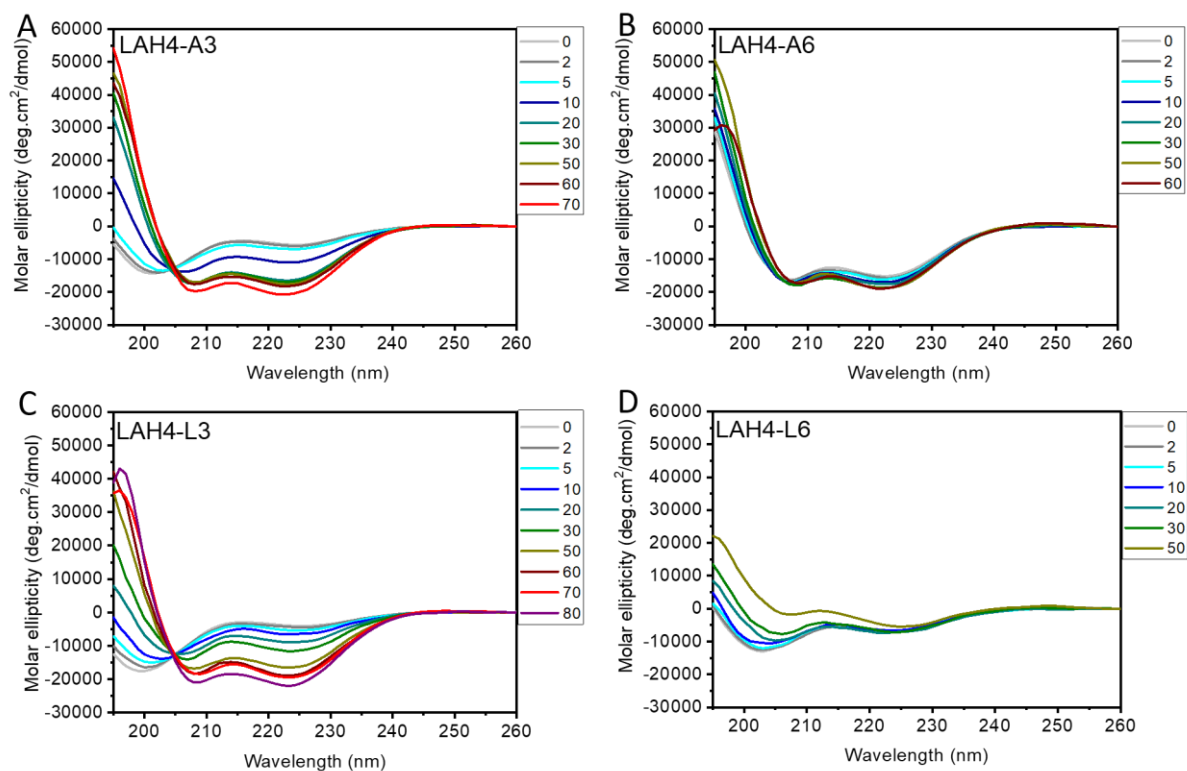
Figure 17: Circular dichroism spectra of the LAH4-An (A, B) and LAH4-Ln (C, D) series of peptides in 10 mM acetate buffer at pH 5 titrated with POPC/POPS (9/1) SUVs. Each curve corresponds to the indicated lipid to peptide ratio (from 0 to 80).

Upon addition of SUVs made of POPC/POPS (9/1 mole/mole at pH 5), almost all isomers adopt more helical secondary structures, notable exceptions being LAH4-A5, LAH4-A6, LAH4-L5 and LAH4-L6, where changes in the CD spectra are small or absent (**Figure 17 B, D** and **Figure SI 4**). For the LAH4-An series, peptides LAH4-A1 to LAH4-A4 reach about the same secondary structure content when membrane associated (**Figure 17 A** and **Figure SI 5**). In contrast, considerable variations of the α-helical content are observed for LAH4-L0 to LAH4-L4 of the LAH4-Ln series (**Figure 17 C** and **Figure SI 5**). For the peptides that already exhibit high helical content in the absence of liposomes (53%), the structural changes when vesicles are added remains small. In contrast, upon addition of liposomes to LAH4-L5 and LAH4-L6, the CD spectra show apparent increases in ellipticity at low wavelengths (190-205 nm). These shifts are assigned to light scattering artifacts due to the agglutination of peptide/vesicles when the amount of lipids increases (**Figure 17 D**).

The degrees of helicity are given in **Figure SI 6** they were estimated using the CDpro software with (CONTINLL) self-consistent method fit [80] obtained from analysis of **Figure SI 4** and **Figure SI 5**. The α-helical secondary structure content expressed in percent is presented in **Table 11**.

PEPTIDE L/P RATIO	LAH4-A1	LAH4-A2	LAH4-A3	LAH4-A4	LAH4-A5	LAH4-A6
0	20±0.9	17±0.3	21±0.4	22±1.1	53±3.6	53±0.4
2	28±1.4	22±0.7	19±1.8	26±1.5	47±3.9	53±1.6
5	36±2.6	27±1.3	21±2.3	32±2.2	47±4.7	57±0.9
10	42±4	35±0.5	41±0.5	37±2.2	43±0.8	59±1.1
20	61±3.3	47±3.5	55±4.4	51±3.4	55±3.6	66±0.5
30	67±0.7	60±2.6	65±2.8	62±2.8	62±1.4	66±2.7
50	71±1.5	70±0.2	75±0.3	71±2.5	61±2.1	80±0.4
60	77±1.6	74±0.8	82±0.5			75±2.5
70	80±6.5	73±1.8	82±0.4			

PEPTIDE L/P RATIO	LAH4-L0	LAH4-L1	LAH4-L2	LAH4-L3	LAH4-L4	LAH4-L5	LAH4-L6
0	22±0.9	23±1.5	17±0.8	19±1	19±0.6	24±1	31±3.8
2	22±0.5	30±1.1	20±0.5	20±0.3	21±0.4	24±1.1	27±1.2
5	27±0.8	34±0.7	24±1.2	26±1.1	23±1.1	29±2.2	27±1.1
10	32±1.4	38±1.2	32±2.9	31±1.1	32±2.5	25±1	30±1.4
20	40±3.2	50±1.3	43±0.8	42±3.4	38±0.3	24±0.3	29±2.2
30	52±3	65±0.8	52±1.6	48±3.8	41±2.7	26±0.9	30±2
50	66±1.2	71±0.9	63±1.3	78±0.9	74±1.9	26±1.8	31±1.5
60	62±2.1			79±1			29
70			70±2	81±0.5	76±2.9		36±3.6

Table 11: α-helical secondary structure content (in percentage) for the LAH4-An and LAH4-Ln peptides at different L/P ratios in acetate buffers at pH 5. SUVs made from POPC/POPS 9/1 were added during the titration experiments to reach the indicated lipid-to-peptide molar ratios.

The LAH4-A1 to LAH4-A4 and LAH4-L0 to LAH4-L4 helix content in solution (25-30%) increases to around 70% when SUVs are added (**Table 11**). The helicity for LAH4-L5 and LAH4-L6 peptides remains around 20%. For LAH4-A5 and LAH4-A6, the CD spectra are not much altered during the lipid titration and the peptide remains in α-helical conformation (**Figure 18 B**). For LAH4-A5, the α-helical content remains relatively stable around 50-60% (**Table 11**). Finally, the LAH4-A6 helical content increases by up to about 20% when vesicles are added (**Table 11**). Because only minor spectral changes are observed for peptides with 160° and 180° hydrophilic angles, these data did not allow to examine the membrane association in a quantitative manner.

When the helix content is used to evaluate the amount of membrane-associated peptide as a function of lipid concentration, in most cases the fraction of membrane-associated peptide increases in close to linear fashion until a plateau is reached [81] (**Figure 18**).
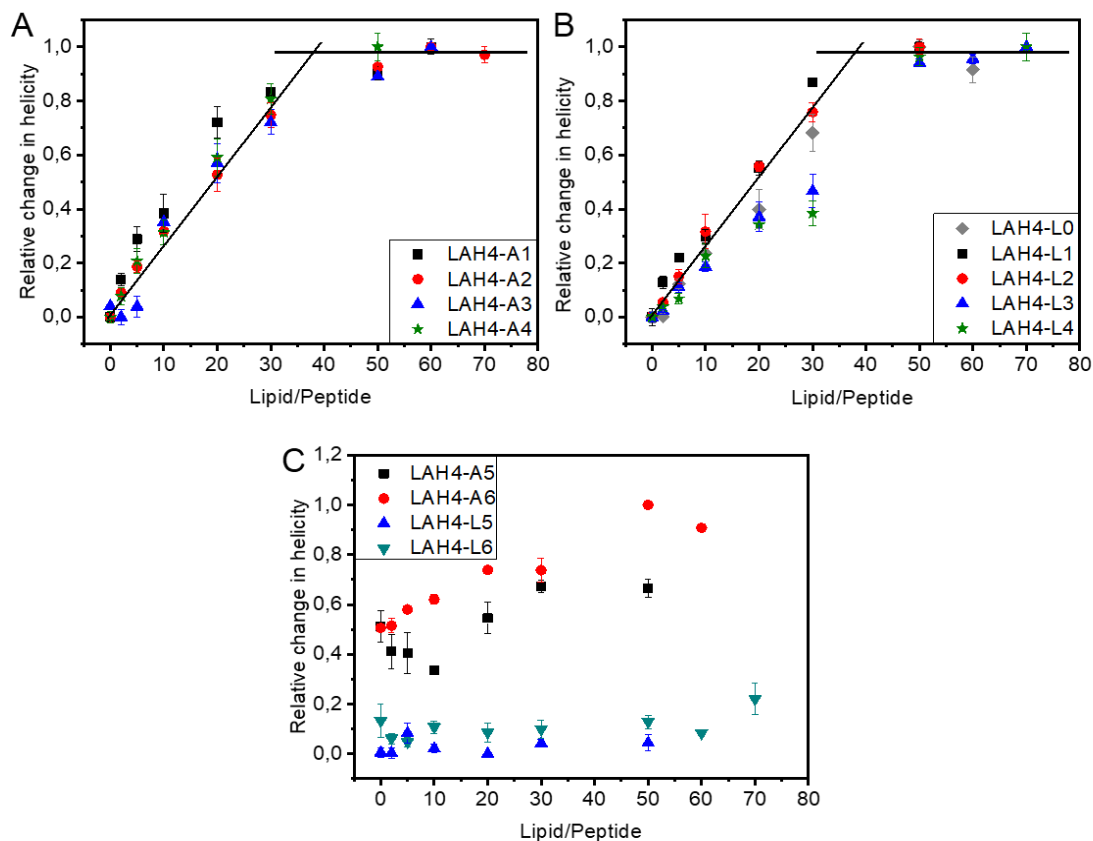

Figure 18: Fraction of membrane-associated peptides from the LAH4-An and LAH4-Ln series as a function of L/P molar ratio determined from the changes in helical content from CD spectra as shown in Figure SI 4 and Figure SI 5. Data for peptides with hydrophilic angle <150º from the LAH4-An series (A), or LAH4-Ln series (B) and with hydrophilic angle> 150º from both series (C). Peptides (36 µM) in 10 mM acetate buffer at pH 5 at different L/P ratios SUVs of POPC/POPS 9/1 mol/mol and the temperature was stabilized at T= 25 °C.

The fitting of these allows us to estimate the point where all peptides are bound to lipid membranes. The two lines cross when all peptides are bound, that is at L/P ratios of about 40 (**Figure 18 A, B**). This behaviour has previously been observed in more elaborate binding studies of LAH4-L1 to POPC/POPS membrane at molar ratios of 3:1, 6:1 and 9:1 using CD spectroscopy and isothermal titration calorimetry (ITC) [82]. As a first approximation, the LAH4-Ln and LAH4-An series peptides exhibit about the same membrane association degree (**Figure 18 A, B**). Because the CD spectral changes of the LAH4-A5, LAH4-A6, LAH4-L5 and LAH4-L6 peptides are small or absent upon lipid addition (**Figure 18 C**). Importantly, the peptides with hydrophobic angle from 60° to 140° (LAH4-A1 to LAH4-A4 and LAH4-L0 to LAH4-L4) all showed the same behaviour when associating with POPC/POPS membranes regardless of the hydrophilic angle. As for LAH4-L5 and LAH4-L6 the helix content matches those of other members of the L-series in solution (25-30%) and does not change much with the titration with SUVs (**Table 11**). It thus appears that at the very large hydrophilic angles the "leucines" (**Figure SI 3**) framed by charged histidines at pH 5 cannot efficiently interact with the membrane interface.

III.5 Characterization of membrane permeabilization

In order to study the LAH4 peptide activity with eukaryotic and bacterial membranes, POPC/POPS and POPE/POPG model phospholipid mixtures are used. POPC/POPS is commonly used as a simple model of the inner lipid leaflet of a eukaryotic membrane [77], while POPE and POPG are the main lipid components of inner bacterial membrane [78]. By studying these two different lipid environments, we can find out if there is a specificity in the interactions of LAH4 peptides with eukaryotic and/or bacterial membranes. In order to test the peptide capability to disrupt membranes, fluorescence dye release experiments were performed (**Figure 19** and **Figure SI 7**). The experiments were done at pH 5 and 7.4 using vesicles either made of POPC/POPS or of POPE/POPG both at molar ratios of 3/1 (mole/mole). The total peptide-to-lipid ratio was adjusted to 1/50 for all experiments. The peptide was injected after 100 seconds of sample stabilization and the calcein release percentage was recorded at least for ~ 600 seconds in total (**Figure 19** and **Figure SI 7**). Each experiment was repeated more than three times, and the calcein release percentage is calculated from the average of the replicates at the 350 seconds time point (i.e., 250 seconds after the peptide addition).
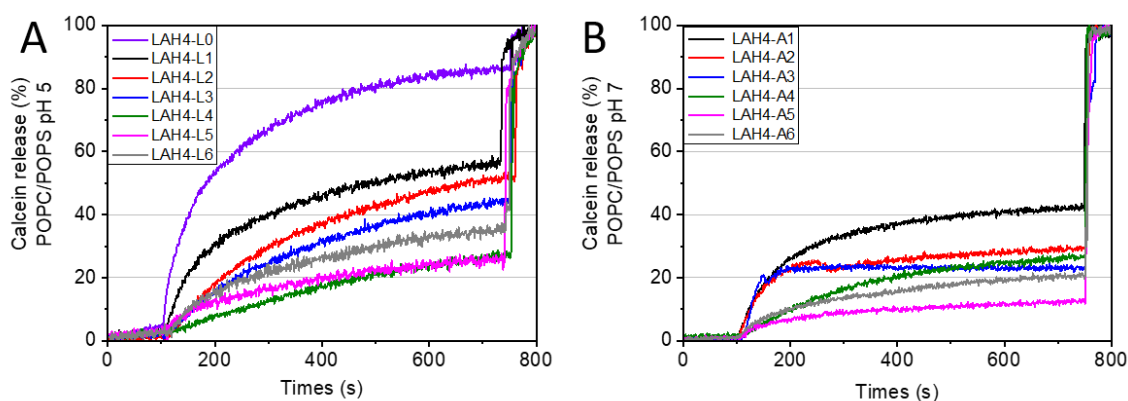

Figure 19: The percentage of calcein release over time from LUVs made of POPC/POPS 3/1 mol/mol in presence of (A) peptides from the LAH4-Ln series at pH 5 or (B) peptides from the LAH4-An series at pH 7. The peptide was injected after 100 seconds of equilibration and the Triton X-100 around 750 seconds The peptide-to-lipid ratio was kept at 1/50 and the temperature was stabilized at T= 25 °C. The percentage of calcein release at t= 250 s after addition of peptide are summarized in Figure 20.

The calcein release obtained at t= 350 seconds (i.e., 250 s after the addition of peptide) from the analysis of **Figure SI 7** are given in **Figure 20** with error bars.
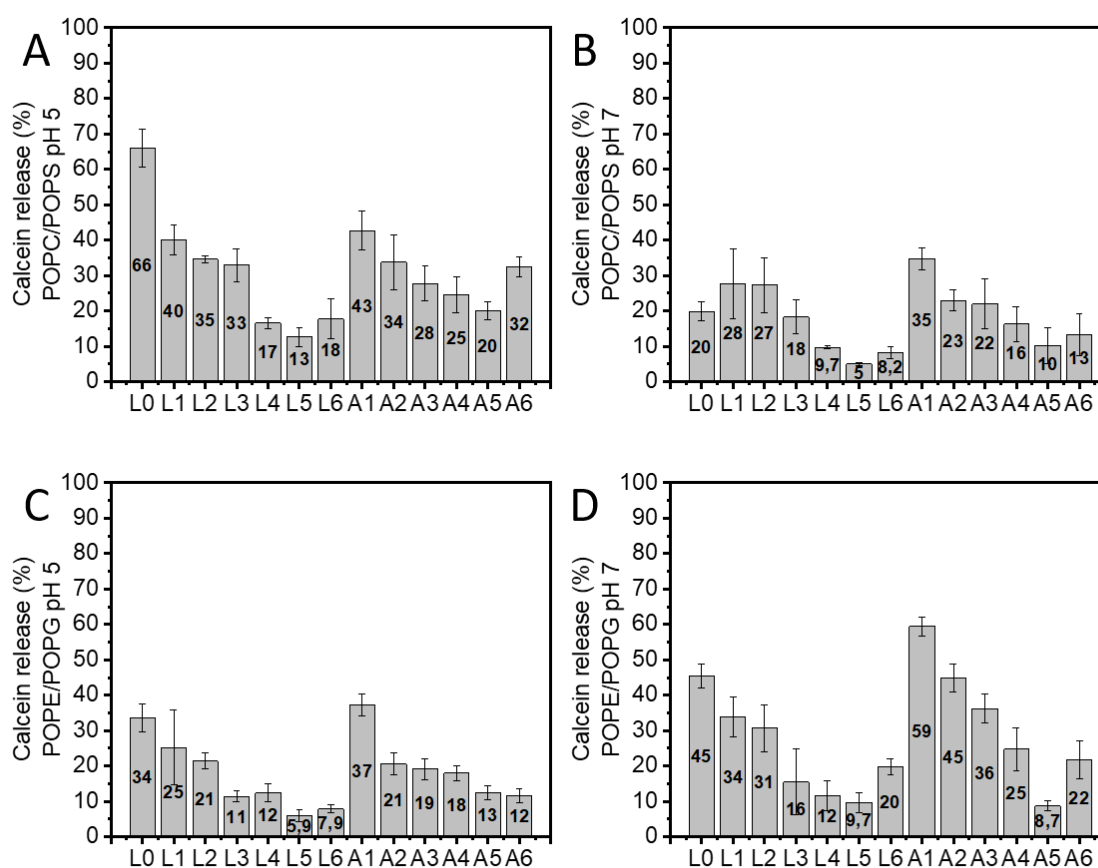

Figure 20: The percentage of calcein release 250 seconds after peptide addition and measured from POPC/POPS 3/1 mole/mole (A, B) or POPE/POPG 3/1 LUVs (C, D) in the presence of peptides from the LAH4-Ln or LAH4-An series at pH 5 (A, C) or pH 7.4 (B, D). Typical traces over time are shown in Figure SI 7.

The fraction of released calcein depends on the lipid composition of the vesicles and the pH. While for POPC/POPS at pH 5 calcein release varies between 10% and 70% (**Figure 20 A**), at pH 7.4 the variation ranges between only 10% and 40% (**Figure 20 B**) indicating that the LAH4 isomers are more efficient at pH 5 in releasing calcein from POPC/POPS vesicles. In contrast, for POPE/POPG liposomes at pH 5 the calcein release percentage varies between 10% and 40% (**Figure 20 C**) and is more efficient at pH 7.4 where 10-70% of the fluorophore escape from the vesicles (**Figure 20 D**).

Notably, the calcein release percentage depends in a systematic manner on the number of residues framed by the two histidines. When the number of residues between the histidines and therefore the hydrophilic angle increases, a decrease in calcein release activity is observed. For example, 250 seconds after the peptide addition, 66% of calcein has escaped from POPC/POPS LUVs at pH 5 in presence of LAH4-L0, but only 40% for LAH4-L1, 35% for LAH4-L2, and it continues to decrease while "hydrophilic angle" increases (**Figure 21**). Similar dependences of the calcein release activity and the hydrophilic angle are observed for the two series of LAH4 peptides of both pH and lipid compositions investigated here (**Figure 21**).
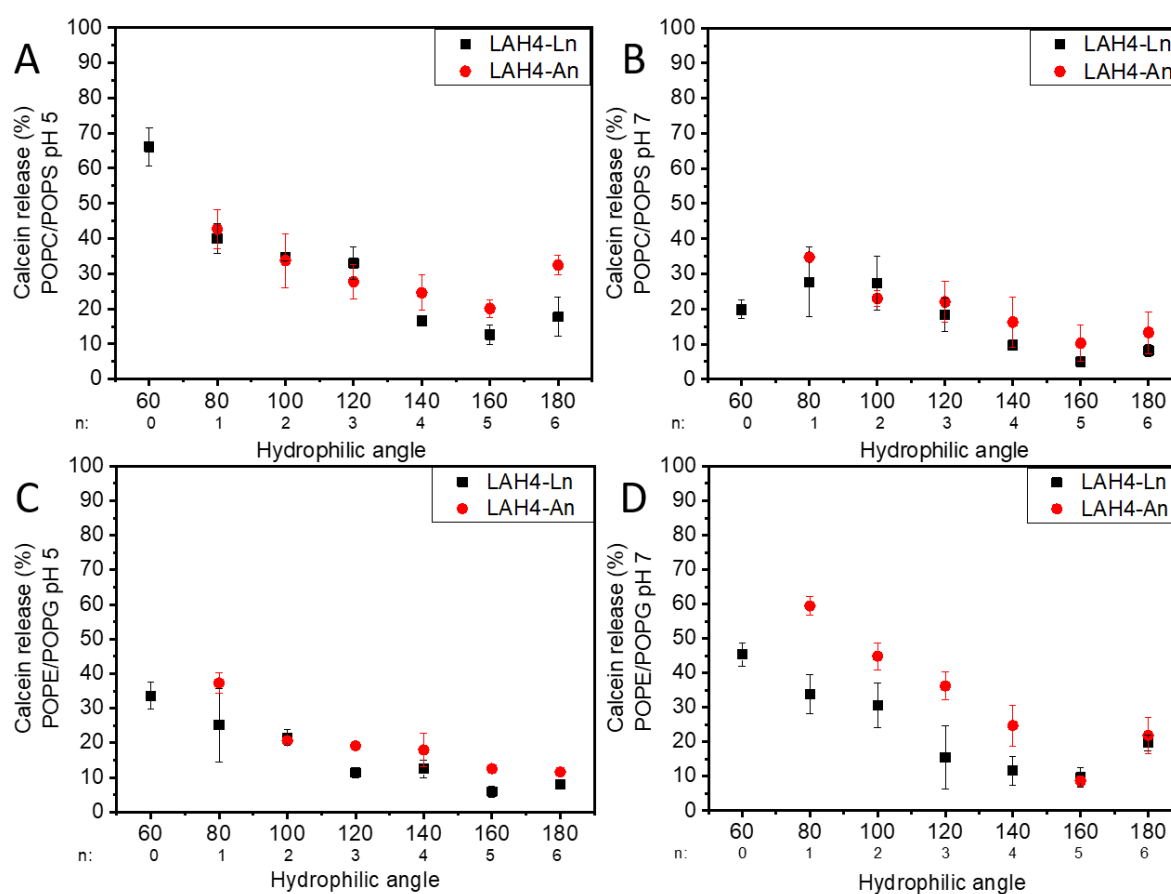
Figure 21: The percentage of calcein release from LUVs composed of POPC/POPS 3/1 at pH 5 (A) and pH 7.4 (B) or from POPE/POPG 3/1 at pH 5 (C) and pH 7.4 (D) driven by LAH4 isomers as a function of the hydrophilic angle. Percentage of calcein release 250 seconds after peptide addition (v.s. Figure 20). The LAH4-Ln series represented as black squares and the LAH4-An series as red dots with the error bars.

The calcein release activity decreases in a continuous manner when the peptides hydrophilic angle increases from 60° to 160°, whatever is the pH value, the vesicles composition, or the amino acid in the hydrophilic angle. This behaviour is interrupted for a hydrophilic angle of 180°, indeed only LAH4-A6 and LAH4-L6 present a higher activity than the previous isomers. This result shows that there is a remarkable correlation between the hydrophilic angle and the calcein release activity for hydrophilic angles ranging from 60° to 160° (see **Figure 21**).

In **chapter III. 3, 4** and **5**, our results show that for peptides with an angle between 160° and 180° membrane-association appears to be weak, which may be related to the low calcein release activities. However, the peptides which exhibit hydrophilic angles inferior to 150° (i.e., LAH4-A1 to LAH4-A4 and LAH4-L0 to LAH4-L4), there is no difference neither in membrane association nor in their secondary structure in solution in absence or presence of membranes whatever is their hydrophilic angle. It is likely that the peptides with small hydrophilic angles which means a wider hydrophobic angle penetrate more deeply into the membrane interface which also develops differences in curvature strain by disordering the lipid fatty acyl chains [82]. Such differences in calcein release promotion could be assign to different peptide-membrane interactions. A previous study [10] had investigated on a much smaller set of the LAH4-Ln peptides their membrane disordering on the fatty acyl chain. This study included 3 peptides, namely LAH4-L1 (80°), LAH4-L2 (100°) and LAH4-AL6 (180°) (*v.s.* **Table 4**). It revealed that LAH4-L1 and LAH4-L2 with small hydrophilic angle cause more disturbance on the lipid chains compared to LAH4-AL6 presenting an angle of 180°. One hypothesis is that the peptides with smaller hydrophilic angles insert themselves into the membrane and have the capacity to disrupt the lipid chains.

III.6 Biological activities of histidine-rich peptides

We have previously investigated the physico-chemical properties including correlation between membrane disruption and hydrophilic angles of two peptide series LAH4-An and LAH4-Ln. Now we will study different biological activities: antimicrobial, transfection and transduction of these two series according to their hydrophilic angles.

Preliminary studies were carried out in our laboratory for the antimicrobial activities and by collaborators on the LAH4-Ln and LAH4-An series transfection activities. In the first section of this part, the peptide series antimicrobial activities will be analysed, i.e., the minimum peptide concentrations to stop the microorganisms' growth (for instance, *E. coli*). In a second phase, the peptide series transfection activities will be studied. Transfection involves transferring nucleic acid via a non-viral vector inside cells. Finally, the peptide transduction activities will be shown. Transduction is used to transfer nucleic acid via a viral vector into the cells. These analyses were carried out to investigate whether the activities of the aforementioned peptides are correlated with their hydrophilic angles.

III.6.1 Antimicrobial activity

In a first step, the antimicrobial activities of both peptide series are analysed by determining the minimal inhibitory concentrations (MIC). For this experiment, each peptide was dissolved to obtain a 300 µM stock solution (three times the desired final concentration). Each peptide aliquot was used to prepare two dilution series: the first for peptide concentrations ranges from 100 µM to 1.75 µM. This wide range allowed us to get an idea about the MIC ranges for most of the LAH4 isomers. However, as the MIC of certain peptides could not be reached (still too high concentration of peptide) and therefore determined accurately within the above concentration range, a second dilution series with concentrations ranging from 30 µM to 0.52 µM was used for more accurate MIC determination. The peptide stock solutions (300 µM or 90 µM) were added to triple concentrated Mueller Hinton broth (MH3X) and successive peptide dilutions by a factor of 1.5 were carried out. Then, bacterial suspension (1-2*10^5 CFU/ml) was added. Each condition was carried out in triplicate. In all cases, after 12 hours of incubation, the $OD_{600\ nm}$ was measured and the bacterial growth percentage was calculated in relation to positive control (control without peptide, 100%) and negative control (control without bacteria, 0%). **Figure 22 A, B** shows the plots of the bacterial growth percentages in function of peptide concentrations. For each peptide, when the bacterial growth percentage reaches a minimum (usually around 0-20%), the corresponding concentration of that peptide is by definition the minimum inhibitory concentration (MIC) [83]. The bacterial growth inhibition performances of some purchased peptides (LAH4-L1 and LAH4-A4) are compared with their equivalents synthesized in our laboratory (LAH4-L1_ML and LAH4-A4_ML), which are comparable with one another. To be precise, MIC is similar for LAH4-L1 and remains within the dilution factor margin of error for LAH4-A4 (**Figure SI 8**). (**Figure 22**) the overlap of these two experiments was carried out, making it possible to obtain the bacterial growth percentage of each peptide for concentrations ranging from 100 µM to 0.52 µM. In order to make parallel comparisons, data of the same peptide series were plotted together. To get better view of each activities, experimental data were fitted with logistics sigmoid function using OriginPro software. Logistics equation is

$$y_{min} + (y_{max} - y_{min}) \Big/ (1 + (x/x_{min})^p$$

with p= slope, y=bacterial growth (%) and x= peptide concentration (µM).
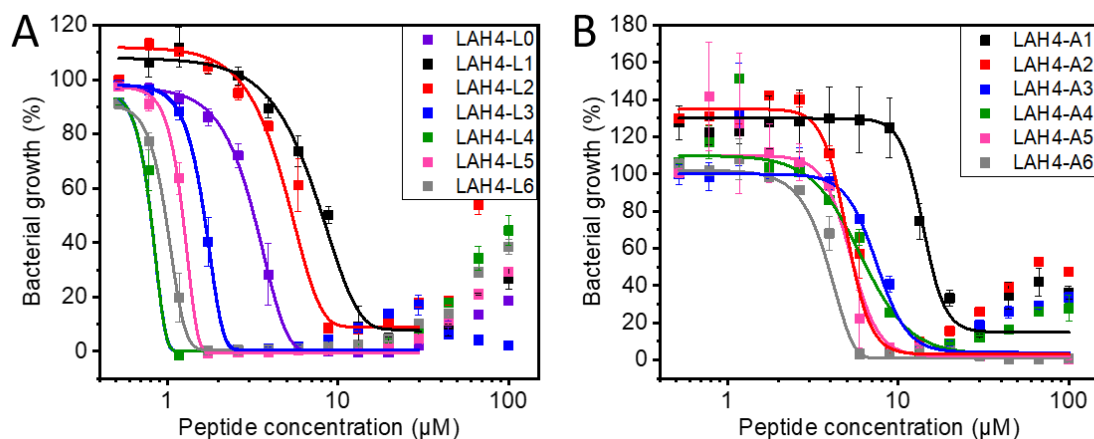
Figure 22: The bacterial growth percentage as a function of peptide concentration for the LAH4-Ln (A) and the LAH4-An series (B) at pH 5. The two experimental data sets (each data point derived from triplicates under the same experiment conditions) covering the concentration range 100 µM-0.52 µM was presented as an average of the bacterial growth percentage compared to the positive control (bacteria without peptide 100%). The tendency curves were fitted with logistics function ($y_{min}+(y_{max}-y_{min})/(1+(x/x_{min})^p)$) using OriginPro software.

As shown in **Figure 22** for some peptides at very low concentrations of the bacterial growth percentages can be greater than 100%. This means that bacteria are better growing in the presence of low concentration of peptides than without peptide at all. In addition, bacterial growth increases again at high peptide concentrations (usually above 20 µM). This increase in bacterial growth may be due to high peptide concentrations. Peptides tends to precipitate when added to the concentrated rich media (MH3X). So, there are less peptide who can interact with bacteria, allowing bacterial growth back to a higher level.

The plots in **Figure 22 A** show us a wide distribution of the LAH4-Ln series tendency curve of bacterial growth. In comparison, most of the bacterial growth curves from the LAH4-An series are grouped (**Figure 22 B**). This analysis allows us to determine the peptide minimum concentration (MIC) that inhibits most of bacterial growth.

The MIC of each peptide was analysed as a function of the hydrophilic angles (**Figure 23**).
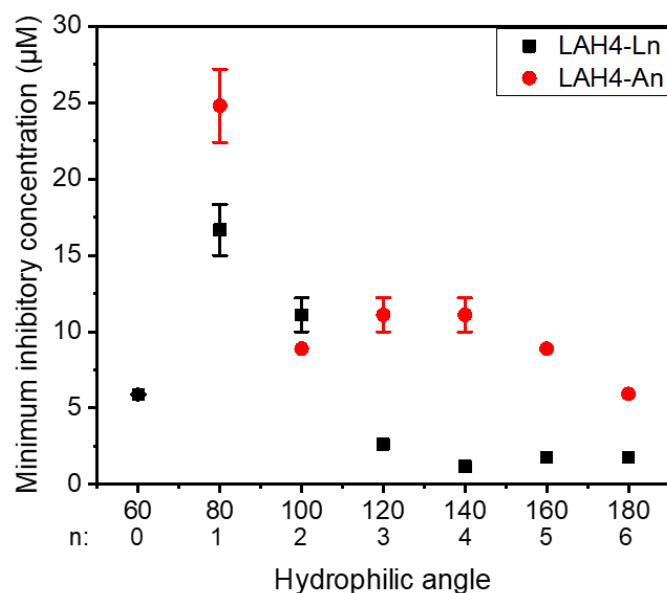
Figure 23: Minimum inhibitory concentration compared to the hydrophilic angle for the LAH4-An (red dots) and the LAH4-Ln series (black squares). For each peptide, the MIC is the concentration when the bacterial growth percentage reaches minima (usually around 0-10%) Figure SI 9.

We can see that for both series, the highest MICs was observed for peptides with a hydrophilic angle of 80° (25 µM for LAH4-A1 and 17 µM for LAH4-L1), suggesting lower antimicrobial activities for the 80° hydrophilic angle. Above 80°, there is clearly higher antimicrobial activities. Indeed, in the LAH4-An series, for hydrophilic angles from 100° to 180°, there is little variation in the MIC (ranging from 5 to 15 µM). While in the LAH4-Ln series, there is a continuous decrease in MIC as the hydrophilic angle increase from 80° to 120°. For angles greater than 120° (LAH4-L4, LAH4-L5 and LAH4-L6) the MIC seems to reach a limit and remains below 2 µM. The exception of this trend is LAH4-L0, whose MIC is as low as 6 µM despite a hydrophilic 60° angle. The peptides with larger hydrophilic angles have better antimicrobial activities. In particular, the best antimicrobial activities observed are the ones from the LAH4-Ln series with angles between 140° and 180° where the MICs are as low as 2 µM. On the other hand, for the LAH4-An series the differences are much less pronounced with somewhat higher antimicrobial activity for LAH4-A6 with a hydrophilic 180° angle. Only for the LAH4-Ln series, there is a correlation between the minimal inhibitory concentration and the hydrophilic angle ranging from 60° to 140°. In addition, the LAH4-Ln series seems more active than the LAH4-An series, especially for hydrophilic angles greater than 120°.

III.6.2 Transfection activity

After having tested the antimicrobial activities, we became interested in the transfection activity of the same series of LAH4 peptides. In this study, our collaborator Antoine Kichler analysed the transfection efficiency for the LAH4-Ln and LAH4-An series.

The transfection allows the transfer of nucleic acids complexed with non-viral vectors into cells (*v.s.* **Figure 3**). In our case, cargo nucleic acid consists in a plasmid containing the gene encoding luciferase that will allow to follow the transfection efficiency by luminescence while the non-viral vector is a member of LAH4 peptide family and the transfected cells are human glioblastoma U87. The peptide/DNA complex realizes cell entry by endocytosis: at first the complex is internalized into endosomes; thereafter the endosome acidification leads to the complex dissociation. The freed LAH4 peptide subsequently disrupts the endosomal membrane and thus allows the release of the cargo plasmid into the cytoplasm from where this later is addressed to the nucleus. Finally, the luciferase gene embedded in the plasmid is expressed into luciferase. The efficiency of the whole transfection process can therefore be measured by the resulting luciferase activity. More specifically, transfection efficacies of 1.5 µg plasmid DNA encoding luciferase complexed to different peptide quantities (µg) were evaluated in human glioblastoma U87 cells.

For transfection tests, we wanted to keep the same buffer conditions than those used in calcein release experiment, so the first step was to test the suitability of the 50 mM phosphate and acetate buffers with 50 mM NaCl used for the transfection experiment by comparing it with the commonly used 150 mM NaCl solution. For this, specific peptides are selected: LAH4 already known to be good transfection activators (**Figure SI 10**) [24] [84] and LAH4-A4 to see if there are differences. The results showed us that the DNA transfection is comparable in the acetate buffer with NaCl or NaCl at pH 5, whereas in the phosphate buffer with NaCl no reproducible transfection activity is observed. Therefore, for the following experiments, we decided to use only acetate.

For all peptides of the LAH4-An and LAH4-Ln series, peptide/DNA complexes were formed by varying the peptide/DNA ratio for a fixed DNA quantity (1.5 µg) in 50 mM acetate buffer with 50 mM NaCl at pH 5. Once created, the complex was added into the cell culture medium of human glioblastoma cell line U87. Luciferase activities for each condition was measured 1 day

after transfection. All experiments were repeated twice for different peptide quantities (7.5 µg to 36 µg) (**Figure 24**).
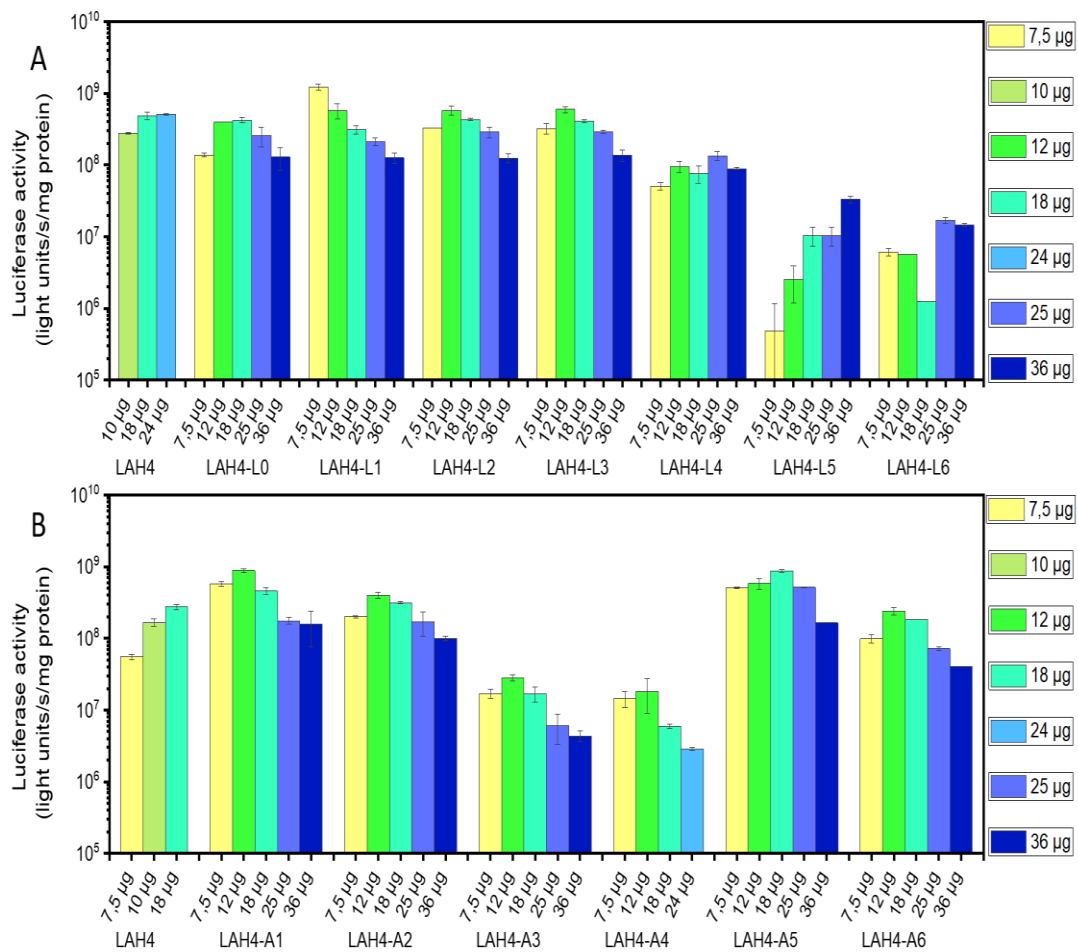

Figure 24: Transfection efficiency of the LAH4-Ln (A) and LAH4-An (B) peptides evaluated on human glioblastoma U87 cells as a function of different peptide quantities (µg) used to complex with 1.5 µg DNA in 50 mM acetate buffer + 50 mM NaCl at pH 5. Luciferase activity was measured 1-day post-transfection. The transfection efficiency is expressed as light units/s/mg protein and the reported values are the mean of duplicates. Error bars represent the standard deviation of the mean.

Figure 24 A show for the LAH4-Ln (LAH4-L0 to LAH4-L4) the same range of luciferase activity that decreases for LAH4-L5 and LAH4-L6. However, considering the LAH4-An, luciferase activity decreases for LAH4-A1 to LAH4-A4 and are a bit higher for LAH4-A5 and LAH4-A6 (**Figure 24 B**). The luciferase activity is analysed depending on the peptide quantity needed to get the best transfection efficiency. For the LAH4-An series, the best luciferase activity is

observed with 12 µg peptides except for LAH4-A5 which has better luciferase activity at 15 µg (**Figure 24 B**). However, the LAH4-Ln series is very different. Indeed, LAH4-L1 has the best luciferase activity with only 7.5 µg peptide. The other members of this series need higher peptide quantity to have their best luciferase activity. Here is the ranking, from the lowest peptide quantity to the highest -L1<-L2-L3<-L0<-L4-L6<-L5 (**Figure 24 A**). In this study we wanted to see if there is a correlation between transfection activities and the peptides hydrophilic angles. For this, we took the highest luciferase intensity for each peptide. For example, for LAH4-L1 the best luciferase activity is obtained with a 7.5 µg peptide quantity while for LAH4-L2 it is 12 µg.

In **Figure 25** we show the best observed luciferase activity on a logarithmic scale for each peptide versus their hydrophilic angle.
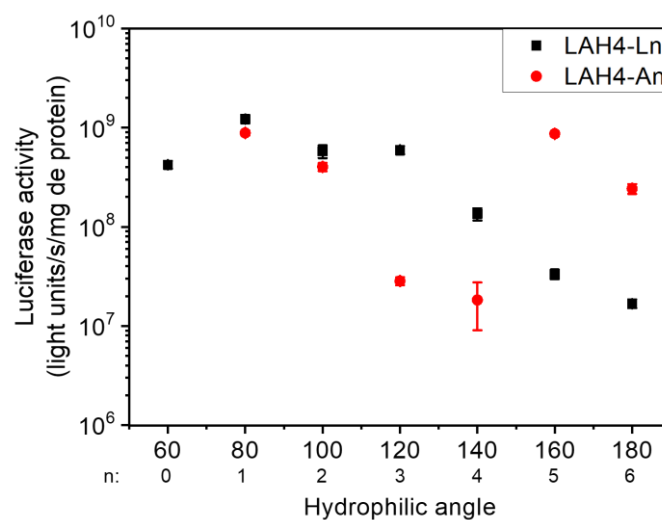

Figure 25: The LAH4-An and LAH4-Ln peptides transfection efficiency evaluated on human glioblastoma U87 cells as a function of hydrophilic angle. The transfection efficiency is expressed as light units/s/mg protein and the reported values are the mean of duplicates (and are shown on a logarithmic scale). Error bars represent the standard deviation of mean. In figure only the conditions giving the highest luciferase expression are reported. The LAH4-An series (red dots) LAH4-Ln series (black squares).

The highest activity is observed for LAH4-L1 and LAH4-A1, i.e., the peptides with 80° hydrophilic angles. However, there is a difference in behaviours between the LAH4-An and LAH4-Ln series. For the LAH4-Ln series, the activity decreases when the hydrophilic angle increases particularly for peptides with hydrophilic angles from 120° up to 180°. At 100° and 120°, they show similar transfection efficacies. There is a difference of 2 orders of magnitude between the 80° and 180° angles (**Figure 25**). A similar trend is also observed from LAH4-A1 to LAH4-A4 for peptides in the LAH4-An series with hydrophilic angles ranging from 80° up to 140°. There is a difference of 1 magnitude orders between 100° and 120° peptides (**Figure 25**). In addition, high activity levels are observed for LAH4-A5 and LAH4-A6 with 160° and 180° angles respectively (**Figure 25**).

The peptides LAH4-L1 and LAH4-A1 (80°) have better transfection activities and these activities decrease depending on hydrophilic angle. The transfection study allows us to say that there is also a correlation between the transfection activity and the hydrophilic angle for the LAH4-Ln and LAH4-An series except for the 160° and 180° angles. There is a relationship between the peptide ability to disrupt the membrane and transfection activity. Indeed, an important step of transfection mechanism is the endosomal membranes permeabilization to release the nucleic acid into the cytoplasm. In this case, the best peptides for membrane permeabilization are the peptides with small hydrophilic angles to better disturb acyl chains.

III.6.3 Transduction efficiency

Finally, after the antimicrobial and transfection activities we compared the transduction activities. In this study, the two series LAH4-An and LAH4-Ln transduction efficiency were studied by our collaborator Anne Galy [33].

Transduction consists to transfer nucleic acid material into cells via lentiviral vector (LV) particles (*v.s.* **Figure 4**). In our case, lentiviral vector particles are obtained from four plasmids: two for the particle expression component: one envelope glycoprotein and one encoding the green fluorescence protein (GFP). LV will adhere and fuse with the target cell membrane. So, the viral entry efficiency is dependent on the envelope glycoprotein that could be here vesicular stomatitis virus G (VSV-G) or modified gibbon ape leukemia virus glycoprotein (GALVTR) which interacts with the cell target receptor. In this study, CD34+ (hematopoietic stem/progenitor) cells transduction was tested by adding LV particles (VSV-G-LVs or GALVTR-LVs) mixed with or without LAH4 peptide derivatives (**Figure 26**).

Transduction efficiency was evaluated by measuring the GFP expression by flow cytometry after 4-6 days. The ability of VSV-G-pseudotypes retroviral vectors to transfer genes into hematopoietic progenitor cells (hCD34+) is proven [33]. Indeed, the transduction efficiency for VSV-G-LVs in the absence of any transduction enhancers are 12% compared to GALVTR-LV who are inefficient for this type of cells with transduction percentage around 1. These results can be explained by the difference between the two pseudotypes. Indeed, VSV-G-LV is a vector for which the action mechanism is pH dependent while that of GALTR-LV is not.
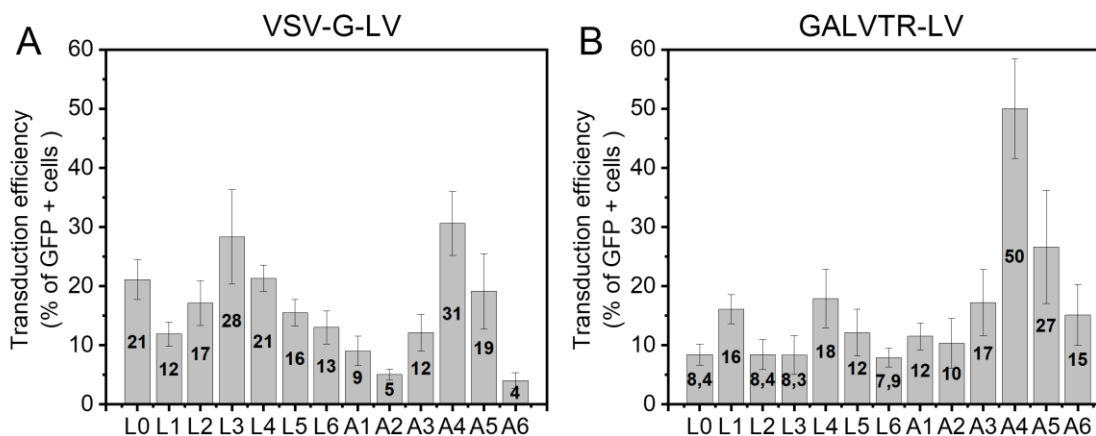
Figure 26: The LAH4 peptides percentage of transduction efficiency. Preactivated hCD34+ cells were transduced with VSV-G-LV (A) or GALVTR-LV (B) in the presence of the LAH4-Ln and LAH4-An series. The percentage of transduction efficiency in absence of peptide is 12% for the VSV-G-LV and 1% for the GALVTR. The plot from the data of [33].

In **Figure 26** adapted from publication [33], only two peptides of the LAH4-Ln and LAH4-An series significantly improve the transduction when complexed to VSV-G-LV: LAH4-A4 and LAH4-L4, peptides with 140° hydrophilic angle (**Figure 26 A**). Surprisingly, LAH4-A2 and LAH4-A6 inhibit the VSV-G-LV transduction compared with the baseline in the absence of peptide. The other peptides had non-significant transduction activity or low for LAH4-L0 and LAH4-L3 with the probability value (p ≤0.05) [33]. **Figure 26 B** for GALVTR-LVs the result is completely different, transduction with LV alone is ineffective with 1% GFP in hCD34+. However, in the presence of any the LAH4-Ln or LAH4-An series member there is a large increase by the GFP percentage. Just like VSV-G-LVs, the best transduction efficiency for GALVTR-LVs is obtained for peptide with a hydrophilic angle 140° (LAH4-A4 and LAH4-L4).

We have included the results of this previous study **Figure 26** in order to show how transduction correlates with a hydrophilic angle. For better visualisation, the GFP expression percentages by the cells are compared to the different hydrophilic angles of the peptides (**Figure 27**).
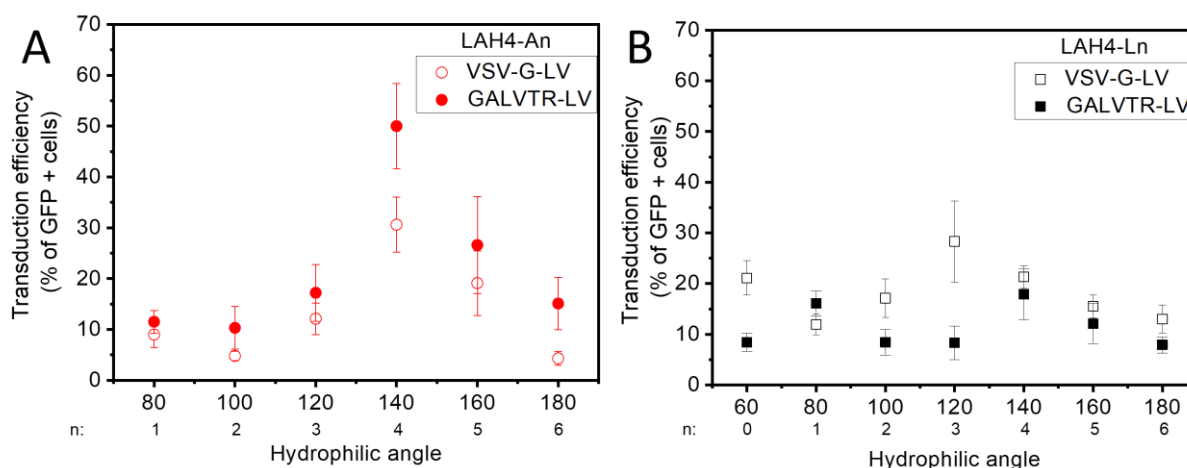
Figure 27: The lentiviral transduction enhancement as reported in [33] is shown as a function of hydrophilic angle. hCD34+ cells are transduced with the VSV-G-LV or GALVTR-LV in presence of peptides from the LAH4-An (A) or LAH4-Ln series (B). Plot from the data of [33] and Figure 26.

The LAH4-An series (**Figure 27 A**), shows us an increase in the transduction efficiency depending on the hydrophilic angle of the peptide. The same profile is observed for both LVs (GALVTR and VSV-G). Indeed, angles ranging from 80° to 140° (LAH4-A1 to LAH4-A4) correlates with an increase in the transduction efficiency and then from 140° to 180° (LAH4-A5; LAH4-A6) it decreases.

However, for the LAH4-Ln series (**Figure 27**) the profile is different according to the type of viral particles contrary to what was observed previously for the LAH4-An series. Moreover, the LAH4-Ln series have the transduction percentage around 15% for both LVs (GALVTR or VSV-G). So, for the LAH4-Ln series no apparent correlation with hydrophilic angle seems to exist.

We can see a difference in the transduction activity depending on the series. It can be noted that the hydrophobic core composition changes these activities. For the LAH4-Ln series transduction activity is almost unaffected by the detailed nature of the peptides while this is not the case for the LAH4-An series. The lentiviral transduction activities are highest for the LAH4-A4 peptide which has a 140° hydrophilic angle for both lentiviral pseudotypes GALVTR and VSV-G-LV compared to no peptide complexation and other vector-peptide complexes.

III.6.4 Peptide activities regarding hydrophilic angles

In this part, the different antimicrobial, transfection, or transduction with the two LVs (VSV-G-LV or GALVTR-LV) activities observed for the LAH4-An and LAH4-Ln peptide series have been discussed. **Table 12** presents the best (+) or the worst (-) activities with respect to the hydrophilic angle for the LAH4-Ln or LAH4-An series.

	Antimicrobial		Transfection		Transduction VSV-G-LV		Transduction GALVTR-LV	
	+	**-**	**+**	**-**	**+**	**-**	**+**	**-**
LAH4-An	180°	80°	80°	140°	140°	100°/180°	140°	100°
LAH4-Ln	140°	80°	80°	180°	120°/140°	80°/180°	140°	180°

Table 12: The antimicrobial, transfection, or transduction with the two LVs (VSV-G-LV or GALVTR-LV) activities as a function of the hydrophilic angle for the LAH4-Ln or LAH4-An peptides. The best and the worst in each series are indicated with (+) and (-) respectively.

We can see that the best antimicrobial activity corresponds to peptides with a hydrophilic angle of 180° for the LAH4-An series and 140° for the LAH4-Ln series. Moreover, peptides with 80° hydrophilic angle have the least antimicrobial activities. In addition, some natural antimicrobial peptides such as cecropin and magainin 2 also have hydrophilic angles of 180° [85] [86].

Antimicrobial activity is favoured by peptides with wide angles, but in the transfection case, it is the other way around: peptides with an 80° hydrophilic angle show the best activity whether it is for the LAH4-An or LAH4-Ln series. The least transfection activity corresponds to peptides with a 140° hydrophilic angle for the LAH4-An series and 180° for the LAH4-Ln series.

Transduction activity is mainly favoured by the peptide presenting 140° hydrophilic angle, but low or absent with hydrophilic angles 100° or 180° for the both lentivirus vectors (VSV-G-LV or GALVTR-LV).

The activity values reported in **Table 13** correspond are those observed for the angles previously shown in **Table 12.**

	Antimicrobial (µM)		Transfection RLU/s/mg protein		Transduction VSV-G-LV (% of GFP + cells)		Transduction GALVTR-LV (% of GFP + cells)	
	+	**-**	**+**	**-**	**+**	**-**	**+**	**-**
LAH4-An	5.93 x	24.8 ±2.4	8.8×10^8 ±5.1×10⁷	1.8×10^7 ±9.2×10⁶	31 ±5.4	4.8/4 ±0.95/±1.4	50 ±8.4	10 ±4.2
LAH4-Ln	1.17 x	16.66 ±1.7	1.2×10^9 ±1.2×10⁸	1.7×10^7 ±1.6×10⁶	28/21 ±8/±2.25	12/13 ±2.05/±2.8	18 ±4.95	7.9 ±1.6

Table 13: The different activity values: antimicrobial, transfection or transduction with the two LVs (VSV-G-LV or GALVTR-LV) as a function of the hydrophilic angle represented in Table 12 for the LAH4-Ln or LAH4-An series. The best and the worst in each series are indicated with (+) and (-) respectively with their error bars (x: no error bars corresponding).

Better antimicrobial activities are observed for peptides of the LAH4-Ln series. Indeed, the minimum inhibitory concentration is as low as 1.17 µM for the best peptide in the LAH4-Ln series and 16.66 µM for the worst among this series whereas for the LAH4-An series, the lowest MIC is 5.93 µM and the highest 24.8 µM. Comparing the best of each series, LAH4-Ln is 5 times better than LAH4-An.

The luciferase activity for the best peptide in the LAH4-Ln series is 1.4 higher than for the LAH4-An series. In addition, the LAH4-Ln series peptides have better transfection abilities at large hydrophilic angles (140°). Like antimicrobial, the transduction activities are favoured by the 140° hydrophilic angle (LAH4-L4 and LAH4-A4, respectively).

The transduction activities are favoured by 140° hydrophilic angles for both lentivirus vectors (VSV-G-LV or GALVTR-LV) (**Table 12**). However, quite important differences (factor about 2.7) are observed in GFP percentage (18% LAH4-L4 and 50% for LAH4-A4), and this for the same lentiviral particles type (GALVTR-LV) (**Table 13**). This difference in transduction activities can be assigned to the type of amino acid exposed in between the histidines, thus not only the hydrophilic angle but also the type of amino acid is to consider. Nevertheless, this is not the case when looking at the VSV-G-LV where LAH4-A4 and LAH4-L4 present similar transduction efficiency (31% and 21% respectively).

These tests showed that transfection was favoured by small angles in the LAH4-Ln series (80°) and antimicrobial activity was favoured by large angles in the LAH4-Ln series, while antimicrobial activity was favoured by large angles in the LAH4-L4 series (140°), and the transduction is again favoured by LAH4-A4 (140°).

III.7 Conclusion

Peptides from the LAH4 family have been shown to exhibit different activities depending on their sequences. To better understand the action mechanisms and optimize activities of these peptides, different aspects are discussed. One of the parameters studied was the hydrophilic angle that already showed different membrane permeabilization activities.

In this chapter, we have studied two series of peptides of the same global amino acid composition. Changing the location of the histidines in the primary sequence allowed to define the hydrophilic angle from 60° to 180° established from Schiffer-Edmundson helical wheel representations.

The first step of this study was to analyse the physico-chemical properties of these peptides: the secondary structure as a function of pH and the interaction with POPC/POPS model membranes. For hydrophilic angles between 60° to 140°, the two series show that secondary structures are modified as a function of the pH. However, wide hydrophilic angles (160° and 180°), while the LAH4-Ln series changes its structure according to pH, the LAH4-An series already presents a high degree of α-helical structure at pH 5. Because LAH4-An (160° and 180°) have a high degree of α-helicoidal structure at pH 5, these peptides interaction with POPC/POPS cannot be monitored by CD. However, the LAH4-Ln series members (160° and 180°) do not show any interaction with the POPC/POPS membrane even if structure changes depending on the pH. For hydrophilic angles between 60° to 140°, the two series all showed the same behaviour when associating with POPC/POPS membranes regardless of the hydrophilic angle.

In addition, this study was able to show a decrease in the calcein release when the hydrophilic angle increased. These measurements revealed a correlation between the hydrophilic angle of the peptides. Indeed, for hydrophilic angles <150° (LAH4-A1 to LAH4-A4 and LAH4-L0 to LAH4-L4), the variations in calcein release activities are probably neither related to differences in membrane association nor their secondary structure in solution or in the membrane. It is likely that the peptides with a small hydrophilic angle penetrate deeply into the membrane which thereby also develops differences in curvature strain, in the disordering of the lipid fatty acyl chains [10] and lipid-mediated interactions between the peptides [87][88][89].

The biophysical and biological activities are put together in perspective in the following studies, the peptide transfection and antimicrobial activities are correlated with the calcein release activity.

Indeed, the transfection efficiency decreases as the hydrophilic angles decrease. The important step in transfection mechanism is when liberated LAH4 peptide disrupt the endosomal membrane to release its nucleic acid cargo [19]. The ability of peptides to disorder the fatty acyl chain of the membrane can be correlated to the transfection activities of various cell line [10].

The antimicrobial activity is favoured when α-helical peptides insert into the membrane interface and destabilize the membrane packing [89]. This activity was favoured by peptides with wide angles, the best was observed for the LAH4-Ln series peptides and more specifically for LAH4-A4 with 140° hydrophilic angle. These results are consistent with those from Torsten Wieprecht [90] for the M2a isomers with an hydrophilic angle between 80° to 180°. The antibacterial activities of these peptides were tested on Gram-negative bacteria (Escherichia coli and Pseudomonas aeruginosa) and Gram-positive bacteria (Staphylococcus aureus). Minimum Inhibitory concentrations against all three investigated bacterial strains was lower for large angles (140°-180°) than for small ones (80°-120°) [90].

The transfection and antimicrobial activities were favoured by peptides containing leucine in the hydrophilic face (LAH4-L1 and LAH4-L4, respectively). The leucine presence in this face favoured the membrane destabilization. Thereby, the calcein release activity observed from eukaryotic or bacterial membrane models correlates with transfection and antimicrobial activities respectively for the LAH4-Ln series (LAH4-L1 to LAH4-L4) (**Figure 28**).
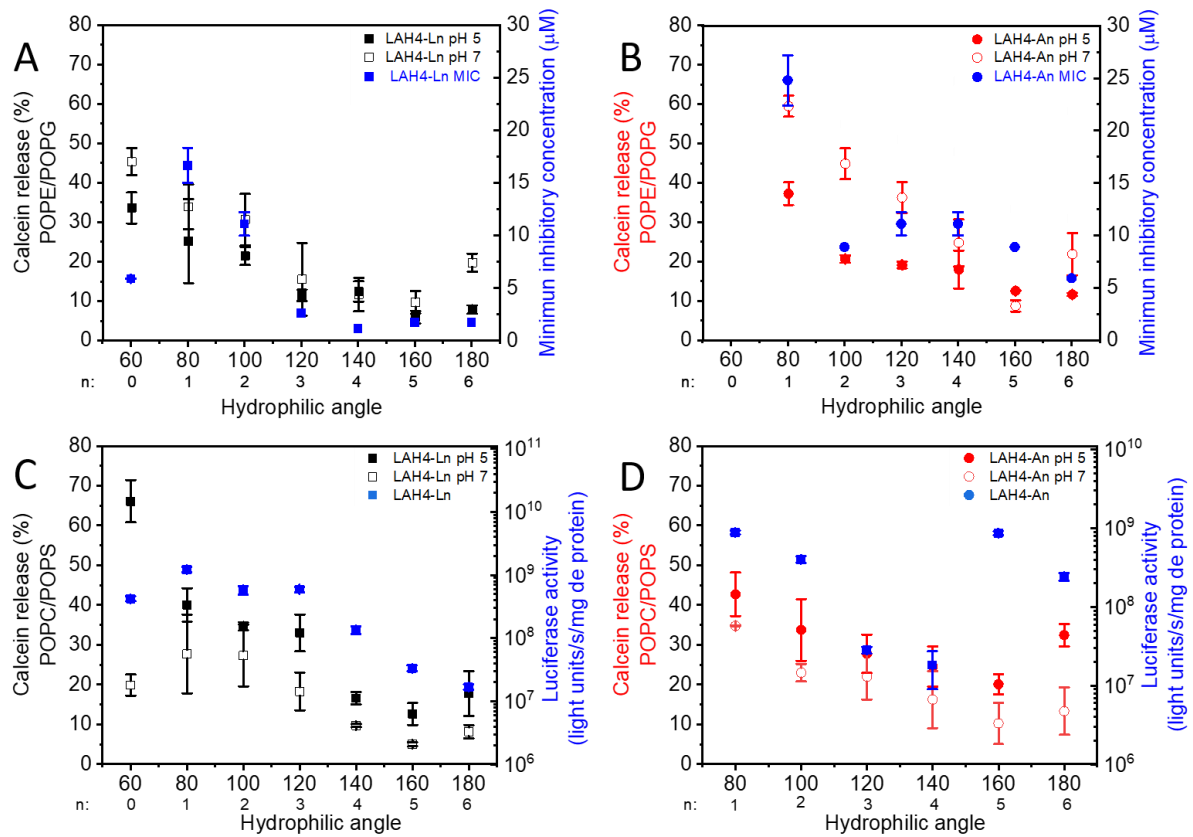
Figure 28: The percentage of calcein release and biological activities driven by LAH4 isomers as a function of the hydrophilic angle. Percentage of calcein release with LUVs composed of POPE/POPG (A, B) or POPC/POPS (C, D) for the LAH4-Ln series (black squares) and LAH4-An series (red circles) at pH 5 (filled symbol) and pH 7.4 (open symbol). LUVs composed of POPE/POPG 3/1 at pH 5 and pH 7.4 with minimum inhibitory concentration (blue) for the LAH4-Ln series (A) and LAH4-An series (B). LUVs composed of POPC/POPS 3/1 at pH 5 and pH 7.4 with luciferase efficiency (blue) for the LAH4-Ln series (C) and LAH4-An series (D).

However, this is not the case for transduction where the highest lentiviral transduction enhancement activities have been found for the LAH4-A4 peptide which exhibits a hydrophilic angle of 140°. Indeed, lentiviral transduction enhancement has been associated with fibrils formation [34], increased lentiviral attachment to cellular membranes and promotion of membrane fusion [40][91], the calcein release investigated here is not adapted to study this biological activity mechanism (**Figure 29**).
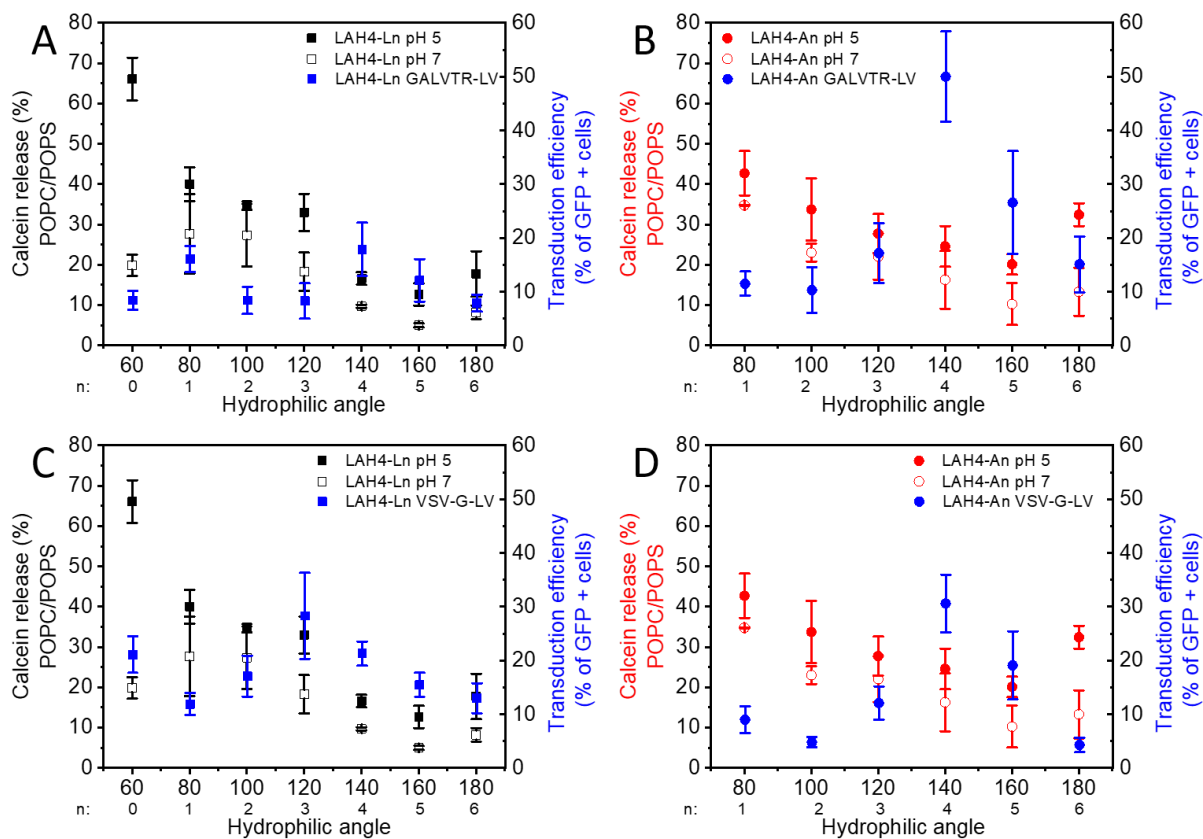
Figure 29: The percentage of calcein release and transduction activities driven by LAH4 isomers as a function of the hydrophilic angle. Percentage of calcein release with LUVs composed of POPC/POPS 3/1 for the LAH4-Ln series (black squares) and LAH4-An series (red circles) at pH 5 (filled symbol) and pH 7.4 (open symbol). Transduction efficiency with lentivirus vectors GALVTR-LV (blue) for the LAH4-Ln series (A) and LAH4-An series (B). Transduction efficiency with lentivirus vectors VSV-G-LV (blue) for the LAH4-Ln series (C) and LAH4-An series (D).

The membrane interactions of the two series LAH4-Ln and LAH4-An are important to explain these activities. The activities are different depending on whether it is the LAH4-Ln or LAH4-An series. The hydrophilic angles and leucine or alanine residues present in the hydrophilic face play a role in the peptides' activity. These observations are interpreted in terms of the difference in the depth of peptide insertion systems in lipid bilayers. LAH4-L1 (80°), LAH4-L2 (100°) and LAH4 AL6 (180°) investigations have shown that small hydrophilic angles disturb more the lipid chains [10]. However, my work was conducted on only two of these peptides. To get more information, effect on acyl chain should be studied by including more peptides from both series LAH4-Ln and LAH4-An.

In addition a study on lytic amphipathic helices showed that an increase in the hydrophilic angle lead to a reduction of hemolytic activity [92].

However, the highest transduction activity for LAH4-A4 directly is referring to its dual ability of binding to vectors and enhance the fusion of vector-cell membranes, hence the name vectofusin-1 [40]. In addition, improvement in lentiviral transduction has been associated with fibrils formation. And recently, the LAH4-A4 has been shown to be able to form fibrils which still increase its transduction activity [34].

IV. Self-assembly of histidine-rich amphipathic peptides

IV.1 Introduction

In recent years, the peptide self-assembly has attracted increased interest in various applications. In fact, the peptides as a building block are easily synthesized, can be modified and allow to follow modular strategies. These peptides, which are synthesized either by imitating natural sequences or by using de novo strategies [93], allowed the design of several nanometric morphologies such as nanotubes, spheres, vesicles and, of course, fibrils or hydrogel matrices [94] [95]. Self-assembly can be defined as the spontaneous and reversible [96] organization of molecules into supramolecular organizations by non-covalent interactions [97]. The peptide self-assembly is principally driven by non-covalent interactions (electrostatic, hydrophobic, hydrogen bonds, etc.) [98] [99]. Indeed, when the peptides are in α-helical conformations the hydrophobic residue on one side will interact with each other, allowing helix-helix intertwining of two or more helices [100]. In short, it has been shown that modifications in the primary sequence modify the fibrils structures [101]. The repartition of hydrophobic (H) and polar (P) residues in the primary sequences determines the self-assembly. For example, the helical components are amphipathic as defined by the heptad repeats HPPHPPP. In contrast, an altered HP repetition tends to adopt β-strand conformations [93]. They are thus suitable for various applications, in fields of nanotechnologies, biology and pharmaceutics [102]. In a biological system, the self-assembled peptides and proteins have been shown to be implicated in human neurodegenerative disorders [103] such as Parkinson's, Alzheimer's and other diseases [104].

To improve the nucleic acid delivery in gene therapy, one approach is to assemble peptides into fibrils which then associate with viral particles, allowing better transmembrane cargo transportation. These fibrils have been shown to facilitate the fusion between viral and cellular membranes [34]. Nanofibrils obtained from self-assembled peptides thus represent a new class

of transduction enhancers. Furthermore, such nanofibrils have shown to be effective in transduction with little cytotoxicity [45] [105].

While β-amyloid nanofibrils have already proven their efficiency in transduction assay, LAH4-A4 (Vectofusin-1, VF-1) [34], a cationic amphipathic peptide, has been described as a new viral entry enhancer of a completely different nanometric assembly [40]. Vectofusin-1 (LAH4-A4) self-assembly, significantly increases the transduction efficiency of various lentiviruses [34]. A previous study has shown an α-helical structure of the peptide [34] within this fibril but they do not correspond to this canonical coiled-coil motif HPPHPPP. So, there is still much to be learned about this nanoobject, such as the detailed structure of the self-assembly complex. Therefore, we are interested in the conditions that lead to the self-assembly of these peptide fibrils.

For the preparation of such nano-assemblies, a previous doctoral student [106] had implemented a fibrillation protocol. The first step was to study the LAH4-A4 peptide (VF-1) aggregation as a function of pH. This study showed that the peptide was not in a monomeric state at low pH (acetate buffer at pH 4.8) presenting at least two components. In addition, by dynamic light scattering (DLS) analyses showed that the particle size increases with pH until it stabilizes at pH 8 [106]. The LAH4 and LAH4-L1 peptide present a size of 2-4 nm at pH 5 or 20-40 nm at pH 7.4 [8]. The peptide aggregation is thus related to the deprotonation of histidines and thus the concomitantly higher propensity for hydrophobic interactions. A dialysis protocol was implemented to avoid peptide aggregation, thereby promoting fibrils formation [106]. This allows a gentle pH increase of the solution allowing self-assembly when the pH was close to the histidines pKa to avoid amorphous aggregation [34]. This previous study has shown the importance of pH for this peptide self-assembly.

The variation in amino acid distribution along the primary sequence can lead to different supramolecular assemblies resulting in a large shift in function. It is for that reason that we studied supramolecular assembly of three peptides of the LAH4 family (LAH4, LAH4-L1 and LAH4-A4). Whereas all three peptides share the same amino acids, the histidine positions define hydrophilic angles of 100° for LAH4, 80° for LAH4-L1 and 140° for LAH4-A4, respectively (*v.s.* **Figure 6**).

In this secondary chapter, the self-assembly fibrillation protocol of LAH4-A4 is optimized and the fibril stabilities with respect to environmental conditions are tested by quantifying the peptide in the fibrils by HPLC and qualitative observations are assessed by TEM. Indeed, with the dialysis protocol, fibrillation takes one week of incubation and the percentage of peptide in fibrils remains below 30%. **Chapter IV.3** shows that a modification of the fibrils structure takes place over time. To improve the yield, a part of my thesis consists in the development of a more efficient preparation protocol. It will be presented in the first part of this chapter how LAH4-A4 peptide can self-assemble into stable fibrils giving more reproducible and comparable results. Structural analysis of LAH4-A4 fibrils by FTIR and solid-state NMR spectroscopy were carried out and compared with the different conditions used for self-assembly. The self-assembly fibrillation for two other peptides of the LAH4 family (LAH4 and LAH4-L1) was also been performed. The optimal fibrillation conditions for these three peptides and the stability of these fibrils in different environments have been investigated by using an HPLC-based assay. It can be adjusted simply by changing the buffer composition (pH, salt, ions) or by modest changes in their sequence. In addition, the secondary structure of the peptides in the fibrils is determined by analysing the ^{13}Cα chemical shifts observed in solid-state NMR spectra and the position of the amide I bands in Fourier transform infrared spectra. Finally, the different biological activities (antimicrobial and transfection) are analysed for LAH4, LAH4-L1 and LAH4-A4 peptides: in solution, when self-assembled or of mixtures of both.

IV.2 Materials and Methods

Peptide synthesis

The size of LAH4 (KKALL ALALH HLAHL ALHLA LALKK A-NH$_2$); LAH4-L1 (KKALL AHALH LLALL ALHLA HALKK A-NH$_2$) and LAH4-A4 (KKALL HAALA HLLAL AHHLL ALLKK A-NH$_2$); is MW= 2778.5 Da. The peptides were prepared by solid-phase synthesis using a Millipore 9050 automatic peptide synthesizer and Fmoc chemistry. The peptides were purified by reverse phase HPLC (Gilson, Villiers-le-Bel, France) using a preparative C18 column (Luna, C18-100 Å-5 µm, Phenomenex, Le Pecq, France), and the fractions collected were determined by the UV absorption of the mobile phase at 214 nm. The gradient of acetonitrile/water with 0.1% TFA was used as the mobile phase: solvent A contains 10% acetonitrile in water, 0.1% TFA and solvent B was made of acetonitrile at 100%, 0.1% TFA. The acetonitrile gradient started at 35% and was going up to 70% acetonitrile. The identity and purity (>90%) of the peptide within the collected fraction were checked by MALDI-TOF mass spectrometry (MALDI-TOF Autoflex, Bruker Daltonics, Bremen, Germany). The purified peptides were dissolved three times in 4% (by volume) acid acetic at a concentration of 1 mg/ml with subsequent lyophilization to ensure the exchange of the TFA anions with acetates. The aliquots of 1 mg peptide were then prepared and stored at -20 °C.

Fibrillation

Fibrillation by dialysis

The fibrillation protocol of LAH4-A4 peptides established by Justine Wolf (e.g., University of Strasbourg, 2018 [106]), relied on dialysis over 2 days to gradually increase the pH of the solution. The peptides were dissolved in water at a concentration of 2 mg/ml in water and dialyzed against 10 mM phosphate buffer at pH 6.2. A dialysis bag of 500 to 1000 MWCO (molecular weight cut off) was used (Spectra/Por®, Bioch CE) and the buffer was exchanged four times for a dialysis lasting about 36-48h. The dialysis bag was washed with 10 mM phosphate buffer at pH 6.2.

Fibrillation test in microtubes

The peptide in microtubes was dissolved in 50% ethanol over 30 minutes at a 10 mM peptide concentration and bath sonicated to having the monomeric peptide. This peptide solution was then diluted in various buffers to a 0.5 mM final peptide concentration. The buffer used for this test includes: 10 mM phosphate buffer at pH 6.2 and pH 7.4; 50 mM phosphate buffer at pH 7.0 and ultrapure filtered water (Merck-Millipore, Molsheim, France) were tested. Fibrillation was conducted under vigorous shaking for two days in the Eppendorf Mixer 5432 at room temperature (20-30°C). The fibrils prepared microtubes were centrifuged at 16,000 g for 1 minute and the supernatant was removed. Pellets with the fibrils were washed with the same buffers. The peptide contents of fibril pellets was analysed by RP-HPLC according to the protocol later described in "quantification of the fibrils amounts by RP-HPLC".

Fibrils stability

Stability of fibrils prepared by dialysis

The LAH4-A4 peptide was fibrillated by dialysis during 1 week in different solutions. 250 µl of the dialysis suspension containing fibrils and monomers (CT) were mixed with 250 µl of different buffers: 10 mM phosphate buffer at pH: 6.2, 7.4 or 8, 10 mM trisaminomethane (Tris) at pH 7 or water. After 1 day of incubation with agitation, the solution was centrifuged at 16,000 g for 30 minutes and the supernatant was removed. The pellet was washed with the same solution and the peptide content of the fibril pellets was analysed according to the protocol described below in "Quantification of the amount of fibrils by RP-HPLC".

Stability of fibrils prepared in microtubes

The fibrils prepared in microtubes were centrifuged at 16,000 g for 30 minutes and the supernatants were removed. The pellets were resuspended to a 0.5 mM final peptide concentration in various solutions: buffers used for this test were 10 mM phosphate buffer at pH 6.2 or pH 7.4, MH1X (Mueller-Hinton) at pH 7 or pH 5 and ultrapure filtered water (Merck-Millipore, Molsheim, France). The pellets resuspended in these different solutions were exposed to vigorous shaking for one day in the Eppendorf Mixer 5432 at room temperature (20-30°C). The suspension was centrifuged at 16,000 g for 30 minutes and the supernatant was removed. The pellets were washed with the same solution was used and

73

peptide content of the fibril pellets was analysed according to the protocol described below in "Quantification of the amount of fibrils by RP-HPLC".

Fibrillation kinetics by dialysis

The fibrillation protocol by dialysis was performed on LAH4-A4 peptide. Transmission Electron Microscopy and Circular Dichroism spectrometry were used to analyse LAH4-A4 evolution during this dialysis. The pH meter was used to analyse the pH variation for all samples. The fibrillation test lasted as long as 4 days, and 1 ml samples of the peptide solution/suspension were taken at different time intervals (0h, 2h, 5h, 24h, 48h and 92h) throughout the fibril preparation to monitor the modification of the LAH4-A4 structure.

Circular dichroism

The dialysis solution (fibrils/peptide) or supernatant of the fibrils in microtubes were diluted to get a peptide concentration of approximately 0.1 mg/ml (36 µM) in the respective buffer and a second dilution was done if necessary.

These concentrations were chosen to ensure a good signal-to-noise ratio when working with a cuvette of 1 mm optical path, while the absorption from the buffer being negligible. The measurements were performed at the "Service d'Analyses et de Mesures physiques" from our institute as previously described. Measurements were performed close to room temperature (T= 25 °C) and standard values for the acquisition parameters were used (1 nm in resolution, 50 nm/min of scanning speed and 1 second for the detector integration time). The data were recorded from λ= 260 nm down to 190 nm and 5-10 acquisitions were accumulated for each spectrum.

Quantification of the amount of fibrils by RP-HPLC

Quantification of the amount of peptides in the fibrils was performed by RP-HPLC. The fibrils prepared in microtubes were centrifuged at 16,000 g for 1 minute and the supernatant was removed. The fibril pellets were washed with the fibrillation buffer to remove any trace of peptides in solution. Then fibril pellets were disassembled by addition of 2 mM HCl, the pH was controlled and centrifugation was performed to control complete pellet dissociation. Then analysis was performed by reverse-phase analytical HPLC (Hitachi Primaide,

Schaumburg, IL, United States) using an analytical C18 column (Luna, C18-100 Å-5 μm, Phenomenex, Le Pecq, France) and a flow rate at 1 ml/min. A gradient of acetonitrile/water with 0.1% TFA was used as the mobile phase with solvent A: 100% water, 0.1% trifluoroacetic acid (TFA) and solvent B: 100% ACN, 0.1% TFA. The gradient used for the three peptides was 45% of solvent B for 3 minutes, an increase to 75% of solvent B within 15 minutes and finally to 95% of solvent B for three minutes before the column was equilibrated at 45% of solvent B for 3 minutes. The concentration of peptides was determined based on standard curves prepared from known LAH4 peptide concentrations. For each concentration, the integration of the LAH4 peak at 214 nm (peptide bond) was determined to get the standard curve equation. For each quantification at least two injections for the same sample are done.

Optimized protocol for LAH4-A4, LAH4-L1 and LAH4 fibrillation in microtubes

The lyophilized peptide in microtubes was dissolved in 50% ethanol over 30 minutes at a 10 mM peptide concentration and bath sonicated to get it well solubilized. These three peptide solutions were then diluted to a 0.5 mM final peptide concentration in 10 mM phosphate buffer at pH 7.4 for LAH4-A4 and LAH4-A1 and at pH 6.2 for LAH4. Fibrillation was conducted under vigorous shaking for two days in the Eppendorf Mixer 5432 at room temperature (20-30°C). The fibrils prepared in microtubes were centrifuged at 16,000 g for 1 minute and the supernatants were removed. Pellets with the fibrils were washed with the buffer used for fibrillation to remove any trace of peptide in solution. The solutions were centrifuged at 16,000 g for 30 minutes, the pellets were analysed by RP-HPLC to determine the amount of peptide in the fibrils to be used in antimicrobial or transfection experiments.

Transmission Electron Microscopy

Sample material was deposited on formvar grids (CFT200-Cu, Electron Microscopy Sciences, Hatfield, PA, United States). After 2 minutes the grids were blotted dry and left to dry on air for 30 minutes. The grids were washed in ultrapure filtered water and the grids were again blotted dry and left to dry on air for 30 minutes. TEM images were collected using a Hitachi H7500 electron microscope, operated at 80 KeV.

FTIR experiments

The fibrils were centrifuged at 16,000 g for 30 minutes at room temperature, the fibrils pellets were washed with fibrillation buffer (10 mM phosphate buffer) and centrifuged again to remove residual monomeric peptides. The pellets were resuspended in 10 µl of 10 mM phosphate buffer of which 2 µl was loaded and dried on the diamond crystal. FTIR spectra (12 scans, from which the background was subtracted) were recorded from 1500 to 2500 cm^{-1} with a Nicolet 6700 spectrometer (Thermo Scientific, Waltham, MA).

MAS solid-state NMR

MAS solid-state NMR experiments were performed at 301 °K on two different Bruker^{TM} spectrometers: an AVANCE 500 MHz wide bore spectrometer operating at a frequency of 500.03 MHz for ^{1}H (125.7 MHz for ^{13}C) or an AVANCE 300 MHz spectrometer (300.33 MHz for ^{1}H and 75.52 MHz for ^{13}C). Samples were spun either at 25 kHz in a triple resonance MAS probe designed for 2.5 mm o.d. zirconia rotors closed with vespel caps (first spectrometer) or 12 kHz in a double resonance 4 mm MAS probe (4 mm o.d. zirconia spinners, closed with Kel-F caps). All solid-state 1D ^{13}C spectra were acquired following the Adiabatic Passage through the Hartmann and Hahn Cross Polarization (APHH-CP) pulse scheme [107] using a tangential radiofrequency field strength function (angle set to 88°). The Hartmann-Hahn modified condition was setup for the n=1 condition with RF fields adjusted to 99 kHz for ^{1}H and 74 kHz for ^{13}C (when using the 2.5 mm MAS probe at 500 MHz) or 66 kHz and 41 kHz for ^{1}H and ^{13}C respectively (for the 4 mm MAS probe at 300 MHz). Proton decoupling was obtained by using SPINAL-64 [108] at a 130 kHz or 75 kHz radiofrequency field for the MAS 2.5 mm probe or the 4 mm MAS probe, respectively. Spectra were acquired with a 24.41 Hz/pt resolution at 125.7 MHz (4096 data points in time domain and 50 kHz, i.e., 397.63 ppm, for the spectral width) while 12.2 Hz/pt was obtained at 75.52 MHz (4096 data points in time domain and 25 kHz, i.e., 333 ppm, for the spectral width). 1024 to 10240 transients per FID were added depending on the samples to get a suitable Signal/Noise ratio. Separated by a 1 s recycle delay total acquisition times per spectrum ranged from 17 minutes to ca 3 hours. A 25 Hz Lorentzian apodization function was applied prior to Fourier transform over 8192 points (zero filling by 4096 points). Chemical shifts are given respective to tetramethysilane (TMS) using adamantane as a secondary reference [109].

Antimicrobial activity assays

A broth microdilution assay is used to determine the minimum inhibitory concentration (MIC) i.e., the lowest peptide concentration able to inhibit bacterial growth for each peptide (solution, fibrils and mixture). The fibrils were prepared using tube fibrillation in a 10 mM phosphate buffer at pH 7.4 for LAH4-L1 and LAH4-A4 and at pH 6.2 for LAH4. Fibrillation was initiated exactly two days before the antimicrobial activity test. The peptides for the "peptide in solution" condition was solubilized in same buffers than those used for fibrillation prior to the test. These last samples were not shaken, a vortex and a sonication period were applied to homogenous peptide solution. Mixtures were obtained by mixing peptide solution (50%) and fibrils (50%) from the two previously prepared samples. The concentrations were assessed by HPLC as described previously and subsequent dilution was then carried out to finally have a peptide stock solution of 300 µM.

For all the activity tests, *E. coli* bacteria (ATCC® 25922™, Thermo Fisher Scientific, Courtaboeuf, France) were spread on Mueller-Hinton agar plates (MH) and incubated at 37 °C overnight. Some colonies were resuspended in 1 ml of Mueller-Hinton broth, at pH 7.4. This suspension was used to seed a preculture (10 ml of MH broth at pH 7.4) at the OD_{550}= 0.005. This preculture was incubated for about 6 hours at 37 °C (OD_{550}= 1-2) and then used to inoculate a culture with a starting OD_{550}= 0.2 in 10 ml of MH at pH 5. The culture was incubated at 37 °C until OD_{550}= 1 to 2 was reached (2-3 hours). According to the Mac Farland standard, OD_{550}= 0.1 to 0.2 should correspond to $1-2*10^8$ CFU/ml. Therefore, from the culture, a standard bacterial suspension was prepared at OD_{550}= 0.2 which was subsequently diluted a thousand-fold to prepare the final bacterial working solution of OD_{550}= 0.0002 that should correspond to $1-2*10^5$ CFU/ml.

The antimicrobial analyses were carried out in 96-well microplates (sterile polystyrene untreated with F-bottom, Thermo Scientific Nunc A/S, Roskilde, Denmark). The first column of the plate contains the highest final concentration (Cf) of peptide to test (Cf 100 µM). 100 µl of peptide stock solution at three times the desired final highest peptide concentration was added to 50 µl of MH3X at pH 5. After pipetting up and down, serial dilution by a factor of 1.5 was successively carried out by transferring 100 µl of peptide solution from one column to the next previously loaded with 50 µl MH1X at pH 5 (from columns 1 to 11). Column 12 was used

for control conditions: bacteria without peptides (CT+) or broth without bacteria (CT-). The bacterial working suspension was distributed (50 µl) in each well, except those for CT-. The final volume was 100 µl/well and the range of peptide concentrations tested was around 100 µM to 1.75 µM. The microplates were incubated at 37 °C for 12 hours and bacterial growth was assessed by the OD_{600} measurement.

To check the bacterial density for each experiment, the working bacterial suspension was diluted 1/100 and 1/500 in MH1X at pH 5 and 100 µl were spread on MH agar plates. After overnight incubation at 37 °C, the CFU were counted and the CFU/ml were determined. The final concentration of peptides was precisely evaluated by HPLC and compared for each experiment with a standard concentration curve known to LAH4. The newly determined concentration was used a posteriori for the experimental analysis.

Cell culture and preparation of peptide/DNA complexes for transfection

The fibrils were prepared using the microtube fibrillation protocol in phosphate buffer 10 mM at pH 7.4 for LAH4-L1 and LAH4-A4 and at pH 6.2 for LAH4. Fibrillation was initiated approximately two days before the antimicrobial activity test as same fibrils solutions was used for both assays. The peptides for the "peptide in solution" condition was solubilized in the same buffers than those used for fibrillation prior to the test. The concentrations were analysed by HPLC as described previously.

The Roswell park memorial institute medium (RPMI) was supplemented with 100 units/ml penicillin, 100 µg/ml streptomycin and 10% of fetal calf serum for the culture of the human glioblastoma cell line U87. A total of 55,000 U87 cells were plated in 48 well plates one day before the experiment. The cells were transfected using the following protocol: a fixed quantity of the plasmid DNA (1.5 µg of the 7.6 kb p-Luc plasmid which is an expression plasmid encoding the firefly luciferase gene under the control of the human cytomegalovirus (CMV) immediate-early promoter) was mixed with increasing amounts of peptide.

The quantity of peptides in solution was fixed to 15 µg. For the fibrils' quantity, LAH4-A4 and LAH4-L1 were fixed at 7.5 µg and 15 µg and LAH4 at 15 µg and 24 µg. Peptide (solution or fibrils) and DNA solutions were each diluted into 25 µl of 10 mM phosphate buffer at pH 6.2 or 7.4. The solutions were gently mixed at room temperature for 20 minutes. DNA complexes were generated using increasing peptide/DNA w/w ratios. These mixtures were then diluted

with serum-free culture medium to obtain a final volume of 0.5 ml. For transfection, culture medium containing the DNA complexes were deposited in duplicate (0.25 ml/well) on human glioblastoma U87 cells. After 2.5 hours of incubation at 37 °C, culture medium was replaced with fresh one containing serum.

Cells were harvested 1 day after transfection, and the luciferase activity was measured. For luciferase activity, cells were harvested in 100 µl of lysis buffer (8 mM MgCl2, 1 mM DTT, 1 mM EDTA, 0.6% Triton X-100, 15% glycerol, and 25 mM Tris-phosphate buffer at pH 7.8). The cell lysate was centrifuged for 7 minutes at 10,000 g to pellet debris. Supernatants (2 µl) were transferred into 96-well plates to measure the luciferase activity with a Centro LB luminometer (Berthold Technologies GmbH & Co. KG, Bad Wildbad, Germany). The measurement was done over 1 s after automatic injection of 50 µl assay buffer (lysis buffer without Triton X-100 but supplemented with 2 mM adenosine triphosphate (ATP)) and 50 µl of a luciferin solution (167 µM in water) to the supernatants. Luciferase background was subtracted from each value and the protein content of the transfected cells was measured by Bradford dye-binding using the BioRad protein assay (Bio-Rad, Marnes-la-Coquette, France). The transfection efficiency was expressed as light units/1s/mg protein (light units measured over a period of 1 s and the values were then normalized after measurement with respect to the amount of protein present in each well). Reported values are the mean of duplicates and error bars represent the standard deviation of the mean.

IV.3 LAH4-A4 peptide self-assembly conditions.

For the dialysis protocol over 4 days, the fibrillation percentage remains below 30% after one week of incubation. In addition, a modification of the fibril structure takes place over time. To better understand the peptide assembly a kinetic analysis of the dialysis process was performed. The dialysis protocol was applied to slowly increase the pH. For fibrillation by dialysis, LAH4-A4 peptide was dissolved in water at a concentration of 2 mg/ml and dialyzed against 10 mM phosphate buffer at pH 6.2 [106]. A fibrillation test was performed over four days, taking 1 ml each time (0h, 2h, 5h, 24h, 48h and 92h).

Each sample was analysed by circular dichroism and the pH was measured. We can see the pH evolution depending on the dialysis time and follow the secondary structure adopted by the peptide (**Figure 30 A, B**). In addition, TEM was performed on the collected samples at different times (**Figure 30 C**). A drastic decrease of the volume in the dialysis bag during the last days of dialysis results in a more concentrated peptide solution (>2 mg/ml). The experiment starts at (T0) with a 2 mg/ml peptide solubilization in water right before the dialysis.
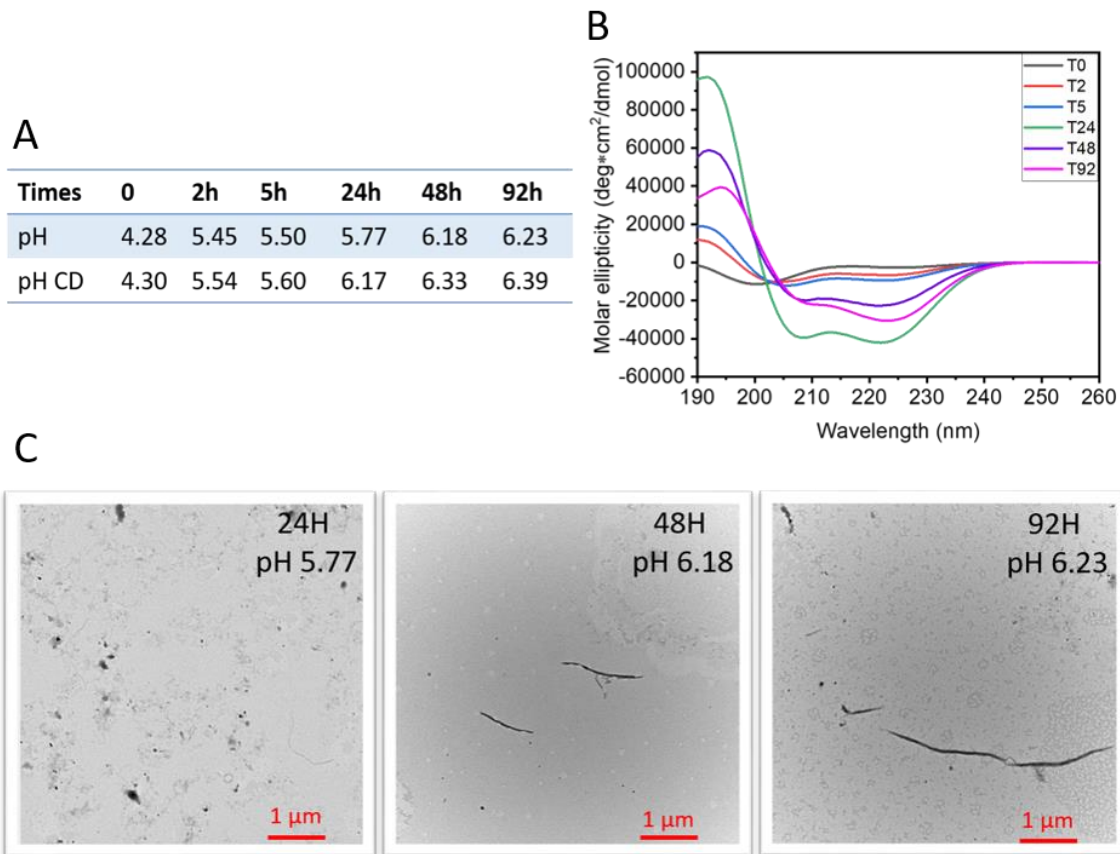
Figure 30: LAH4-A4 fibril formation. pH of the solution as a function of time during the dialysis (A). The pH of the aliquots and after dilution for CD experiments. Evolution of the CD spectra as a function of dialysis time (B). Fibril formation over time by TEM (C).

The peptide adopts a random coil conformation at T0 and the pH of the solution is around 4.28. During the first few hours (2h and 5h), no changes are visible by CD while the pH increases. At T24, the pH reaches 5.8, the CD spectra (**Figure 30 B**, green) show two minima at 209 nm and 222 nm which correspond to an α-helical structure and the TEM analysis shows small fibrils (**Figure 30 C** 24h). After 48 hours, the pH continued to increase up at pH 6.1 approaching the histidines' pKa and the fibrils elongated and increased in diameter (**Figure 30**). At 92 hours, the solution reaches the pH of the dialysis buffer and the TEM shows large and long fibrils. The CD follows the peptide conformation during dialysis indicating an α-helical structure after 24 hours of dialysis. Moreover, small fibrils begin to form after 24 hours. However, TEM analysis showed that the appearance of the fibrils' changes during the dialysis. Indeed, the fibrils become longer and larger that could be related to several factors including changes in pH and/or concentration overtime.

In order to have more information, the same samples (24h, 48h and 92h) that were stored in suspension at room temperature on the bench were deposited on TEM one month later to see if further fibrils elongation occurred with times (**Figure SI 12**). This study showed us, that the fibrils have further elongated without modification of pH or concentration. Indeed, the remaining monomers in solution also self-assembled thereby the fibrils undergo an elongation and become more compact and linear.

This study confirms previous results published by Louis S. Vermeer which agree that the fibrils are made of LAH4-A4 in predominantly α-helical conformation [34]. However, after 92 hours dialysis the yield (fraction of the initial peptide transformed into fibrils) is only 30% obtained (**data not shown**). In order to be able to perform reliable structural analyses, stable samples that do not evolve over time are needed. In addition, the dialysis technique does not give optimal yields and it takes 1 week to obtain samples.

In order to see the fibrils stability carried out by dialysis, the dialysis suspension containing fibrils and monomers (250 µl) were mixed with 250 µl of different buffers: 10 mM phosphate buffer at different pH (pH 6.2, 7.4 and 8), 10 mM trisaminomethane (Tris) at pH 7 and water. Phosphate buffers of different pH were analysed to test the influence of pH on self-assembly [34]. Furthermore, Tris buffer at pH 7 and water were used to see if the phosphate ions influence on the self-assembly [34]. After 1 day of incubation, the solution was centrifuged to recover the pellet. This pellet was washed to remove all monomers. Then pellet/fibril disassembly was carried out by the addition of 2 mM HCl and centrifugation was performed to control complete pellet dissociation. The pH was controlled before the fibrils quantification by reverse phase HPLC. **Figure 31** shows the percentage of peptide associated with the fibrils determined by HPLC as a function of buffer composition. The 13.5% observed for the control (CT) corresponds to the initial fibrils' percentage contained in the dialysis suspension from which 250 µl were distributed in different buffers.
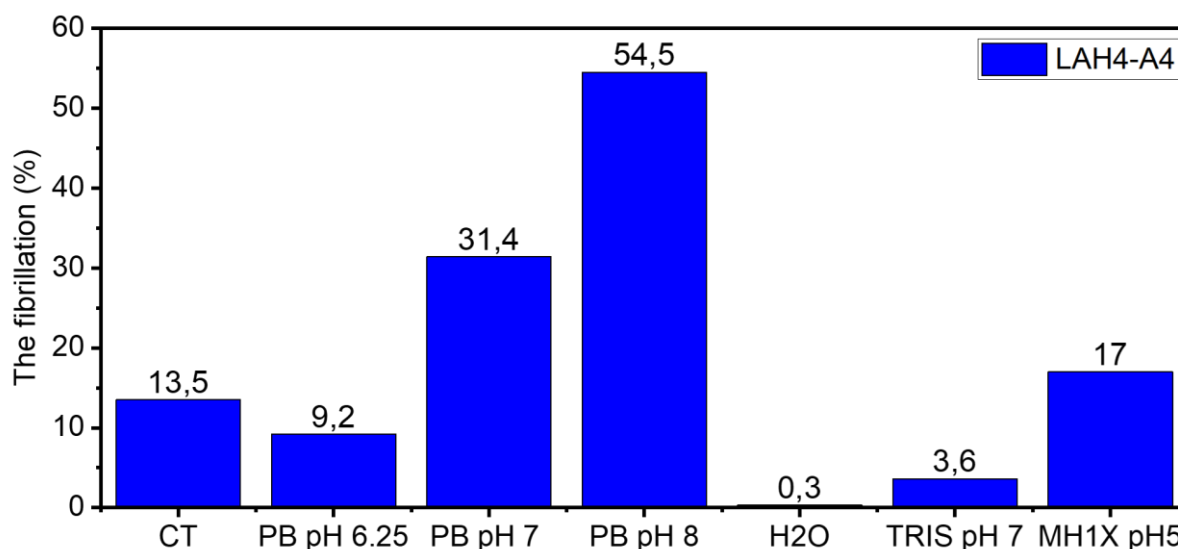
Figure 31: Stability in different buffers of LAH4-A4 fibrils formed by dialysis. The fibrillation percentage as a function of buffer composition to which 250 µl of the dialysis solution containing fibrils and monomers were added. Analysis was performed after 1 day under shaking at 25 °C in different buffers: 10 mM phosphate buffer at pH: 6.2, 7.4 and 8, 10 mM trisaminomethane (Tris) at pH 7 and water. The control (CT) represents the initial fibrils in the dialysis suspension from which 250 µl were distributed in different buffers.

The importance of phosphate ions is noteworthy to maintain fibrillation. Indeed, when adding H_2O or Tris buffer even at pH 7 (which is the pH used during fibrillation), the content of fibrils decreases below 3.6% compared to 13.5% of the control (**Figure 31**). But phosphate ions are not the only parameter to consider, pH is essential too. Indeed, to see the pH effect the CT is diluted in phosphate buffer of different pH. The fibrils percentage for the CT and in PB at pH 6.25 is 13% and 9%, respectively, i.e., not much different. In contrast, between pH 6 and 7 there is an increase by 20%. Upon increase in pH, the fibrils content reaches 31.4% at pH 7 and 54.5% at pH 8 (**Figure 31**). The presence of phosphate ions and a high pH value play a crucial role for fibril formation [106]. However, this experiment was carried out only once and the pH variation during dialysis was not taken into account. The fibrils appearance by TEM was not carried out for this assay, the solution modification can cause peptide aggregation.

In order to optimize the yield and to better control the sample evolution over time, a new fibrillation technique was established. The new fibrillation protocol was inspired by conditions

used for other antimicrobial peptides studied in our laboratory, in particular PGLa and Magainin 2 (Mag2) [110].

The peptide is dissolved in 50% ethanol during 30 minutes at a 10 mM peptide concentration and bath sonicated to have the monomeric peptide [111]. We decided to test different buffers in order to see which one will best promote formation of LAH4-A4 fibrils: the buffer used during dialysis (10 mM phosphate at pH 6.25) and as these peptides are very sensitive to the pH the same buffer with a higher pH (10 mM phosphate at pH 7.4). In addition, Mag2 aggregates into fibrils at high salt, so we tested the same buffer with a higher salt concentration (50 mM phosphate buffer at pH 7.4). The peptide is diluted to a final peptide concentration of 0.5 mM using the previously described buffers and incubated while shaking for one day to test peptide fibrillation (**Figure 32**). Fibrillation percentage was determined by using the same protocol as for dialysis fibrillation. **Figure 32** shows the fibrillation percentage determined by HPLC as well as the TEM images based on different fibrillation buffers.
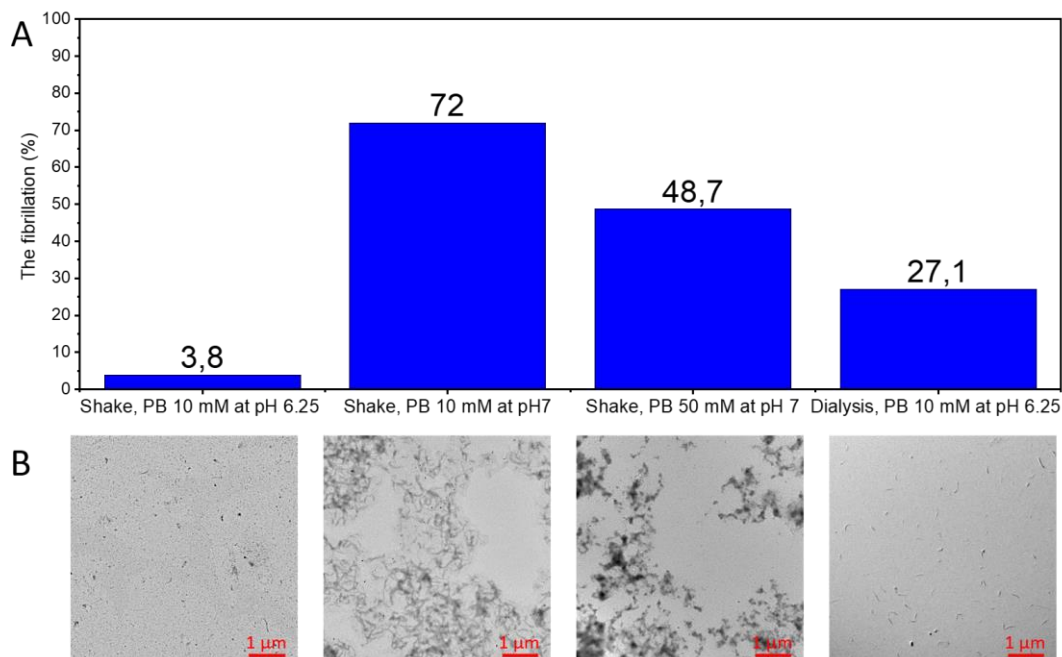

Figure 32: Different fibrillation conditions for LAH4-A4. The fibrillation percentage (A) and the corresponding TEM images of the fibrils (B). Pellet quantification by HPLC after 1 day of shaking peptide in different solution: 10 mM phosphate buffer (PB) at pH 6.2 or 7 and with 50 mM phosphate buffer at pH 7 or 1 week of dialysis with 10 mM phosphate buffer at pH 6.2 at 25 °C.

These results show that after 24 hours (**Figure 32**) in the presence of 10 mM phosphate at pH 6.25, the dialysis method shows that 27.1% of fibrils are formed compared to 3.8% under agitation using the same buffer. In this condition the agitation is not favourable for fibril formation. However, when the pH increased to 7.4 the fibrils percentage increases to 72%. However, when the phosphate concentration is increased to 50 mM there is an amorphous aggregation of the peptide (**Figure 32**), unlike the fibrillation observed for Mag2 and PGLa under such conditions [110].

This study allowed us to improve the fibrillation conditions for LAH4-A4. LAH4-A4 fibrillation by vigorous shaking in a 10 mM phosphate buffer at pH 7.4 occurs faster, with less material loss and a better fibril yield around 80%. The samples are easy to handle, the fibrils are washed to remove any traces of monomers quickly. In addition, the samples are reproducible, and the fibrils appearance by TEM remains the same.

Despite all the advantages of this fibrillation protocol, we need to ensure whether the fibrils structure is the same than the one obtained by the dialysis method.

IV.4 LAH4-A4 peptide self-assembly structure as a function of conditions.

Even if the LAH4-A4 fibrils look similar by transmission electronic microscopy regardless of the protocol used, studies are necessary to check whether the fibrils have the same structure. The Fourier transform infrared (ATR-FTIR) and MAS solid-state NMR spectroscopy, two techniques will allow us to check the fibrils structure.

The Fourier transform infrared spectroscopy is a technique that can be used to determine secondary structures of peptides by looking at the amide I region. The absorption associated with C=O stretching is denoted as amide I and the exact position allows one to differentiate between α-helix and β-sheet secondary structure of peptide [56]. Indeed, bands observed around 1645 cm^{-1} to 1655 cm^{-1} are preferentially in favour of random coil signatures and from 1650 cm^{-1} to 1658 cm^{-1} of α-helix structure. The bands indicating β-sheet structure are around wavenumbers from 1620 cm^{-1} to 1640 cm^{-1} and 1670 cm^{-1} to 1695 cm^{-1} [56].

The fibrils were formed either by shaking or by following the dialysis protocol. They were washed with their fibrillation buffer to remove peptide in solution and the pellet has been deposited on the crystal. The samples have been dried slowly to remove all water traces.

ATR-FTIR spectra were recorded from 1500 cm^{-1} to 2500 cm^{-1} and 12 scans were accumulated. The background from the buffer was subtracted. **Figure 33** presents the FTIR spectrum of the amide I region from two fibrillation protocols.
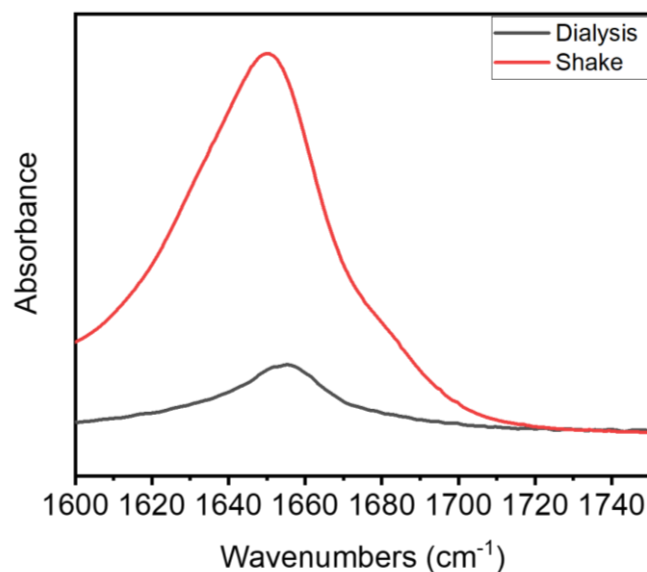
Figure 33: ATR-FTIR of LAH4-A4 in the amide I region, the spectra were recorded from dried fibrils. Spectra from fibrils formed during dialysis (black) or when prepared by vigorous shaking (red). The fibrillation was conducted in 10 mM phosphate buffer at pH 6.2 for dialysis or pH 7.4 for shaking both at room temperature and the pellet was washed. The pellet fibrils were also checked by TEM analysis.

The FTIR spectra show us one peak at wavenumbers around 1650 cm^{-1} for the fibrils formation method by shaking (**Figure 33** red) or 1655 cm^{-1} by dialysis (**Figure 33** black). The signal at wavenumbers around 1650-1655 cm^{-1} is characteristic of the α-helical secondary structure (**Figure 33**). There is no modification of secondary structure according to the fibril's formation methods (by shaking or dialysis). In both cases the ATR-FTIR spectrum indicates that LAH4-A4 a made from α-helical peptides.

In order to have more information on the structure of the LAH4-A4 fibrils these were analysed by solid-state NMR spectroscopy. The ^{13}C chemical shifts of the Cα, Cβ and CO positions are sensitive to the peptides or proteins secondary structure [112]. We have used this correlation to analyse the peptide in a residue dependent manner. For example, the alanine carbonyl chemical shift is around 175.3 (± 1.61) ppm for a β-strand structure and around 179.58 (± 1.39) ppm for an α-helix conformation [112].

The fibrils were formed by shaking or dialysis protocol. They were washed with their fibrillation buffer to remove peptide in solution and the pellet was concentrated before incorporation into a 2.5 mm MAS spinner. One dimensional {^{1}H}^{13}C CP/MAS ssNMR spectra were acquired for both fibrillation techniques to investigate whether shaking or dialysis do modify the fibrils secondary structure (**Figure 34**).
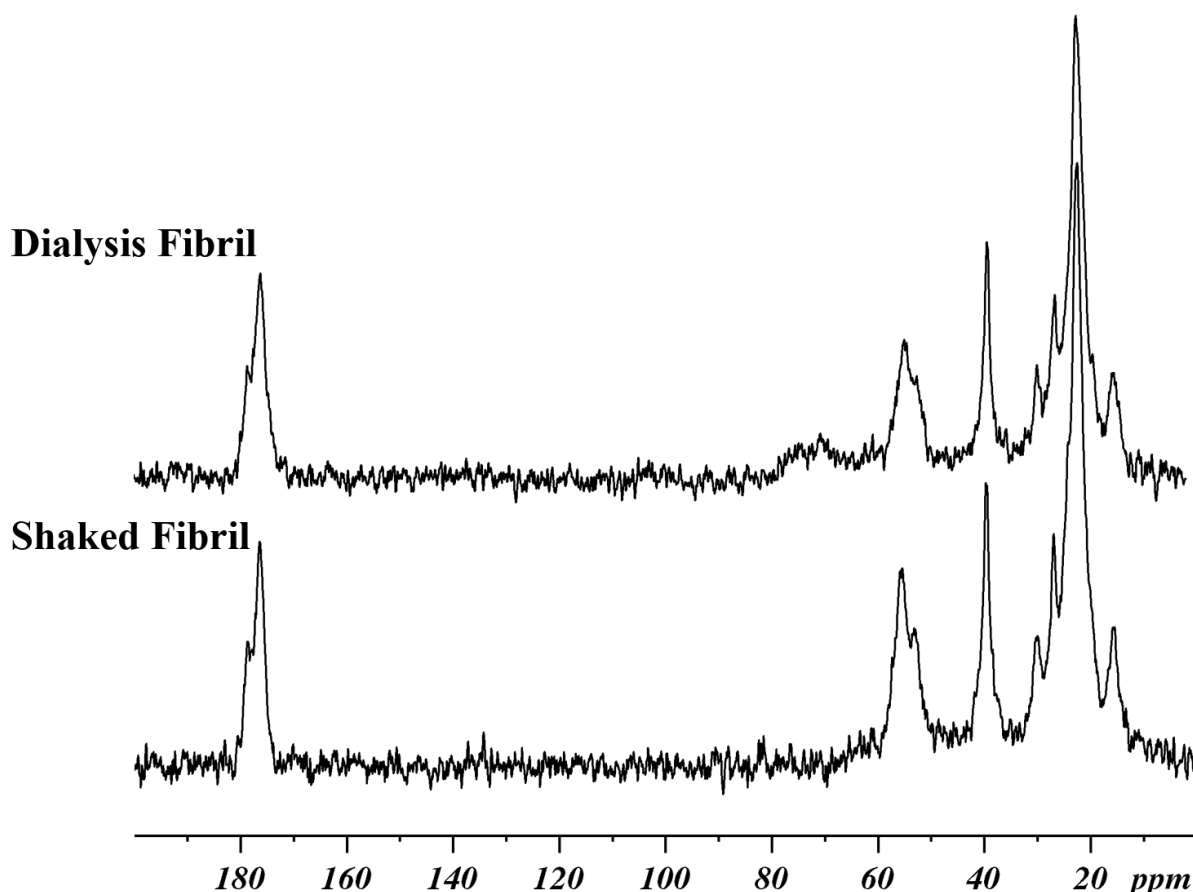

Figure 34: {^{1}H}^{13}C CP-MAS solid-state NMR spectra of LAH4-A4 fibrils as function of protocol. Spectra according to the protocol by dialysis (top) or vigorous shake (bottom). The fibrillation was conducted in 10 mM phosphate buffer at pH 6.2 for dialysis or pH 7.4 for shaking both at room temperature and the pellet was washed. The spectra were recorded on a Bruker^{TM} Avance 500 MHz NMR spectrometer, samples were packed inside 2.5 mm zirconia rotors, spun at 25 kHz and the number of scans was 1024.

The solid-state NMR spectra present the same profile whatever the fibrils formation methods used (shaking or dialysis) (**Figure 34**). When we focus on the carbonyls' region (170-180 ppm), we find chemical shifts around 178 ppm, which is characteristic of α-helical, structure for both preparation methods.

In this part, we have shown that we were able to establish a new protocol for LAH4-A4 fibril formation. It consists of first solubilizing 10 mM peptide in 50% ethanol and then diluting it in 10 mM phosphate buffer at pH 7.4 to get a final concentration of 0.5 mM and agitation for 2 days. In order to stop fibrillation, the fibrils are washed with the same buffer used for fibrillation to remove any trace of free peptide remaining in solution. The TEM shows us that the fibrils are more homogenous when they are formed by agitation and the peaks are much better resolved. This protocol allows the formation of more homogenous fibrils with a yield around 80% and faster. The new fibrillation protocol (shaking) does not change the secondary structure with respect to the previous protocol (dialysis), as we could see the peptides adopt α-helical conformations in both cases.

The study is extended to LAH4-L1 and LAH4. The LAH4-L1 had already shown the ability to form fibrils by dialysis [106]. We focused on the fibrillation conditions for the other two peptides.

IV.5 LAH4 and LAH4-L1 histidine-rich peptides self-assembly conditions

Interestingly, LAH4, LAH4-L1 and LAH4-A4 exhibit distinct biological activities and small changes in the amino acid sequence can modify the activity (*v.s.* **Figure 6**). Indeed, these peptides exhibit antimicrobial [9][18], transfection [10][31][44], and transduction [33][40] activities, respectively. It is interesting to note that modest differences in primary sequence affect the physico-chemical characteristics of the resulting secondary structures (e.g., distribution of amino acid side chains and charge, hydrophobic moment based on the α-helical structure, etc.) and result in supra-molecular assemblies of different shapes and thereby large shifts in function [113][114]. The goal of this study is to investigate the capacity of the three peptides (LAH4-A4, LAH4-L1 and LAH4) to form fibril. The previous study described a rapid fibrillation protocol for LAH4-A4 with good yield, more stable fibrils over time and with reproducible structure. We will rely on this protocol to form LAH4 and LAH4-L1 fibrils. However, for fibrils with these peptides the salts and pH used in the buffer system are of additional importance. As we have seen previously, the pH plays a crucial role in the fibril's formation ([106] and *v.s.* **chapter IV.3**). Therefore, for this study we carried out the protocol as described before: fibrillation was performed by shaking the peptide in solution in 10 mM phosphate buffer at two different pH 6.2 and 7.4 (**Figure 35**). As described before, the fibrillation percentage after 1-day incubation was obtained by washing and collecting the fibrils. Then the pellet was dissociated into HCl (2 mM), analysed by reverse phase HPLC to determine the peptide quantity (**Figure 35**).
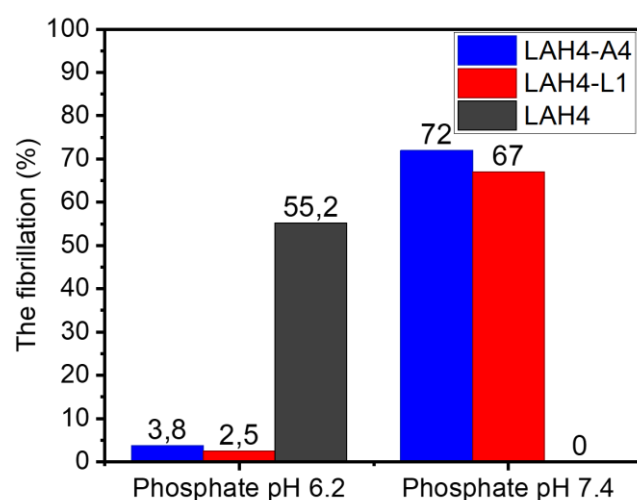
Figure 35: Fibrillation yield of peptides involved in fibrils compared to the total peptide using the shaking protocol. The fibrillation was conducted by shaking over 1 day in 10 mM phosphate buffer at pH 6.2 or pH 7.4 at room temperature. The pellet was washed before analysing, quantified by HPLC and analysed by TEM. LAH4-A4 (blue), LAH4-L1 (red) and LAH4 (black).

Strikingly, the three peptides do not have the same fibrillation conditions and a change in pH has a big effect (**Figure 35**). The best fibril conditions for LAH4-L1 are the same conditions than for LAH4-A4. At pH 6.2, the LAH4-L1 fibril fraction remains below 5%, while at pH 7.4 it approaches 70%. The self-assembly of these two peptides is favoured at pH 7.4 (**Figure 35** red and blue). For LAH4 on the other hand the fibrillation fraction at pH 6.2 tends towards 55%, whereas at pH 7.4 no fibrillation is observed. As a matter of fact, no LAH4 pellet is detected at pH 7.4 which could have been used for quantification by HPLC. On the contrary, at pH 6.2, a large pellet is observed for LAH4, similar to LAH4-L1 and LAH4-A4 at pH 7.4. This first step tells us that the pH dependence is very different for the peptides' fibrillation.

However, obtaining a pellet does not mean that the peptide adopts an organized self-assembly. Therefore TEM was performed in order to verify the resulting supramolecular assembly that is obtained with the applied protocol (**Figure 36**).
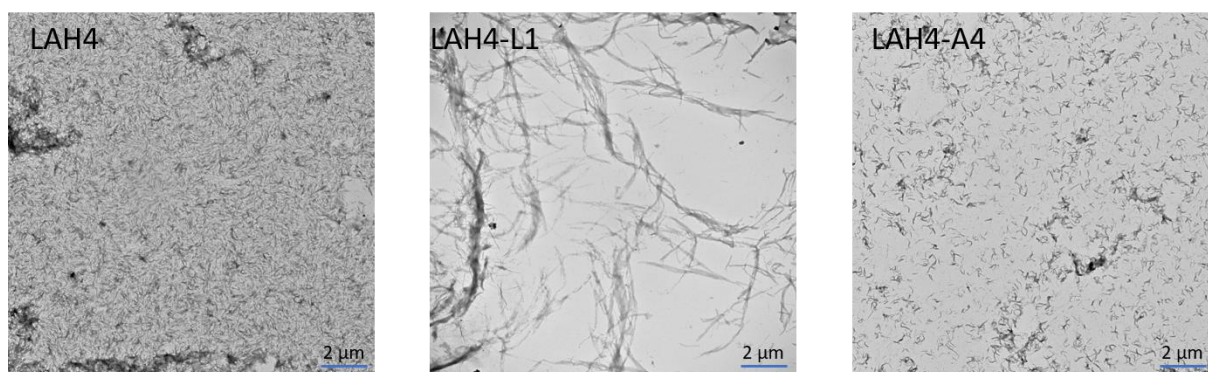
Figure 36: Transmission Electron Microscopy on the fibrils obtained by shaking. The fibrillation is conducted over 1 day at room temperature in 10 mM phosphate buffer at pH 6.2 for LAH4 and at pH 7.4 for LAH4-L1 and LAH4-A4.

TEM pictures show that different kind of fibrils are formed by the three peptides. LAH4 tends to have short linear fibrils (**Figure 36** LAH4). Unlike LAH4, LAH4-L1 tends to cluster together and to form more compact and long structures (**Figure 36** LAH4-L1). As previously described [34]LAH4-A4 forms wavy and very short fibrils structures (**Figure 36** LAH4-A4).

In the next step, we focused on the stability of the fibrils in four buffer solutions. Because self-assembly of the peptides is highly dependent on the pH and ions (v.s. **Figure 31**), the fibrils stability was analysed in the two fibrillation buffers (10 mM phosphate at pH 7.4 and 6.2) but also in the Mueller Hinton broth (MH) used for testing antimicrobial activity and in pure water. The goal was to verify if the fibrils were stable at different conditions (**Figure 37**). After fibril formation, centrifugation at 16,000 g for 30 minutes was carried out to remove the non-fibrillated peptide which remains in the supernatant. The pellet was resuspended in the previously cited solutions. After 1 hour of stirring the samples were centrifuged again to recover the pellets which were dissolved it in 2 mM HCl. An HPLC separation was carried out to quantify the amount of peptide involved in fibrils (**Figure 37**). Results are represented as a percentage of the peptide found by quantification compared to the expected amount of peptide if fibrillation was total and fibrils fully stable (100%).
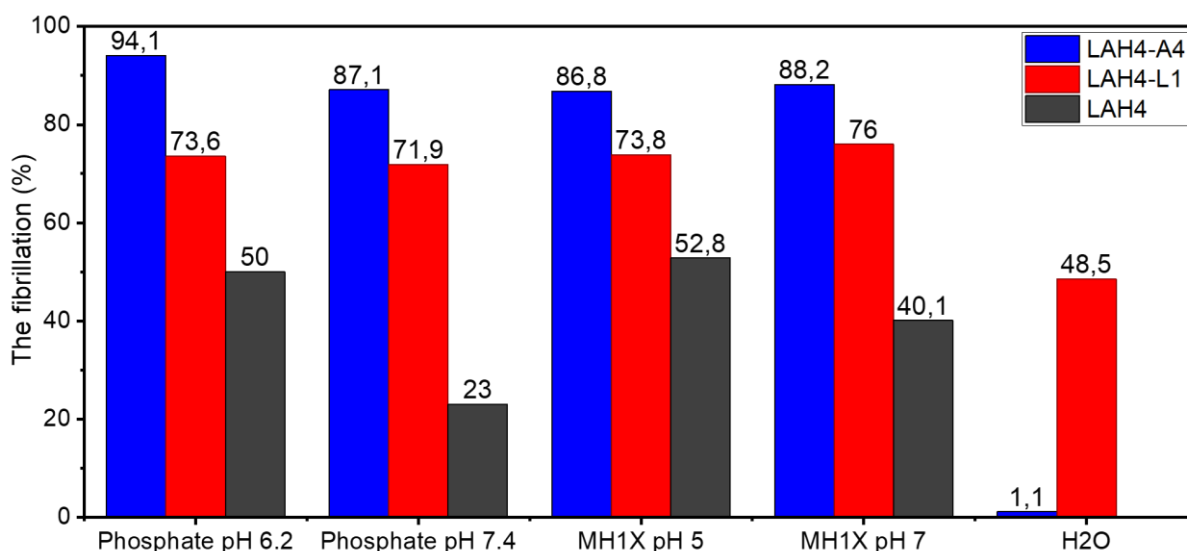
Figure 37: The influence of buffer composition on fibrils. The fibrillation yield was determined by HPLC after 24 hours of continuous shaking in various environments. All phosphate buffers are 10 mM at pH 6.2 or 7.4, MH1X at pH 5 or 7 and water. LAH4-A4 (blue), LAH4-L1 (red) and LAH4 (black).

In the same condition as used for fibrillation (10 mM phosphate buffer at pH 7.4), LAH4-A4 and LAH4-L1 show 87% and 72% fibril, respectively, whereas LAH4 shows 50% in 10 mM phosphate buffer at pH 6.2. **Figure 37** shows that LAH4-A4 fibrils are stable in 10 mM phosphate buffer at pH 6.2 and 7.4 and MH1X at pH 5 and 7 with fibrils percentage around 80%. LAH4-L1 fibrils are also stable under different conditions (phosphate and MH1X at both pH) with a percentage of the fibrils state of around 70%. LAH4 is more sensitive to the pH: in phosphate buffer at pH 6.2 as well as MH1X, pH 5 LAH4 fibrils are relatively stable, however at increased pH towards 7.4 the LAH4 fibrils dissolve. In addition, the fibrils are stable in the rich medium (MH) used for antimicrobial activities, no defibrillation was observed during this analysis. Also, in the LAH4 case treated with pure water, no pellet could be detected and quantified, which could be interpreted as a total dissociation of the fibrils in the water. Indeed, peptides were found to be in the supernatant (**data not shown**). **Figure 37** shows that the LAH4 fibrils are not stable in pure water. For LAH4-A4 fibrils same observation is done, in the presence of water there is defibrillation and we detect only 1% of the peptides in the remaining fibrils. However, LAH4-L1 does not completely disassemble in water and 48% of the peptides could be detected in a fibrillar form.

This study allowed us to optimize the protocol for LAH4-A4, LAH4-L1 and LAH4 fibrillation: 10 mM phosphate buffer at pH 7.4 for LAH4-A4 and LAH4-L1 and at pH 6.2 for LAH4. In fact, LAH4 fibrils formation is favoured at a lower pH than LAH4-L1 and LAH4-A4. In addition, these different peptides do not react in the same way depending on the pH used. These results could be due to the different peptides secondary structures: amino acid distribution, side chains and charge, hydrophobic moment.

IV.6 The fibrils structure of the LAH4 and LAH4-L1 histidine-rich peptides

We have seen previously that modifications in the sequence generate modifications in the self-assembly conditions. These can lead to different supramolecular assemblies resulting in a great change of function. In order to evaluate the fibrils structural details, biophysical techniques such as TEM, FTIR, CD and solid-state NMR spectroscopy are used. The fibrils are formed under the conditions previously described.

After shaking in the best fibrillation condition for each peptide, centrifugation at 16,000 g was carried out and the supernatant was recovered and analysed by CD. The pellet was washed with the fibrillation buffer before it was further analysed by FTIR. The supernatant analysis by CD shows that LAH4, LAH4-L1 and LAH4-A4 peptide in solution are in α-helical conformations (**data not shown**). To analyse the pellets by FTIR they were deposited on the crystal and dried slowly to remove all water traces. The FTIR spectrum recorded in the amide I region shows us different secondary structures of the peptides (**Figure 38**).
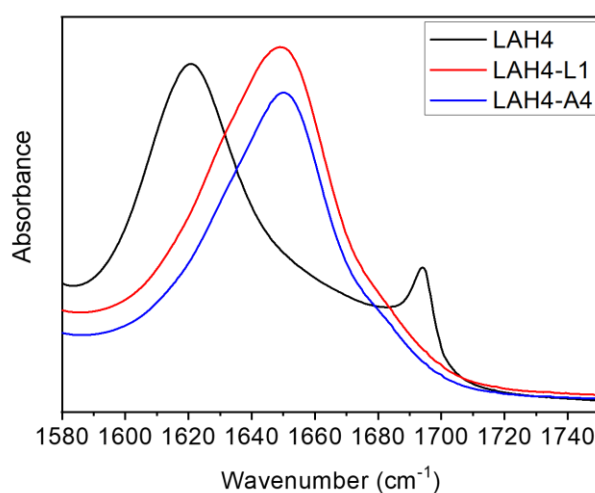

Figure 38: ATR-FTIR spectra of LAH4-A4, LAH4-L1 and LAH4 in the amide I region, the spectra were recorded from dried fibrils. The fibrillation was conducted by shaking over 1 day in 10 mM phosphate buffer at pH 6.2 or pH 7.4 at room temperature. The pellet was washed and the pellet fibrils were checked by TEM. LAH4-A4 (blue), LAH4-L1 (red) and LAH4 (black).

The LAH4-A4 and LAH4-L1 FTIR spectra from fibrils prepared in the same phosphate buffer at pH 7.4 present both a peak with a maximum around 1650 cm^{-1}. Hence, the LAH4-A4 and LAH4-L1 FTIR spectra are characteristic of an α-helical structure. However, the LAH4 fibrils (phosphate buffer at pH 6.2) are dominated by a band around 1620 cm^{-1}, typical range for β-sheet secondary structures. Moreover, the second band around 1690 cm^{-1}, typical pattern for antiparallel β-sheet secondary structures.

The three peptides would therefore not have the same secondary structure in their fibrillar self-assemblies. In order to confirm this secondary structure analysis, natural abundance {^{1}H}^{13}C CP/MAS solid-state NMR spectra of the fibrils were recorded.

The ^{13}C peptide chemical shifts allow us to distinguish between the two different secondary structures (α-helix and β-sheet) [112]. For this study, we focus on the alanines' chemical shift. In **Figure 39** the expected chemical shift region for α-helix conformation are labelled in light blue and those corresponding to β-sheet in dark blue (**Figure 39**).

Alanine Conformation	Cα (ppm)	Cβ (ppm)	C=O (ppm)
α-helix	54.86 (0.94)	18.27 (1.08)	179.58 (1.39)
β-sheet	50.86 (1.28)	21.72 (1.77)	175.3 (1.61)

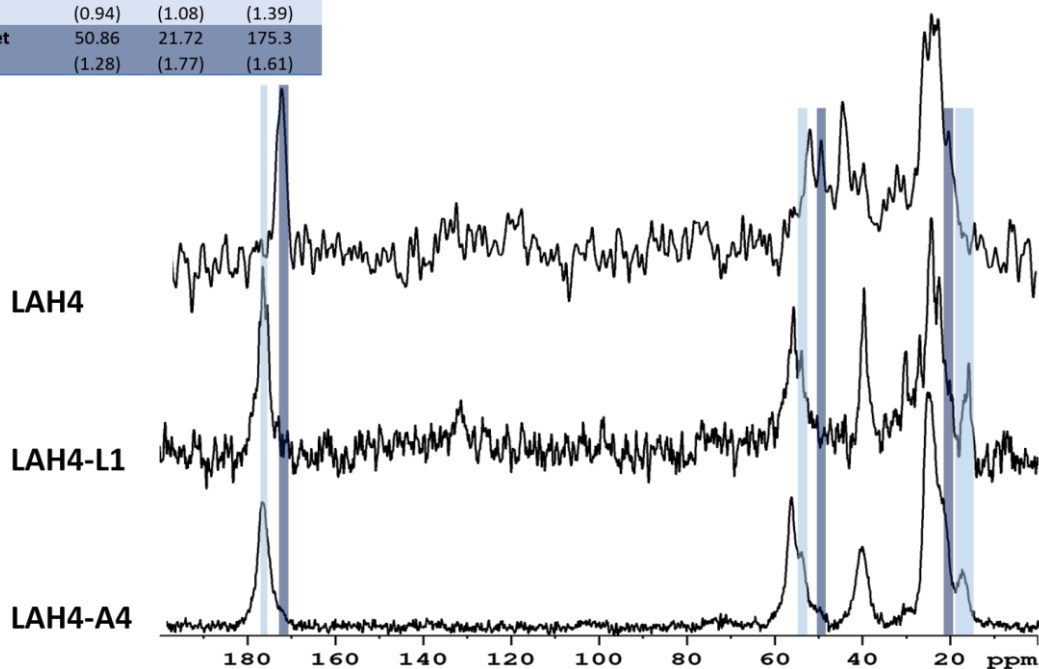*Figure 39: $\{^1H\}^{13}C$ CP-MAS solid-state NMR spectra of LAH4, LAH4-L1 and LAH4-A4. The alanine chemical shifts [112] for β-sheet (dark blue) and for the α-helix conformation (light blue) are highlighted. The fibrils were formed in 10 mM phosphate buffer at: pH 6.2 for LAH4 or at pH 7.4 for LAH4-A4 and LAH4-L1 and the pellet was washed. The LAH4-A4 spectrum was recorded on a Bruker^{TM} Avance 500 MHz NMR spectrometer, samples packed inside 2.5 mm zirconia rotors and spun at 25 kHz at 301 K. LAH4 and LAH4-L1 spectra were recorded on a Bruker^{TM} Avance 300 MHz NMR spectrometer, samples packed inside 4 mm zirconia rotors and spun at 12 kHz at 301 K.*

The LAH4-A4 and LAH4-L1 carbon spectra show chemical shifts of the carbonyls' groups around 177 ppm characteristic of an α-helix structure. The LAH4 spectrum exhibits carbonyl chemical shifts around 172 ppm characteristic for β-sheets (**Figure 39**). These spectra clearly show the secondary structures of these three peptides when assembled in fibrils. The fibrils of LAH4 tend to adopt β-sheet structures, whereas LAH4-L1 and LAH4-A4 to have α-helical conformations.

As peptide self-assembly originates from non-covalent interactions, including hydrogen-bonding, π-π stacking, electrostatic, hydrophobic, and van der Waals interactions [99] the presence of negative or positive charges on the peptide at specific positions stabilizes the assemblies. Then the structural modifications of the LAH4 family peptide could be directly linked to the primary sequence modification (**Figure 40**).

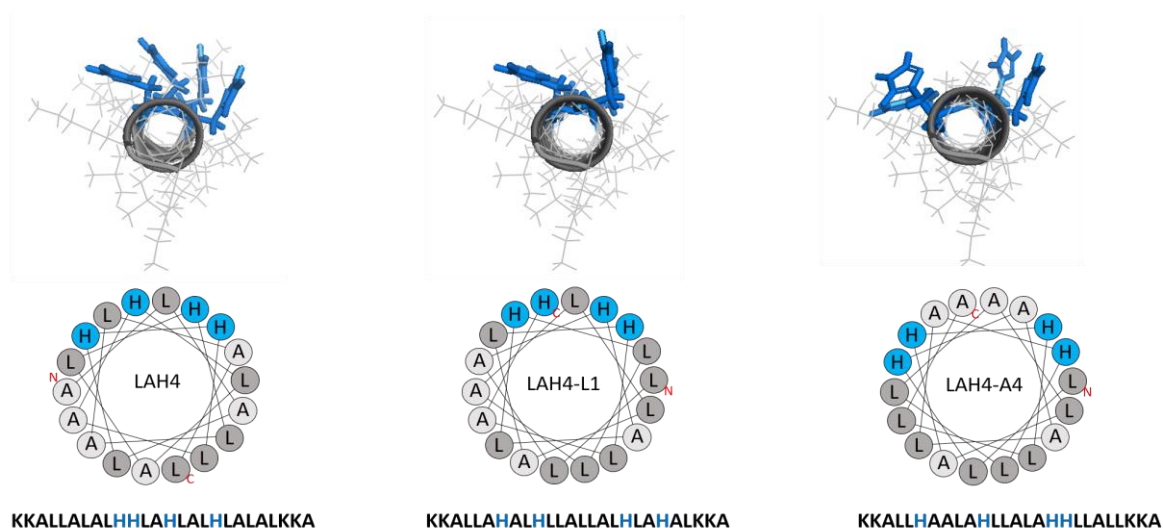KKALLALALHHLAHLALHLALALKKA   KKALLAHALHLLALLALHLAHALKKA   KKALLHAALAHLLALAHHLLALLKKA

Figure 40: Schiffer-Edmundson helical wheel representations of the core region (residues 6-23) for LAH4, LAH4-L1 and LAH4-A4 peptides. LAH4, LAH4-L1 and LAH4-A4 helical wheels and their primary sequence. The polar residues so histidines (blue), the hydrophobic residues (grey): leucine (dark grey) and alanine (light grey). Figures are created using the Heliquest software [73].

One hypothesis for this structural modification is that when the peptide is in α-helical secondary structure, the distribution of the four histidine residues is different for LAH4 when compared to the other peptides (**Figure 40**) [115]. One hypothesis is that this structural variation is related to the histidines distribution around the α-helix. For LAH4, the four histidine residues are distributed on the same side giving it a strong polar character while the other side has a highly hydrophobic character due to leucine and alanine residues. This is not the case for LAH4-L1 and LAH4-A4 for which histidines are paired with alanine or leucine residues in between which alters the bimodal amphipathic character of LAH4. There is a hydrophilic/hydrophobic character that can be characterized either by the hydrophilic angle or by the hydrophobic moment. LAH4, LAH4-L1 and LAH4-A4 have a different hydrophobic moment 0.19, 0.23 and 0.34, respectively. LAH4 has a weaker hydrophobic moment than

LAH4-L1 and LAH4-A4. These differences between the three peptides will affect intermolecular interactions.

For LAH4 the self-assembled fibrils are characterized by β-sheet conformations and for LAH4-A4 and LAH4-L1 the self-assembled fibrils are characterized by α-helical conformations. The structure can be predicted as a function of the hydrophobic (H) and polar (P) residue repartition in the primary sequence [97]. The helical components are amphipathic as defined by the heptad sequence repeats HPPHPPP [116]. Even if these two peptides have α-helical structure when they self-assemble, assemble they do not correspond to this canonical coiled coil motif HPPHPPP. In addition, an altered HP repetition tends to adopt β-strand conformation [93], LAH4 does not correspond to this motif too. In contrast, one study show when the peptides are in α-helical conformations the hydrophobic residue on one side will interact, allowing helix-helix self-assembly with two or more helices [100]. For more information on the structure of the LAH4-A4 fibrils, RX diffraction and the solid-state NMR spectroscopy (*v.s.* **chap V**) analysis should be carried out.

IV.7 The antibiotic activity of fibrils formed by histidine-rich peptides

Amphipathic peptides can assemble in different ways: nanotubes, nanovesicles, nanofibers, etc. [117]. Molecule assembly to form complexes has attracted attention in different fields, from biomaterials [100][118], biomedical applications [45][119][120] or amyloidogenic diseases [121][122][123]. The α-helical peptides from the LAH4 family have already proven their efficiency as amphipathic peptides. In addition, variations in the primary sequence allow the increase of antimicrobial activity or to promote other activities such as transfection or transduction. For the latter, peptide self-assembly was carried out to increase activity as already reported for other peptides.

Moreover, the LAH4-A4 belongs to a novel class of α-helical fibrils-forming transduction enhancers [34]. Maybe that the LAH4-A4, LAH4-L1 and LAH4 activities are modified when they are self-assembled. In addition, as these three peptides present different structures it may be interesting to see if the kind of fibril structure alters the activity. In this part, fibrillar assemblies and non-aggregated peptides in solution were evaluated and compared with their antimicrobial and transfection activities. This study will allow us to clarify whether the change in the functionality of it is peptide is directly related to their different supramolecular assemblage form. This will allow us to know whether the supramolecular structure rather than the secondary structure impacts the functionality.

IV.7.1 Antimicrobial activity

Studies have already shown antimicrobial activity for some peptides present in the LAH4 family. They exhibit antimicrobial activity in an acid solution at pH 5, however when the pH is increased to around 7 the peptides have little or no activity [9] [18]. Since the fibrils were obtained at pH 6.2 and 7.4, the antimicrobial activities of LAH4, LAH4-L1 and LAH4-A4 in solution were tested at both pH 5 and 7 to keep similar conditions. These experiments will allow to get an idea about the range of activities of these three peptides and thus allow to adapt the experimental conditions for the fibrils. The fibrils stay stable in the MH1X at pH 5 and 7, the solution used to test antimicrobial activities. The peptides in solution are first analysed at two different pH to be able to later compare them to the corresponding self-assemblies to keep similar experimentation conditions and to optimize them.

At first the solutions (possibly monomers) were tested at pH 5 and 7.4. Peptide aliquots were dissolved in water to obtain 300 µM stock solutions then sequentially diluted in MH medium at pH 5 or 7 to get, after addition of bacterial suspension a final peptide concentration ranging from 100 to 1 µM. After 12h of incubation in a static incubator, the bacterial density is measured. Three independent experiments were performed with triplicates for each condition. For data analysis, we considered that bacterial growth control without peptides (CT+) corresponding to 100% bacterial growth and without bacteria (CT-) corresponding to 0% bacterial growth. **Figure 41** presents the bacterial growth percentage at both pH according to the peptide concentration.

At first, three different peptide minimal inhibitory concentrations are determined at pH 5 (**Figure 41**). For all three peptides, a small but regular decrease in bacterial growth is observed before reaching its maximum of inhibition. The increase in bacterial growth after the MIC had been reached could be due to the fact that at high concentrations the peptides aggregate. The thus obtained MIC for all three peptides in acidic conditions are summarized in **Table 14**.
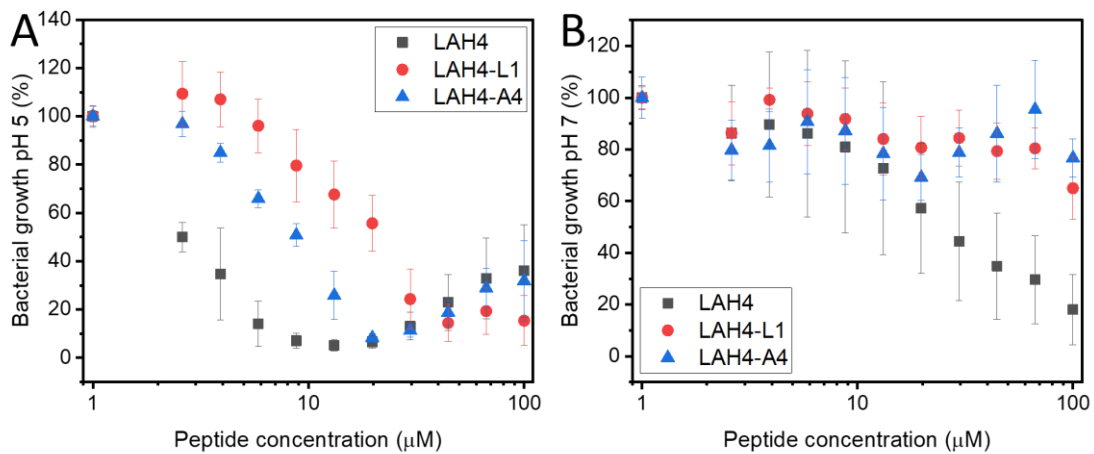
Figure 41: The bacterial growth percentage as a function of peptide concentration (1-100 µM) at pH 5 (A) and pH 7 (B) for LAH4 (black), LAH4-L1 (Red) and LAH4-A4 (blue). The average of the three independent experiment data sets (each condition repeated in triplicates) is represented as a percentage compared to bacterial growth control without peptides (CT+) after background subtraction condition without bacteria (CT-).

For pH 7, the percentage of bacterial growth did not reach minima and remain around 80% even at 100 µM (the highest peptide concentration tested) for LAH4-L1 and LAH4-A4. Only LAH4 presents activity as the percentage decreases down to 20% for 100 µM. Moreover, error bars are considerable and no MIC was determined.

Peptide/MIC	pH 5	pH 7
LAH4	8.8 μM	>100
LAH4-L1	44.4 μM	None
LAH4-A4	19.8 μM	None

Table 14: MIC values obtained for LAH4, LAH4-L1 and LAH4-A4 at two different pH 5 and 7.4 for static incubation.

The peptides minimum inhibitory concentration (MIC) at acid pH is about 9 μM for LAH4, 20 μM for LAH4-A4 and 44 μM for LAH4-L1. This first experiment is able to highlight the activities of LAH4, LAH4-L1 and LAH4-A4 peptides in solution at two different pH. In addition, confirming what was already observed at pH 7, LAH4 is the most active of the three peptides in these antimicrobial assays since it only needs 9 μM to inhibit bacterial growth. This study had already been carried out with only LAH4 [9] and is consistent with those previously achieved, the peptide concentration in which full growth inhibition is observed (10 μM) and at pH≈ 7, the LAH4 histidines are uncharged and growth inhibition is only observed at much higher peptide concentrations [9].

In the next step, the antimicrobial activity of fibrils formed by shaking was analysed. For this, the fibrils were formed while stirring in 10 mM phosphate solution at pH 6.2 for LAH4 and pH 7.4 for LAH4-L1 and LAH4-A4. After two days the fibrils were centrifuged, the supernatant removed and the pellet washed with their fibrillation buffer to remove all non-aggregated peptide traces. The fibrils were quantified by HPLC to determine the exact amount of peptide, and thus to be able to work with well-defined stock solutions. The antimicrobial activity was tested at final peptide concentrations ranging from approximately 100 to 1 μM. Experiments were performed in parallel with peptide either in solution or as fibrils and finally as an equal mixture of both. These tests were carried out once in duplicate on a 96-well plates with shaking.

First, the LAH4-A4 antimicrobial activities for the fibrillar form or when dissolved in buffer were tested (**Figure 42**). **Figure 42 A** present the antimicrobial activities from different concentrations of fibrils stock solution at 150 μM, 300 μM and 500 μM in the phosphate buffer at pH 7. **Figure 42 B** presents different conditions of LAH4-A4 in solution either in H_2O or

phosphate buffer at pH 7. The serial peptide dilutions were done in MH1X at pH 5 to get final peptide concentrations ranging from approximately 100 to 1 µM.
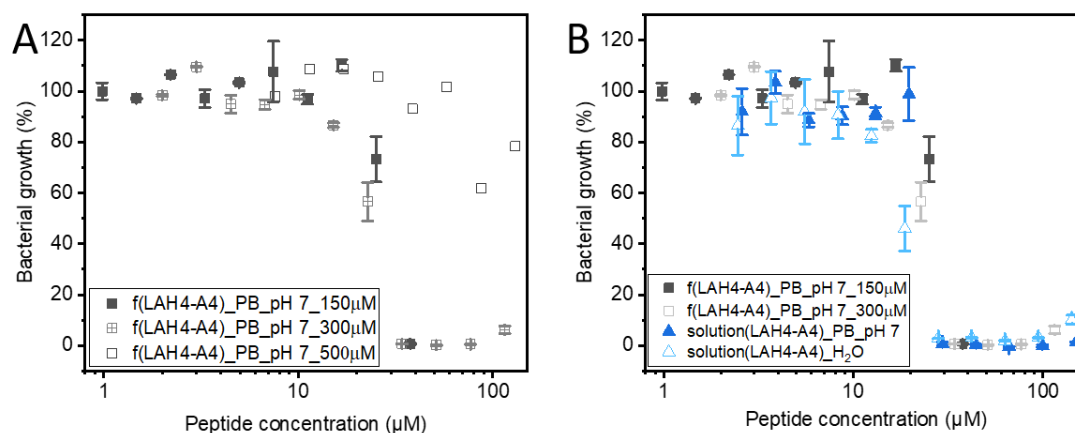

Figure 42: The bacterial growth percentage as a function of peptide concentration for LAH4-A4 starting from different concentrations of stock suspension of fibrils in 10 mM phosphate buffer at pH 7.4 (A) or from peptide solutions in H₂O or 10 mM phosphate buffer at pH 7.4 (B). The experiment is done in MH at pH 5 with static incubation. Results are represented as the average of experimental triplicates in comparison to bacterial growth control without peptides (CT+) after background subtraction of the condition without bacteria (CT-).

In order to know if the LAH4-A4 fibrils have an antimicrobial activity and if it can be influenced according to the fibrils stock solutions different concentrations at 150 µM, 300 µM and 500 µM were tested (**Figure 42 A**). The experiment reveals the same MIC of fibrils from a 150 µM or 300 µM starting stock solution. However, the bacterial growth inhibition is lost when a 500 µM stock solution was used suggesting the formation of inactive aggregates. Secondly, solubilization conditions have been tested. In order to reconcile the conditions used for fibrils in antimicrobial tests, the peptide was tested in water or in the fibrillation buffer. LAH4-A4 peptide is solubilized in 50% ethanol (a 0.5 mM) to have the least aggregated peptide in the solution, then diluted either in the water or in the fibrillation buffer (10 mM phosphate at pH 7.4). The MIC is about 30 µM for both conditions: the peptide solubilized in water or in fibrillation buffer (**Figure 42 B**). In order to have the fibrillation conditions and stay

homogenous for all tested conditions for each peptide, we decided to continue the antimicrobial tests by solubilizing the peptide in the fibrillation buffer.

This allowed us to determine the best conditions for antimicrobial assays. The 300 µM peptide stock solutions were all prepared in fibrillation buffer whatever the conditions: peptides in solution, fibrillated or their equal mixture (1:1; v:v). So LAH4 (solution, mix and fibrils) are in 10 mM phosphate buffer at pH 6.2. LAH4-L1 and LAH4-A4 (solution, mix and fibrils) are in 10 mM phosphate buffer at pH 7.4. The antimicrobial activities were tested at final peptide concentrations ranging from 100 to 1 µM in a MH medium at pH 5. These tests have been performed twice. Furthermore, the same experiment was performed either under static or shaking conditions (**Figure 43 A, B**).
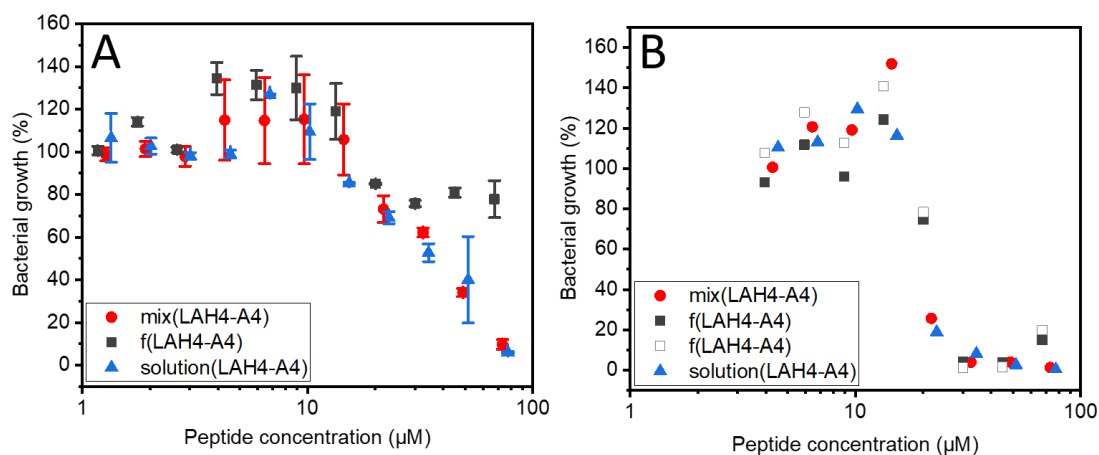

Figure 43: The bacterial growth percentage as a function of LAH4-A4 concentration for a static (A) or shaking incubation (B). Peptide in 10 mM phosphate buffer at pH 7.4 in solutions (blue triangles), fibrils (grey squares) and equal mixtures (red dots). The experiments were performed in MH at pH 5 and results are represented as the average of the experimental data in triplicates in comparison to bacterial growth control without peptides (CT+) after background subtraction of the condition without bacteria (CT-).

When looking at the bacterial growth percentage (**Figure 43**) undergone without (A) or with stirring (B), we can observe a huge difference in the profile between the static plate and the plate under agitation. Indeed, within static incubation, bacterial growth decreases at a slower rate while the peptide concentration increases when compared to the plate under agitation. The decrease in bacterial growth starts approximately at the same peptide concentration

(15 µM), but the slow rate in the static mode makes a precise determination of the MIC impossible (**Figure 43**). However, when the plaque is under agitation, characteristic curves of antimicrobial activity with a rapid decrease in bacterial growth within a short peptide concentration increase are observed. Similar observations were made with the LAH4-L1 and LAH4 peptides (**data not shown**).

For the rest of this study, we tested antimicrobial activity on microplates under agitation. The experiments are currently underway but have been repeated at least twice for each peptide. The bacterial growth percentages for each experiment (noted: 1 to 4, and made in duplicates for some conditions, noted: ') are presented in **Figure 44 A, C, E** in function of peptide concentrations. Their combination for each condition is shown as the average (**Figure 44 B, D, F**). These experiments have been done the same way for LAH4-L1 and LAH4 peptides. The results for the three peptides are displayed as the average obtained for each condition: fibrils, mix and in solution (**Figure 45**). To get better view of each activities, experimental data were fitted with logistics function using OriginPro software. Logistics equation is $y_{min}+(y_{max}-y_{min})/(1+(x/x_{min})^p$ with p= slope, y= bacterial growth (%) and x= peptide concentration (µM).
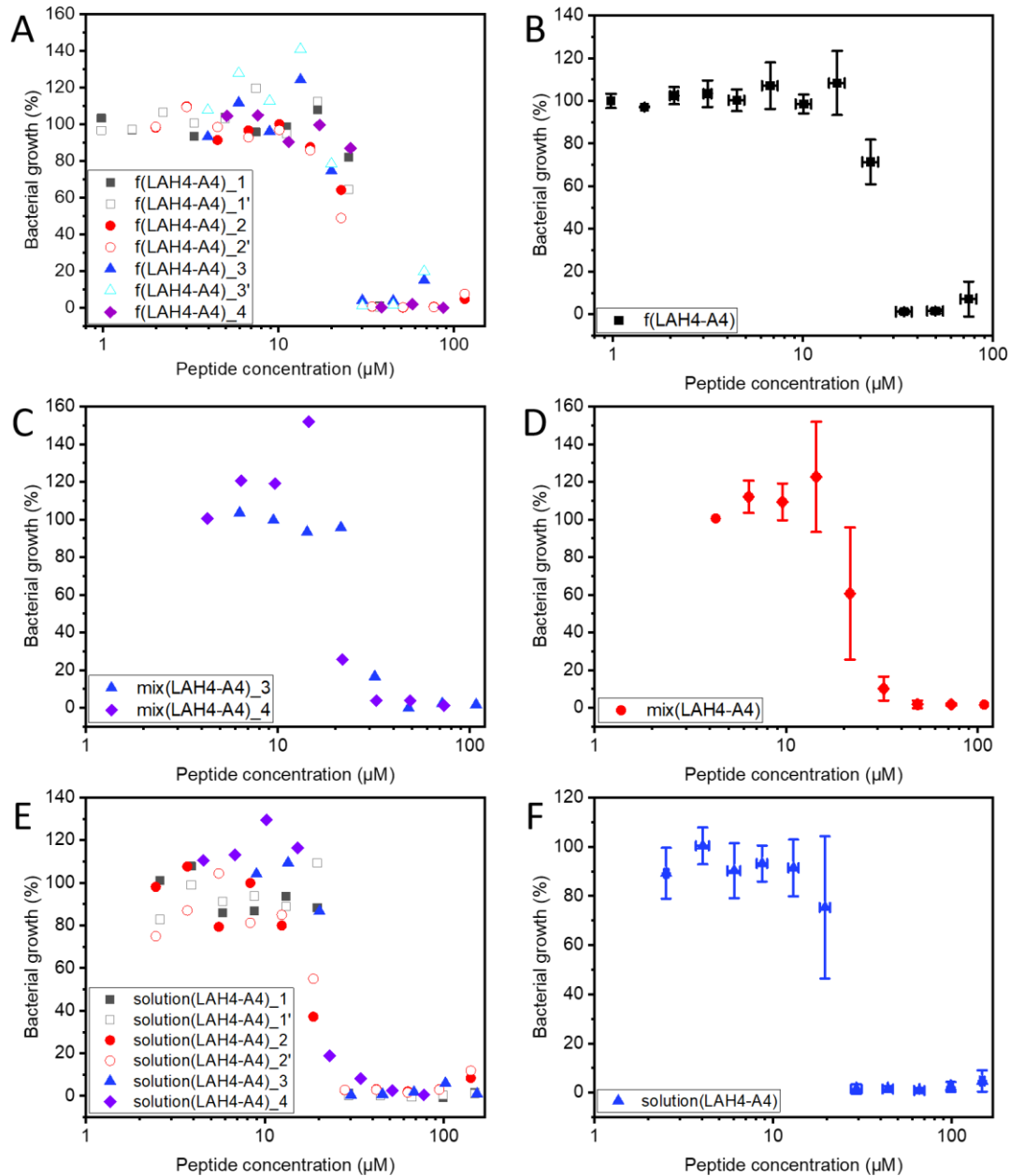
Figure 44: The bacterial growth percentage as a function of LAH4-A4 peptide concentration for three different conditions: Fibrils (A, B), mix with 50% of peptide in solution and 50% of fibrils suspension (C, D) and peptide in solution (E, F). Results of each experiment (noted from 1 to 4) and each duplicate (noted ') are presented in A, C, E. They are shown as average in B, C and F. Error bars in x include the variability in peptide concentration inter-experiments. The peptides (solution, fibrils or mix) are in 10 mM phosphate buffer at pH 7.4 and the experiments are done in MH at pH 5 with incubation at 37 °C under shaking.
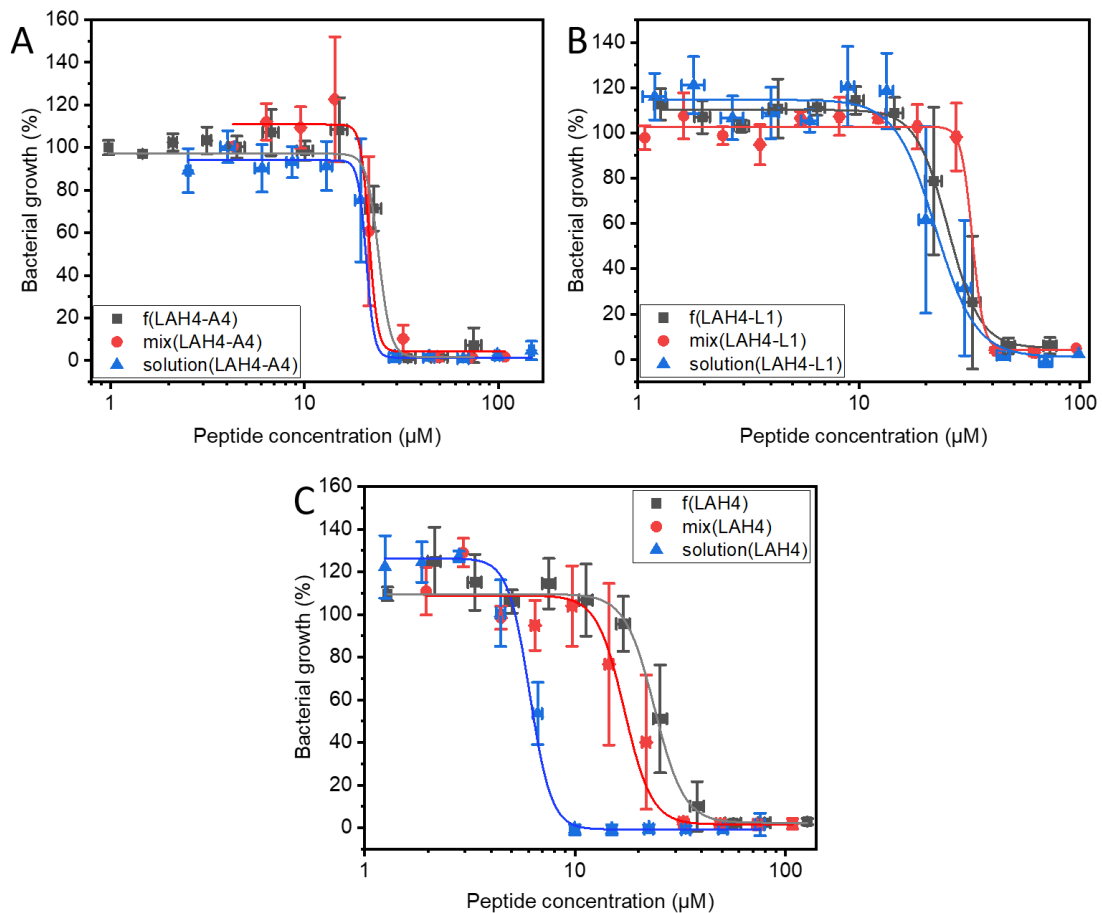
Figure 45: The bacterial growth percentage as a function of peptide concentration for LAH4-A4 (A), LAH4-L1 (B) and LAH4 (C) in the three conditions: peptide in solution (blue triangles), fibrils suspensions (grey squares) and mixtures (red dots). The average of the experimental data is shown as a percentage of bacterial growth of control without peptides (CT+) after background subtraction from control without bacteria (CT-). The tendency curves were fitted with the function $(y_{min}+(y_{max}-y_{min})/(1+(x/x_{min})^p)$ using the OriginPro software. All peptide preparations were done in 10 mM phosphate buffer either at pH 7.4 for LAH4-L1 and LAH4-A4 or at pH 6.2 for LAH4. The experiments are done in MH at pH 5 with incubation at 37 °C under shaking.

Antimicrobial assays have been used to determine MIC values for each peptide suspension of fibrils, in solution or a mixture of both (50/50). However, the experiments need to be repeated in order to have a more accurate MIC for some conditions (**Table 15**).

Peptide/MIC	Fibrils	Mixture	Solution
LAH4	56.4 ±4.8	32.6 ±1.5	9.9 ±0.5
LAH4-L1	47.4 ±3.1	41.2 ±0.9	44.9 ±3.1
LAH4-A4	34.1 ±3.2	48.4 ±0.5	29.3 ±1.9

Table 15: Summarizing the Minimum Inhibitory Concentration (MIC) including the standard deviation (SD) for LAH4, LAH4-L1 and LAH4-A4 depending on whether it is applied in solution, in fibrillar suspension or as a mixture of both (50/50). LAH4-L1 and LAH4-A4 (solution, fibrils or mix) are in 10 mM phosphate buffer either at pH 7.4 for LAH4-L1 and LAH4-A4 or at pH 6.2 for LAH4. The experiments are done in MH at pH 5 with incubation at 37 °C under. Error bars reflect the variability in peptide concentration inter experiments.

For LAH4-A4 and LAH4-L1 (**Figure 45 A, B**), bacterial growth curves almost overlapped whatever the peptide preparation: in solution, in fibrils, or a mixture of both. Even if they slightly differed for the LAH4-L1 peptide, the MIC remains in the same range around 40 µM (**Table 15**). For LAH4-A4 bacteria growth inhibition is observed around 29 µM for the peptide in solution, while for the fibrils around 34 µM is required. For the mixture, a concentration of 32 µM already leads to drastic bacterial growth inhibition (10% compared to CT+, **Figure 45 A**), but the MIC is considered to be at 48 µM (quasi-complete inhibition of bacterial growth) (**Table 15**). Moreover, these experiments are repeated just twice, and differences are reflected by the error bars in x and y axes, which are within the dilution factor range. In contrast, the LAH4 peptide antimicrobial activity varies depending on whether the peptide is in solution, as a fibrils suspension, or applied as a mixture of both (**Figure 45 C**). We find that LAH4 is much more active in solution than fibrils or as a mixture. Indeed, the needed peptide concentration to inhibit bacterial growth is either 10 µM or 56 µM or 33 µM respectively (**Figure 45 C**).

Although the three peptides are identical amino acid composition and secondary structure (in solution), they exhibit distinct antimicrobial activities where LAH4 presents the best activity. When added as a fibrils' suspension, they tend to decrease in antimicrobial activities. The LAH4 fibrils exhibit β-sheet conformation and a lower antimicrobial activity between 38 µM ≤MIC≤ 57 µM. The LAH4-A4 and the LAH4-L1 assemble into fibrils in an α-helical conformation with MICs of 34 µM and 47 µM, respectively (**Table 15**).

Interestingly, fibrillation of antimicrobial peptides results in no/moderate loss for peptides that have already low antimicrobial activities in solution (LAH4-L1 and LAH4-A4). However, a significant loss of antimicrobial activity is observed for LAH4 which exhibits good activity in solution. In this study, we can see any antimicrobial activity modification depending on the peptide state in the same buffer. LAH4-A4 and LAH4-L1 peptides are both in phosphate buffer at pH 7.4 where they show α-helix structure whatever in solution or in a fibrillar state. On the contrary, LAH4 peptides (in phosphate at pH 6.2) have different activities in solution or self-assembled as well as different structures into a β-sheet.

The reduction in fibrils activity can be explained by a different factor. The fibrils may have difficulty passing the bacterial outer membrane. Moreover, peptide self-assembly may lower the number of lipid molecules in contact with the peptide and is therefore expected to decrease the peptide influence on the membrane physical properties. The peptide aggregation can decrease the perturbation on the membrane by reducing the membrane surface area in contact with the peptide. In addition, the membrane partition of these large complexes may be more difficult to achieve or different mechanisms apply that our conventional models suggest [124].

IV.7.2 Transfection activity

After having tested the antimicrobial activities for these three peptides, we became interested in their transfection activity. Indeed, they have also increased efficiency of in vitro transfection of eukaryotic cell lines which has already enabled the design of LAH4-L1 [10] with the greatest transfection activity (*v.s.* **chapter I.2**). The peptides ability to transfect cells depending on whether they are in solution or assembled has been analysed. The analysis carried out by the Antoine Kichler group, consist only of preliminary results done in duplicate on a single experiment. Therefore, results will be analysed only in a qualitative manner since no statistical test can be carried out to be conclusive.

At first, we compared the three peptides LAH4, LAH4-L1 and LAH4-A4 transfection activity when applied to a solution containing 150 mM NaCl. In this test, different amounts of peptide were used from 5 µg to 24 µg for a constant amount 1.5 µg DNA. The DNA/peptide ratio play a role for transfection activity and may differ from one peptide to another. The optimal transfection conditions were determined to use increasing concentrations of peptide.

Efficiency of transfection of LAH4/DNA complexes has been compared with other known transfection agents of DNA. The effectiveness of the transfection of LAH4 in solution has already been shown to be better (>1 log) than other transfection compounds [17]. Therefore, it will be used as our reference. This analysis allowed us to determine the peptide with the greatest transfection activity.
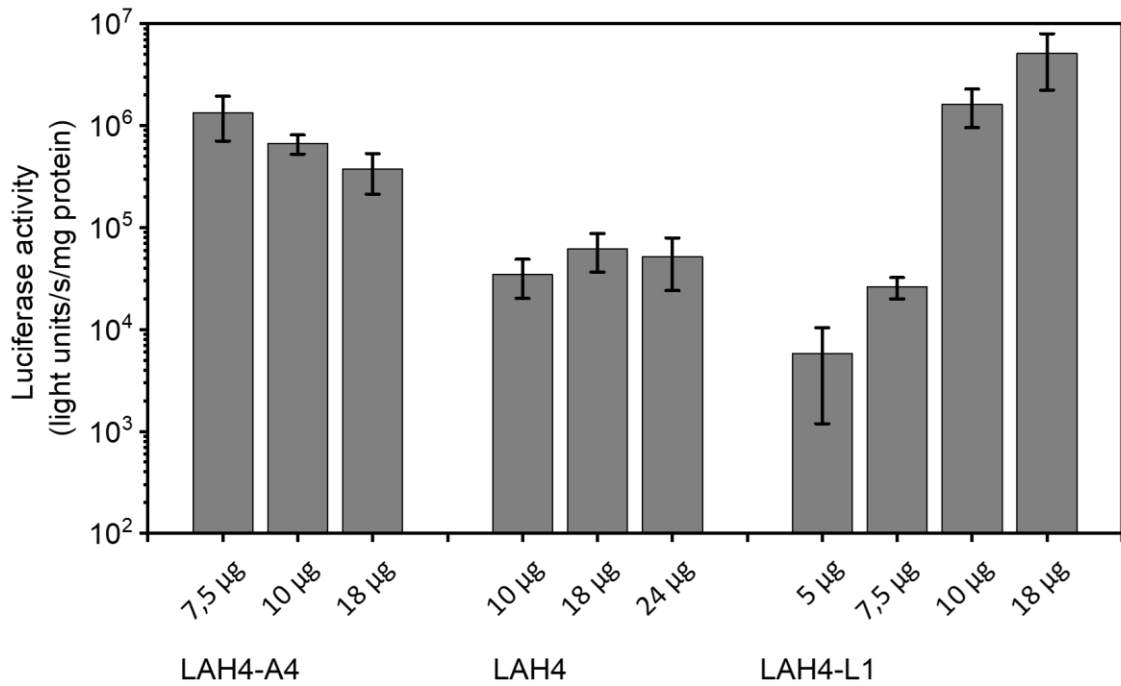
Figure 46 : LAH4-A4, LAH4 and LAH4-1 transfection efficiencies evaluated on human glioblastoma U87 cells as a function of peptide quantity (µg). Increasing amounts of peptide were mixed with a constant amount of reporter plasmid (1.5 µg of pDNA). The complexes were incubated for 2.5 hours with the cells plated in 48-well plates and medium was then replaced with fresh culture medium. Luciferase activity was measured 1-day post-transfection. Error bars represent the standard deviation of the mean of duplicates of a single experiment (and are shown on a logarithmic scale).

Figure 46 shows the LAH4-A4, LAH4 and LAH4-L1 and transfection activity. For the LAH4-A4, the best peptide quantity for transfection activity is 7.5 µg. When this quantity increases the luciferase activity decreases (**Figure 46**). The LAH4 peptide has a lower transfection activity by at least one log when compared to LAH4-A4. The transfection is favoured with 18 µg of peptide but does not vary much when different amounts of peptide are tested; indeed the error bars overlap. When 18 µg of LAH4-L1 peptide were added the highest transfection activity was observed. This transfection efficiency decreases when the amount of peptide is reduced. The variation in transfection activity with the peptide quantity covers +2 log in efficiency when doubling peptide quantity from 5 µg to 10 µg.

In a second step, the fibrils transfection activity was tested under conditions where we have shown that fibrils are stable, i.e., in phosphate buffer at pH 6.2 and 7.4. The rich MH medium used for antimicrobial experiment was also tested at pH 5 and 7, but the peptides in solution have transfection activity lower in presence of MH medium (**data not shown**).

The transfection activity was performed for the peptide in solution or in its fibrillar state. The LAH4, LAH4-L1 and LAH4-A4 peptides in solution have a different transfection activity depending on the quantity. The transfection activities for LAH4-L1 and LAH4 are highest with 18 µg of peptide but LAH4-A4 is more active with a lower quantity of 7.5 µg.

Based on the peptides' quantities giving the best transfection efficiency, two quantities were tested for LAH4, LAH4-L1 and LAH4-A4 in solution or for their self-assemblies: 7.5 µg and 15 µg for LAH4-L1 and LAH4-A4 while 15 µg and 25 µg of LAH4 peptide were mixed with 1.5 µg pDNA. The fibrils were quantified by HPLC to determine the exact amount of peptide before analysis. In addition, to be able to compare conditions between each peptide and with the antimicrobial activity experiment different buffers were used. These were both fibrillation buffers, namely 10 mM phosphate buffer at 6.2 and 7.4. For the peptide in solution, 10 mM acetate buffer at pH 5 was also included because it gives the best transfection activity for the peptide in solution (**Figure SI 10**). However, the fibrils are not stable in this buffer; therefore, it could not be used to test the self-assembled peptide activity. The luciferase activity after transfection with the LAH4-L1 peptide is shown in **Figure 47**.
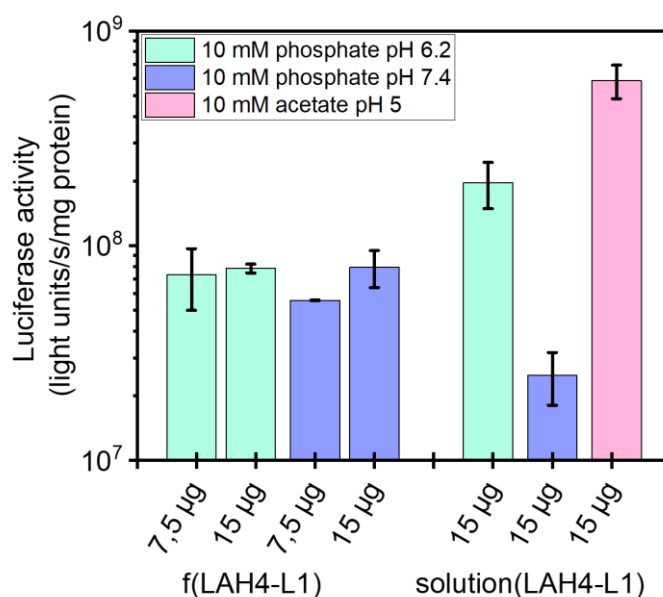
Figure 47: The LAH4-L1 transfection efficiency evaluated on human glioblastoma U87 cells as a function of the buffer used to transfect the pDNA complexed either with the peptide in solution or as fibrils. The experiment has been performed with two different peptide quantities (7.45 and 15 µg) and in 10 mM phosphate buffer at pH 6.2 (green) or pH 7.4 (purple) and in 10 mM acetate buffer at pH 5 (pink). Peptides were mixed with a constant amount of reporter plasmid (1.5 µg of pDNA). The complexes were incubated for 2.5 hours with the cells plated in 48-well plates and medium was then replaced with fresh culture medium. Luciferase activity was measured 1-day post-transfection. The transfection efficiency is expressed as light units/s/mg protein. Error bars represent the standard deviation of the mean of duplicates of a single experiment (and are shown on a logarithmic scale).

Figure 47 shows the best transfection efficiencies are obtained when the experiments are performed with solubilized peptide at acid pH with 10 mM acetate buffer. The peptide in solution in 10 mM phosphate is more active at pH 6.2 when compared at pH 7.4 (**Figure 47**). When the solution pH increases (pH 5, 6.2 or 7.4) the peptide is less effective in transfection with loss of one log from 5 to 7.4 and this for the same amount of peptide. At pH around 6.2, the peptide solution is more active when compared to the fibril. The fibril transfection activity remains in the same range whether at pH 6.2 or 7.4. The pH does not play a role in fibril activity. However, in the transfection assays at pH 7 LAH4-L1 fibrils are more active than the corresponding peptide solutions.

In a second experiment the luciferase activity after transfection with the LAH4-A4 peptide is tested and the results shown in **Figure 48**.
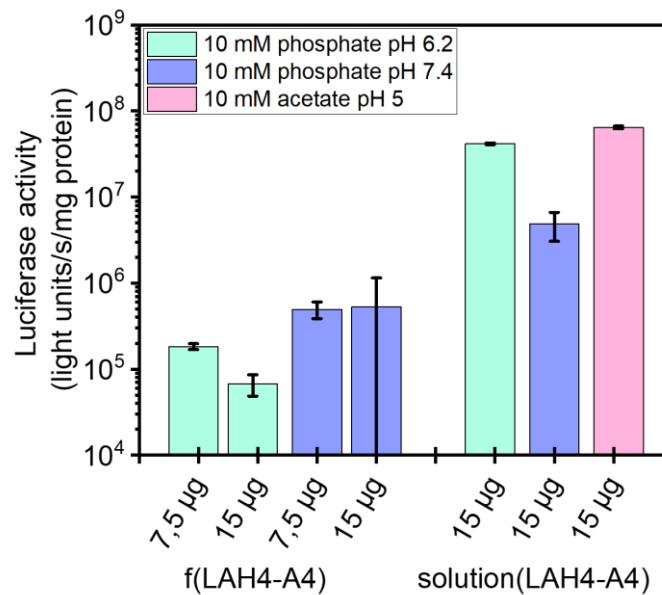

Figure 48: LAH4-A4 transfection efficiency evaluated on human glioblastoma U87 cells as a function of the buffer used to transfect the pDNA complexed either with the peptide in solution or as fibrils. The experiment has been performed with two different peptide quantities (7.45 and 15 µg) and in 10 mM phosphate buffer at pH 6.2 (green) or pH 7.4 (purple) and in 10 mM acetate buffer at pH 5 (pink). Peptides were mixed with a constant amount of reporter plasmid (1.5 µg of pDNA). The complexes were incubated for 2.5 hours with the cells plated in 48-well plates and medium was then replaced with fresh culture medium. Luciferase activity was measured 1-day post-transfection. Error bars represent the standard deviation of the mean of duplicates of a single experiment (and are shown on a logarithmic scale).

Figure 48 shows that the transfection activity of the LAH4-A4 is highest in the presence of acetate buffer at pH 5 or phosphate buffer at pH 6.2, but the transfection activity decrease with the phosphate buffer at pH 7.4 as previously observed for the LAH4-L1. The LAH4-A4 and LAH4-L1 in solution is more active at acidic pH (**Figure 48** and **Figure 47**). The LAH4-A4 fibril state are less active compared to in solution at both pH 6.2 and 7. The luciferase activity of LAH4-A4 fibrils at pH 6.2 is around 10^5 light units/s/mg of protein for the both quantities but at pH 7 is around 10^6 light units/s/mg of protein for 7.5 µg. For LAH4-A4 fibrils at pH 7 with

15 µg the experiment could not be conclusive. Indeed, one of the duplicates realized showed luciferase activity while the other did not which explains the huge error bar.

To finish, the luciferase activity after transfection with the LAH4 peptide is shown in **Figure 49**.
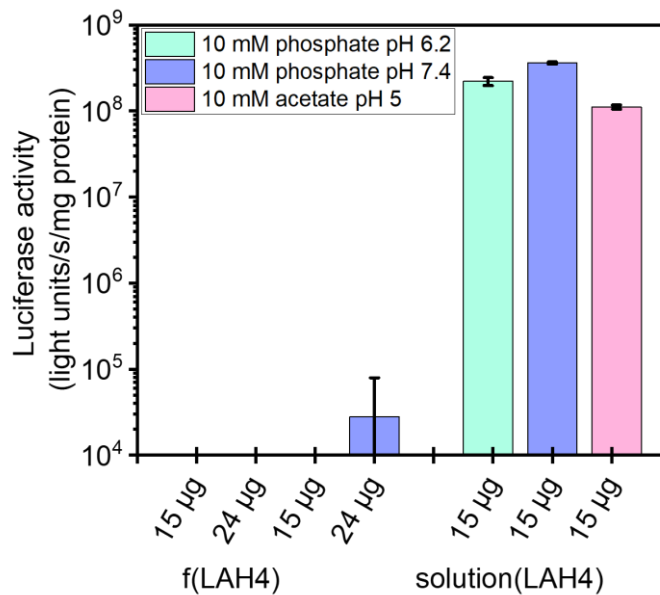

Figure 49: LAH4 transfection efficiency evaluated on human glioblastoma U87 cells as a function of the buffer used and if the peptide is added in solution or as fibrils. The experiments has been performed with two different peptide quantities (15 µg and 24 µg) and in 10 mM phosphate buffer at pH 6.2 (green) or pH 7.4 (purple) and in 10 mM acetate buffer at pH 5 (pink). Peptides were mixed with a constant amount of reporter plasmid (1.5 µg per duplicate of pDNA). The complexes were incubated for 2.5 hours with the cells plated in 48-well plates and medium was then replaced with fresh culture medium. Luciferase activity was measured 1-day post-transfection. Error bars represent the standard deviation of the mean of duplicates of a single experiment (and are shown on a logarithmic scale).

Figure 49 shows for LAH4 transfection activity in the same range for the three-buffers used, i.e., around 10^8 light units/s/mg of protein. There is no activity decrease observed with LAH4 when compared to LAH4-L1 and LAH4-A4 in the phosphate buffer at pH 7.4. However, in its fibril form the peptide shows no transfection activity in phosphate neither at pH 6.2 nor 7.4 (**Figure 49**). Like for LAH4-A4 fibrils, the experiment with 24 µg of LAH4 fibrils could not be conclusive, again only one of the duplicates showed luciferase activity.

IV.7.3 Biological conclusion

In this part, the different antimicrobial and transfection activities observed for the LAH4, LAH4-L1 and LAH4-A4 in solution or fibril state have been grouped in **Table 16**.

In order to be able to compare the results between antimicrobial peptides and transfection and also compare the peptides in the fibrils form or in solution, the conditions of peptide preparation were identical for both types of experiments. Therefore, we will consider the following condition for both tests: 10 mM phosphate buffer at pH 6.2 for LAH4 and at pH 7.4 LAH4-L1 and LAH4-A4; for transfection assays: 15 µg of peptide. In **Table 16** we can see antimicrobial or transfection results either fibrils or peptide in solution.

	Antimicrobial (µM)			Transfection Light units/s/mg protein	
	fibrils	mixture	solution	fibrils	solution
LAH4-L1	47.4 ±3.1	41.2 ±0.9	44.9 ±3.1	7.93×10^7 ±6.9×10^6	2.5×10^7 ±1.6×10^7
LAH4-A4	34.1 ±3.2	48.4 ±0.5	29.3 ±1.9	5.29×10^5 ±6.2×10^5	4.8×10^6 ±1.8×10^6
LAH4	56.5 ±4.8	32.6 ±1.5	9.9 ±0.5	None	2.2×10^8 ±$2.3 * 10^7$

Table 16: Summarizing the Minimum Inhibitory Concentration (MIC) for E.coli or transfection efficiency on human glioblastoma U87 cells for LAH4, LAH4-L1 and LAH4-A4. The results are shown depending on peptide preparation in solution, in fibrillar suspension or as a mixture of both (50/50). All peptide preparations were performed in 10 mM phosphate buffer either at pH 7.4 for LAH4-L1 and LAH4-A4 or at pH 6.2 for LAH4. For antimicrobial assays, all experiments are performed in MH at pH 5 with incubation at 37 °C under shaking. Error bars in x reflect the variability in peptide concentration between experiments repeated at least twice. For transfection experiments 15 µg peptide were mixed with 1.5 µg of pDNA. Error bars represent the standard deviation of the mean of duplicates of a single experiment (and are shown on a logarithmic scale).

The LAH4-L1 has the same tendency whether for antimicrobial activities or transfection in the fibrillation buffer. Indeed, LAH4-L1 does not vary so much in antimicrobial activity, its MIC is around 40 μM in solution or fibril state (**Table 16**). Similarly, transfection activities in the fibrillation buffer this peptide (solution or fibril) are in the same logarithmic range around 10^7 light units/s/mg of protein. The LAH4-A4 is a little more active in solution than in fibrils for both antimicrobial and transfection activities. Indeed, the LAH4-A4 peptide has antimicrobial activity with MIC at 29 μM when the peptide is in solution while when it is in the fibrils form its MIC increases to 34 μM and for the transfection efficiency there is one log of difference between the peptide in solution and fibrils (**Table 16**).

LAH4-L1 and LAH4-A4 are finally two peptides that do not present to much change in transfection activity whatever they are in solution or added as fibrils in their fibrillation buffer. However, this comparison is made with the fibrillation buffer which does not show the best transfection activities for LAH4-L1 and LAH4-A4 in solution. Indeed, the transfection activity of these two peptides is favoured in the presence of acetate buffer at pH 5 with an increase of 1 log.

The LAH4 peptide is much more active in solution with a MIC at 9.9 μM against bacteria while in the fibrils form its MIC increases to 56.5 μM. in a similar way, LAH4 completely loses its transfection activity when it is self-assembled (**Table 16**).

Although the three peptides share identical amino acid composition, they behave quite differently. All of them are structured as α-helix when in solution. Whereas the fibrils formed by LAH4-L1 and LAH4-A4 also present α-helical structure, LAH4 fibrils a made-up form β-sheet structures.

Interestingly, the fibrils formed by LAH4 have completely lost their antimicrobial and transfection activities. It would be interesting to study the ability of the β-sheet fibrils to insert into the membrane [125] as it may influence this decrease in antimicrobial and transfection activity [24]. Loss of transfection activity can be explained by a blocking at different stages of the transfection process (*v.s.* **Figure 3**): complexation with DNA, membrane interaction, complex internalization or dissociation.

For the α-helical peptides LAH4-L1 and LAH4-A4, their antimicrobial activities are identical for the peptide in solution or fibril with fibrillation buffer. The LAH4-L1 and LAH4-A4 fibrils have transfection activity found in the same logarithmic scale 10^7 light units/s/mg of proteins

whether in 10 mM phosphate at pH 6.2 or 7.4. For LAH4-A4, the transfection activity with 15 μg could not be conclusive given the huge error bar but with less fibrils (7.5 μg) in the same buffer transfection activity decreases by 1 log when compared to the solution. The LAH4-A4 and LAH4-L1 the fibrils in α-helical structure do not completely lose their activities, which is not the case for LAH4 with β-sheet structure. The transfection activities of LAH4-L1 and LAH4-A4 fibrils are lower compared to peptides in an acetate buffer. Phosphate especially at high pH may cause aggregates to form in a manner related to the fibril formation under more specific conditions. This may explain why acetate buffer is much more active: pH and the absence of the bivalent phosphate. Indeed, this experiment shows best transfection when using the acetate buffer, at pH 5 for all three peptides in solution.

This modification of pH (6.2 to 7.4) for fibrillation may impact the self-assembly. Indeed, LAH4-A4 and LAH4-L1 adopt an α-helical structure in the presence of 10 mM phosphate buffer at pH 7.4, while LAH4 fibrils adopt a β-sheet structure with phosphate at pH 6.2. The pH of fibrillation buffer next to the histidine pKa could alter the conformation and activities [126].

In the laboratory, Magainin 2 and PGLa, two antimicrobial peptides, have been shown to be able to form fibrils with a β-sheet/turn signature [110]. As published, these peptides forms fibrils in the presence of Mueller Hinton medium or phosphate buffers at different pH, they may dissociate inversely when exposed to watery environments of appropriate composition (e.g., acidic conditions, absence of phosphate or presence of detergent). In addition, the peptide fibrillation results in a decrease of their individual antimicrobial activities as found for LAH4 peptides. There are three antimicrobial peptides with different sequences adopting β-sheet secondary structures in fibrils. Maybe the interactions with these peptides have a similar action mode [125].

IV.8 Conclusion

In this chapter, we were able to monitor the different self-assembly conditions for the three peptides LAH4, LAH4-L1 and LAH4-A4.

First, the experiments were carried out on LAH4-A4, making it possible to note the pH importance of pH on the fibrillation of these peptides. Moreover, the phosphate plays an important role in the self-assembly in fibrils [34]. Whereas a high concentration of phosphate ions causes peptide aggregation ([106], *v.s.* **Figure 32**) this process is reversible when transferred in water (**Figure 37**). In addition, stability studies on the fibrils formed by dialysis has shown a reversible process dependent on the presence of phosphate where defibrillation occurs in Tris or acetate buffer while in phosphate buffer the fibrils are stable (**Figure 31**).

In addition, the fibrillation conditions have been optimized allowing better yields of around 70% for LAH4-A4, 60% LAH4-L1 and 50% for LAH4.

Secondly, self-assembly of LAH4-L1 and LAH4 was carried out. Conditions for self-assembly are different for LAH4 when compared to LAH4-A4 and LAH4-L1. Indeed, LAH4-A4 and LAH4-L1 self-assemble in the presence of 10 mM phosphate buffer at pH 7.4 and the peptides secondary structure in the fibrils is α-helical. In contrast, LAH4 fibrils form in phosphate buffer at pH 6.2 close to the histidines' pKa and the peptides adopt a β-sheet structure.

This structural modification must be directly linked to the histidine position. In addition, the self-assembly mechanism may be different, LAH4 needs a pH close to the histidines pKa otherwise it does not structure at pH 7.4 (0%). There may be charge distributions between the histidines of the different peptide molecules, restructuring itself by adopting a β-sheet. While LAH4-A4 is less sensitive to pH variation and the fibrillation percentage increases from pH 6.2 to pH 7.4, there may be association of the peptides via hydrophobic interactions allowing then to keep their assembly in an α-helical conformation. Their histidine orientation in the secondary structure can alter self-assembly of the peptide, resulting in two different conformations: α-helix or β-sheet.

To identify the factors influencing the formation of fibrils, it would be interesting to analyse in more detail the stability conditions of these fibrils and the kinetics of fibrillation [99]. We have seen the influence of phosphate in self-assembly of these peptides. In addition, it would be interesting to see if phosphate is involved in fibrillation, which can be investigated by

120

solid-state NMR ^{13}C-^{31}P distance measurements to eventually detect spatial proximities between peptides and phosphates.

In addition, preliminary analyses of the antimicrobial and transfection activities showed differences depending on the peptide whether they are in solution or self-assembled. These analyses showed a loss of activity for LAH4 peptides when it is self-assembled in β-sheet. In addition, LAH4-L1 and LAH4-A4 do not promote antimicrobial or transfection activity when they are self-assembled as α-helical fibrils. The transduction activities still need to be tested to find out if the fibrils have more activity than the peptides in solution.

The peptides in solution have already shown a capacity to insert and deform the model membranes. So it would be interesting to check the bilayer interaction of fibrils and to compare their insertion and deformation on model membranes by solid-state NMR spectroscopy [62], infrared spectroscopy [125], calcein release according to their fibril structure. Loss of transfection activity for LAH4 can be explained by a blocking at different stages of the transfection process. The inactivity of LAH4 fibrils in transfection which may be related to their structure is due to the absence of association with DNA or the lack of dissociation inside the endosome or the cytoplasm. Solid-state NMR spectra [127] or electrophoretic mobility shift assays may show the formation of complex peptide/DNA. In order to get more information on these fibrils, the peptide-peptide interactions will be interesting to analyse by solid-state NMR spectroscopy in order to decipher the self-assemblies of these peptides and the differences between peptides. These peptide-peptide interactions were investigated for LAH4-A4 by solid-state NMR spectroscopy and RX diffraction technics and are presented in the following (**chapter V**).

V.   LAH4-A4 structural studies

V.1 Introduction

The functionalities and supramolecular assemblies of peptides of the LAH4 family can be finely tuned by changing the buffer composition (pH, salt, ions) or by modest changes in their sequence [10] [17] [40] [84]. **Chapter IV** shows the LAH4-A4 peptide self-assembly conditions. In addition, the LAH4-A4 fibrils secondary structure was characterized by ssNMR spectroscopy and FTIR showing an α-helical structure. In order to collect detailed information on the peptide structure in fibrils self-assembly, solid-state NMR spectroscopy was used. Magic-angle spinning (MAS) solid-state NMR spectroscopy (ssNMR) has proven to be a method allowing for structural and dynamic studies in particular for biological samples. Examples are structural investigations of protein, amyloid fibrils and membrane peptides and proteins or oligomeric assemblies [128] [129] [130] [131] [132].

LAH4-A4 (vectofusin-1) is composed of 26 residues, but only four different types of amino acids are present namely leucines, alanines, lysines and histidines. Because of the high redundance in composition it is difficult to assign the resonances in the NMR spectra. Indeed, the chemical shifts of the 8 alanines are expected in the same spectral region. By preparing the peptides by solid-phase peptide synthesis, they can be labelled specifically with ^{15}N and ^{13}C. The labelling strategy is summarized in **Table 17**.

LAH4-A4	Sequence label with ^{15}N and ^{13}C (red)
Sample 1	KKALL HAALA HLLAL AHHLL ALLKK A
Sample 2	KKALL HAALA HLLAL AHHLL ALLKK A
Sample 3	KKALL HAALA HLLAL AHHLL ALLKK A
Sample 4	KKALL HAALA HLLAL AHHLL ALLKK A

Table 17: Sequence of LAH4-A4 where the ^{15}N and ^{13}C labelled regions are shown in red KKALLHAALAHLLALAHHLLALLKKA.

Different regions in the sequence were selected to cover the extremities (Nter and Cter) or the peptide central parts, consequently almost all the entire peptide was labelled at some point. Alanines, leucine and lysines were chosen as amino acids in this first study for their moderate cost. In addition, only four or five amino acids were labelled at the same time to be able to assign them easily.

Initially, the solution-state NMR from samples labelled with $^{13}C/^{15}N$ was carried out to have the LAH4-A4 assignment and structure in solution. Thereafter self-assembled structures were formed from peptides labelled at different positions to analyse the LAH4-A4 fibril structure by solid-state NMR.

Comparison between the structure determined in liquid and in fibril form of the peptide will be performed. First the secondary structure can be determined using the chemical shift values (TALOS+ and CSI) then distance information can be obtained based on two-dimensional solid-state NMR experiments such as DARR or hNCO/hNCα from samples labelled with ^{13}C and ^{15}N. Besides, to get more information about the self-organization of these fibrils small-angle X-ray scattering (SAXS) and wide-angle X-ray scattering (WAXS) experiments were carried out. The part of solid-state MAS ssNMR work to obtain structural models of these fibrils already started but is still in progress.

V.2 Materials and Methods

Peptide synthesis

The LAH4-A4 peptides (KKALLHAALAHLLALAHHLLALLKKA-NH$_2$) were prepared by solid-phase synthesis using a Millipore 9050 automatic peptide synthesizer and Fmoc chemistry. The sequences and their abbreviations or colour used in the text are the following. At the underlined and red positions, the amino acids were uniformly labelled with ^{15}N and ^{13}C (**Table 17**).

The peptides were purified by reverse phase HPLC (Gilson, Villiers-le-Bel, France), the chromatograms were recorded at 214 nm using a preparative C18 column (Luna, C-18-100 Å-5 µm, Phenomenex, Le Pecq, France) using an acetonitrile/water gradient buffered with 0.1% TFA. The gradient runs from 35% to 70% acetonitrile. The identity and purity (>90%) of the peptides were checked by MALDI-TOF mass spectrometry (MALDI-TOF Autoflex, Bruker Daltonics, Bremen, Germany). The purified peptides were dissolved three times in 4% (vol) acid acetic at 1 mg/ml concentration with subsequent lyophilization to ensure exchange of the TFA counter anions to acetate. The lyophilized peptides were stored at -20 °C.

Solution-state NMR sample preparation

The peptide (2 mg) was dissolved in 500 µl of a mixture of 50% (*v/v*) deuterated trifluoroethanol (TFE-d$_3$) and 50% of aqueous (H$_2$0) 25 mM d$_{11}$-Tris buffer with 2,2-dimethyl-2-sila-pentane-5-sulphonic acid (DSS) (2.5 mM) as 1H chemical shift reference. All solutions have a pH of around 5.

The experiments were performed on a 500 MHz liquid-state NMR spectrometer (Bruker Avance III) with a 5 mm cryo-probe X-^{1}H (with ^{31}P≤X≤^{15}N) and were recorded at a temperature of 300 K. One-dimensional ^{1}H, as well as two-dimensional correlation experiments (^{1}H-^{1}H TOCSY, ^{1}H-^{1}H NOESY, ^{1}H-^{15}N HSQC, ^{1}H-^{13}C HSQC, ^{1}H-^{13}C HSQC-NOESY, ^{1}H-^{15}N HSQC-NOESY) were recorded from labelled and natural abundance peptides. The 90° and water suppression pulses were optimized on the first spectrum in natural abundance and the same conditions were used for the labelled sample. The measurements are performed by the "service de résonance magnétique nucléaire" from our institute.

For one dimensional ¹H, the following parameters were used: 90° pulse of 12 μs; 20 ppm spectral width; 3 ms acquisition time; 1 s recycle delay; 50 μs dwell time; 59998 time domain data points; and 32 number of scans.

For two-dimensional correlation experiment (HSQC, HSQC-NOESY, HSQC-TOCSY for ¹H-¹⁵N and ¹H-¹³C).

¹H-¹H TOCSY were measured with a Bruker standard pulse sequence "dipsi2esgpph", the following parameters were used: 90° pulse of 11.9 μs (¹H); 10 ppm and 10 ppm spectral width; 999 ms and 51 ms acquisition time; 9998 and 512 time domain data points; respectively for the two dimensions (F2 and F1). Recycle delay of 2 s; 100 μs dwell time; 8 number of scans.

¹H-¹H NOESY were measured with a Bruker standard pulse sequence "noesyesgpph", the following parameters were used: 90° pulse of 11.9 μs (¹H); 10 ppm and 10 ppm spectral width; 999 ms and 51 ms acquisition time; 9998 and 512 time domain data points; respectively for the two dimensions (F2 and F1). Recycle delay of 2 s; 100 μs dwell time; 200 ms mix time and 8 number of scans.

¹H-¹³C HSQC were measured with a Bruker standard pulse sequence "hsqcctetgpsp.2", the following parameters were used: 90° pulse of 11.9 μs (¹H) and 9.5 μs (¹³C); 15 ppm and 20 ppm spectral width; 250 ms and 12 ms acquisition time; 3748 and 512 time domain data points; (F2 and F1) respectively. Recycle delay of 2 s; 66.66 μs dwell time; 90 ms mix time and 8 number of scans.

¹H-¹⁵N HSQC were measured with a Bruker standard pulse sequence "hsqcetgpsisp2.2", the following parameters were used: 90° pulse of 11.9 μs (¹H) and 14 μs (¹⁵N); 15 ppm and 160 ppm spectral width; 200 ms and 126 ms acquisition time; 2998 and 256 time domain data points; respectively for the two dimensions (F2 and F1). Recycle delay of 2 s; 83.2 μs dwell time; 16 number of scans.

¹H-¹³C HSQC-NOESY were measured with a Bruker standard pulse sequence "hsqcetgpnosp", the following parameters were used: 90° pulse of 11.9 μs (¹H) and 9.5 μs (¹³C); 12 ppm and 60 ppm spectral width; 250 ms and 34 ms acquisition time; 3004 and 512 time domain data points; 300 ms and 60 ms mix time; respectively for the two dimensions (F2 and F1). Recycle delay of 2.2 s; 83.2 μs dwell time; 8 number of scans and 300 ms mix time.

¹H-¹⁵N HSQC-NOESY were measured with a Bruker standard pulse sequence "hsqcetgpnosp", the following parameters were used: 90° pulse of 11.9 µs (¹H) and 14 µs (¹⁵N); 12 ppm and 4 ppm spectral width; 200 ms and 552 ms acquisition time; 2402 and 224 time domain data points; 200 ms and 90 ms mix time; respectively for the two dimensions (F2 and F1). Recycle delay of 2.2 s; 83.2 µs dwell time, 20 number of scans and 200 ms mix time.

¹H-¹³C HSQC-TOCSY were measured with a Bruker standard pulse sequence "hsqcdietgpsisp.2", the following parameters were used: 90° pulse of 11.9 µs (¹H) and 9.5 µs (¹³C); 12 ppm and 60 ppm spectral width; 250 ms and 34 ms acquisition time; 3004 and 512 time domain data points; respectively for the two dimensions (F2 and F1). Recycle delay of 2.2 s; 83.2 µs dwell time; 8 number of scans and 60 ms mix time.

¹H-¹⁵N HSQC-TOCSY were measured with a Bruker standard pulse sequence "hsqcdietgpsisp.2" the following parameters were used: 90° pulse of 11.9 (¹H) µs and 14 µs (¹⁵N); 12 ppm and 6 ppm spectral width; 200 ms and 631 ms acquisition time; 2402 and 384 time domain data points; respectively for the two dimensions (F2 and F1). Recycle delay of 2.2 s; 83.2 µs dwell time; 20 number of scans and 50 ms mix time.

Fibrillation protocol in microtubes

The peptide was dissolved in 50% ethanol over 30 minutes to reach a concentration of 10 mM and sonicated in a bath to obtain the monomeric peptide. The peptide solution was then diluted in 10 mM phosphate buffer at pH 7.4 to a 0.5 mM final peptide concentration. Fibrillation was conducted under vigorous shaking for two days in the Eppendorf Mixer 5432 at room temperature (20-30°C). The fibrils were transferred in tubes and centrifuged at 16,000 g during 1 minute and the supernatant was removed. The pellet was washed with 10 mM phosphate buffer at pH 7.4 to avoid defibrillation. The solution was again centrifuged at 16,000 g for 30 minutes to remove the "free" peptide in solution.

Solid-state NMR sample preparation

The fibrils were resuspended in 10 mM phosphate buffer at pH 7.4 and transferred into a 200 µl pipette tip previously sealed by heat. Several centrifugation steps at 16,000 g for 30 minutes were executed to remove the maximum of phosphate buffer and concentrate the pellet. The fibrils were transferred to a 2.5 mm MAS rotor by centrifugation at 6,000 g maximum until the rotor was full.

MAS solid-state NMR

All 1D and 2D solid-state NMR spectra were recorded on a Bruker[TM] AVANCE 500 MHz wide bore spectrometer operating at a frequency of 500.03 MHz for ^{1}H (125.7 MHz for ^{13}C), with the same experimental and processing conditions for 1D's as given in previous **chapter II.2.2** and **IV.2** for ^{13}C (probe, spinning frequency, temperature, radiofrequency fields, apodization function, etc.). ^{15}N 1D spectra (**data not shown**) are only differing by their spectral windowing and Hartmann-Hahn conditions that were set as follow: fields adjusted to 72 kHz for ^{1}H and 47 kHz for ^{15}N and a 24.41 Hz/pt resolution at 50.67 MHz (2048 data points in time domain and 25 kHz, i.e., 493.35 ppm, for the spectral width and a 50 Hz Lorentzian apodization function was applied prior to Fourier transform over 4096 points (zero filling by 2048 points). Chemical shifts are given respective to TMS following standard substitution methods: adamantane for ^{13}C and NH$_4$Cl for ^{15}N [109] [133].

2D ^{13}C-^{13}C spectra

2D ^{13}C-^{13}C spectra were acquired using a Dipolar Assisted Rotational Resonance (DARR) pulse sequence [65]. Spectral parameters and radiofrequency fields were identical to 1D's, including recycling time, and a 25 kHz ^{1}H RF-field was used during the t1 evolution time (equal to the spinning speed). 384 increments of 512 scans each were acquired, spaced by a 40 µs evolution time and leading to a 130 Hz/pt spectral resolution in the indirect dimension. A squared sinebell window (π/2 shifted) were applied in both dimensions before Fourier transform over 4096 (F2 dimension) and 1024 points (F1 dimension).

2D hNCO and hNCα spectra

2D hNCO and hNCα spectra were acquired following the principles described previously (**chapter II.2.2**) [66]. The RF conditions for the first CP step, from ^{1}H to ^{15}N, was kept identical to the preceding 1D description (72 kHz for ^{1}H and 47 kHz for ^{15}N). ^{13}C Decoupling during evolution (sandwiched π pulse) relied on a 42 kHz B1 field while ^{1}H decoupling was done by a 75 kHz RF field, ensuring no CP from ^{1}H to ^{13}C could occur. The final selective magnetization transfer from ^{15}N to ^{13}C was carefully set to only polarize CO's or Cα's, i.e.: 5 kHz for ^{13}C and 30 kHz for ^{15}N while keeping ^{1}H decoupling set to 70 kHz (avoiding any other magnetization transfer than ^{15}N to ^{13}C). 32 increments of 2048 scans each were acquired, spaced by a 1315 μs evolution time, leading to a 47 Hz/pt spectral resolution in the indirect dimension (15 ppm ^{15}N spectral width, centered at 116.7 ppm). A 25 Hz Lorentzian broadening was applied in the direct dimension while a squared sinebell window (π/2 shifted) in the indirect dimension before Fourier transform over 2048 (F2 dimension, no zero filling) and 1024 points (F1 dimension, 992 points zero-filling).

V.3 Characterization of LAH4-A4 in solution

Various studies have been carried out previously using solution NMR spectra giving structural information on the LAH4 peptide [12] [127]. Of special interest is the LAH4 in presence of TFE, in this solvent peptide adopts an α-helical structure in the L4-L23 region [12].

In this part the LAH4-A4 peptide will be analysed for the first time by liquid-state NMR spectroscopy, this analysis will allow us to collect the full assignment (^1H, ^{13}C, ^{15}N) and collect structural information [134]. This study will then allow us to compare the peptide solution structure with its fibrillar form.

In previous liquid-state NMR experiments, the LAH4 peptide was solubilized in 50% trifluoroethanol (TFE). TFE often causes an increase in peptide helicity [135]. The same conditions were used here for the spectral acquisition for LAH4-A4 peptides. LAH4-A4 peptides (1.5 mM) was solubilized in (v/v) 50% TFE-d_3 and d_{11}-Tris (25 mM) in water at pH around 7. In addition, different parts of the sequence were labelled uniformly with ^{15}N and ^{13}C (KKALLHAALAHLLALAHHLLALLKKA) and were studied under the same conditions allowing for easy assignment.

For assignment ^{15}N and ^{13}C assignments one-dimensional ^1H, as well as two-dimensional correlation experiments ^1H-^{15}N HSQC, ^1H-^{13}C HSQC, ^1H-^{13}C HSQC-NOESY, ^1H-^{15}N HSQC-NOESY spectra were performed. The experiments were performed on a 500 MHz solution state NMR spectrometer at T=300 K.

First, we have compared the protons' 1D NMR to ensure that there no modification occurred between the different samples.
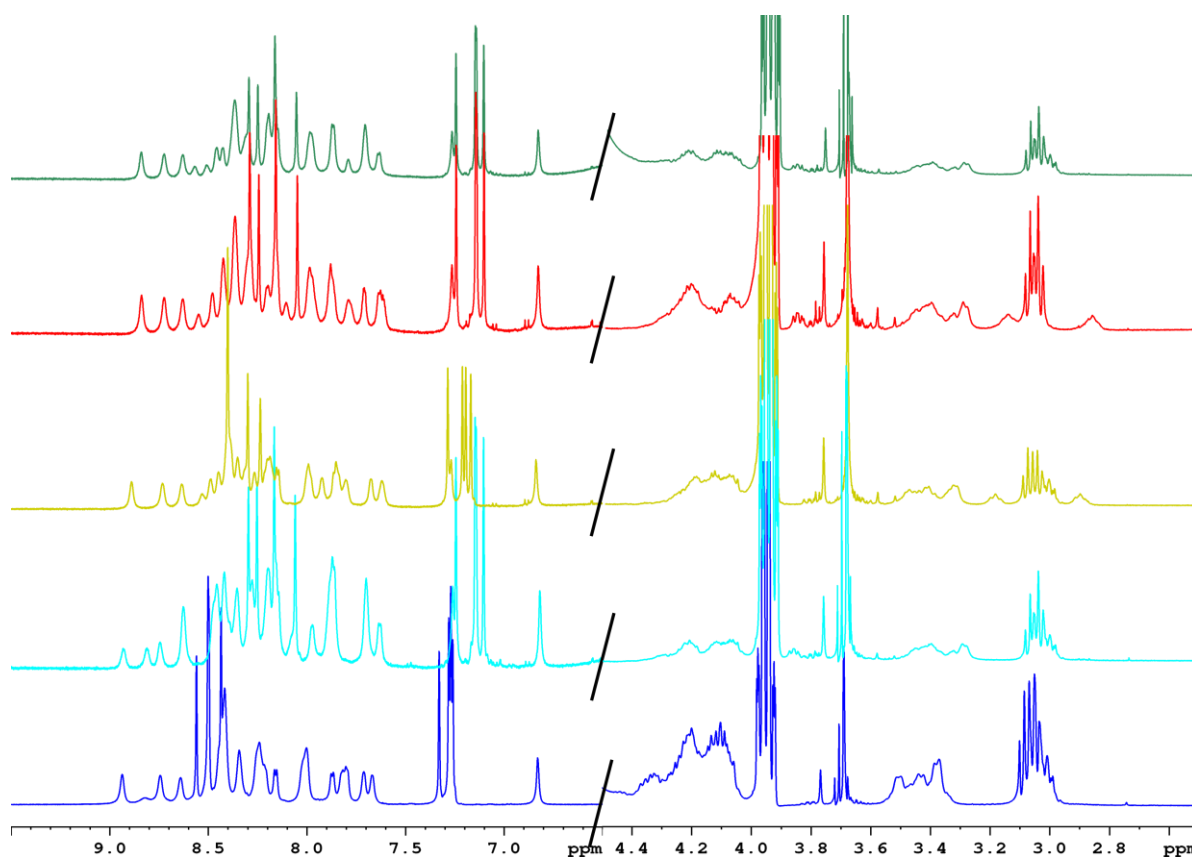
Figure 50: 1D proton liquid-state NMR spectra of LAH4-A4 in solution with 50% of TFE at pH around 6. The unlabelled peptide (dark blue) and the different labelled regions (^{15}N and ^{13}C). KKALLHAALAHLLALAHHLLALLKKA are shown.

Figure 50 shows the LAH4-A4 1D proton spectra, different colours are used according to the labelled region in the sequence KKALLHAALAHLLALAHHLLALLKKA and in dark blue LAH4-A4 spectra in natural abundance. In **Figure 50** the characteristic amino acids chemical shift is seen in the amides' proton around 8 ppm and the α protons around 4 ppm [136]. We can see that there is no chemical shift modification in 1D spectra for the peptides labelled in the α protons in the region around 4 ppm. In addition, the region between 6.8 ppm and 7.2 ppm corresponding to the side chains of lysines and imidazole rings of the histidines [134]. Structural changes should manifest themselves by change in chemical shift, changes in the proton chemical shifts are observed between the spectra labelled (**Figure 50**) (KALL, AALA, LLALA and ALLK) and natural abundance (**Figure 50** dark blue). Knowing that LAH4 peptide secondary structure change with pH, a pH check has been carried out on the different peptides after acquisition. Indeed, for all the labelled sample presented pH was around 5= (5.42, 5.34, 4.90 and 5.23) instead of the expected at pH 7. However, for the natural abundance sample pH is

6.1 this could explain the chemical shift change in the region between 6.8 ppm and 7.2 ppm. However, we have used the different labelled samples to facilitate the assignment.

Peptide labelled in different regions (in colour) KKALLHAALAHLLALAHHLLALLKKA were assigned. 2D ^{1}H-^{15}N HSQC shows the correlation between protons and the directly bound nitrogen nuclei for each amino acid and the ^{1}H-^{15}N HSQC-NOESY shows further protons close in space (**Figure 51**).
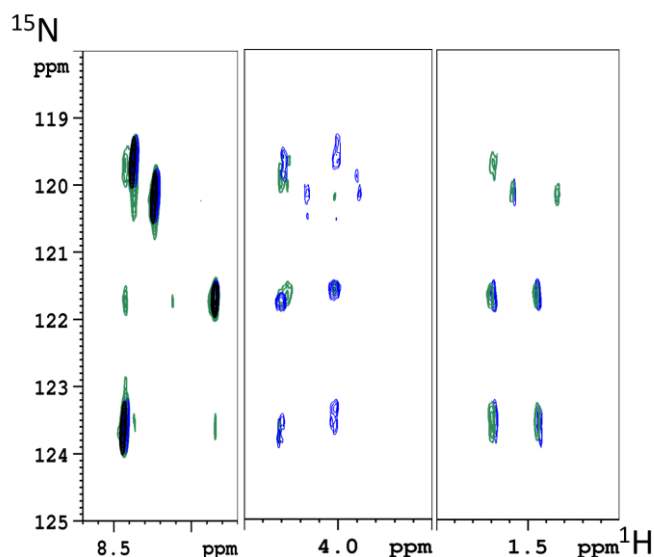

*Figure 51: 2D solution state spectra of LAH4-A4 in 50% TFE/50% water solution. ^{1}H-^{15}N HSQC (black) and ^{1}H-^{15}N HSQC-NOESY (green) and ^{1}H-^{15}N HSQC-TOCSY (blue) shows the correlations for a peptide labelled in the region: **KKALLHAALAHLLALAHHLLALLKKA.***

This allowed for each labelled region establish the connectivity between neighbouring residues through the NOE contacts allowing the assignment of the ^{1}Hα nuclei. ^{1}H-^{15}N HSQC-TOCSY creates correlations between all protons allows to have more detail (**Figure 51**). 2D ^{1}H-^{15}N HSQC in black shows the N-H correlations, and ^{1}H-^{15}N HSQC-NOESY in green shows the correlation between the residues and ^{1}H-^{15}N HSQC-TOCSY in blue shows all correlations.

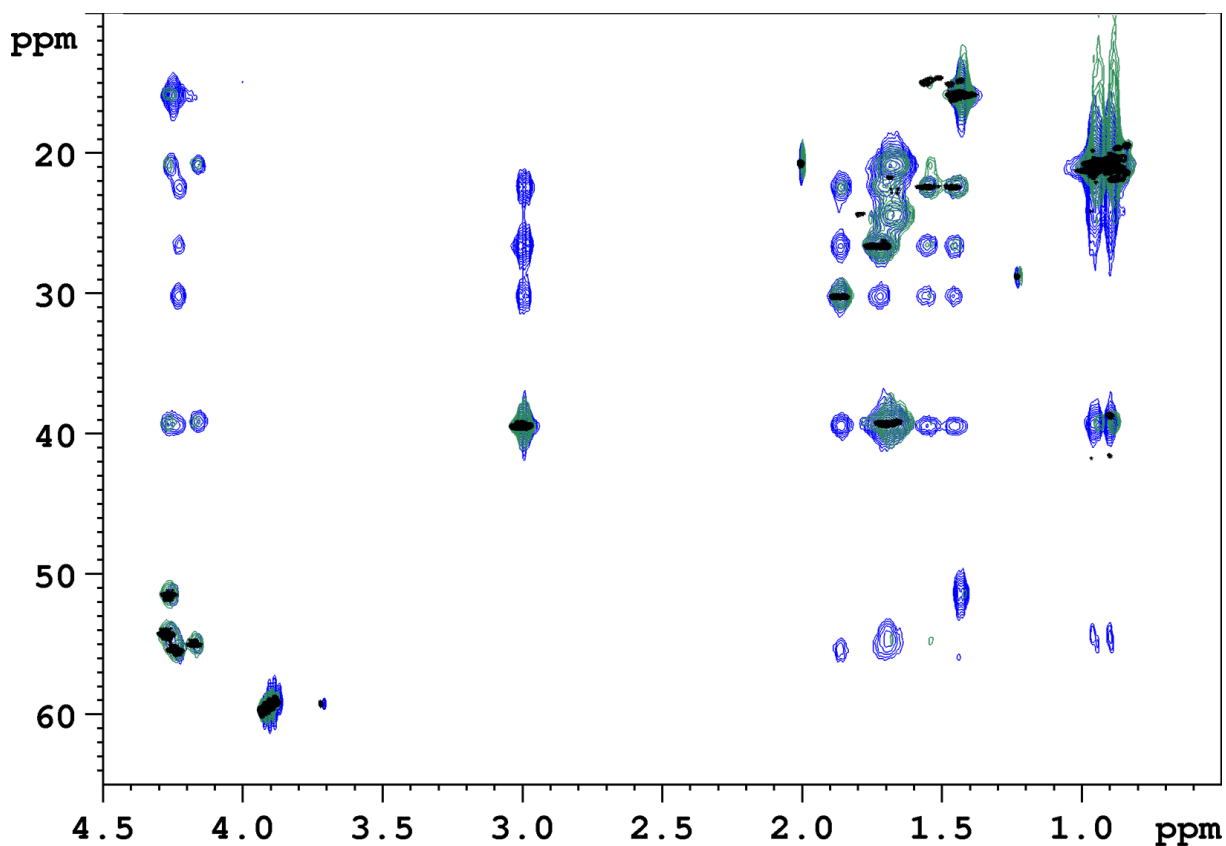The same experiments are done with ^{13}C (**Figure 52**).

Figure 52: ^{1}H-^{13}C HSQC (black), ^{1}H-^{13}C HSQC-NOESY (green) and ^{1}H-^{13}C HSQC-TOCSY (blue) liquid-state NMR spectra of LAH4-A4 in 50% TFE in water for the following labelling scheme: KKALLHAALAHLLALAHHLLALLKKA.

2D ^{1}H-^{13}C HSQC shows the bond correlations, ^{1}H-^{13}C HSQC-NOESY in addition shows the distance correlations between spins. In order to confirm the ^{13}C assignment, complementary spectra (^{1}H-^{13}C HSQC-NOESY and ^{1}H-^{13}C HSQC-TOCSY) are carried out (**Figure 52**).

Once the selectively labelled spectra of the different peptides were analysed, the LAH4-A4 unlabelled spectrum was recorded. First the 2D ^{1}H-^{15}N-HSQC and ^{1}H-^{13}C-HSQC were performed for unlabelled LAH4-A4 in the same condition. The chemical shift previously found for labelled amino acids were assigned on the ^{1}H-^{15}N-HSQC and ^{1}H-^{13}C-HSQC spectra of unlabelled LAH4-A4. Then 2D ^{1}H-^{1}H TOCSY and NOESY were performed to find the chemical shift of unlabelled amino acids and verify the assignment.

These assignments are summarized in **Figure 53** and **Table 18**. The labelled amino acids are in colour depending on their localization in the sequence KKALLHAALAHLLALAHHLLALLKKA.
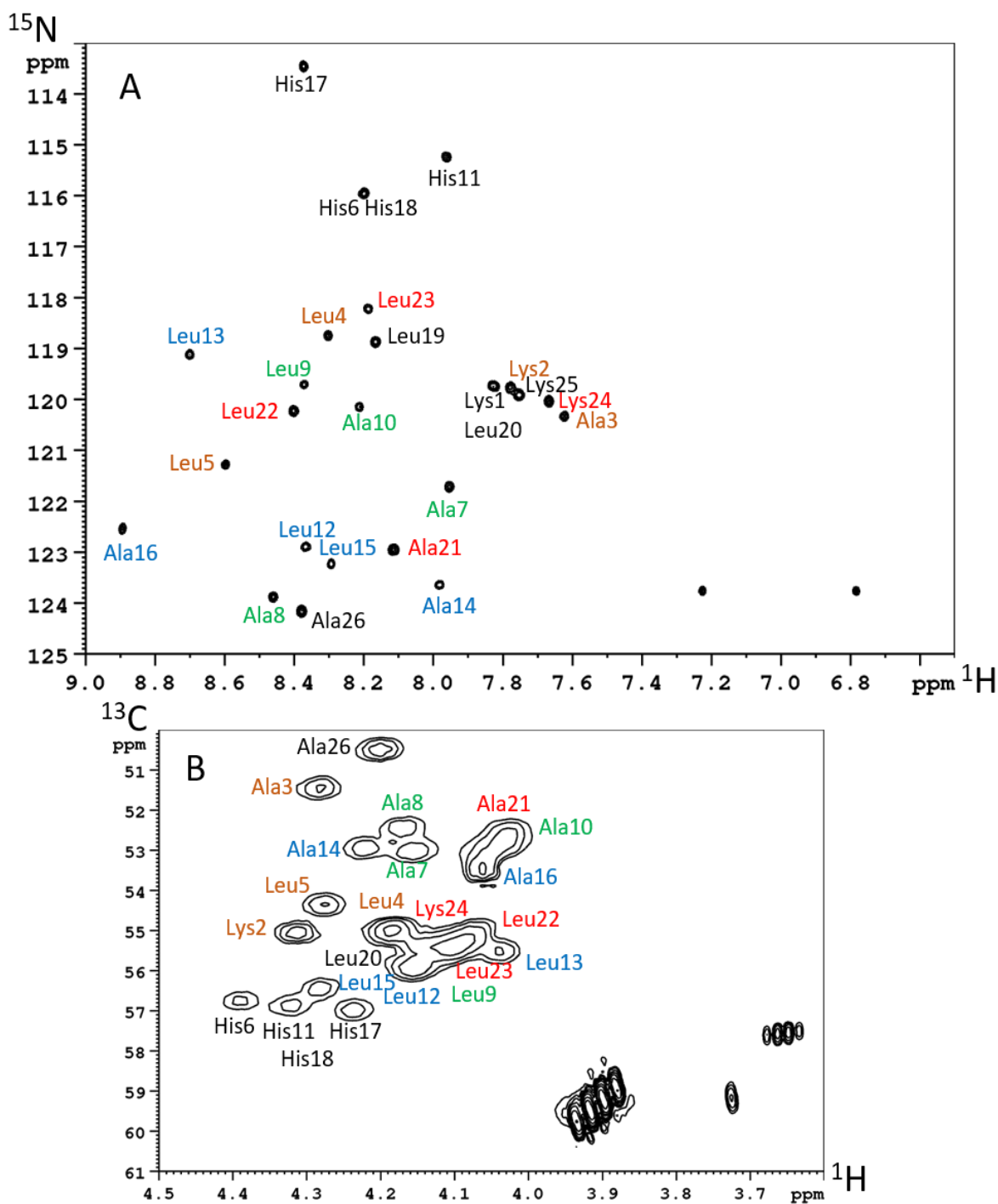
Figure 53: Natural abundance 2D ¹⁵N-HSQC and ¹³C-HSQC liquid-state NMR spectra of unlabelled LAH4-A4 in 50% TFE in water: ¹H-¹⁵N (A) and the Cα region ¹H-¹³C (B). Different colours are used to highlight the labelled sites in the different peptide preparations KKALLHAALAHLLALAHHLLALLKKA that are used for assignment.

In **Figure 53** the peaks at 6.8 ppm (^{1}H) and 7.2 ppm (^{1}H) in the 2D ^{15}N-HSQC spectra correspond to the side chains of lysines with the ^{15}N resonances folded. Histidine backbones show up at the chemical shift between 116 ppm (^{15}N) and 113 ppm (^{15}N).

Table 18 present the assignments for LAH4-A4 in the presence of TFE. This data will allow us to compare peptide chemical shifts in solution and when self-assembled.

aa \ppm	^{15}N	^{1}H$_N$	^{13}C$_\alpha$	^{1}H$_\alpha$
K1	119.7	7.8		
K2	119.8	7.8	55.1	4.1
A3	120.3	7.6	52.6	4.0
L4	118.7	8.3	55.5	4.0
L5	121.3	8.6	55.4	4.1
H6	115.9	8.2	56.8	4.4
A7	121.7	8.0	52.4	4.2
A8	123.9	8.5	53.2	4.1
L9	119.7	8.4	55.3	4.1
A10	120.1	8.2	52.6	4.0
H11	115.2	8.0	56.9	4.3
L12	122.9	8.4	55.9	4.1
L13	119.1	8.7	55.1	4.1
A14	123.7	8.0	52.9	4.2
L15	123.3	8.3	55.9	4.2
A16	122.5	8.9	53.0	4.1
H17	113.4	8.4	57.0	4.2
H18	115.9	8.2	56.4	4.3
L19	118.9	8.2	55.4	4.1
L20	119.7	7.8	54.9	4.2
A21	122.9	8.1	52.4	4.1
L22	120.2	8.4	55.1	4.2
L23	118.2	8.2	55.4	4.1
K24	120.0	7.7	55.0	4.2
K25	119.9	7.8		4.3
A26	124.2	8.4	50.4	4.2

Table 18: Chemical shift for ^{15}N, ^{13}C$_\alpha$, ^{1}H$_N$ and ^{1}H$_\alpha$ of LAH4-A4 in solution with 50% of TFE at pH 6.1 when adopting an α-helical structure. Chemical shift given through internal DSS calibration.

V.4 Characterization of LAH4-A4 fibrils

In this part, we will focus on the fibrillar form of L1H4-A4. As previously mentioned, the peptide is composed by only 4 different amino acids (alanine, lysine, leucine, histidine). Therefore, we have used the same labelling strategy, and the regions labelled one at a time are represented with different colours: KKALLHAALAHLLALAHHLLALLKKA. The previously found optimal fibrillation conditions were used (*v.s.* **chapter IV.3**).

A previous PhD student had labelled the methyl of alanine 14 and formed peptides fibrils by dialysis. Solid-state NMR spectroscopy had shown a duplication of the ^{13}Cβ peak around 15 ppm both resonances occurring with equal intensity. She had hypothesized that the duplication of this resonance corresponds to the specific arrangement of the peptide when assembled into fibrils. I could be the result of different peptide conformations, resulting from a mixture of peptides in α-helical, random coil or β-sheet.

To avoid a peak duplicate depending on peptide conformation the fibril was washed to have only the chemical shifts of the fibril in α-helical structure. Washing with the same buffer allow to remove all traces of monomeric peptides still in solution. The pellet was then concentrated by centrifugation cycle to remove the maximum amount of buffer, then the fibrils were packed into a 2.5 mm rotor.

Before performing a time-consuming structural investigation, the quality and reproducibility of the sample preparations was tested by recording 1D ^{13}C CP-MAS solid-state spectra (**Figure 54**). The different functional groups of amino acids were identified by their literature ^{13}C chemical shift. The carbonyl peak appears around 170-180 ppm, the Cα around 60-50 ppm and the Cβ/γ in the region <50 ppm (**Figure 54**).
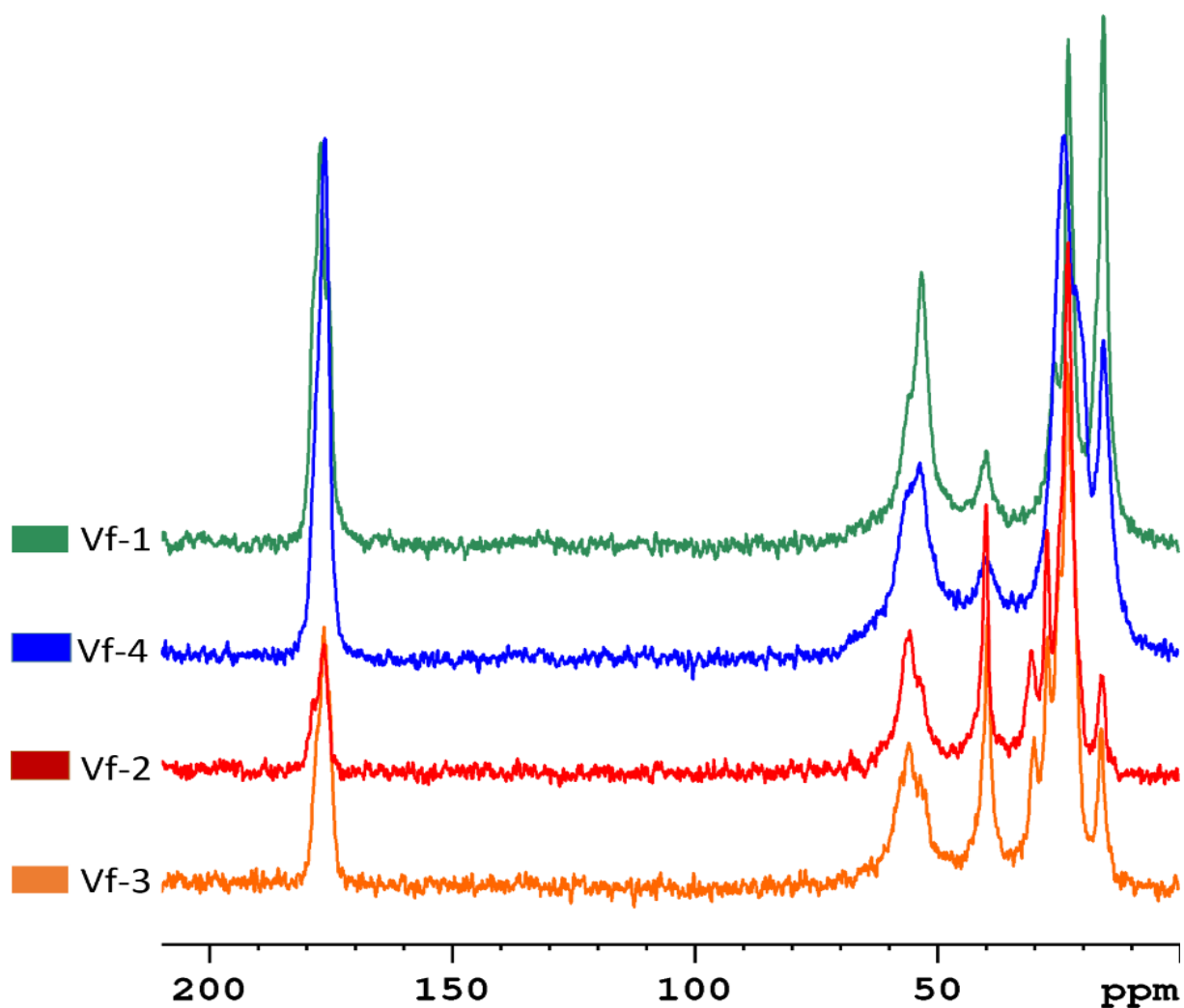
Figure 54: {¹H}¹³C CP-MAS solid-state NMR spectra of LAH4-A4 labelled in different regions of the peptide. The spectra are shown in the corresponding colour: KKALLHAALAHLLALAHHLLALLKKA. LAH4-A4 spectra recorded on a Bruker™ Avance 500 MHz NMR spectrometer, samples packed inside 2.5 mm zirconia rotors and spun at 25 kHz at 301 K.

Figure 54 CP-MAS ¹³C solid-state NMR spectra, shows one peak of the ¹³Cβ of alanine around 16 ppm. Therefore, the two peaks observed previously had to be two different peptide conformations, resulting from a mixture of peptides in fibrils with α-helicoidal and the peptide in solution. By washing the fibrils' pellet, the peptide solution is not present in the sample. Moreover, **Figure 54** does not show chemical shifts variation for the different samples, so there is reproducibility of the sample preparations.

To assign the carbons, 2D DARR spectra were recorded with 2 different mixing times: short (75 ms) or long (400 ms). Indeed, a mixing time of 75 ms give close contacts (CO-Cα, Cα-Cβ, Cβ-Cγ) while a long mixing time gives information about long range contact involving labelled residues. This experiment therefore allows us to have the carbon chemical shift correlations within amino acids. The assignment procedure is exemplified in **Figure 55** and **Figure 56** for sample 2 (KKALLHAALAHLLALAHHLLALLKKA).
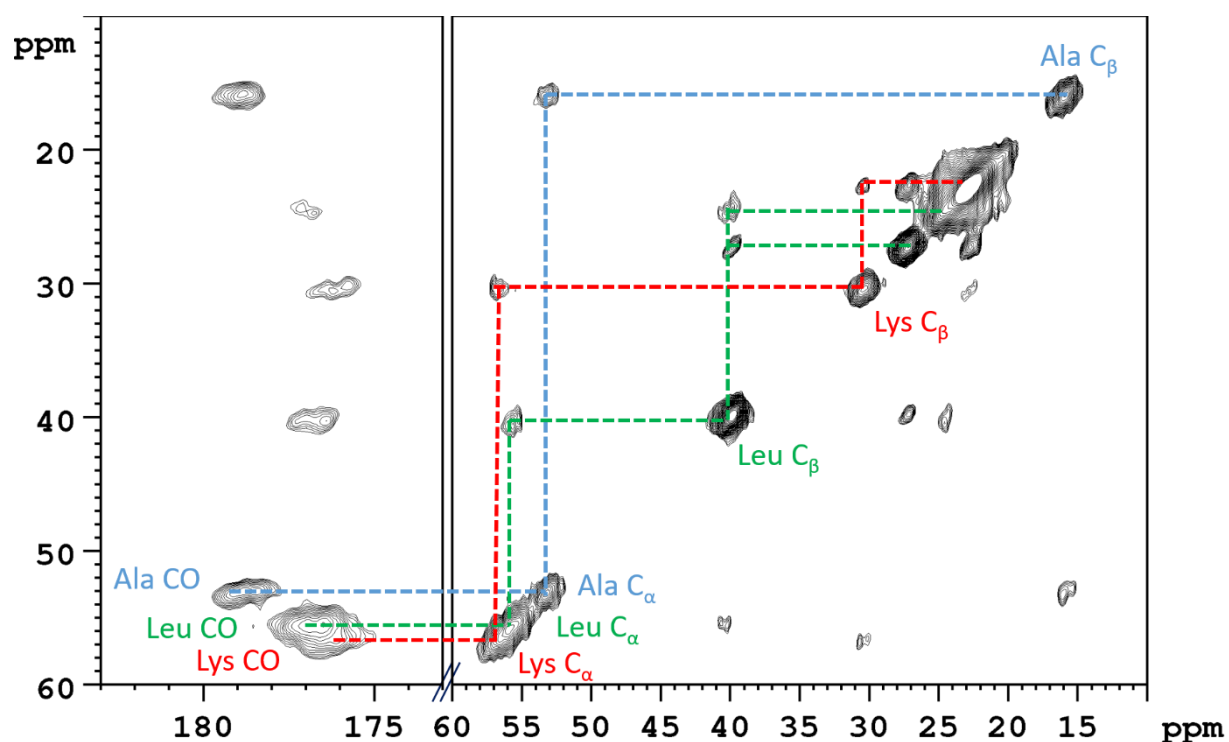
*Figure 55: 2D ^{13}C-^{13}C DARR spectrum at 75 ms mixing time of LAH4-A4 fibrils for the sample 2 labelling scheme: KKALLHAALAHLLALAHHLL*ALLK*KA. The spectra correlate the different amino acid functional groups: CH$_3$, Cα, Cβ and carboxyl group (CO). Correlation peaks assigned to alanine (blue), leucine (green), and lysine (red) of the labelled residues are indicated. LAH4-A4 spectrum recorded on a Bruker^{TM} Avance 500 MHz NMR spectrometer, samples packed inside 2.5 mm zirconia rotors and spun at 25 kHz at 301 K.*

Figure 55 shows the correlation between different amino acid functional groups: CH_3, $C\alpha$, $C\beta$ and carboxyl group (CO). Correlation peaks assigned to alanine (blue), leucine (green), and lysine (red) of the labelled residues. Sample 2 is labelled with ^{15}N and ^{13}C on one alanine, two leucines and one lysine with the sequence ALLK. In ^{13}C-^{13}C DARR spectrum, the alanine chemical shift of $C\beta$ is around 16 ppm and correlates to $C\alpha$ about 53 ppm which itself correlated to carbonyl at about 177 ppm (**Figure 55**). The ^{13}C-^{13}C DARR spectra allow to distinct the chemical shift of different labelled amino acids. In this example, we can easily assign labelled alanine thanks to the characteristic chemical shift of the $C\beta$ at about 16 ppm. Likewise, for leusine which has a chemical shift of $C\beta$ towards 40 ppm.

To discriminate the two leucines, hNCO and hNCα experiments were carried out (**Figure 56**). hNCO allows us to correlate the chemical shift of the carbonyl of a preceding amino acid (i-1) with the nitrogen of an amino acid (i). hNCα allows to correlate the chemical shift of the α-carbon (Cα) with the nitrogen from the same amino acid (i). The two leucines have different neighbours in the labelled fragments they are distinguished by identifying the previous amino acid (i-1).
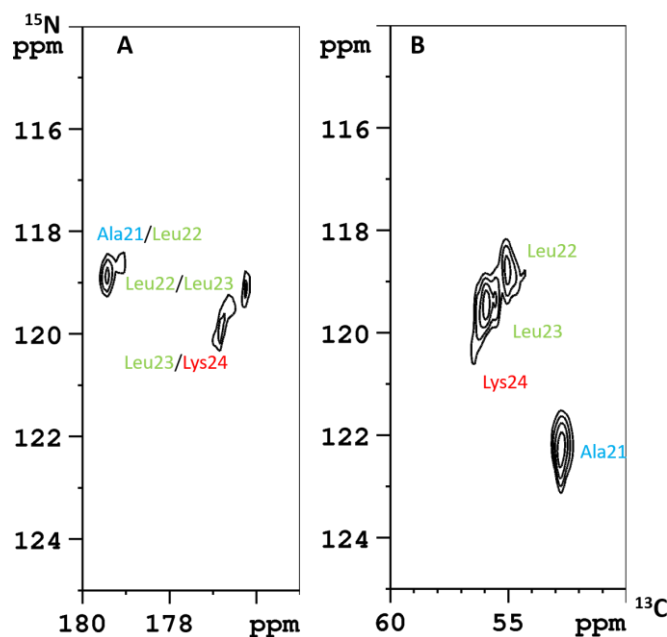
*Figure 56: 2D hNCO and hNCα spectrum of LAH4-A4 fibrils for the sample 2 labelling scheme: KKALLHAALAHLLALAHHLL**ALLK**KA. hNCO spectrum (A) and hNCα spectrum (B). Correlation peaks assigned to alanine (blue), leucine (green), and lysine (red) of the labelled residues are indicated. LAH4-A4 spectra recorded on a Bruker^TM Avance 500 MHz NMR spectrometer, samples packed inside 2.5 mm zirconia rotors and spun at 25 kHz at 301 K.*

Figure 56, shows an example of the sample 2 region labelling corresponding to the chemical shift of amide carbons from the L21 to K24 residues of the hNCO and hNCα spectrum. The hNCα and hNCO spectra are side-by-side to distinguish the Cα chemical shift from a residue (i) from the Cα chemical shift of the previous residue (i-1) thus we can assign this part of the sequence.

The same procedure is then carried out on the four samples, allowing to assign the ^{13}C and [15] N chemical shifts for all the labelled amino acid, the results are summarized in **Table 19**.

aa \ppm	^{15}N	^{13}CO	$^{13}C\alpha$	$^{13}C\beta$	$^{13}C\gamma$	$^{13}C\delta 1$	$^{13}C\delta 2$	$^{13}C\epsilon$
K1								
K2	120.6	175.3	57.3	30.1	21.5	27.2		39.5
A3	122.4	177.7	52.7	16.2				
L4	119.2	176.8	56	40.2	25.1	23.4	22.3	
L5	119.4	176.4	55.5	39.6	24.9	23.1	21.5	
H6								
A7	121.9	177.3	53.1	15.7				
A8	120.4	177.4	52.9	15.8				
L9	119	175.6	56.2	39.8	25.8	22.9	22.2	
A10	121.8	178.9	53.5	15.4				
H11								
L12	120.3	176.5	56.1	39.2	23.8	19.5		
L13	119.9	176.1	56	38.4	24.2	20.6		
A14	121.7	178.5	53	15.5				
L15	120.8	176.2	55.6	39.6	24.4	20.9		
A16	122.3	177.2	52.9	15.6				
H17								
H18								
L19								
L20								
A21	122.3	178.8	52.9	15.7				
L22	118.8	176.9	55.3	39.6	24.5	23.1	21.6	
L23	119.6	176.5	55.02	40.01	24.1	23	20	
K24	120.4	176.2	56.6	30.2	22.5	27		39.6
K25								
A26								

Table 19: Chemical shift for ^{15}N and ^{13}C for fibrils of LAH4-A4 labelled in different regions of the peptide. The spectra are shown in the corresponding colour: KKALLHAALAHLLALAHHLLALLKKA. LAH4-A4 spectrum recorded on a Bruker^TM Avance 500 MHz NMR spectrometer, samples packed inside 2.5 mm zirconia rotors and spun at 25 kHz at 301 K. Assignment with 2D ^{13}C-^{13}C DARR spectrum of 75 ms or 400 ms mixing time, 2D hNCO and hNCα spectrum. Chemical shifts given respective to TMS through standard substitution methods (adamantane for ^{13}C and NH₄Cl for ^{15}N [109 133]).

V.5 Difference between the monomeric form of LAH4-A4 in solution and its fibrillar form

NMR spectroscopy can determine the secondary structure of a protein but also precisely locates secondary structure elements within the peptide chain [137]. The chemical shift provides information on the secondary structure and allows one to monitor structural changes. NMR chemical shifts in proteins depend strongly on local structure. Spectra have been referenced in the same way to compare spectra [138]. Indeed, the spectra of peptides in solution are calibrated using DSS as reference while for ^{13}C solid-state NMR adamantane is used and fixed to 38.2 ppm (corresponding to 0 ppm for TMS) [109]. To guarantee the same referencing as in liquid with DSS calibration, +1.7 ppm is added to the values measured by solid-state NMR spectroscopy [139].

In this part, the chemical shift of the monomeric peptide in solution (**chapter IV.3**) or in the form of fibril (**chapter IV.4**) were analysed and compared by two methods. First, the chemical shift index [68] provides information about the secondary structure and secondly the TALOS+ software [140] establishes a relationship between ^{13}C, ^{15}N and ^{1}H chemical shifts and the dihedral angle φ/ψ.

The ^{13}Cα chemical shift depends of secondary structure: it is lower when the protein adopts a α-helical structure and higher for a β-sheet conformations when compared to its random coil structure [112]. Therefore, secondary structure information is obtained by calculating the difference of observed ^{13}Cα chemical shift and the chemical shifts of an ideal random coil conformation established by using a great number of published structures according to [68]:

$$\Delta\delta = \delta_{observed} - \delta_{random\ coil}$$

It indicates the propensity of an amino acid to be involved in α-helix (+1), β-sheet (-1) and others (0). The chemical shifts for random coils structure [112] compared for the chemical shift obtained in solution or in fibril (**Figure 57**).
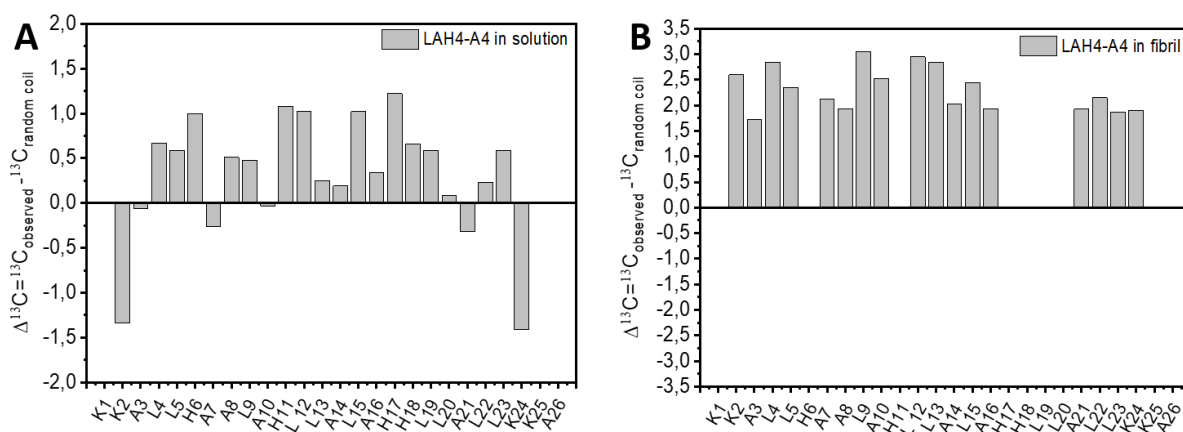
Figure 57: Secondary chemical shifts of LAH4-A4 in solution at pH 6.4 (A) or fibrils at pH 7.4 (B). The diagrams represent the difference between chemical changes of $^{13}C\alpha$ compared to random coil values for amino acid residues. The chemical shift are referencing with DSS.

The secondary chemical shifts indicate that in TFE/water solution LAH4-A4 adopts predominantly α-helical structure (**Figure 57 A**). However, residues at the extremities especially lysines tend not to participate in this helical structure. A previous study investigated the secondary structure of LAH4 in the presence of 50% TFE. This experiment indicates an α-helix between the L4 to L23 region [12]. The LAH4-A4 peptide probably adopts the same configuration in this solution (**Figure 57 A**). In fibrils LAH4-A4 peptide is also α-helical but, in this case, the α-helical conformation extends from positions K2 to K24 (**Figure 57 B**). Therefore, there is a change in the structure at the Nter and Cter. The comparison between LAH4-A4 in solution and its self-assembled form shows us a modification from random coils to α-helix for the terminal lysines K2 and K24 (**Figure 57 A, B**).

In order to have more information on the secondary structure of the peptide the TALOS+ software was used [98]. The TALOS+ software allows one to determine the torsion angles of the peptide backbone [97] [68]. The software will predict the values of the φ/ψ dihedral angles and from the chemical shift values of the residue: Cβ, Cα and CO and NH. For each residue TALOS+ considers the environment with the chemical shifts of its two neighbours. Based on this tripeptide, the chemical shift values will be compared to the database composed of proteins with known structure. TALOS+ looks at the similarities of chemical shifts and preserve the corresponding φ/ψ dihedral angle values. The dihedral angles are shown in a Ramachandran

diagram where different regions represent the different structure such as α-helix or β-sheet as a function of the angles φ/ψ [69]. Furthermore, the chemical shifts of Cβ, Cα and CO shown in **Table 18** and **Table 19** allow one to determine the secondary structure of the peptide in solution or in fibrils using TALOS+. First, **Figure 58** shows the results of the first TALOS+ step for LAH4-A4 in solution or in fibrils. In this step TALOS+ predicts the distribution of φ and ψ within an α-region (-160<φ <0 & -70<ψ <60), a +φ-region (0<φ <160 & -60<ψ <95) or a β-region (all other angle combinations) using an artificial neuronal network.
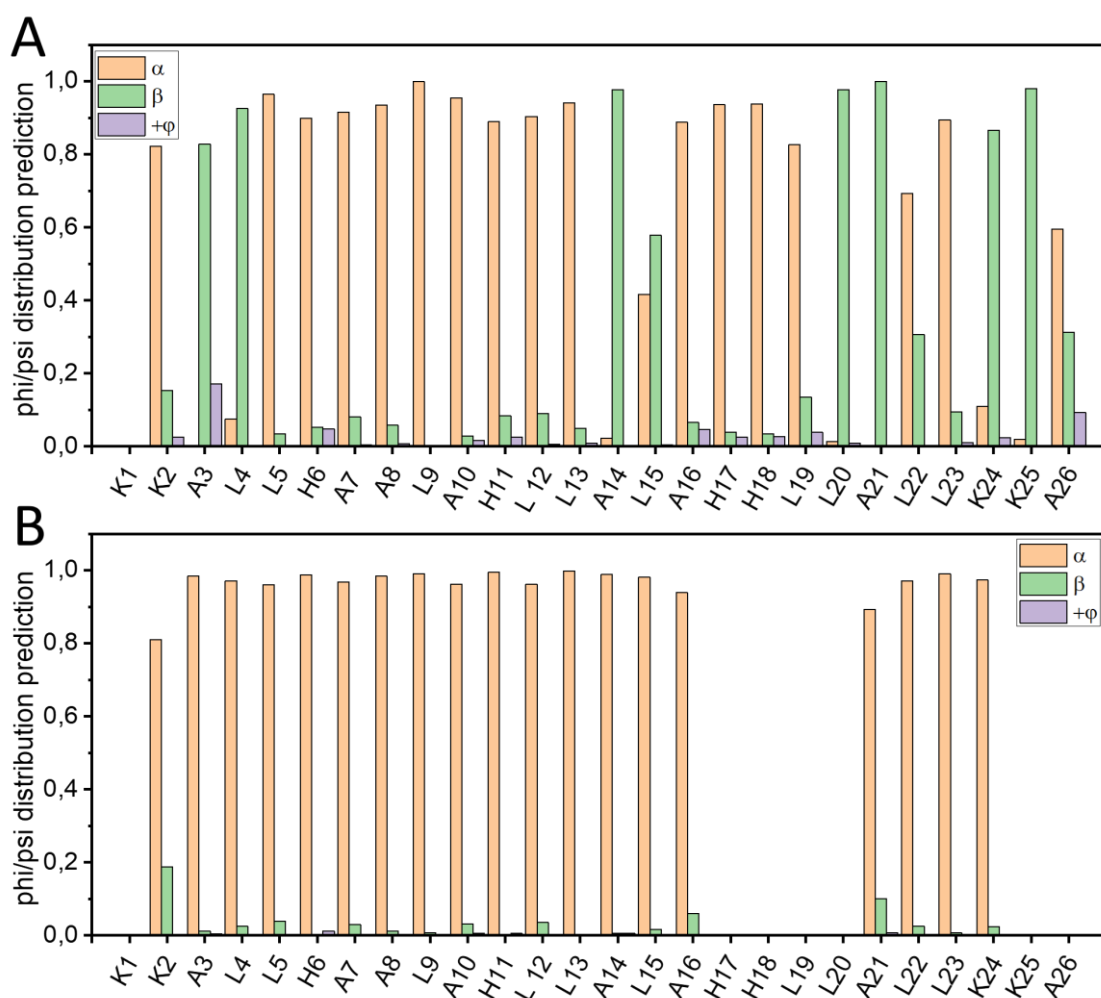

Figure 58: Secondary structure prediction by TALOS+. The horizontal axes show amino acid residue numbers and vertical phi or psi distribution prediction in the peptide in solution (A) or in fibrils (B). Alpha is -160<Phi<0 & -70<psi<60 (orange), the +φ is (0<Phi<160 & -60<psi<95 (purple) and Beta are all others (green) corresponding to the Ramachandran graph.

The secondary structure in solution of L5 to L19 predicted by TALOS+ is α-helical (**Figure 58 A**). According to the software, the residues A14 and L15 are "dynamic" and no predictions were available. The extremity of the peptide is more in the β-sheet region. **Figure 58 B** shows the angles prediction when the peptide is in fibrils. We can see that all amino acids are in α-helical conformation even the termini of the peptide (Nter and Cter). We find the same results as previously obtained by the secondary chemical shift (**Figure 57**).

Once the angles φ and ψ were predicted by TALOS+, they were reported into PyMol to generate a three-dimensional structural model of the peptide in fibrils. The predicted structure of LAH4-A4 in the fibrils or in solution are shown in **Figure 59**.
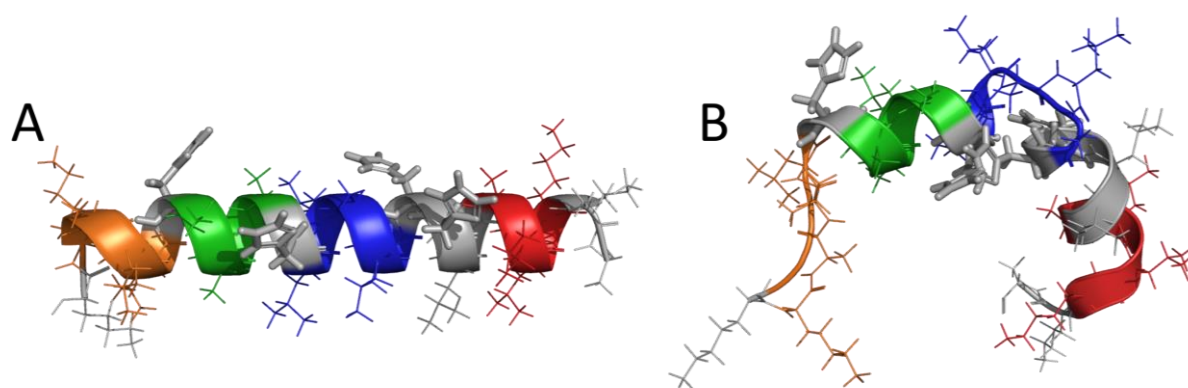

Figure 59: Structure of LAH4-A4 (VF-1) in fibril form (A) or in monomeric form in solution (B) with TALOS+ prediction for angles φ and ψ.

Chemical shift analysis (by TALOS and chemical shift index) lead to the same conclusions: the peptide in fibrils or in solution is mostly α-helical (**Figure 59**). In the fibrillar form, it adopts an almost perfect regular α-helical structure even the extremities are incorporated in the α-helix. However, the extremities of the peptide in solution are not incorporated in the α-helical structure. In addition, the amino acids A14 and L15 are defined as "dynamic" in TALOS+, forming this "loop" between the two α-helical segments in the representation of the peptide in solution. However, the pH of the solution is around 6.1 the peptide has can exhibit a "loop" between the two helical as it has already been shown for LAH4 peptides in the presence of DPC micellar solutions at pH 6.1 [12].

V.6 Structural characterization of the LAH4-A4 fibrils

V.6.1 SWAXS experiment for fibril characterization

In order to gain information about self-assembly into fibrils, Small angles X-ray scattering (SAXS) or wide-angle X-ray scattering (WAXS) experiments are performed. SAXS and WAXS provides information about the secondary and tertiary structure of proteins or peptide and is sensitive to small conformational changes. The secondary structures of proteins or peptides can be determined by the molecular dimensions reflected in WAXS or SAXS patterns. The α-helical structure has three characteristic peaks [141]: 1.5 Å axial separation of amino acid, 5.4 Å pitch and 10 Å diameter (center-to-center distance). β-sheet structures have two characteristic peaks: 4.7 Å strand-to-strand distance and 7 Å pleat distance. The structure of the amyloid-β was studied with similar methods. Amyloid-β assemblies exhibit cross-β structures with the diffraction pattern showing two characteristic signals: 4 Å on the orthogonal axis to the fibril axis and 10-12 Å parallel to the fibril axis [142] [143].

In order to gain more structural information on the self-assembly of the peptide an initial SAXS and WAXS analysis was performed in collaboration with the laboratory of Jérôme Combet. This allows to detect repetition distances of self-assembled fibrils in their dried form. The SAXS and WAXS is the same technique except the distance from the sample to the detector. The modification of the distance between the sample and the detector allows the maximum diffraction to vary at larger angles than at smaller angles (WAXS and SAXS, respectively).

This study allows us to see repetition distances based on a meridian or equatorial plane as a function of the fibril orientation. The combination of SAXS and WAXS (so called SWAXS) measurements performed by the laboratory of Jérôme Combet are presented in **Figure 60**.
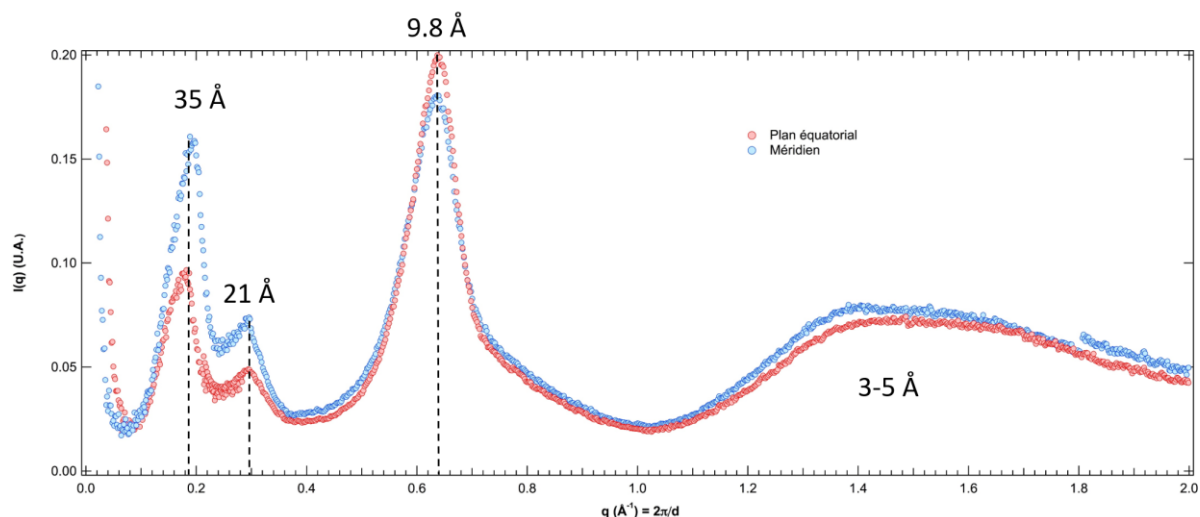
Figure 60: SWAXS experiment with dried LAH4-A4 fibrils. Intensity following the equatorial direction (red) and the meridian (blue) depending on the diffusion vector q=2π/d. SAXS image and WAXS image Figure SI 13.

Figure 60 shows two peaks in the meridian plane corresponding to 35 Å and 21 Å. In addition, one peak in the equatorial plane at 9.8 Å. Also, one isotropic reflection at 4-5 Å.

In order to understand what these distances can correspond to the structure predicted with TALOS+ in the **chapters V.5** with the dihedral angles φ and ψ are used. Using the Pymol software, we were able to calculate the distances within the monomeric peptide (**Figure 61**).
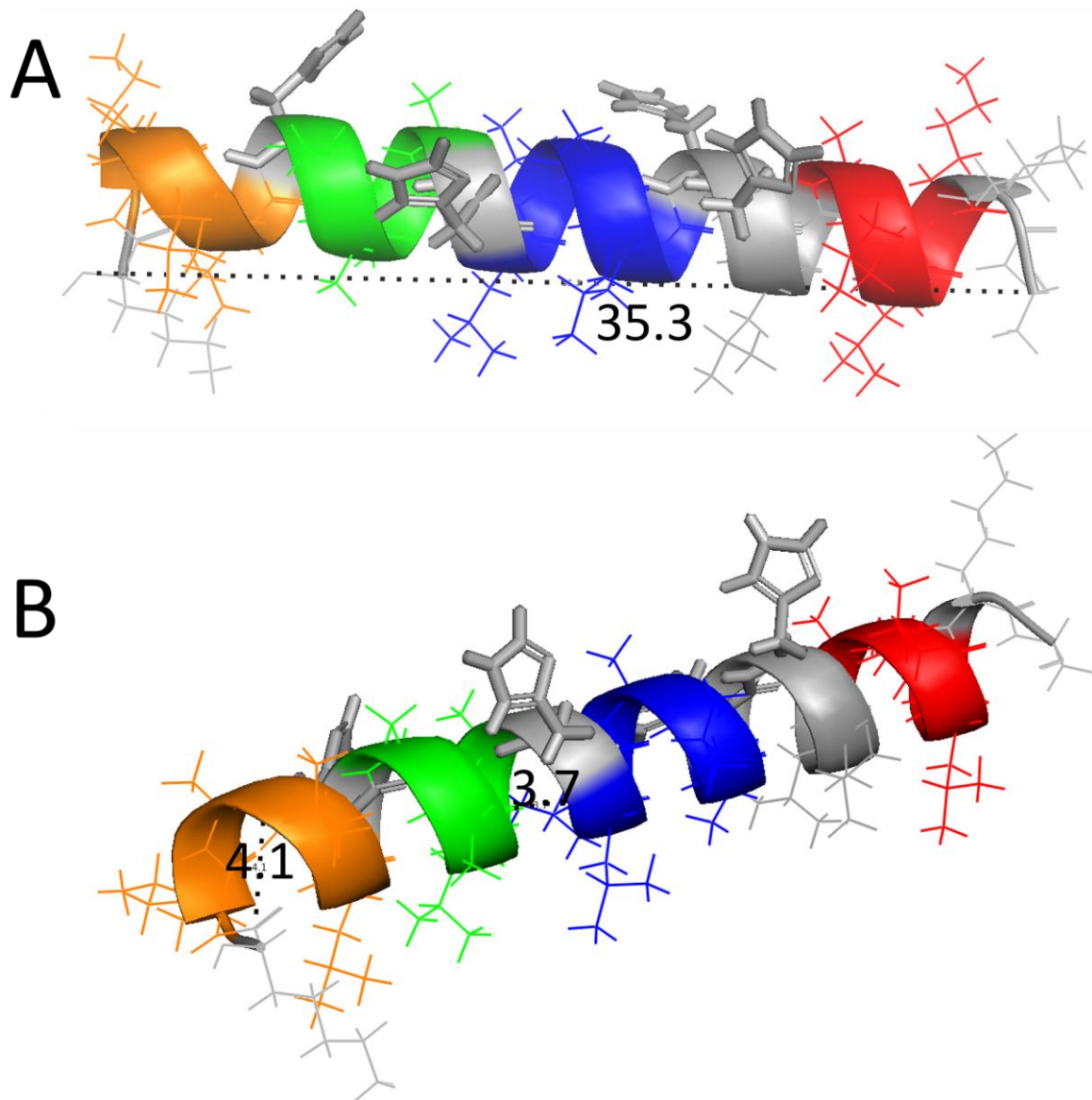
Figure 61: The α-helical peptides' representation based with TALOS+ prediction for angles φ and ψ. The different labelled positions are in colour and the distance calculate by PyMol of this α-helix. (A) the distance of the Cα from the first amino acid to the last. (B) inter loop distances.

The peptide has a length of 34.5 Å from its Nter to its C_{ter} when it is an α-helix conformation (**Figure 61 A**). It can therefore be assumed that the repetition of 35 Å is related to the length of the peptide that will be in the meridian axis. In addition, the isotropic diffusion of 4-5 Å can correspond to the distances between the α-helix pitch (**Figure 61 B**). This isotropic diffusion of 4-5 Å can be characteristic of α-helices since there is diffusion in the meridian and equatorial plane. However, the distance corresponding to 9.8 Å is characteristic of center-to-center

distance between two helices in the equatorial plane. In order to verify with this model, two peptides were placed next to each other using PyMol, by paying attention to the surface of these two peptides having contact with each other. Then the distance between the two peptides are evaluated (**Figure 62**).
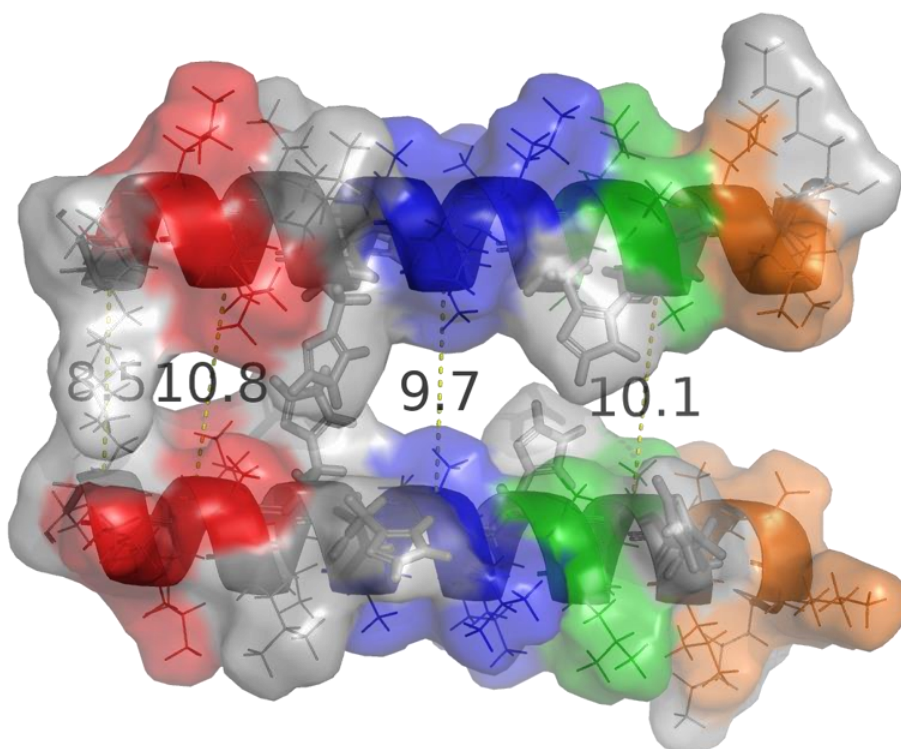
Figure 62: Representation of two α-helical peptides based on TALOS+ prediction for angles φ and ψ. The different labelled position in colour and the distance calculate by PyMol between the two peptides in agreement with close contact of their mesh surface.

Figure 62, shows that a distance between 9 Å and 10 Å can separate the two peptides. It may therefore be that the inter-peptide distance is 9.8 Å.

The characteristic peaks of α-helical structures are: 1.5 Å axial separation of amino acid, 5.4 Å pitch and 10 Å diameter [141]. In this study, we find peaks a 10 Å corresponding to the distance between helices side by side and the peaks corresponding to the pitch at 5.4 Å is isotropic and not defined by a preferential axis. In addition, a peak at 32 Å is visible, characteristic to the length of the peptide.

In the meridian plane, the distance of 21 Å does not correspond to distances within the α-helical structure. Therefore, it can be assumed that this distance is related to repetitions within fibril structure. One study [144], shows that PSMa3 self-assembles in such a manner that

the α-helices interact via their hydrophobic face, creating a tight interface. Based on the previous study [144], we can assume a fibril structure where the peptides are aligned to each other depending on their hydrophilic or hydrophobic face with a distance of 9.8 Å. So, we hypothesized that fibrils could be structured a way illustrated in **Figure 63**.
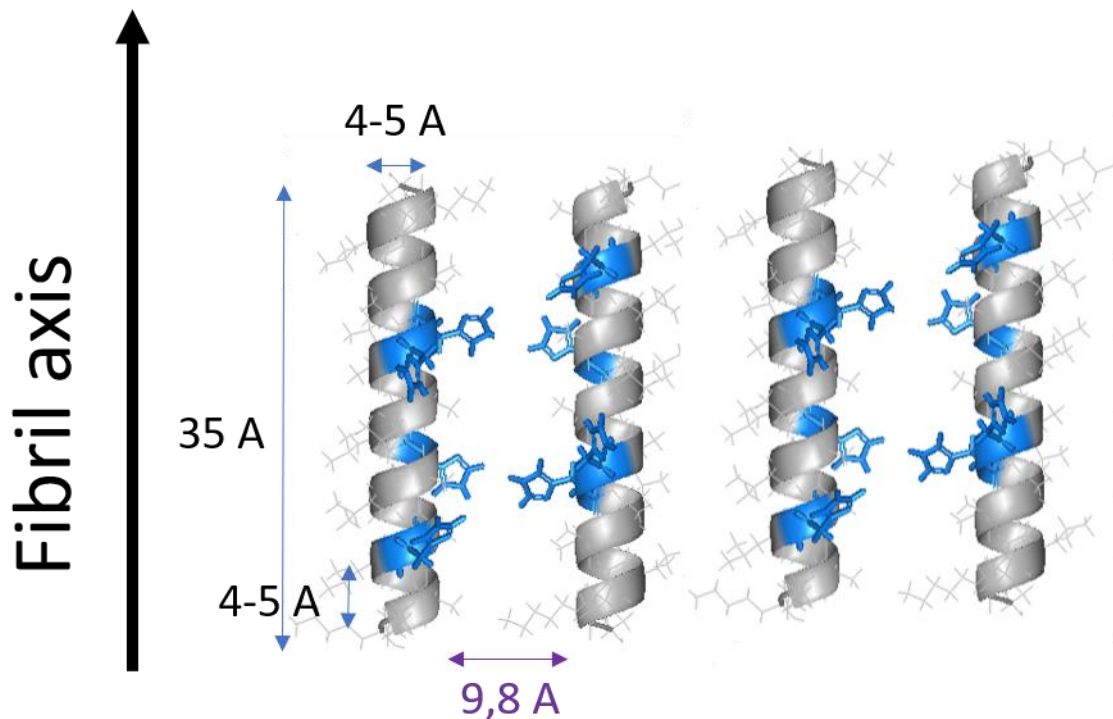
Figure 63: Hypothetical fibrils structure of LAH4-A4 inspired by the publication [144] with the fibril representation based with TALOS+ prediction for angles φ and ψ.

We hypothesized on the distances between the two peptides and clearly this remains a model. The peptide can be self-assembled in different ways and with different contacts. To gain more information of this self-assembly, a study by solid-state NMR spectroscopy was carried out.

V.6.2 Nuclear magnetic resonance for fibril characterization

Self-assembly of many molecules can be monitored by NMR by revealing intramolecular and intermolecular contacts. In order to have intermolecular information of the fibril LAH4-A4 peptides with different regions labelled were incorporated into the fibrils. 50% of LAH4-A4 sample 1 and 50% of LAH4-A4 sample 2 were fibrillated together: If there are contacts between these two regions, we should see an intermolecular interaction. **Figure 64** shows the different samples prepared.
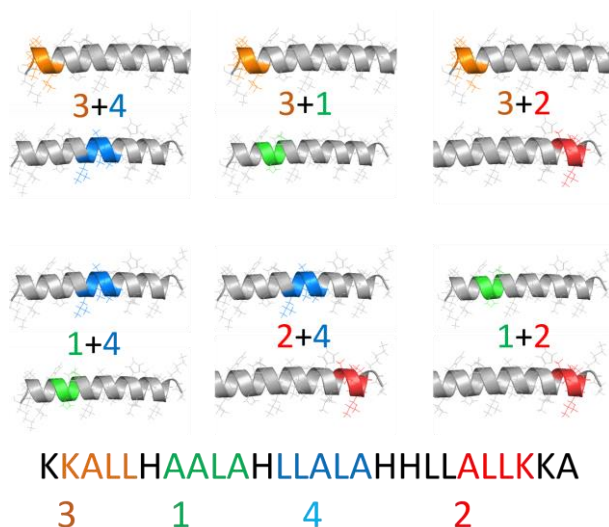
Figure 64: The six different associations analysed by ssNMR. The labelling region are represented with different colours as a function of our labelling KKALLHAALAHLLALAHHLLALLKKA.

Figure 64 shows six different samples including one prepared with 50% of LAH4-A4 sample 1 and 50% of LAH4-A4 sample 2. These sequences were used to form fibrils with the optimal conditions found previously. The labelling region is represented with different colours as a function of our labelling KKALLHAALAHLLALAHHLLALLKKA. During the rest of the thesis, this colour code will be kept.

The previous chapter suggests a distance of 9 Å between two peptides. But different self-assembly can take place. **Figure 65** shows the different possibilities of peptide-peptide association.
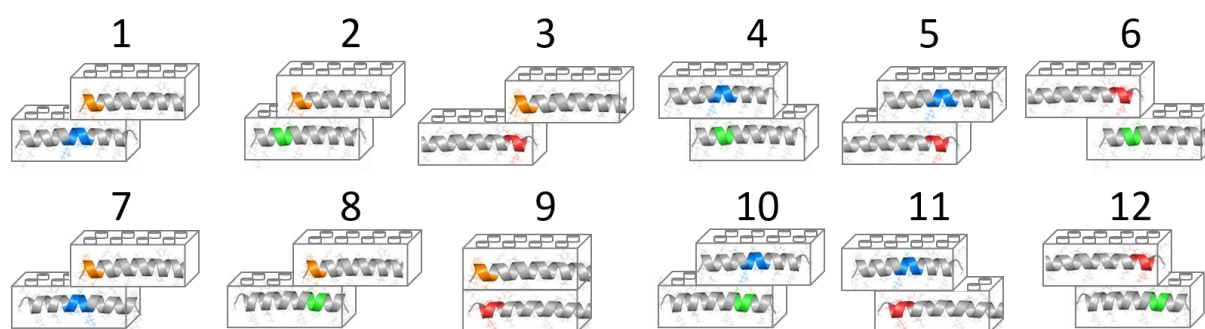
Figure 65: Different hypothetical self-assemblies of LAH4-A4 α-helices.

The peptide helices can be antiparallel (**Figure 65,** 1 to 6) or parallel (**Figure 65**, 7 to 12). In addition, the peptide helix may exhibit an offset to each other creating thus different contact between the peptides. That is why we started analysing the six different samples by mixing two distinct markings at a time (**Figure 64** and **Figure 65**).

The spectra consisting of a single labelling was analysed in **chapter V.4** whose chemical shift of each amino acid is assigned and can be found in **Table 19**. The fibrils of samples containing two types of labelled peptide were formed so that intermolecular contacts between these two labels eventually show up in the NMR spectra.

The study is still ongoing and could only be carried out in full on the sample labelled at one region in the core of the sequence. We have dedicated ourselves to the C{δ, ε}-region because if there are intermolecular interactions, they should most probably take place in that region. Indeed, when the peptide self-assembles the lateral chains of the peptide in α-helical form will come into contact. The contact of its lateral chains will result in the appearance of a peak showing correlation between the two carbons. 2D ^{13}C-^{13}C DARR spectra with different intensity of the cross peak is modulated by the DARR mixing time: at short mixing time cross peak appear only for nearby ^{13}C, when the mixing time is increased longer contacts appear. To see cross peak the 2D ^{13}C-^{13}C DARR spectra were acquired with 400 ms mixing time.

The spectrum of the mixture of the two samples labelled in one region and fibril together can be seen in black. The other colour spectra are samples is labelled 100% and, in the region corresponding to the colour. The colour represents the label area of the sample. Examples in **Figure 66** the spectrum 2D ^{13}C-^{13}C of the samples labelled at region 2 in red and 1 in green **Figure 66 A, B**. The black spectrum represents a fibrillation with 50% sample 1 and 50%

sample 2 (**Figure 66 C**). In order to see the differences between the spectra, they were superimposed (**Figure 66 D**).
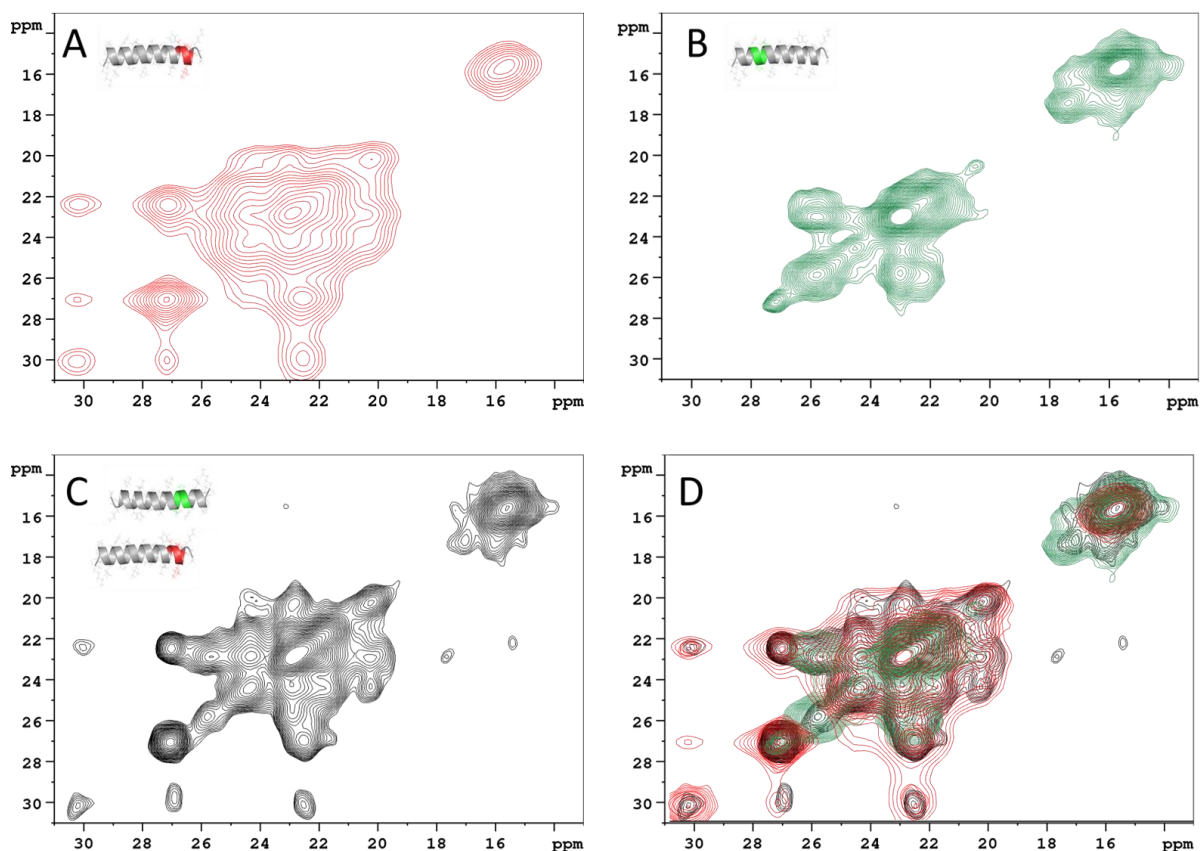
Figure 66: 2D ^{13}C-^{13}C DARR spectra of LAH4-A4 fibrils for the sample 2 (A, in red) sample 1 (B in green), the mixture of this two sample 50%/50% (C in black) and the overlay of the three spectra (D) **KKALLHAALAHLLALAHHLLALLKKA.** *The spectra recorded on a Bruker^{TM} Avance 500 MHz NMR spectrometer, samples packed inside 2.5 mm zirconia rotors and spun at 25 kHz at 301 K with a mixing time of 400 ms. Zoom on the C{β, γ, δ} region.*

The mix of two sample labelled can be seen a small correlation peak between ^{13}C at 24 ppm and 20 ppm. However, the closest resonance of sample 1 is one labelled leucine with chemical shifts at around $^{13}Cγ$ 25.8 ppm and $^{13}Cδ$ at 22.9-6 ppm. The peak therefore cannot be correlated with the leucine of this labelling. Therefore, we cannot assign this peak to an intermolecular interaction.

In addition, if the level of sample 2 is raised the spectrum covers it. Maybe the peak is already present in the 100% marked sample. The same process is carried out for samples with another labelling position in the sequence 1 + 3 and 1 + 4 (**Figure 67**).
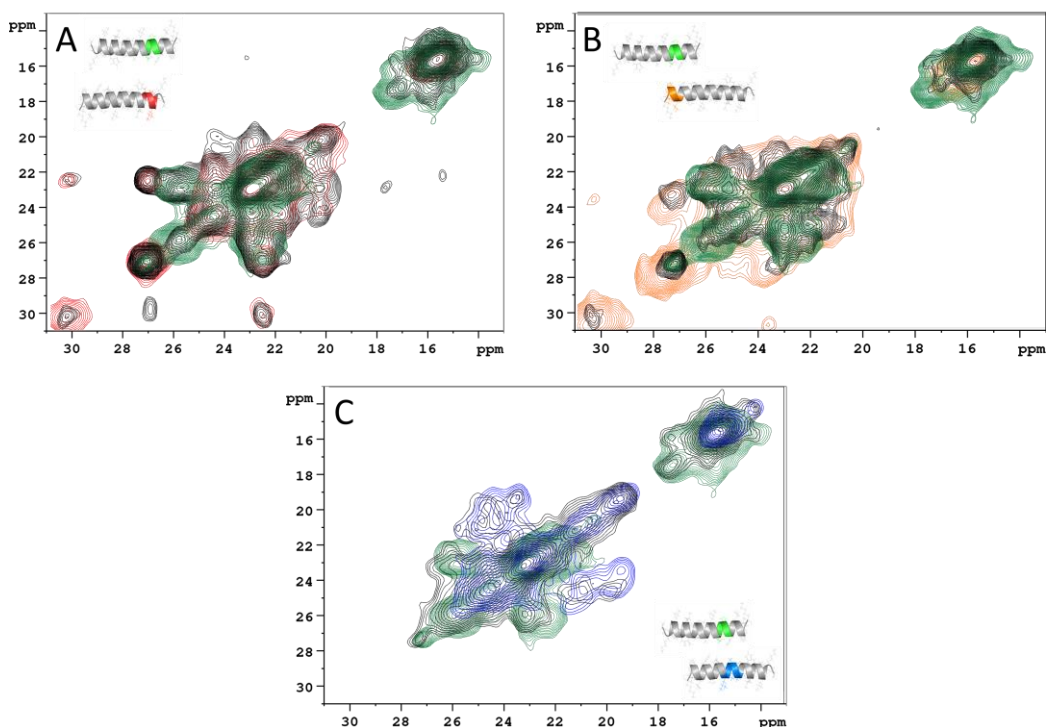
Figure 67: 2D ^{13}C-^{13}C DARR spectra of LAH4-A4 fibrils as a function of the labelled overlay of the three spectra. The spectra coloured (100% labelling) and Black (50%/50%). The mix between: sample 1 and 2 (A), sample 1 and 3 (B) and sample 1 and 4 (C) KKALLHAALAHLLALAHHLLALLKKA. The spectra recorded on a Bruker^{TM} Avance 500 MHz NMR spectrometer, samples packed inside 2.5 mm zirconia rotors and spun at 25 kHz at 301 K with DARR mixing time of 400 ms. Zoom on the C{β, γ, δ} region.

This study has so far not provided any information of intermolecular contacts between amino acid in the C{β, γ, δ} region. When we extend the inspection to Cβ and Cα, we cannot identify a peak of intermolecular correlation. The study of the self-assembly of LAH4-A4 fibrils is still not complete; it would be necessary to have more contact information. However, it already allowed us to draw some hypothesis about the possibility's interactions of the peptide. In addition, spectra with better resolution could remove suspicions about correlation peaks. This would allow us to determine the structure of the LAH4-A4 fibrils. This study would extend to LAH4 and LAH4-L1 as well as having the structure of these three peptides in the fibrils form. This structure could be directly related to their respective function.

V.7 Conclusion

In this study we were able to first determine the structure of the LAH4-A4 peptide in solution in the presence of TFE allowing the peptide to be in the α-helical form in solution. This NMR analysis allowed us to assign the various amino acid chemical shifts of LAH4-A4 in its α-helical conformations. The results found for this peptide are not so different than those found for LAH4. Indeed, in TFE solution the peptide adopts a preferential α-helix conformation of the L4-L23 region but not including the peptide termini.

In the following, the LAH4-A4 structure in the fibril was determined by solid-state NMR spectroscopy. The samples were selectively labelled, and the chemical shift of these amino acids measured. In the fibril the ends will also be part of the α-helical structure. In this conformation the peptide is able to self-assemble concomitant with a change in the lysines mobility. Thereby, we were able to differentiate the peptide structure when it is in solution is in the fibril form.

In order to have more information when the peptide self-assembles SAXS and WAXS experiments were carried out in order to gain repeated distances of the peptide in the fibril. The results show repetitions in the meridian plane at 35 Å and 21 Å, in the equatorial plane at 9.8 Å and isotropic diffusion at 4-5 Å. The distances corresponding to the α-helix are 4-5 Å for the turn and 35 Å for the peptide length when being α-helical. However, the distances of 9.8 Å and 21 Å are not part of the characteristic distances of the α-helical peptide. Therefore, these distances can be linked to inter-fibril repetition distances.

In order to obtain more details on the self-assembly of LAH4-A4 fibrils, solid-state NMR spectroscopy studies are underway. This study will allow to identify intra-fibril contacts. However, the study of intramolecular interactions is still ongoing hopefully leading to an exact LAH4-A4 fibril structure.

VI. General conclusion

This manuscript is dedicated to the LAH4 family peptides with a particular interest on how, changes in the sequence can influence their or self-assembly structure and/or lead modification in their activity.

First, two peptide series LAH4-Ln and LAH4-An by making vary the histidines positioning in the LAH4 sequence were studied. This modification provided hydrophilic angles ranging from 60° to 180° with an increasing number (n=0 to 6) of either alanines or leucines present in between the histidines in a helical wheel peptide representation. This study shows that, for hydrophilic angles between 60° to 140°, peptides of both series present the same physico-chemical properties, which are secondary structures dependent on pH or on the interaction with POPC/POPS model membranes. However, for wide hydrophilic angles (160° and 180°), the peptides do not show interactions with POPC/POPS model membranes. While the LAH4-Ln series get structured by an increase of the pH from 5 to 7, the LAH4-An series already presents a high degree of α-helical structure at pH 5. In addition, calcein release activity are correlated with the hydrophilic angle of the peptides. Indeed, a decrease in the percentage of calcein release was observed when the hydrophilic angles increased. These variations are likely related to the membrane penetration degree depending on the hydrophilic angle of the peptide. These membrane interactions for the two series LAH4-Ln and LAH4-An are important to explain the transduction, transfection, or antimicrobial activities. The transfection and antimicrobial activities showed the same trend as calcein release activity, which is not the case for transduction. These different activities can be related to their mechanisms of action: while transfection and antimicrobial activities are underlined by the destabilization of the membrane, transduction needs a fusion with the membrane.

In order to understand and increase transfection activity, the LAH4-A4 peptide shown to be the best enhancer of all the LAH4-An and LAH4-Ln series was studied in the second chapter. Indeed, LAH4-A4 has already shown strong transfection activity in solution and has even shown the ability to form fibrils that further increase its transduction activity. Optimization of a fibrillation protocol of the LAH4-A4 peptide has been performed to have more reproducible results over time. This study resulted in the determination of the parameters essential to obtain more stable fibrils and better yield around 70%. These well-defined conditions are the following: fibrillation occur in 10 mM phosphate buffer at pH 7 under vigorous agitation. In addition, the improvement of the fibrillation protocol (from dialysis to shaking) does not alter the secondary structure of the LAH4-A4 fibrils. This study is extended to LAH4 and LAH4-L1 to investigate correlations between peptide-sequences, self-assembly and activities. The fibrillation protocol for both peptides were developed. LAH4-L1 and LAH4-A4 fibrils under the same conditions at pH 7.4 while LAH4 develop fibrils in the same buffer but requires a lower pH of 6.2. The pH and phosphate play a critical role in the fibrillation of these peptides. Indeed, this process is reversible as shown by the stability tests that show reversible dissociation of fibrils when phosphate is absent or low pH. The fibril structure was analysed by TEM: LAH4-A4 tends to form short structures of non-linear fibrils, LAH4 tends to form short linear fibrils and LAH4-L1 tends to group together and form more compact and longer structures. In addition, the fibrils structure by ssNMR and FTIR was analysed, showing that LAH4-A4 and LAH4-L1 form α-helical fibrils while LAH4 form fibrils of β-sheets. The supramolecular assemblies of peptides of the LAH4 family can be finely tuned by changing the buffer composition (pH, salt, ions) or by modest changes in their sequence. Moreover, transfection and antimicrobial activities were tested to see the effect of these self-assembled peptides on these activities. In their fibrillar state, the α-helical LAH4-L1 and LAH4-A4 peptides remain active albeit at a lower level. Interestingly, the β-sheet LAH4 fibrils drive to the complete loss of antimicrobial and transfection activities. However, transduction activities have not been tested yet to see if fibrils could improve the activity compared to peptides in solution. In order to get more information on these is fibrils and to better understand their self-assembly, we dedicated ourselves to determine the structure of the LAH4-A4 fibrils by ssNMR.

Due to the high redundancy in the amino acid composition of LAH4-A4, it is difficult to assign resonances from NMR spectra. The strategy used was to synthesize LAH4-A4 peptides with specifically labelled segments at different positions on the peptide sequence, with segments being labelled with ^{15}N and ^{13}C consisting each of four consecutive residues. In this study we were able to first determine that the structure of all these LAH4-A4 peptides in solution and in the fibrils was α-helical. This study allowed us to obtain the amino acids chemical shifts of LAH4-A4 when it is in solution or in the fibril form. The secondary structure of the peptide in solution or fibril was analysed. This shows that the peptide in solution with TFE adopts an α-helical structure between L4 and L23. The residues at the extremities especially lysines tend not to participate in this helical structure. When the peptides are in their fibrillar form, the flexibility of the lysine side chains changes. Indeed, residue K2 and K24 are part of the α-helix structure when the peptide is in the form of fibrils. There is therefore a change in the secondary structure of the ends of the peptide when it is in solution or self-assembly. The loss of transfection activity may be related to these modifications of the peptide when it is assembled. The peptide/DNA complex caused by electrostatic interaction between lysine residues and DNA phosphate groups may be prevented. SWAXS experiments were performed to get information about self-assembly into fibrils. This allowed us to find the characteristic peaks of an α-helical structure namely 5.4 Å for pitch and 10 Å for peptide-peptide distance as well as 35 Å corresponding to the characteristic length of a peptide helix. One peak at 21 Å does not correspond to any distances within the α-helix structure, this distance is probably related to repetitions within fibril structure. In order to determine the peptide self-assembly and then to acquire a better structural understanding of these fibrils, MAS solid-state NMR work started but is still in progress. The strategy consists of having intermolecular information by making fibrils of two differently labelled peptides and by analysing them with ssNMR to look for inter-peptide through-space correlation peaks.

VII. Bibliography

1. D. Chow, M. L. Nunalee, D. W. Lim & A. J. Simnick. Peptide-based Biopolymers in Biomedicine and Biotechnology. *Early Human Development* **62**, 125–155 (2008).

2. D. A. Phoenix, S. R. Dennison & F. Harris. *Antimicrobial Peptides: Their History, Evolution, and Functional Promiscuity*. *Antimicrobial Peptides* (2013).

3. G. Diamond. Nature's antibiotics : the potential of as new drugs. *Biologist* **48**, 209–212 (2001).

4. K. V. R. Reddy, R. D. Yedery & C. Aranha. Antimicrobial peptides: Premises and promises. *International Journal of Antimicrobial Agents* **24**, 536–547 (2004).

5. A Joliot & A. Prochiantz. Protein transduction, from technology to physiology. *Nature cell biology* **6**, 189–196 (2004).

6. R. E. W. Hancock & R. Lehrer. Cationic peptides: A new source of antibiotics. *Trends in Biotechnology* **16**, 82–88 (1998).

7. B. Bechinger. Towards membrane protein design: pH-sensitive topology of histidine-containing polypeptides. *Journal of Molecular Biology* **263**, 768–775 (1996).

8. A. Marquette, A. J. Mason & B. Bechinger. Aggregation and membrane permeabilizing properties of designed histidine-containing cationic linear peptide antibiotics. *Journal of Peptide Science* **14**, 488–495 (2008).

9. T. C. B. Vogt & B. Bechinger. The interactions of histidine-containing amphipathic helical peptide antibiotics with lipid bilayers. *Journal of Biological Chemistry* **274**, 29115–29121 (1999).

10. A. J. Mason, A. Martinez, C. Glaubitz, O. Danos, A. Kichler & B. Bechinger. The antibiotic and DNA-transfecting peptide LAH4 selectively associates with, and disorders, anionic lipids in mixed membranes. *The FASEB Journal* **20**, 320–322 (2006).

11. B. Bechinger. The structure, dynamics and orientation of antimicrobial peptides in membranes by multidimensional solid-state NMR spectroscopy. *Biochimica et Biophysica Acta - Biomembranes* **1462**, 157–183 (1999).

158

12. J. Georgescu, V. H. O. Munhoz & B. Bechinger. NMR Structures of the histidine-rich peptide LAH4 in micellar environments: Membrane insertion, pH-dependent mode of antimicrobial action, and DNA transfection. *Biophysical Journal* **99**, 2507–2515 (2010).

13. B. Bechinger, R. Kinder, M. Helmle, T. C. B. Vogt, U. Harzer & S. Schinzel. Peptide structural analysis by solid-state NMR spectroscopy. *Biopolymers - Peptide Science Section* **51**, 174–190 (1999).

14. N. Voievoda. Biophysical Investigation of the Membrane and Nucleic Acids Interactions of the Transfection Peptide LAH4-L1. *Thesis* (2014).

15. B. Bechinger, J. M. Ruysschaert & E. Goormaghtigh. Membrane helix orientation from linear dichroism of infrared attenuated total reflection spectra. *Biophysical Journal* **76**, 552–563 (1999).

16. B. Bechinger. Insights into the mechanisms of action of host defence peptides from biophysical and structural investigations. *Journal of Peptide Science* **17**, 306–314 (2011).

17. A. Kichler, C. Leborgne, J. März, O. Danos & B. Bechinger. Histidine-rich amphipathic peptide antibiotics promote efficient delivery of DNA into mammalian cells. *Proceedings of the National Academy of Sciences of the United States of America* **100**, 1564–1568 (2003).

18. A. J. Mason, C. Gasnier, A. Kichler, G. Prévost, D. Aunis, M. H. Metz-Boutigue & B. Bechinger. Enhanced membrane disruption and antibiotic action against pathogenic bacteria by designed histidine-rich peptides at acidic pH. *Antimicrobial Agents and Chemotherapy* **50**, 3305–3311 (2006).

19. A. Kichler, B. Bechinger & O. Danos. Des peptides cationiques antibactériens comme vecteurs de transfert de gènes. *Medecine/Sciences* **19**, 1046–69 (2003).

20. Ülo Langel. Cell-Penetrating Peptides Methods and Protocols. in *Cell-Penetrating Peptides* vol. 1324 177–190 (2015).

21. T. Lehto, K. Ezzat & Ü. Langel. Peptide nanoparticles for oligonucleotide delivery. *Progress in Molecular Biology and Translational Science* **104**, 397–426 (2011).

22. E. Eiríksdóttir, K. Konate, Ü. Langel, G. Divita & S. Deshayes. Secondary structure of cell-penetrating peptides controls membrane interaction and insertion. *Biochimica et Biophysica Acta - Biomembranes* **1798**, 1119–1128 (2010).

23. I. R. De Figueiredo, J. M. Freire, L. Flores, A. S. Veiga & M. A. R. B. Castanho. Cell-penetrating peptides: A tool for effective delivery in gene-targeted therapies. *IUBMB Life* **66**, 182–194 (2014).

24. L. Prongidi-Fix, M. Sugawara, P. Bertani, J. Raya, C. Leborgne, A. Kichler & B. Bechinger. Self-promoted cellular uptake of peptide/DNA transfection complexes. *Biochemistry* **46**, 11253–11262 (2007).

25. W. Li, F. Nicol & F. C. Szoka. GALA: A designed synthetic pH-responsive amphipathic peptide with applications in drug and gene delivery. *Advanced Drug Delivery Reviews* **56**, 967–985 (2004).

26. F. Milletti. Cell-penetrating peptides: Classes, origin, and current landscape. *Drug Discovery Today* **17**, 850–860 (2012).

27. A. Gräslund, F. Madani, S. Lindberg, Ü. Langel & S. Futaki. Mechanisms of cellular uptake of cell-penetrating peptides. *Journal of Biophysics* **2011**, 1–10 (2011).

28. M. E. Martin & K. G. Rice. Peptide-guided gene delivery. *AAPS Journal* **9**, 18–29 (2007).

29. N. Nayerossadat, P. Ali & T. Maedeh. Viral and nonviral delivery systems for gene delivery. *Advanced Biomedical Research* **1**, 1–11 (2012).

30. H. Yin, R. L. Kanasty, A. A. Eltoukhy, A. J. Vegas, J. R. Dorkin & D. G. Anderson. Non-viral vectors for gene-based therapy. *Nature Reviews Genetics* **15**, 541–555 (2014).

31. G. Moulay, C. Leborgne, A. J. Mason, C. Aisenbrey, A. Kichler & B. Bechinger. Histidine-rich designer peptides of the LAH4 family promote cell delivery of a multitude of cargo. *Journal of Peptide Science* **23**, 320–328 (2017).

32. N. Liu, B. Bechinger & R. Süss. The histidine-rich peptide LAH4-L1 strongly promotes PAMAM-mediated transfection at low nitrogen to phosphorus ratios in the presence of serum. *Scientific Reports* **7**, 1–12 (2017).

33. S. Majdoul, A. K. Seye, A. Kichler, N. Holic, A. Galy, B. Bechinger & D. Fenard. Molecular determinants of vectofusin-1 and its derivatives for the enhancement of lentivirally mediated gene transfer into hematopoietic stem/progenitor cells. *Journal of Biological Chemistry* **291**, 2161–2169 (2016).

34. L. S. Vermeer, L. Hamon, A. Schirer, M. Schoup, J. Cosette, S. Majdoul, D. Pastré, D. Stockholm, N. Holic, P. Hellwig, A. Galy, D. Fenard & B. Bechinger. Vectofusin-1, a potent peptidic enhancer of viral gene transfer forms pH-dependent α-helical nanofibrils, concentrating viral particles. *Acta Biomaterialia* **64**, 259–268 (2017).

35. A. Kichler, C. Leborgne, O. Danos & B. Bechinger. Characterization of the gene transfer process mediated by histidine-rich peptides. *Journal of Molecular Medicine* **85**, 191–201 (2007).

36. B. Bechinger, V. Vidovic, P. Bertani & A. Kichler. A new family of peptide-nucleic acid nanostructures with potent transfection activities. *Journal of Peptide Science* **17**, 88–93 (2011).

37. B. L. Davidson & X. O. Breakefield. Viral vectors for gene delivery to the nervous system. *Nature Reviews Neuroscience* **4**, 353–364 (2003).

38. J. H. M. Anthony J.F. Griffiths, Susan R. Wessler, Richard C. Lewontin, William M. Gelbart, David T. Suzuki. The genetics of bacteria and their viruses. *An Introduction to Genetic Analysis* (2004).

39. Y. Liu, Y. J. Kim, M. Ji, J. Fang, N. Siriwon, L. I. Zhang & P. Wang. Enhancing gene delivery of adeno-associated viruses by cell-permeable peptides. *Molecular Therapy - Methods and Clinical Development* **1**, 12 (2014).

40. D. Fenard, D. Ingrao, A. Seye, J. Buisset, S. Genries, S. Martin, A. Kichler & A. Galy. Vectofusin-1, a new viral entry enhancer, strongly promotes lentiviral transduction of human hematopoietic stem cells. *Molecular Therapy - Nucleic Acids* **2**, 1–10 (2013).

41. Y. Lan, B. Langlet-bertin, V. Abbate & L. S. Vermeer. Incorporation of 2 , 3-diaminopropionic acid in linear cationic amphipathic peptides produces pH sensitive vectors. *ChemBioChem* **11**, 1266–1272 (2010).

42. D. Fenard, S. Genries, D. Scherman, A. Galy, S. Martin & A. Kichler. Infectivity enhancement of different HIV-1-based lentiviral pseudotypes in presence of the cationic amphipathic peptide LAH4-L1. *Journal of Virological Methods* **189**, 375–378 (2013).

43. A. J. Mason, W. Moussaoui, T. Abdelrahman, A. Boukhari, P. Bertani, A. Marquette, P. Shooshtarizaheh, G. Moulay, N. Boehm, B. Guerold, R. J. H. Sawers, A. Kichler, M. H. Metz-Boutigue, E. Candolfi, G. Prévost & B. Bechinger. Structural determinants of antimicrobial and antiplasmodial activity and selectivity in histidine-rich amphipathic cationic peptides. *Journal of Biological Chemistry* **284**, 119–133 (2009).

44. A. Kichler, A. J. Mason & B. Bechinger. Cationic amphipathic histidine-rich peptides for gene delivery. *Biochimica et Biophysica Acta - Biomembranes* **1758**, 301–307 (2006).

45. C. Meier, T. Weil, F. Kirchhoff & J. Münch. Peptide nanofibrils as enhancers of retroviral gene transfer. *Wiley Interdisciplinary Reviews: Nanomedicine and Nanobiotechnology* **6**, 438–451 (2014).

46. B. Langlet-Bertin, C. Leborgne, D. Scherman, B. Bechinger, A. J. Mason & A. Kichler. Design and evaluation of histidine-rich amphipathic peptides for siRNA delivery. *Pharmaceutical Research* **27**, 1426–1436 (2010).

47. X. Tian, F. Sun, X. R. Zhou, S. Z. Luo & L. Chen. Role of peptide self-assembly in antimicrobial peptides. *Journal of Peptide Science* **21**, 530–539 (2015).

48. S. M. Kelly, T. J. Jess & N. C. Price. How to study proteins by circular dichroism. *Biochimica et Biophysica Acta* **1751**, 119–139 (2005).

49. A. J. Miles & B. A. Wallace. Circular dichroism spectroscopy of membrane proteins. *Chemical Society Reviews* **45**, 4859–4872 (2016).

50. C. Bonduelle. Secondary structures of synthetic polypeptide polymers. *Polymer Chemistry* **9**, 1517–1529 (2018).

51. L. Whitmore & B. A. Wallace. Protein secondary structure analyses from circular dichroism spectroscopy: Methods and reference databases. *Biopolymers* **89**, 392–400 (2008).

52. N. Sreerama & R. W. Woody. Estimation of protein secondary structure from circular dichroism spectra: Comparison of CONTIN, SELCON, and CDSSTR methods with an expanded reference set. *Analytical Biochemistry* **287**, 252–260 (2000).

53. T. Shimanouchi, H. Ishii, N. Yoshimoto, H. Umakoshi & R. Kuboi. Calcein permeation across phosphatidylcholine bilayer membrane: Effects of membrane fluidity, liposome size, and immobilization. *Colloids and Surfaces B: Biointerfaces* **73**, 156–160 (2009).

54. D. Titus, E. James Jebaseelan Samuel & S. M. Roopan. Nanoparticle characterization techniques. *Green Synthesis, Characterization and Applications of Nanoparticles* (Elsevier Inc., 2019).

55. R. Asmatulu & W. S. Khan. Characterization of electrospun nanofibers. *Synthesis and Applications of Electrospun Nanofibers* (2019).

56. K. Bakshi, M. R. Liyanage, D. B. Volkin & C. R. Middaugh. Fourier transform infrared spectroscopy of peptides. *Methods in Molecular Biology* **1088**, 255–269 (2014).

57. S. J. Matthews. NMR of proteins and nucleic acids. *The Royal Society of Chemistry* **36**, 262–284 (2007).

58. R. Verardi, N. J. Traaseth, L. R. Masterson, V. V Vostrikov & G. Veglia. *Isotope Labeling for Solution and Solid-State NMR Spectroscopy of Membrane Proteins Polarization Inversion Spin Exchange at Magic Angle*. (2012).

59. J. Mispelter. Principes de la détermination de la structure tridimensionnelle de protéines en solution par Résonance Magnétique Nucléaire (RMN). 1–30 (2007).

60. L. Braunschweiler & R. R. Ernst. Coherence transfer by isotropic mixing: Application to proton correlation spectroscopy. *Journal of Magnetic Resonance* **53**, 521–528 (1983).

61. J. G. Beck, A. O. Frank & H. Kessler. RMN of peptide in *NMR of Biomolecules: Towards Mechanistic Systems Biology* 329–344 (2012).

62. E. Strandberg & A. S. Ulrich. NMR methods for studying membrane-active antimicrobial peptides. *Concepts in Magnetic Resonance Part A: Bridging Education and Research* **23**, 89–120 (2004).

63. A. A. Arnold & I. Marcotte. Studying natural structural protein fibers by solid-state nuclear magnetic resonance. *Concepts in Magnetic Resonance Part A: Bridging Education and Research* **34**, 24–47 (2009).

64. A. G. T. Polenova & R. Gupta. Magic Angle Spinning NMR Spectroscopy: A Versatile Technique for Structural and Dynamic Analysis of Solid-Phase Systems. *anal chem* **87**, 5458–5469 (2016).

65. T. T. K. Takegoshi & S. Nakamura. 13C-1H dipolar-assisted rotational resonance in magic-angle spinning NMR. *Chemical Physics Letters* **344**, 631–637 (2001).

66. J. Raya, B. Perrone & J. Hirschinger. Chemical shift powder spectra enhanced by multiple-contact cross-polarization under slow magic-angle spinning. *Journal of Magnetic Resonance* **227**, 93–102 (2013).

67. Y. Shen, F. Delaglio, G. Cornilescu & A. Bax. TALOS+: A hybrid method for predicting protein backbone torsion angles from NMR chemical shifts. *Journal of Biomolecular NMR* **44**, 213–223 (2009).

68. S. Spera & A. Bax. Empirical Correlation between Protein Backbone Conformation and Cα and Cβ 13C Nuclear Magnetic Resonance Chemical Shifts. *Journal of the American Chemical Society* **113**, 5490–5492 (1991).

69. C. Ramakrishnan. Stereochemical criteria for polypeptide and protein chain conformations - Part I. Evaluation of helical parameters. *Proceedings of the Indian Academy of Sciences - Section A* **59**, 327–343 (1964).

70. B. B. He. Small angle X-ray scattering. in *two-dimensional X-ray diffraction* 357–377 (2018).

71. Rigaku. Advanced SAXS/WAXS for nanostructure analysis. 1–4 (2015).

72. M. Schiffer & A. B. Edmundson. Use of Helical Wheels to Represent the Structures of Proteins and to Identify Segments with Helical Potential. *Biophysical Journal* **7**, 121–135 (1967).

73. R. Gautier, D. Douguet, B. Antonny & G. Drin. HELIQUEST: a web server to screen sequences with specific α-helical properties. *Bioinformatics* **24**, 2101–2102 (2008).

74. M. Lointier, C. Aisenbrey, A. Marquette, J. H. Tan, A. Kichler & B. Bechinger. Membrane pore-formation correlates with the hydrophilic angle of histidine-rich amphipathic peptides with multiple biological activities. *Biochimica et Biophysica Acta - Biomembranes* **1862**, 1–9 (2020).

75. L. Ivo H. M. van Stokkum & F. C. A. Hans J. W. Spoelder, Michael Bloemendal, Rienk van Grondelle. Estimation of Protein Secondary Structure and Error Analysis from Circular Dichroism Spectra. *Analytical Biochemistry* **191**, 110–118 (1990).

76. S. W. Provencher & J. Glöckner. Estimation of Globular Protein Secondary Structure from Circular Dichroism. *Biochemistry* **20**, 33–37 (1981).

77. P. Jurkiewicz, L. Cwiklik, A. Vojtíšková, P. Jungwirth & M. Hof. Structure, dynamics, and hydration of POPC/POPS bilayers suspended in NaCl, KCl, and CsCl solutions. *Biochimica et Biophysica Acta - Biomembranes* **1818**, 609–616 (2012).

78. K. Murzyn, T. Róg & M. Pasenkiewicz-Gierula. Phosphatidylethanolamine-phosphatidylglycerol bilayer as a model of the inner bacterial membrane. *Biophysical Journal* **88**, 1091–1103 (2005).

79. C. Aisenbrey, R. Kinder, E. Goormaghtigh, J. M. Ruysschaert & B. Bechinger. Interactions involved in the realignment of membrane-associated helices: An investigation using oriented solid-state NMR and attenuated total reflection Fourier transform infrared spectroscopies. *Journal of Biological Chemistry* **281**, 7708–7716 (2006).

80. N. J. Greenfield. Using circular dichroism spectra to estimate protein secondary structure. *Nature Protocols* **1**, 2876–2890 (2007).

81. C. Aisenbrey, A. Marquette & B. Bechinger. The mechanisms of action of cationic antimicrobial peptides refined by novel concepts from biophysical investigations. *Advances in Experimental Medicine and Biology* vol. 1117 (2019).

82. N. Voievoda, T. Schulthess, B. Bechinger & J. Seelig. Thermodynamic and Biophysical Analysis of the Membrane-Association of a Histidine-Rich Peptide with Efficient Antimicrobial and Transfection Activities. *Journal of Physical Chemistry B* **119**, 9678–9687 (2015).

83. E. C. for A. S. T. (EUCAST) of the E. S. of C. M. & I. D. (ESCMID). Determination of minimum inhibitory concentrations (MICs) of antibacterial agents by broth dilution. *The European Society of Clinical Microbiology and Infectious Diseases* **9**, 1–7 (2003).

84. A. J. Mason, C. Leborgne, G. Moulay, A. Martinez, O. Danos, B. Bechinger & A. Kichler. Optimising histidine rich peptides for efficient DNA delivery in the presence of serum. *Journal of Controlled Release* **118**, 95–104 (2007).

85. B. Bechinger. Structure and Functions of Channel-Forming Peptides: Magainins, Cecropins, Melittin and Alamethicin. *J. membrane Biol.* **156**, 197–211 (1997).

86. T. Wieprecht, M. Dathe, E. Krause, M. Beyermann, W. L. Maloy, D. L. Macdonald & M. Bienert. Modulation of membrane activity of amphipathic , antibacterial peptides by slight modifications of the hydrophobic moment. *FEBS Letters* **417**, 135–140 (1997).

87. E. Glattard, E. S. Salnikov, C. Aisenbrey & B. Bechinger. Investigations of the synergistic enhancement of antimicrobial activity in mixtures of magainin 2 and PGLa. *Biophysical Chemistry* **210**, 35–44 (2016).

88. R. Leber, M. Pachler, I. Kabelka, I. Svoboda, D. Enkoller, R. Vácha, K. Lohner & G. Pabst. Synergism of Antimicrobial Frog Peptides Couples to Membrane Intrinsic Curvature Strain. *Biophysical Journal* **114**, 1945–1954 (2018).

89. N. Harmouche & B. Bechinger. Lipid-Mediated Interactions between the Antimicrobial Peptides Magainin 2 and PGLa in Bilayers. *Biophysical Journal* **115**, 1033–1044 (2018).

90. T. Wieprecht, M. Dathe, R. M. Epand, M. Beyermann, E. Krause, W. L. Maloy, D. L. MacDonald & M. Bienert. Influence of the angle subtended by the positively charged helix face on the membrane activity of amphipathic, antibacterial peptides. *Biochemistry* **36**, 12869–12880 (1997).

91. D. Ingrao, S. Majdoul, A. K. Seye, A. Galy & D. Fenard. Concurrent measures of fusion and transduction efficiency of primary CD34+ cells with human immunodeficiency virus 1-based lentiviral vectors reveal different effects of transduction enhancers. *Human Gene Therapy Methods* **25**, 48–56 (2014).

92. E. M. Tytler, J. P. Segrest, R. M. Epand, S. Q. Nie, R. F. Epand, V. K. Mishra, Y. V. Venkatachalapathi & G. M. Anantharamaiah. Reciprocal effects of apolipoprotein and lytic peptide analogs on membranes. Cross-sectional molecular shapes of amphipathic α helixes control membrane stability. *Journal of Biological Chemistry* **268**, 22112–22118 (1993).

93. J. L. Beesley & D. N. Woolfson. The de novo design of α-helical peptides for supramolecular self-assembly. *Current Opinion in Biotechnology* **58**, 175–182 (2019).

94. N. Habibi, N. Kamaly, A. Memic & H. Shafiee. Self-assembled peptide-based nanostructures: Smart nanomaterials toward targeted drug delivery. *Nano Today* **11**, 41–60 (2016).

95. R. Fairman & K. S. Åkerfeldt. Peptides as novel smart materials. *Current Opinion in Structural Biology* **15**, 453–463 (2005).

96. D. W. H. Frost, C. M. Yip & A. Chakrabartty. Reversible assembly of helical filaments by de novo designed minimalist peptides. *Biopolymers - Peptide Science Section* **80**, 26–33 (2005).

97. D. N. Woolfson. The design of coiled-coil structures and assemblies. *Protein chemistry* vol. 70 (2005).

98. G. M. Whitesides & B. Grzybowski. Self-assembly at all scales. *Science* **295**, 2418–2421 (2002).

99. J. Wang, K. Liu, R. Xing & X. Yan. Peptide self-assembly: Thermodynamics and kinetics. *Chemical Society Reviews* **45**, 5589–5604 (2016).

100. J. L. Beesley & D. N. Woolfson. ScienceDirect The de novo design of a -helical peptides for supramolecular self-assembly. *Current Opinion in Biotechnology* **58**, 175–182 (2019).

101. J. Jyoti & V. Singh. Polymer Chemistry nanostructures : implications in drug delivery and. 4418–4436 (2014).

102. J. J. Panda & V. S. Chauhan. Short peptide based self-assembled nanostructures: Implications in drug delivery and tissue engineering. *Polymer Chemistry* **5**, 4418–4436 (2014).

103. C. Viney. Natural Protein Fibers. *Encyclopedia of Materials: Science and Technology (Second Edition)* (2001).

104. C. J. Bowerman & B. L. Nilsson. Self-assembly of amphipathic β-sheet peptides: insights and applications. *Biopolymers* **98**, 169–184 (2012).

105. M. Yolamanova et al. Peptide nanofibrils boost retroviral gene transfer and provide a rapid means for concentrating viruses. *Nature Nanotechnology* **8**, 130–136 (2013).

106. J. Wolf. Biophysical investigations of the LAH4 family peptides : enhancer of gene delivery , from peptide-peptide interactions to peptide-membrane interactions Biophysical investigations of the LAH 4 family of peptides enhancer of gene delivery , from pep. *Thesis* (2019).

107. S. Hediger, B. H. Meier, N. D. Kurur, G. Bodenhausen & R. R. Ernst. NMR cross polarization by adiabatic passage through the Hartmann-Hahn condition (APHH). *Chemical Physics Letters* **223**, 283–288 (1994).

108. B. M. Fung, A. K. Khitrin & K. Ermolaev. An Improved Broadband Decoupling Sequence for Liquid Crystals and Solids. *Journal of Magnetic Resonance* **142**, 97–101 (2000).

109. C. R. Morcombe & K. W. Zilm. Chemical shift referencing in MAS solid state NMR. *Journal of Magnetic Resonance* **162**, 479–486 (2003).

110. D. W. Juhl, E. Glattard, M. Lointier, P. Bampilis & J. A. Carver. The Reversible Non-covalent Aggregation Into Fibers of PGLa and Magainin 2 Preserves Their Antimicrobial Activity and Synergism. *Frontiers in Cellular and Infection Microbiology* **10**, 1–11 (2020).

111. M. Bouchard, D. R. Benjamin, P. Tito, C. V. Robinson & C. M. Dobson. Solvent effects on the conformation of the transmembrane peptide gramicidin A: Insights from electrospray ionization mass spectrometry. *Biophysical Journal* **78**, 1010–1017 (2000).

112. Y. Wang & O. Jardetzky. Probability-based protein secondary structure identification using combined NMR chemical-shift data. *Protein Science* **11**, 852–861 (2002).

113. S. Lou, X. Wang, Z. Yu & L. Shi. Peptide Tectonics: Encoded Structural Complementarity Dictates Programmable Self-Assembly. *Advanced Science* **6**, 1–24 (2019).

114. S. E. Paramonov, H. W. Jun & J. D. Hartgerink. Self-assembly of peptide-amphiphile nanofibers: The roles of hydrogen bonding and amphiphilic packing. *Journal of the American Chemical Society* **128**, 7291–7298 (2006).

115. D. M. Raymond & B. L. Nilsson. Multicomponent peptide assemblies. *Chemical Society Reviews* **47**, 3659–3720 (2018).

116. S. Mondal & E. Gazit. The self-assembly of helical peptide building blocks. *ChemNanoMat* **2**, 323–332 (2016).

117. P. Chakraborty & E. Gazit. Amino Acid Based Self-assembled Nanostructures: Complex Structures from Remarkably Simple Building Blocks. *ChemNanoMat* **4**, 730–740 (2018).

118. B. Sun, K. Tao, Y. Jia, X. Yan, Q. Zou, E. Gazit & J. Li. Photoactive properties of supramolecular assembled short peptides. *Chemical Society Reviews* **48**, 4387–4400 (2019).

119. A. W. P. Fitzpatrick et al. Atomic structure and hierarchical assembly of a cross-β amyloid fibril. *Proceedings of the National Academy of Sciences of the United States of America* **110**, 5468–5473 (2013).

120. K. M. Hainline, C. N. Fries & J. H. Collier. Progress Toward the Clinical Translation of Bioinspired Peptide and Protein Assemblies. *Advanced Healthcare Materials* **7**, 1700930 (1–12) (2018).

121. Y. Yano, A. Takeno & K. Matsuzaki. Trace amounts of pyroglutaminated Aβ-(3–42) enhance aggregation of Aβ-(1–42) on neuronal membranes at physiological concentrations: FCS analysis of cell surface. *Biochimica et Biophysica Acta - Biomembranes* **1860**, 1603–1608 (2018).

122. G. Fusco, A. De Simone, P. Arosio, M. Vendruscolo, G. Veglia & C. M. Dobson. Structural Ensembles of Membrane-bound α-Synuclein Reveal the Molecular Determinants of Synaptic Vesicle Affinity. *Scientific Reports* **6**, 1–9 (2016).

123. W. Qiang, W. M. Yau, J. X. Lu, J. Collinge & R. Tycko. Structural variation in amyloid-β fibrils from Alzheimer's disease clinical subtypes. *Nature* **541**, 217–221 (2017).

124. B. Bechinger. Structure and function of membrane-lytic peptides. *Critical Reviews in Plant Sciences* **23**, 271–292 (2004).

125. S. Galdiero, A. Falanga, M. Cantisani, M. Vitiello, G. Morelli & M. Galdiero. Peptide-lipid interactions: Experiments and applications. *International Journal of Molecular Sciences* **14**, 18758–18789 (2013).

126. S. P. Edgcomb & K. P. Murphy. Variability in the pKa of histidine side-chains correlates with burial within proteins. *Proteins: Structure, Function and Genetics* **49**, 1–6 (2002).

127. V. Vidovic. Production du peptide P-LAH 4 chez E . coli et études par RMN de ses propriétés antibactérienne et de transfection d ' ADN. *Thesis* (2011).

128. H. Heise. Solid-state NMR spectroscopy of amyloid proteins. *ChemBioChem* **9**, 179–189 (2008).

129. M. Baldus. Magnetic resonance in the solid state: Applications to protein folding, amyloid fibrils and membrane proteins. *European Biophysics Journal* **36**, 37–48 (2007).

130. R. Tycko. Solid-state NMR studies of amyloid fibril structure. *Annual Review of Physical Chemistry* **62**, 279–299 (2011).

131. M. Hong. Structure, topology, and dynamics of membrane peptides and proteins from solid-state NMR spectroscopy. *Journal of Physical Chemistry B* **111**, 10340–10351 (2007).

132. A. Loquet, N. G. Sgourakis, R. Gupta, K. Giller, D. Riedel, C. Goosmann, C. Griesinger, M. Kolbe, D. Baker, S. Becker & A. Lange. Atomic model of the type III secretion system needle. *Nature* **486**, 276–279 (2012).

133. P. Bertani, J. Raya & B. Bechinger. 15N chemical shift referencing in solid state NMR. *Solid State Nuclear Magnetic Resonance* **61–62**, 15–18 (2014).

134. N. J. S. John Cavanagh, Wayne J. Fairbrother, Arthur G. Palmer III, Mark Range. Sequential assignment, structure, Determination and other applications. *Protein NMR Spectroscopy* (2007).

135. A. Cammers-Goodwin, T. J. Allen, S. L. Oslick, K. F. McClure, J. H. Lee & D. S. Kemp. Mechanism of stabilization of helical conformations of polypeptides by water containing trifluoroethanol. *Journal of the American Chemical Society* **118**, 3082–3090 (1996).

136. D. S. Wishart & B. D. Sykes. Chemical shifts as a tool for structure determination. *Methods in Enzymology* **239**, 363–392 (1994).

137. D. S. Wishart, B. D. Sykes & F. M. Richards. Relationship between nuclear magnetic resonance chemical shift and protein secondary structure. *Journal of Molecular Biology* **222**, 311–333 (1991).

138. J. L. Markley, A. D. Bax, Y. Arata, C. W. Hilbers, R. Kaptein, B. D. Sykes, P. E. Wright & K. Wuthrich. Recommendations for the presentation of RMN structures of proteins and nucleic acids. *Pure & Appl. Chem.* **70**, 117–142 (1998).

139. D. S. Wishart, C. G. Bigam, J. Yao, F. Abildgaard, H. J. Dyson, E. Oldfield, J. L. Markley & B. D. Sykes. 1H, 13C and 15N chemical shift referencing in biomolecular NMR. *Journal of Biomolecular NMR* **6**, 135–140 (1995).

140. G. Cornilescu, F. Delaglio & A. Bax. Protein backbone angle restraints from searching a database for chemical shift and sequence homology. *Journal of Biomolecular NMR* **13**, 289–302 (1999).

141. L. Makowski, D. Gore, S. Mandava, D. Minh, S. Park, D. J. Rodi & R. F. Fischetti. X-ray solution scattering studies of the structural diversity intrinsic to protein ensembles. *Biopolymers* **95**, 531–542 (2011).

142. I. W. Hamley. Peptide fibrillization. *Angewandte Chemie - International Edition* **46**, 8128–8147 (2007).

143. O. S. Makin & L. C. Serpell. Structures for amyloid fibrils. *FEBS Journal* **272**, 5950–5961 (2005).

144. E. Tayeb-Fligelman, O. Tabachnikov, A. Moshe, O. Goldshmidt-Tran, M. R. Sawaya, N. Coquelle, J. P. Colletier & M. Landau. The cytotoxic Staphylococcus aureus PSMα3 reveals a cross-α amyloid-like fibril. *Science* **355**, 831–833 (2017).

145. V. Iacobucci, F. Di Giuseppe, T. T. Bui, L. S. Vermeer, J. Patel, D. Scherman, A. Kichler, A. F. Drake & A. J. Mason. Control of pH responsive peptide self-association during endocytosis is required for effective gene transfer. *Biochimica et Biophysica Acta - Biomembranes* **1818**, 1332–1341 (2012).

146. R. Gerbier et al. Development of original metabolically stable apelin-17 analogs with diuretic and cardiovascular effects. *FASEB Journal* **31**, 687–700 (2017).

VIII. Supporting information

Name	Sequences	Transfection efficiency (%)	cells	ref
LAH4	KKALLALALHHLAHLALHLALALKKA	100		
H4-LAK4	HHALLALALKKLAKLALKLALALHHA	2	HepG2	[17]
LAH4-K2-E2	KKLALALHHLAHLALHLALALEE	≤0.1	HepG2	X
LAH4-K4-E4	KKKKLALALHHLAHLALHLALALEEEE	≤0.1	HepG2	X
LAH4-L6	KKKKALLHLHLLALHLHLLALLALKKK	1	HepG2	[17]
LAH4-A6	KKKKALAHLHALAAHLHALAAALKKK	14	HepG2	[17]
LAH4-G6	KKKKALGHLHGLAGHLHGLAGGALKK	≤0.1	HepG2	[17]

Figure SI 1: LAH4 derivatives, histidine modification in the LAH4 sequence with their corresponding transfection activity percentage compared to LAH4 (100%). The publications where the results are found and X: unpublished.

Name	Sequences	Transfection efficiency (%)	cells	ref
LAH4-L1	KKALLALALHHLAHLALHLALALKKA	≥100	HepG2	[10]
LAH6-L1	KKALLAHALHHLALLHHLAHALKKA	37 44	MRC5-V2 HepG2	[18] [84]
LAH4-L1-30	KKALLAAHLAHLLAALLAHLLHALLALKKA	37 44	MRC5-V2 HepG2	[84]
LAH4-L1-30-D	KKALLAAHLAHLLAALLAHLLHALLALKKA	39 6	MRC5-V2 HepG2	[84]
LAH4-D	KKALLALALHHLAHLALHLALALKKA	39 6	MRC5-V2 HepG2	[84]
LAH6-L1-80	KKHLLAHALHLLALLALHLAHALAHLKKA	59 46	MRC5-V2 HepG2	[84]
LAH4-X1	KKLALHALHLLALLWLHLAHLALKK	8	MRC5-V2	[145]
LAH4-X1F1	FKKLALHALHLLALLWLHLAHLALKK	18	MRC5-V2	[145]
LAH4-X1F2	FFKKLALHALHLLALLWLHLAHLALKK	1	MRC5-V2	[145]
LAH6-X1	KHKALHALHLLALLWLHLAHLAKHK	17	MRC5-V2	[145]
LAH6-X1L-W	KHKLLHLLHLLALLWLHLLHLLKHK	57	MRC5-V2	[145]
LAH6-X1L	KHKLLHLLHLLALLALHLLHLLKHK	54	MRC5-V2	[145]
LAH6-X1L-26	KHKLLHLLHLLALLALHLLHLLAHKK	50	MRC5-V2	[145]
LAH6-X1L-P13	KHKLLHLLHLLAPLALHLLHLLKHK	2	MRC5-V2	[145]
LAH-P10	KKLAHALHLPALLWLHLAHALKKA	24	MRC5-V2	[145]
LAH4-Leu	KKALLALLLHHLLHALLHLLLALKKA	100	911	[46]
LAH4-L1-Leu	KKALLAHLLHLLLALLLHLLHALKKA	53	911	[46]
LAH4-L1-R	RRALLAHALHLLALLALHLAHALRRA	87	911	[46]
LAH4-L1-F	FFKKLAHALHLLALLALHLAHALKKA	33	911	[46]
LAH4-L1-F4	KKALLAHFFHLLALLALHFFHALKKA	100	HepG2/HEK293	[18]
LAH4-L1-F2d	KKALLAHFLHLLALLALHLFHALKKA	100	HepG2/HEK293	X
LAH4-L1-Opt	KKLALAHALHLALLLALHLAHALKKA	40 5	HepG2 HEK293	X
LAH4-L1-β	KKALAHALHLLALALLHLAHALAKK	56	MRC5-V2	X
LAH4-L1-IP	LALALKHALHKLALLAKHLAHKLALA	≤0.1	MRC5-V2	[43]
LAH6-L1-80-K2	KHALAHALHLALLLALHLAHALAHKA	0.1	MRC5-V2	X
D-LAH4-L1-rev	AKKLAHALHLALLALLHLAHALLAKK	0.5	HepG2/GM3P51	X
D-LAH4-L1-β	KKALAHALHLLALALLHLAHALAKK	14	MRC5-V2	X
D-LAH4-L1	KKALLAHALHLLALLALHLAHALKKA	0.1 3	HepG2 MRC5-V2	X
LAH	KKLAHALHLLALLWLHLAHALKKA	33.4	MRC5-V2	[41]
LAK	KKLAKALKLLALLWLKLAKALKKA	0.2	MRC5-V2	[41]

Figure SI 2: LAH4-L1 derivatives, histidine modification in the sequence with their corresponding transfection activity percentage compared to LAH4-L1 (100%). The publications where the results are found and X: unpublished.
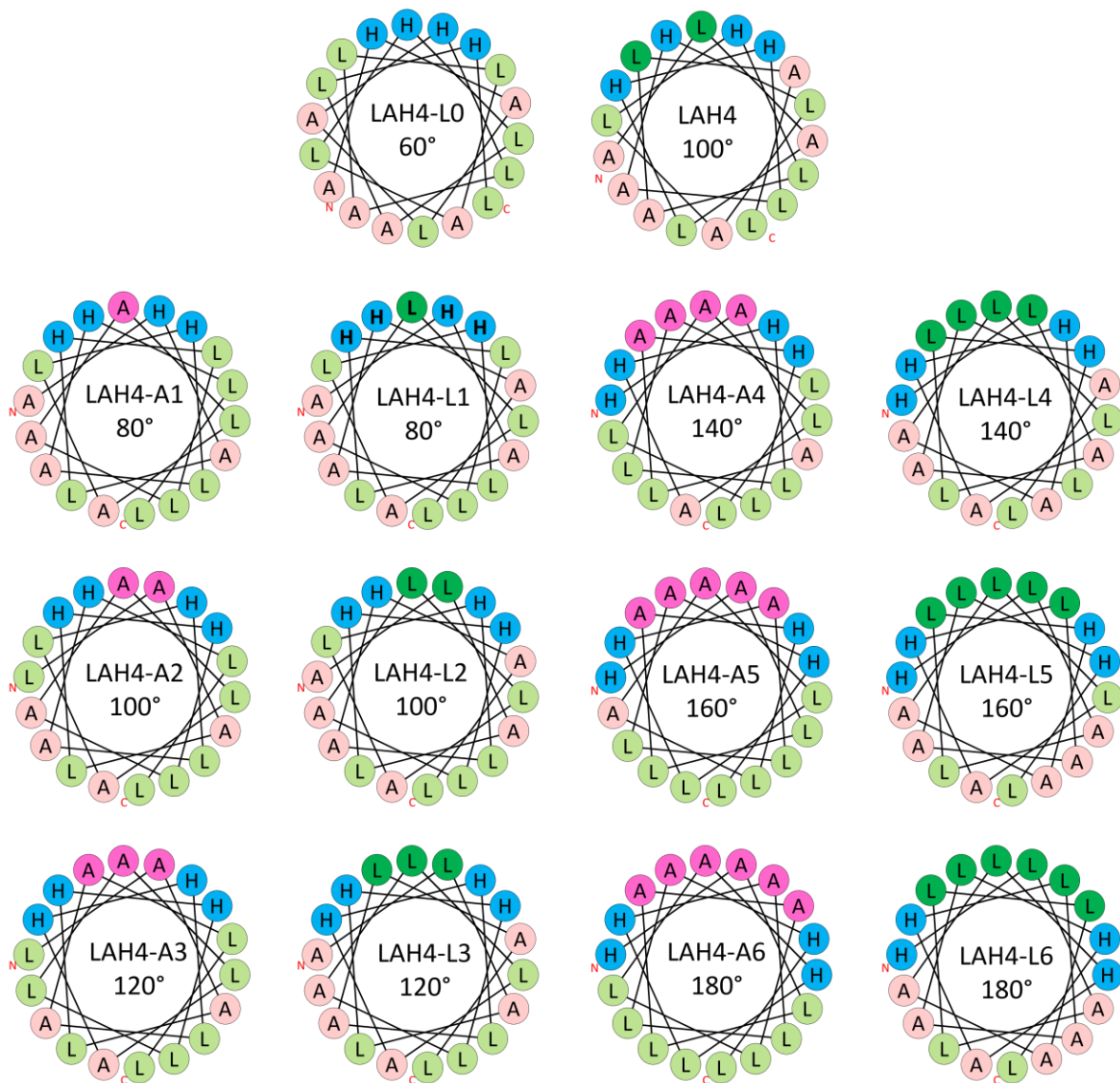
Figure SI 3: Schiffer-Edmundson helical wheel representations of the putative amphipathic α-helical region (residues 6-23) of the LAH4-An and LAH4-Ln peptides and their hydrophilic angle corresponding.
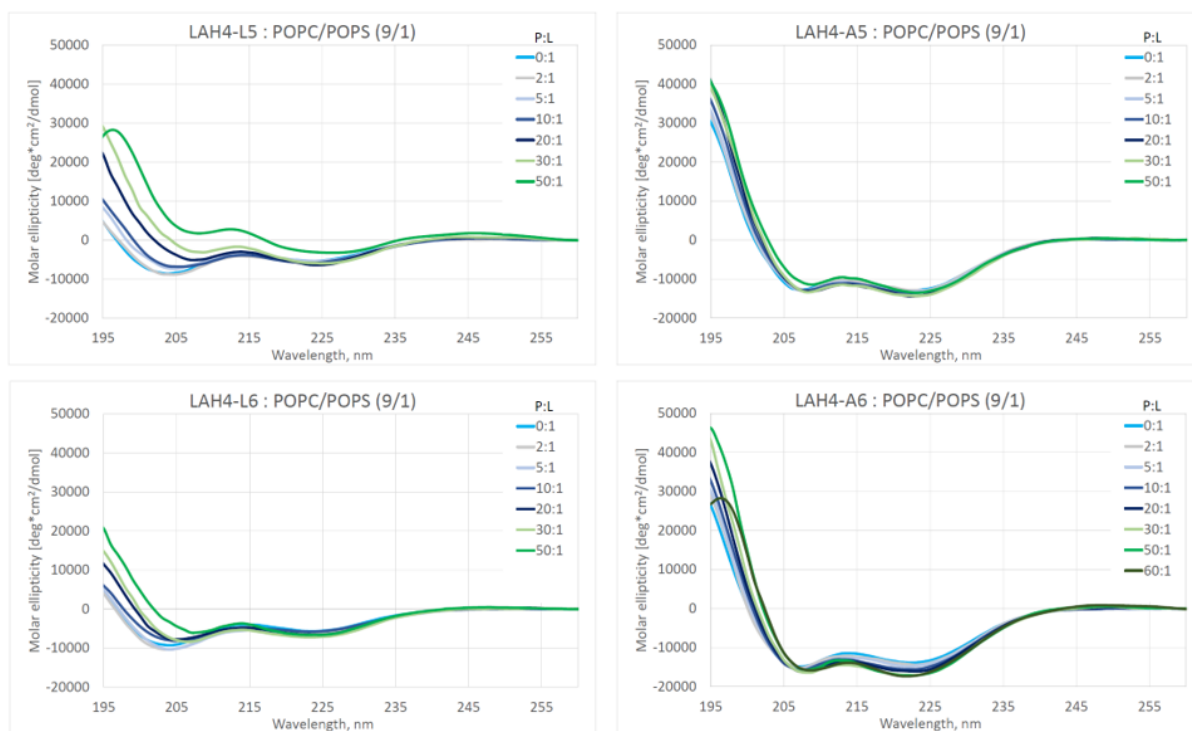
Figure SI 4: Circular dichroism curves of the LAH4-L5, LAH4-L6, LAH4-A5 and LAH4-A6 series peptide solution in 10 mM acetate buffer titrated with POPC/POPS (9/1) SUVs. Each curve corresponds to the indicated lipid to peptide ratio.

Figure SI 5: Circular dichroism curve of the LAH4-Ln or LAH4-An series peptide solution in 10 mM acetate buffer titrated with POPC/POPS (9/1) SUVs. Each curve corresponds to the indicated lipid to peptide ratio.

| LAH4-A1 RATIO L/P	0	2	5	10	20	30	50	60	70	80
ALPHA-HELIX	20	28	36	42	61	67	71	77	80	
BETA	14	13	9	10	9	8	8	10	5	
RANDOM COIL	38	37	35	31	22	17	15	9	9	
OTHER	27	22	23	18	8	8	6	4	6	

LAH4-A2 RATIO L/P	0	2	5	10	20	30	50	60	70	80
ALPHA-HELIX	17	22	27	35	47	60	70	74	73	78
BETA	14	14	13	11	10	9	9	12	10	13
RANDOM COIL	38	37	37	31	31	22	14	10	13	6
OTHER	31	27	23	25	12	9	7	4	4	4

LAH4-A3 RATIO L/P	0	2	5	10	20	30	50	60	70	80
ALPHA-HELIX	21	19	21	41	55	65	75	82	82	
BETA	14	7	8	13	10	8	9	9	13	
RANDOM COIL	38	25	25	36	27	20	12	6	3	
OTHER	27	16	12	10	8	8	4	2	2	

LAH4-A4 RATIO L/P	0	2	5	10	20	30	50	60	70	80
ALPHA-HELIX	22	26	32	37	51	62	71	58	61	
BETA	14	13	9	8	11	8	9	4	18	
RANDOM COIL	35	37	36	32	28	21	13	13	12	
OTHER	24	23	23	10	9	7	25	9	24	

LAH4-A5 RATIO L/P	0	2	5	10	20	30	50	60	70	80
ALPHA-HELIX	53	47	47	43	55	62	61			
BETA	10	11	11	12	9	8	5			
RANDOM COIL	26	31	32	36	26	20	16			
OTHER	11	10	11	9	8	11	19			

LAH4-A6 RATIO L/P	0	2	5	10	20	30	50	60	70	80
ALPHA-HELIX	53	53	57	59	66	66	80	75		
BETA	8	10	9	9	8	6	8	9		
RANDOM COIL	30	28	25	23	17	18	7	12		
OTHER	9	9	9	9	9	10	4	4		

LAH4-L0 RATIO L/P	0	2	5	10	20	30	50	60	70	80
ALPHA-HELIX	22	22	27	32	40	52	66	62	50	
BETA	14	14	14	11	12	9	7	7	8	
RANDOM COIL	38	35	36	34	34	26	17	11	15	
OTHER	27	29	22	23	15	13	10	19	27	

LAH4-L1 RATIO L/P	0	2	5	10	20	30	50	60	70	80
ALPHA-HELIX	23	30	34	38	50	65	71			
BETA	15	10	9	12	9	7	10			
RANDOM COIL	36	37	38	37	31	19	15			
OTHER	25	23	20	12	10	9	4			

LAH4-L2 RATIO L/P	0	2	5	10	20	30	50	60	70	80
ALPHA-HELIX	17	20	24	32	43	52	63		70	
BETA	15	14	13	9	13	10	9		13	
RANDOM COIL	34	35	34	33	34	29	18		9	
OTHER	31	32	29	30	11	9	11		8	

LAH4-L3 RATIO L/P	0	2	5	10	20	30	50	60	70	80
ALPHA-HELIX	19	20	26	31	42	48	78	79	81	82
BETA	13	14	14	13	11	12	12	13	11	14
RANDOM COIL	39	41	38	38	33	31	8	6	5	0
OTHER	29	25	26	20	14	9	2	2	3	4

LAH4-L4 RATIO L/P	0	2	5	10	20	30	50	60	70	80
ALPHA-HELIX	19	21	23	32	38	41	74		76	
BETA	13	14	14	12	9	8	10		17	
RANDOM COIL	39	37	37	34	35	22	4		2	
OTHER	28	28	26	23	17	10	12		5	

LAH4-L5 RATIO L/P	0	2	5	10	20	30	50	60	70	80
ALPHA-HELIX	24	24	29	25	24	26	26			
BETA	13	13	12	24	15	14	12			
RANDOM COIL	36	39	34	37	27	26	23			
OTHER	26	24	25	25	35	34	38			

LAH4-L6 RATIO L/P	0	2	5	10	20	30	50	60	70
ALPHA-HELIX	31	27	27	30	29	30	31	29	36
BETA	12	12	13	10	8	11	11	12	16
RANDOM COIL	38	38	39	38	32	33	30	20	19
OTHER	19	22	22	66	30	27	27	40	28

Figure SI 6: The secondary structure composition (in %) of the LAH4-An and LAH4-Ln peptides from the CD spectra recorded at different L/P ratios at pH 5. SUVs made from POPC/POPS 9/1 were added during the titration experiments to the peptide in solution to reach the indicated lipid-to-peptide ratios. The data shown averages from three independent measurements. The secondary structure elements were estimated using the DICROPROT software using the algorithms SELCON3.
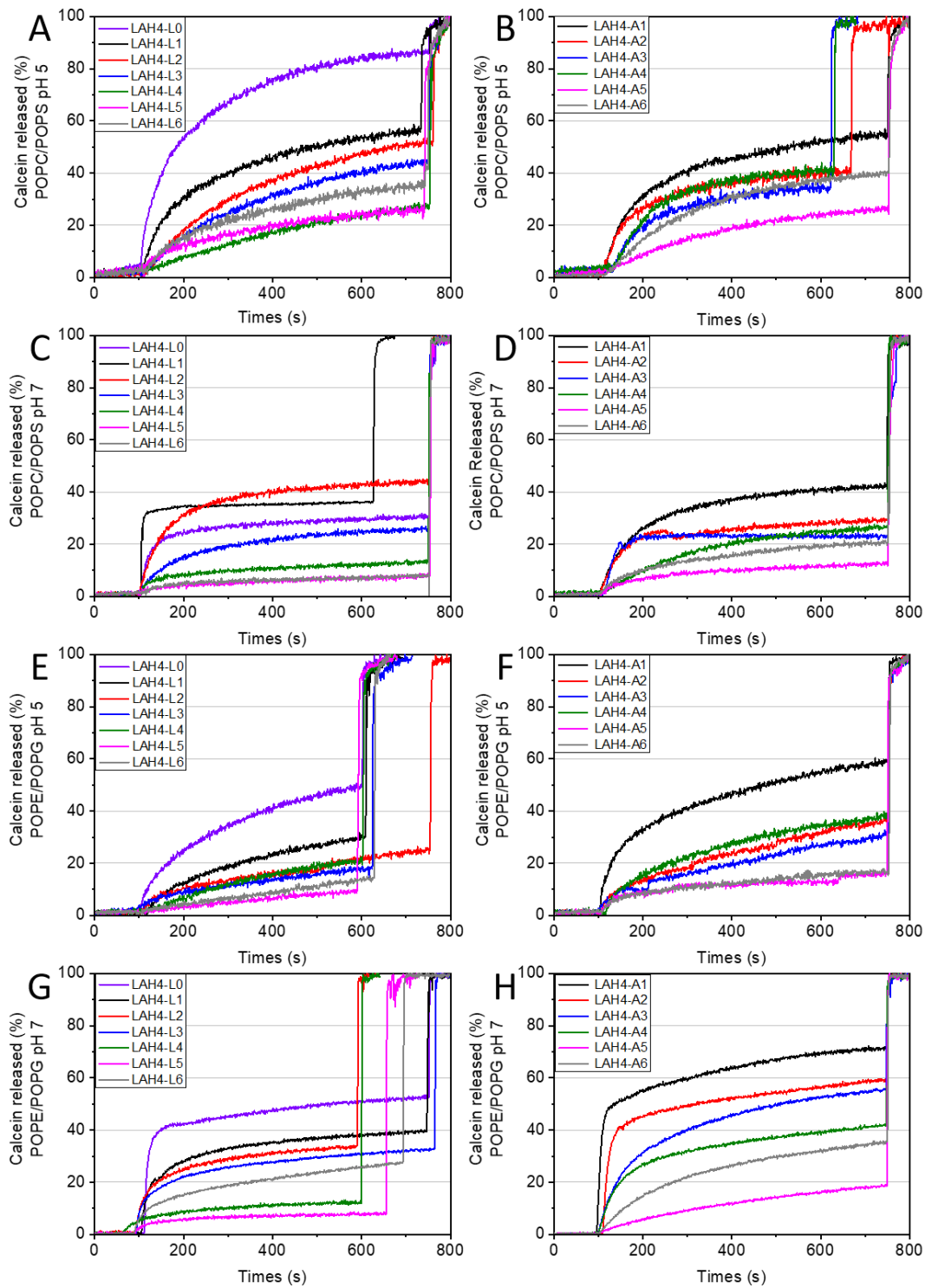
Figure SI 7: Calcein release performed by the LAH4-Ln (left) and LAH4-An (right) series on different vesicles and pH: POPC/POPS (3/1) at pH 5 (A, B) and pH 7 (C, D). POPE/POPG (3/1) at pH 5 (E, F) and pH 7 (G, H).
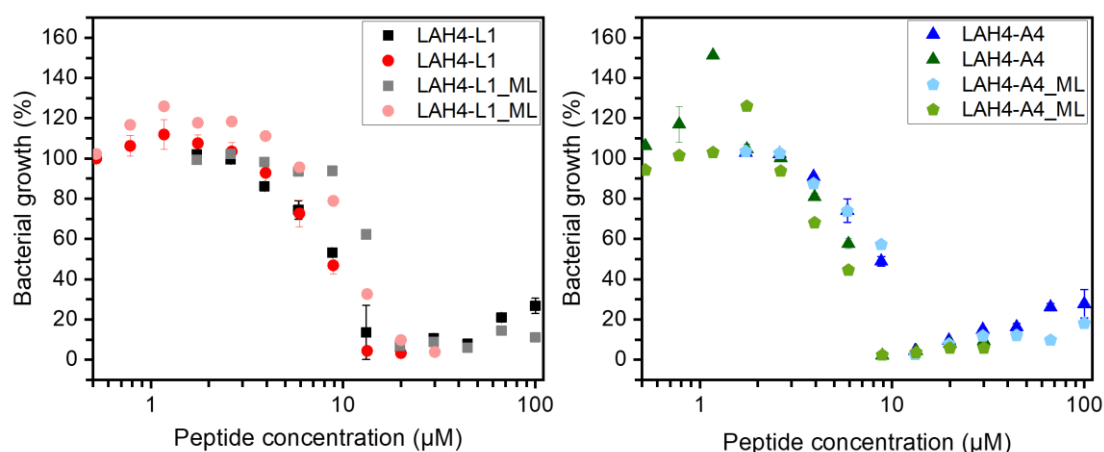
Figure SI 8: Percentage of bacterial growth as a function of the peptide concentration for commercial vs. synthetic preparations of LAH4-L1 and LAH4-A4. The two tested peptide concentration ranges are 100 µM-1.73 µM and 30 µM-0.52 µM, they are represented in black and red respectively for LAH4-L1; in blue and green for LAH4-A4. LAH4-L1 and LAH4-A4 are commercial peptide (dark) whereas LAH4-L1_ML and LAH4-A4_ML are synthesized in the laboratory (light). Averages and standard deviations were obtained from the experimental data set of triplicates after subtraction of the CT- average (control without bacteria, 0%) and as a percentage of the CT+ average (control without peptides, 100%).

PEPTIDE	LAH4-L0	LAH4-L1	LAH4-L2	LAH4-L3	LAH4-L4	LAH4-L5	LAH4-L6
MIC	6.06	19.75	8.77	2.6	1.17	1.73	1.73

PEPTIDE	LAH4-A1	LAH4-A2	LAH4-A3	LAH4-A4	LAH4-A5	LAH4-A6
MIC	30	9.02	13.3	13.3	8.8	5.9

Figure SI 9: Summarizing the Minimum Inhibition Concentration (MIC) for the LAH4-Ln and LAH4-An series. The two experimental data sets (each including triplicates) therefore covering the concentration range 100 µM-0.52 µM. When the percentage of bacterial growth reach minima usually around 0-10%, we can determine the minimum concentration of each peptide that allows to inhibit bacterial growth (MIC).
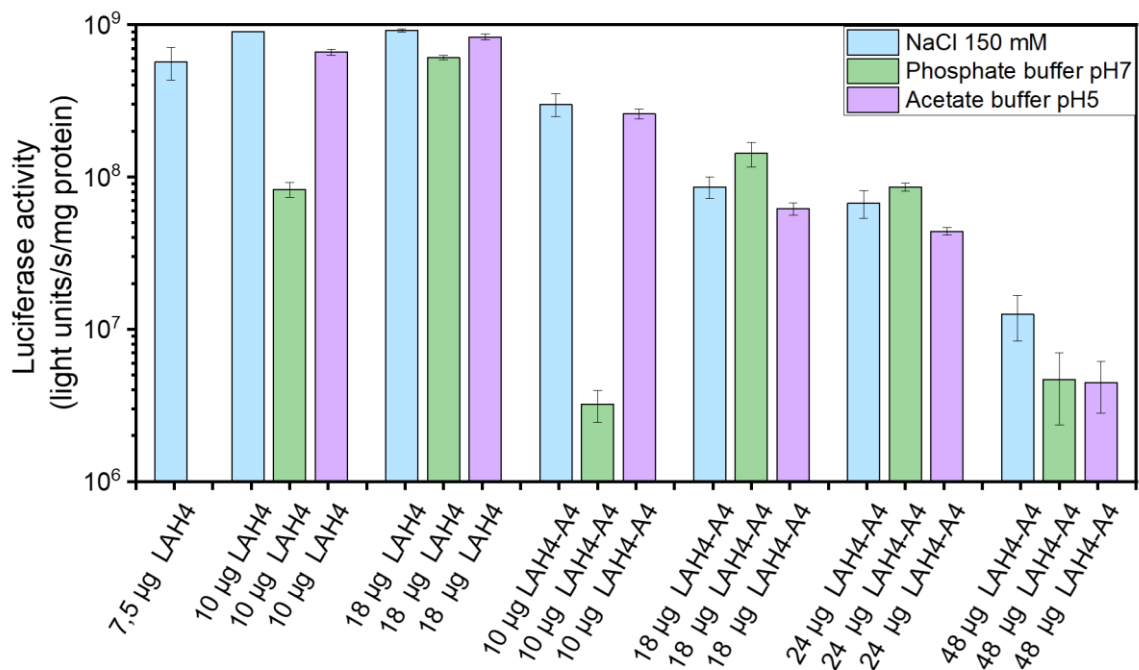
Figure SI 10 Luciferase activity for LAH4 and LAH4-A4 with different buffer and peptide quantity.

PEPTIDE	LAH4-L0	LAH4-L1	LAH4-L2	LAH4-L3	LAH4-L4	LAH4-L5	LAH4-L6
RLU/S/MG	$4.2*10^8$	$1.2*10^9$	$5.8*10^8$	$6*10^8$	$1.5*10^8$	$3.3*10^7$	$1.7*10^7$
ERROR	$3.7*10^7$	$1.2*10^8$	$8.5*10^7$	$5.7*10^7$	$1.9*10^7$	$3.7*10^6$	$1.6*10^6$

PEPTIDE	LAH4-A1	LAH4-A2	LAH4-A3	LAH4-A4	LAH4-A5	LAH4-A6
RLU/S/MG	$8.8*10^8$	$4*10^8$	$2.8*10^7$	$1.1*10^7$	$8.7*10^8$	$2.4*10^8$
ERROR	$5.1*10^7$	$3.9*10^7$	$2.6*10^6$	$9.2*10^6$	$5*10^7$	$2.7*10^7$

Figure SI 11: Summarizing the luciferase efficiency for the LAH4-Ln and LAH4-An series. Only the conditions giving the highest luciferase expression are reported.
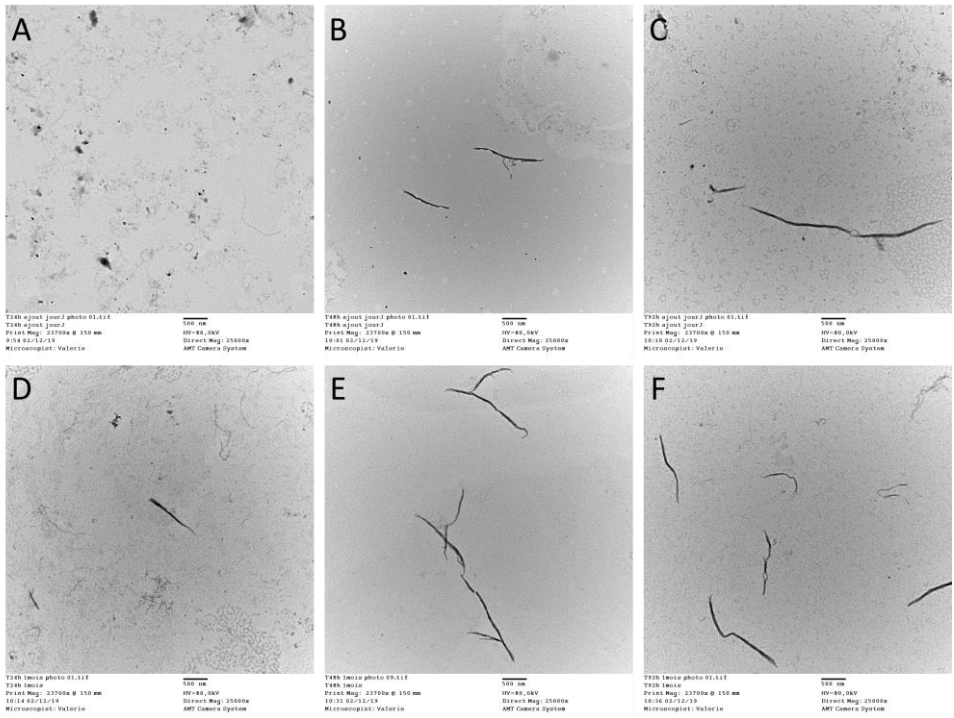
Figure SI 12: Transmission Electron microscopy of the fibrils depending of the time. Images of samples deposited after 24h (A) 48h (B) and 92h (C) of dialysis. The image of the same samples (24h (D) 48h (E) and 92h (F) of dialysis), deposited after been left one month on the bench.
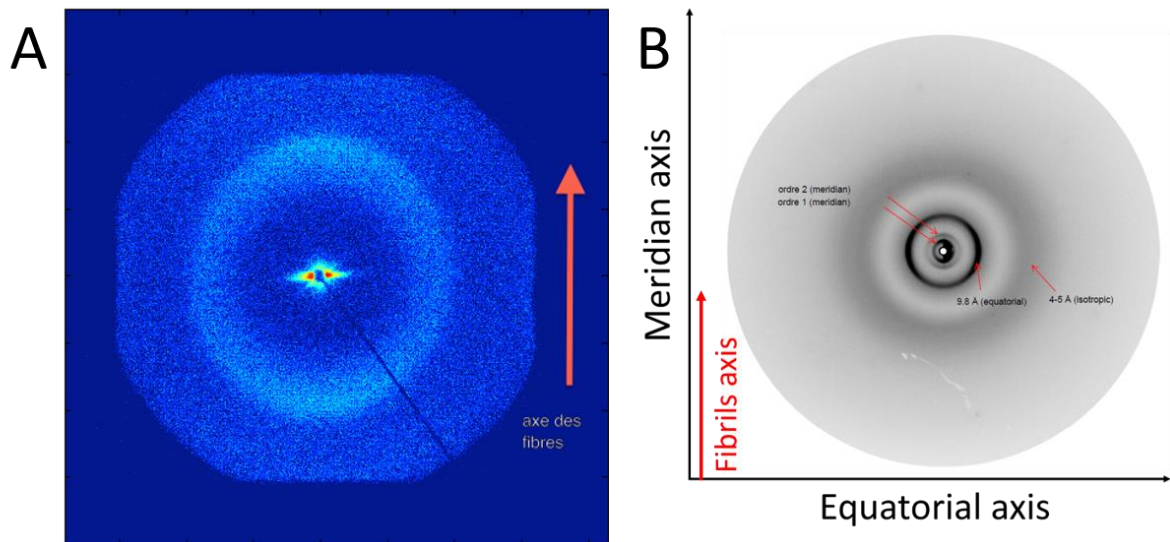
Figure SI 13: the image of small-Angle X-ray Scattering (A) and Wide-Angle X-ray Scattering (B). The image measured on a flat image for the WAXS. The fibrillation was conducted by shaking over 2 days in 10 mM phosphate buffer at pH 7.4 at room temperature. The pellet was washed and the pellet fibrils were checked after by TEM analysis. The pellets were dried slowly to remove all water traces.

IX. Résumé

IX.1 Introduction

Notre laboratoire a conçu un peptide modèle le LAH4 riche en histidine comme un peptide antimicrobien (AMP) [1]. Le LAH4 est composé de 26 résidus dont seulement 4 acides aminés différents : deux lysines à chaque extrémité assurent une bonne solubilité dans l'environnement aqueux, le corps composé d'alanines et de leucines, est interrompu par quatre histidines (Figure 1). Le peptide a une charge globale de + 9 à pH acide et de + 5 à pH neutre du fait de la présence des histidines dans la séquence [2]. En solution, à pH acide (<6), les histidines du peptide sont protonées et le peptide a une conformation aléatoire. Lorsque la valeur du pH dépasse celle du pKa des histidines vers 6, les histidines deviennent neutres, et le peptide adopte une structure en hélice α [1] [2] (Figure 1).

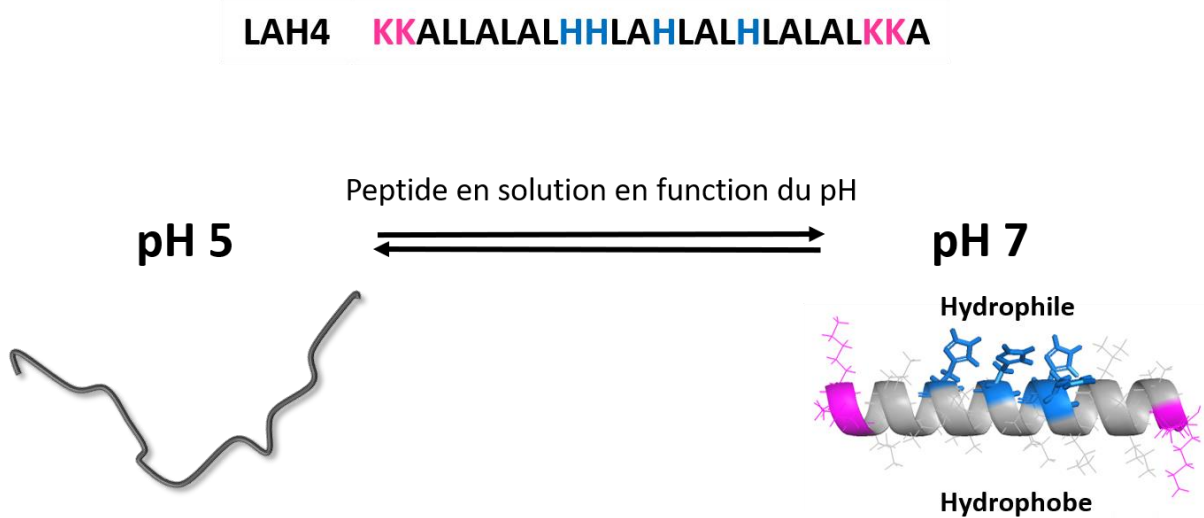**LAH4   KKALLALALHHLAHLALHLALALKKA**

Figure 1: Les deux conformations du LAH4 en fonction du pH de la solution. A pH 5 le peptide est dans une conformation aléatoire. Lorsque le pH augmente, le peptide adopte une structure en hélice α. Le peptide LAH4 en structure hélice α présente un caractère amphipatique avec : une face hydrophobe et l'autre hydrophile. En gris, les résidus d'alanine et de leucine, en magenta les résidus lysines et en bleu les histidines.

Le peptide est amphipathique lorsqu'il adopte une structure en hélice α et présente deux faces : l'une hydrophobe constitué d'alanines et de leucines, l'autre hydrophile avec des histidines (Figure 1) [1].

Dans un environnement membranaire, le LAH4 adopte une conformation amphipathique en hélice α [1]. L'orientation peptidique dans les membranes dépend de l'état de protonation des histidines [3]. En effet, à pH 5, LAH4 adopte une orientation parallèle à la surface de la membrane [4][5]. A pH 6.1 (c'est-à-dire autour des valeurs de pKa des histidine : 5,8; 5,4; 5,7 et 6,0 respectivement pour H10, H11, H14 et H18), il y a une rupture dans l'hélice α entre L9 et H14 [6]. A pH neutre, les histidines sont déprotonées et le peptide passe d'une orientation planaire à une orientation transmembranaire. L'orientation membranaire de l'hélice peut être déterminée par résonance magnétique nucléaire (RMN) à l'état solide orientée. Le déplacement chimique de l'azote ^{15}N [7], est inférieur à 100 ppm pour une orientation planaire ou environ 200 ppm pour une orientation transmembranaire (Figure 2) [4].
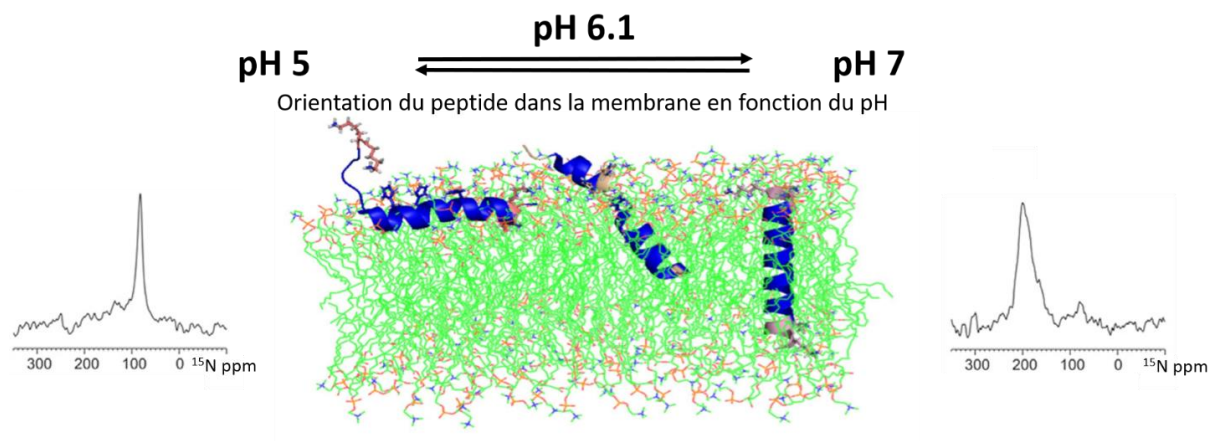

Figure 2: Les différentes orientations du LAH4 en fonction du pH dans un environnement membranaire. Le peptide adopte dans les membranes une orientation planaire a pH 5 alors qu'à pH autour de 7 il adopte une orientation transmembranaire. Les spectres RMN orienté à l'état solide du ^{15}N correspondent à ces deux orientations (adaptés des publications [4][8]).

Outre ces propriétés structurales, le LAH4 présente également des activités biologiques intéressantes [9]. Le peptide LAH4 présente des activités de formation de pores dans les membranes et des activités antimicrobiennes aux pH neutre et acide, même s'il est plus efficace à pH acide [1][10].

De plus, le LAH4 appartient à la catégorie des peptides à pénétration cellulaire (CPP) définis par leur capacité à interagir avec la membrane cellulaire et à entrer dans la cellule par différents mécanismes [11][12][13].

Le peptide a montré une efficacité pour améliorer l'internalisation cellulaire pour une grande variété de vecteur qui peut être divisée en deux types: virale ou non virale [14][15]. Le processus d'administration par système non viral est appelé transfection (Figure 3 A) tandis que celui via un vecteur viral est appelé transduction (Figure 3 B).
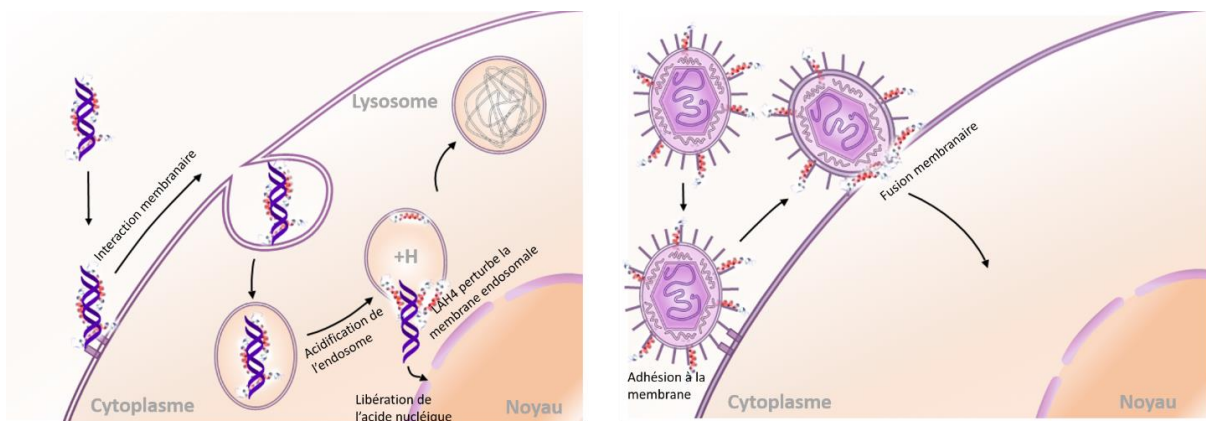

Figure 3: Représentation schématique du mécanisme de transfection (A) et de transduction (B) (extrait de [16] et [17])

Afin d'accroître ces activités, des dérivés LAH4 ont été conçus constituant la famille LAH4. Dans la famille des peptides LAH4, les réarrangements d'acides aminés entraînent un changement de fonctionnalité [18]. Comme il a pu être montré avec deux membres de cette famille: LAH4-L1 et LAH4-A4, permettent d'améliorer les activités de transfection [18][19] et de transduction, respectivement [20][21].

La famille des peptides LAH4 présente des activités : antimicrobiennes [1][10], de pénétration cellulaire [2], de transfection [3][18][22] et de transduction [20][23]. L'étude de la relation entre la similitude des séquences et la variété des activités biologiques présentée par les peptides de la famille LAH4 est d'un grand intérêt. En effet, la compréhension du mécanisme de ces activités basées sur de petits changements dans leur séquence aiderait à la conception de peptides plus actifs.

Une autre façon d'améliorer l'efficacité du peptide est de considérer la structure comme un modulateur de l'activité. L'auto-assemblage peptidique permet de nouvelles fonctions ou une

augmentation de leurs activités biologiques [24]. En effet, pour certains peptides l'assemblage supramoléculaire comme la formation de fibres s'est montré important pour la transduction de lentiviral [21].

Dans une première étude, pour mieux comprendre le mécanisme d'insertion sur la membrane et les différences, des peptides de la famille LAH4 ont été étudiés et comparés. Nous nous sommes concentrés sur les peptides des séries "LAH4-Ln" et "LAH4-An" décrits plus loin dans la section résultats [20] comprenant ainsi LAH4-A4 et LAH4-L1. Leur structure secondaire a été déterminée par dichroïsme circulaire. Leur activité antimicrobienne, de transduction, de transfection et leur capacité à former des pores ont été testées. Leurs caractéristiques biophysiques ont été corrélées avec leurs activités biomédicales. La transduction nécessite une formation de fibres qui guide et accumule les particules virales à la surface de la membrane [21]. Les fibres peuvent également être impliquées dans les interactions directes avec la membrane, non seulement pour assurer l'adhérence mais également pour favoriser la fusion membranaire.

Dans une deuxième étude, nous nous sommes donc consacrés aux conditions fibrillation de LAH4-A4 afin de mieux comprendre son autoassemblage. Les meilleures conditions de fibrillation de LAH4-A4 ont été déterminées et cette étude s'est étendue à deux autres peptides LAH4-L1 et LAH4. Une fois les fibres obtenues, leur stabilité a été testée dans le temps et dans des environnements différents (milieu, pH). La structure de ces trois fibres a été analysée par Microscopie à Transmission Electronique, Résonnance Magnétique Nucléaire à l'état solide et spectroscopie InfraRouge à Transformée de Fourier.

Une troisième étude a été initiée pour déterminer la structure des fibres de LAH4-A4. La structure des fibres est essentielle pour comprendre leurs mécanismes d'action. Dans un premier temps, l'étude structurale du LAH4-A4 en solution a été effectuée par spectroscopie RMN à l'état liquide. Puis les fibres de LAH4-A4 ont été étudiées par spectroscopie RMN à l'état solide. Afin de simplifier l'assignement des acides aminées le peptide a été marqué spécifiquement à différents segments de la séquence, décrits plus loin dans la section résultats. Cette étude permettra de comparer le peptide en solution ou en fibres afin de

déterminer les changements liés à l'auto-assemblage du peptide, puis d'acquérir une meilleure compréhension structurale de ces fibres. Les interactions intramoléculaires des fibres déterminées, nous nous sommes intéressés aux interactions intermoléculaires des fibres du LAH4-A4. De plus, les techniques de diffusion des rayons X aux petits et grands angles (SAXS et WAXS) ont permis d'obtenir des renseignements sur l'arrangement des fibres avec des distances intermoléculaires.

IX.2 Résultats et discussions

Pour mieux comprendre le rôle de l'angle hydrophile, les isomères de la famille LAH4 qui présentent différents angles formés par les résidus d'histidine lorsque le peptide est en conformation hélice α ont été étudiés. Ces isomères ont été obtenus en modifiant le positionnement des quatre histidines dans la séquence du LAH4, permettant d'avoir deux séries de peptides LAH4-Ln et LAH4-An. Ces peptides sont nommés en fonction du nombre de "n" de Leucine (L) ou Alanine (A) qui sont présents entre les histidines lorsqu'ils sont vus dans une projection de roue hélicoïdale (Figure 4). Cette modification a permis de moduler un angle hydrophile θ allant de 60° à 180.
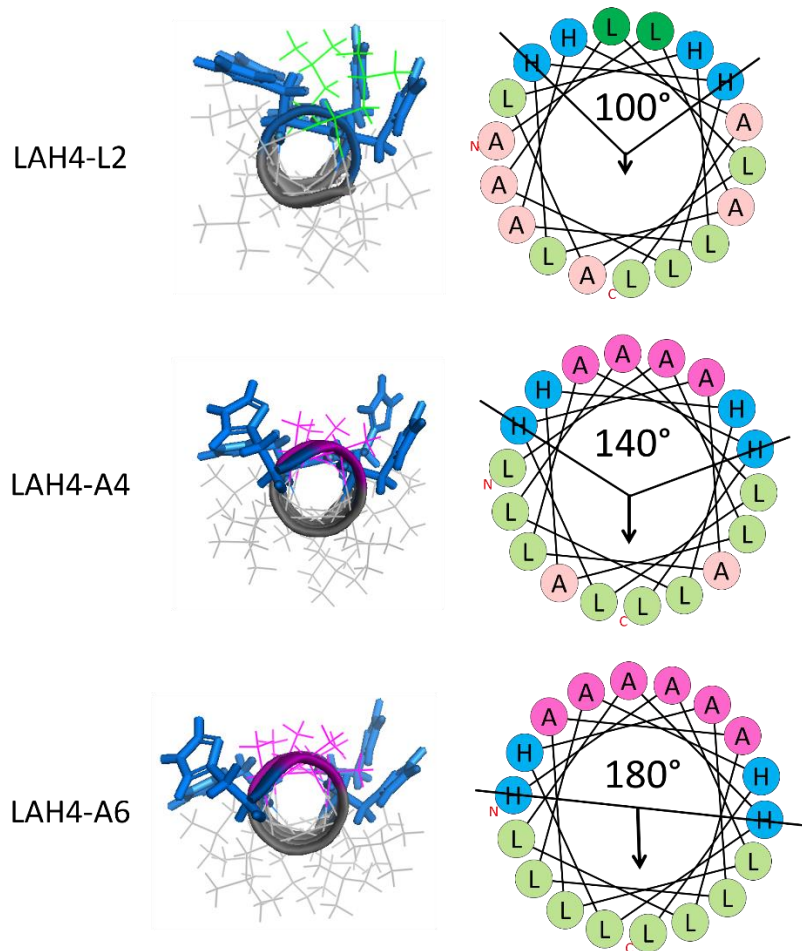
Figure 4: Représentations hélicoïdales de la région centrale (résidus 6-23) pour certains peptides LAH4-An et LAH4-Ln. Ce schéma montre le LAH4-L2 (100°), le LAH4-A4 (140°) et le LAH4-A6 (180°) avec leur angle hydrophile. Représentation PyMol du peptide en structure hélice α parfaite avec la distribution des histidines sur une face hydrophile (à gauche) et des représentations de roues hélicoïdale de Schiffer Edmundson dessinées à l'aide du logiciel Heliquest [25] pour la détermination de l'angle hydrophile. Les histidines (bleues) délimitent l'angle hydrophile, les acides aminés présents dans l'angle : leucine (vert foncé) et alanine (magenta). La flèche noire représente le moment hydrophobe.

La structure secondaire adoptée par les peptides des séries "LAH4-Ln" et "LAH4-An" a été étudiée par dichroïsme circulaire afin de rechercher s'il existait une corrélation en fonction de l'angle hydrophile présenté (allant de 60° à 180° selon les positions des histidines) [26]. La structure secondaire du peptide est l'un des paramètres qui peut influencer l'activité avec les membranes lipidiques [2].

L'étude effectué par dichroïsme circulaire montre que, pour les angles hydrophiles entre 60° et 140°, les peptides des deux séries présentent les mêmes propriétés physico-chimiques, qui sont des structures secondaires dépendantes du pH ou de l'interaction avec les membranes modèles POPC/POPS. Toutefois, pour les grands angles hydrophiles (160° et 180°), les peptides ne montrent pas d'interactions avec les membranes modèles POPC/POPS. Alors que la série LAH4-Ln se structure par une augmentation du pH de 5 à 7, la série LAH4-An présente déjà un haut degré de structure en hélice α à pH 5.

L'interaction des peptides avec des membranes modèles a été testée grâce à des expériences de relargage de calcéine mesuré par fluorescence. L'efficacité de cette famille de peptides à perturber les membranes modèles a ainsi été évaluée en suivant la libération du fluorochrome contenu dans des vésicules lipidiques. Nous observons une corrélation entre les angles hydrophiles des peptides et les activités mesurées (Figure 5). L'activité de libération de calcéine diminue de façon linéaire lorsque l'angle hydrophile des peptides passe de 60° à 160°. Ce résultat montre qu'il existe une corrélation notable entre l'angle hydrophile et l'activité de libération de calcéine.
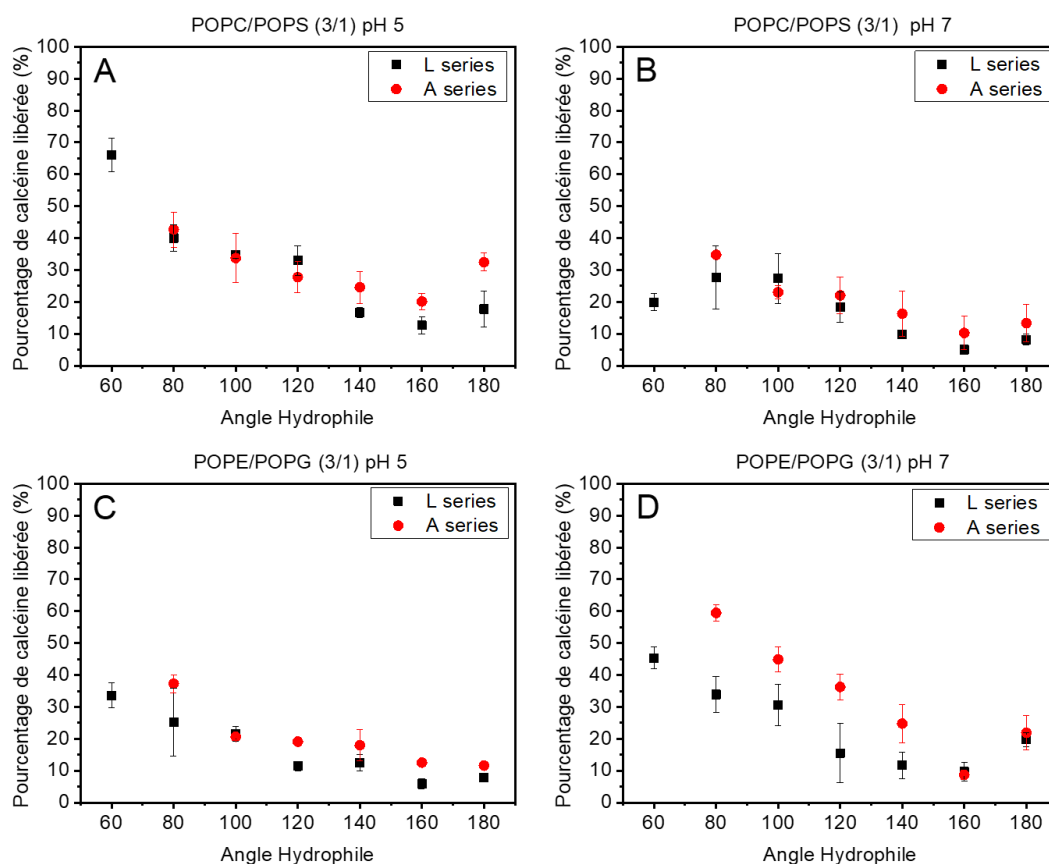
Figure 5: Le pourcentage de calcéine libérée par la famille de peptides LAH4 en fonction de l'angle hydrophile pour des vésicules lipidiques composées de POPC/POPS à pH 5 (A) et à pH 7.4 (B) ou de POPE/POPG à pH 5 (C) et à pH 7.4 (D). La série "LAH4-Ln", carrés noirs et la série "LAH4-An" cercles rouges.

Toutefois, pour les peptides qui présentent des angles hydrophiles de 60° à 160° (c.-à-d. LAH4-A1 à -A4 et -L0 à L4), l'étude par dichroïsme circulaire montre qu'il n'y a pas de différence dans l'association membranaire ni dans leur structure secondaire en solution ou en présence de membrane. Il est probable que les peptides avec un grand angle hydrophobe pénètrent plus profondément dans l'interface membranaire [27].

Les activités biophysiques et biologiques sont mises en perspective dans les études suivantes, la transfection peptidique et les activités antimicrobiennes sont corrélées avec l'activité de libération de calcéine. Les activités transfection et antimicrobiennes ont montré la même tendance que l'activité de libération de calcéine (Figure 6), ce qui n'est pas le cas pour la transduction (Figure 7). Ces différentes activités peuvent être liées à leurs mécanismes

d'action : alors que les activités transfection et antimicrobiennes sont soulignées par la déstabilisation de la membrane, la transduction a besoin d'une fusion avec la membrane.
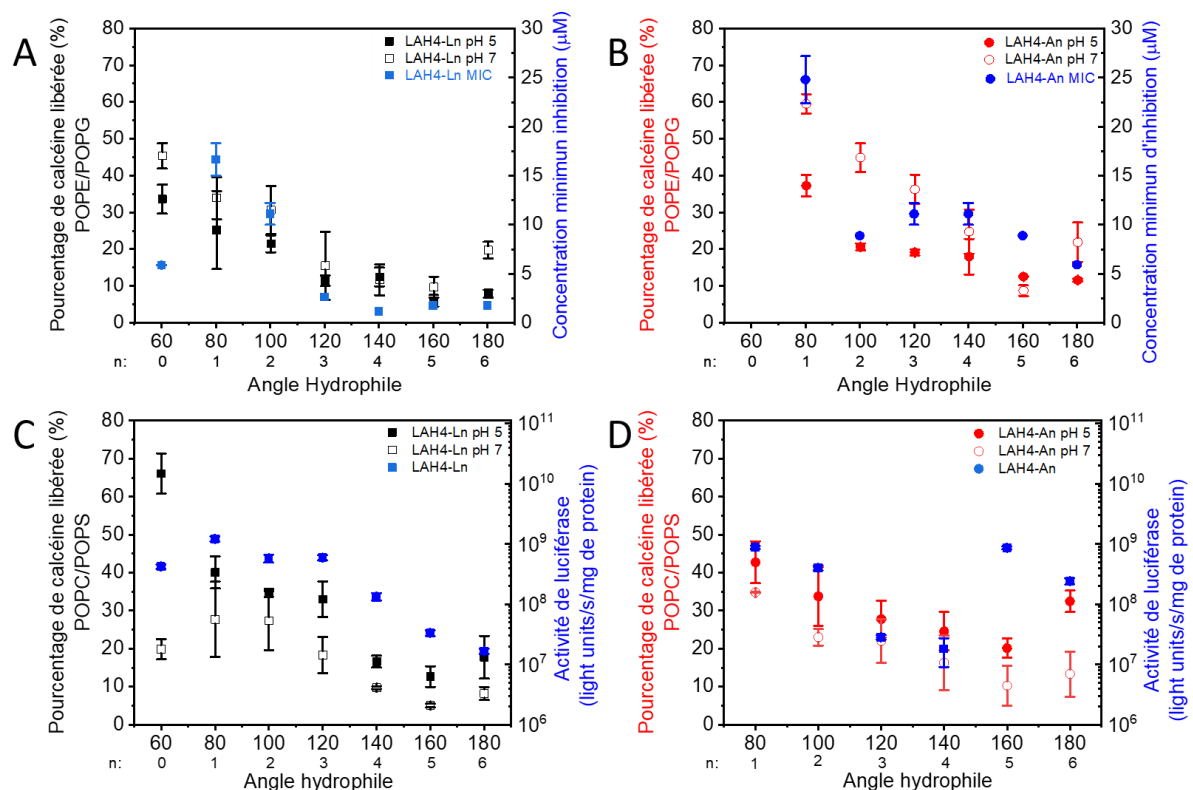

Figure 6: Le pourcentage de calcéine libérée et les activités biologiques entraînées par les isomères LAH4 en fonction de l'angle hydrophile. Pourcentage de rejet de calcéine encapsulée dans de larges vésicules unilamellaires composées de POPE/POPG (A, B) ou POPC/POPS (C, D) pour la série LAH4-Ln (carrés noirs) et LAH4-An (cercles rouges) à pH 5 (symboles pleins) et pH 7.4 (symbole ouvert). Sur le panel du haut, les larges vésicules unilamellaires composées de POPE/POPG 3/1 à pH 5 et pH 7.4 avec les concentrations minimales inhibitrices (bleu) pour les séries LAH4-Ln (A) et LAH4-An (B). Sur le panel du bas, les larges vésicules unilamellaires composées de POPC/POPS 3/1 à pH 5 et pH 7.4 avec l'efficacité de l'activité de luciférase (bleu) pour les séries LAH4-Ln (C) et LAH4-An (D).

En effet, une des étapes critiques dans le mécanisme de transfection est quand le peptide de la famille du LAH4 perturbe la membrane endosomique pour libérer sa cargaison d'acides nucléiques [16]. La capacité des peptides à perturber les chaînes d'acyl gras de la membrane peut être corrélée aux activités de transfection de diverses lignées cellulaires [3]. L'activité antimicrobienne est favorisée lorsque les peptides en hélice α s'insèrent dans l'interface membranaire et déstabilisent l'organisation de la membrane [28]. Les activités transfection et

antimicrobiennes ont été favorisées par des peptides contenant de la leucine sur la face hydrophile (LAH4-L1 et LAH4-L4, respectivement). La présence de leucine dans cette face pourrait favorisée la déstabilisation de membrane.
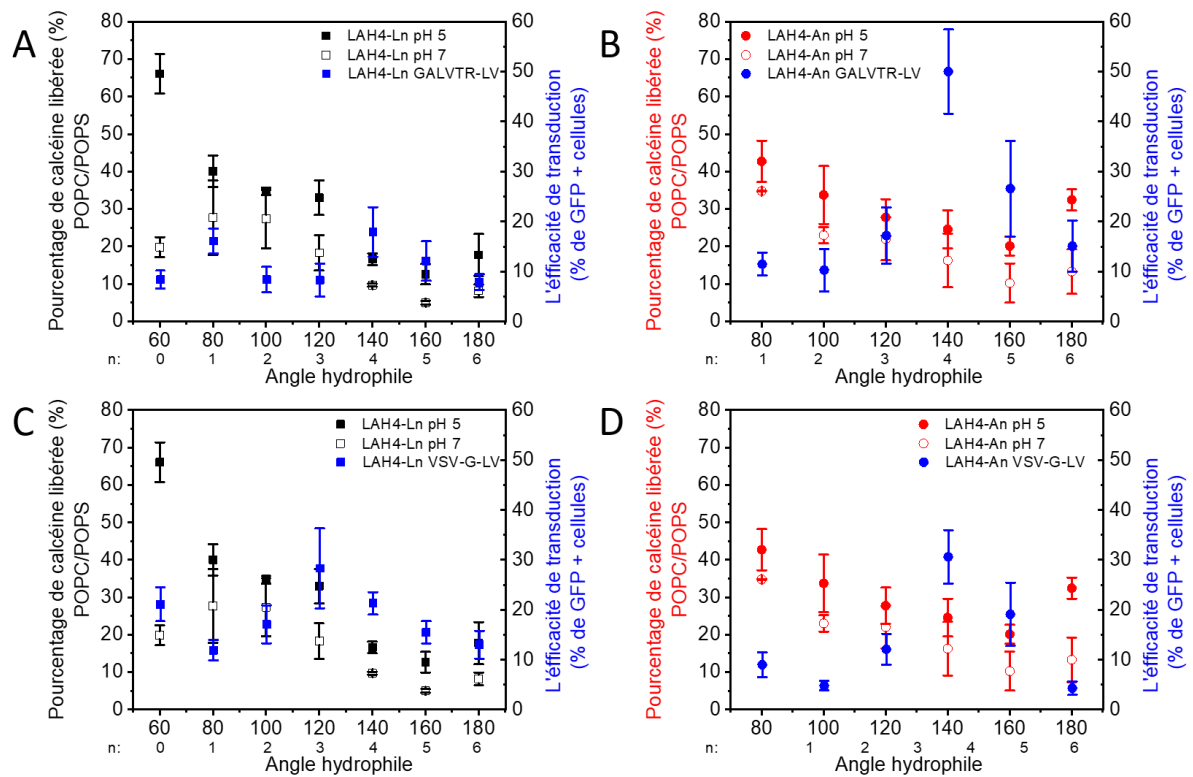

Figure 7: Le pourcentage de calcéine libérée et l'activité de transduction entraînée par les isomères LAH4 en fonction de l'angle hydrophile. Pourcentage de rejet de calcéine encapsulée dans de larges vésicules unilamellaires composées de POPC/POPS 3/1 pour la série LAH4-Ln (carrés noirs) et la série LAH4-An (cercles rouges) à pH 5 (symboles pleins) et pH 7,4 (symbole ouvert). Sur le panel du haut, l'efficacité de transduction avec les vecteurs de lentivirus GALVTR-LV (bleu) pour les séries LAH4-Ln (A) et LAH4-An (B). Sur le panel du bas, l'efficacité de transduction avec les vecteurs de lentivirus VSV-G-LV (bleu) pour les séries LAH4-Ln (C) et LAH4-An (D).

Cependant, ce n'est pas le cas pour la transduction, il n'y a pas de corrélation entre l'angle hydrophile et le pourcentage de calcéine libérée. Le peptide qui permet d'améliorer les activités de transduction de lentivirus est le LAH4-A4 qui présente un angle hydrophile de 140°. En effet, l'amélioration de transduction lentiviral a été associée à la formation de fibre [21], à l'attachement de lentivirus aux membranes cellulaires et à la fusion de la membrane [23][29], la

libération de calcéine étudiée ici n'est pas adaptée pour étudier ce mécanisme biologique d'activité.

Après avoir examiné l'angle hydrophile, dans un deuxième temps, nous nous sommes intéressés aux modifications dans les distributions des chaînes latérales des acides aminés, et comment elles peuvent conduire à différents assemblages supramoléculaires résultant en un grand changement de fonction. En effet, de petits changements pourraient considérablement augmenter les activités. Chaque membre de la famille présente des activités biologiques distinctes par rapport aux petits changements dans la séquence des acides aminés [3] [9] [22] [30]. Nous nous sommes concentrés sur les trois membres LAH4, LAH4-L1 et LAH4-A4 en fonction de leur activité biologique spécifique : LAH4 exerce principalement des activités antimicrobiennes [1] [10], LAH4-L1 est un excellent agent transfection d'acide nucléique [3] [18] [22] et LAH4-A4 est un transducteur de lentiviral [20] [23] (Figure 8). Leur composition en acides aminés est identique, mais l'emplacement des histidines diffère (Figure 8). Lorsque le peptide est représenté sous forme de roue hélicoïdale [20], la distribution des histidines offre différents angles hydrophiles. LAH4 a sur son côté hydrophile une distribution d'histidines formant un angle de 100° tandis que pour LAH4-L1 et LAH4-A4 leurs histidines sont alignées sur un certain angle. LAH4-L1 présente une leucine entre ses deux paires d'histidine formant un angle de 80° et LAH4-A4 quatre alanines pour un angle hydrophile de 140° (Figure 8).

LAH4
KKALLALAL**HH**LA**H**LAL**H**LALALKKA
Antimicrobien

LAH4-L1
KKALLA**H**AL**H**LLALLAL**H**LA**H**ALKKA
Transfection

LAH4-A4
KKALL**H**AALA**H**LLALA**HH**LLALLKKA
Transduction

Figure 8: La séquence et la projection en roue hélicoïdale des trois peptides LAH4, LAH4-L1 et LAH4-A4 avec leur activité correspondante.

Nous nous sommes concentrés sur ces trois peptides de la famille des LAH4 (LAH4, LAH4-L1 et LAH4-A4) afin de répondre aux questions suivantes comment la séquence des acides aminés est transposée dans la structure supramoléculaire et comment cette dernière détermine la fonction biologique. Les conditions de fibrillation de ces trois peptides et la stabilité des fibres obtenues dans différents environnements ont été étudiées [31]. Elles peuvent être ajustées simplement en changeant la composition tampon (pH, sel, ions) ou par des changements modestes dans leur séquence [31]. La première étape portait sur les conditions de fibrillation optimisées à partir de LAH4-A4.

Un protocole de fibrillation avait été établi au laboratoire par la doctorante précédente, Justine Wolf. Il consistait à solubiliser le peptide à faible concentration dans l'eau plutôt que dans du tampon afin d'éviter l'agrégation puis à effectuer une dialyse pendant 24h, permettant ainsi d'augmenter lentement le pH vers le pKa des histidines [32].

Pour la suite de cette étude, une cinétique a été effectuée afin de mieux comprendre l'assemblage du peptide durant la dialyse. Elle nous montre un rendement assez faible de fibrillation vers 30 % et une évolution des fibres en fonction du temps et du pH. Celles-ci deviennent plus longues, plus épaisses et non homogènes en solution rendant difficile la reproductibilité des expériences. Une étude sur les conditions de fibrillation ainsi que sur la stabilité des fibres a été réalisée, un nouveau protocole de fibrillation par agitation en microtube a ainsi pu être établi permettant d'obtenir des fibres plus stables dans le temps

(suivi sur maximum 1 mois), plus homogènes et avec un meilleur rendement de 70 % de fibrillation et moins de perte de matériel. Cette étude a également été réalisée sur LAH4-L1 ainsi que LAH4 (Figure 9). Les résultats nous ont montré l'importance du tampon phosphate 10 mM pour la formation des fibres. En effet, le phosphate joue un rôle important dans l'auto-assemblage dans les fibres [34]. Alors qu'une forte concentration d'ions phosphatés provoque l'agrégation du peptide [104], ce processus est réversible lorsqu'il est transféré dans l'eau. En outre, le LAH4 fibrille à pH 6,25 alors que la fibrillation de LAH4-A4 et de LAH4-L1 est favorisée à pH 7.4.

Pour la suite des études, les fibres ont été obtenues à pH 6,25 pour le LAH4 alors que la fibrillation de LAH4-A4 et de LAH4-L1 a été réalisée à pH 7.4. Les fibres ont été observées par microscopie électronique à transmission (MET) ce qui nous permet de visualiser une différence dans l'apparence de ces trois fibres (Figure 9).
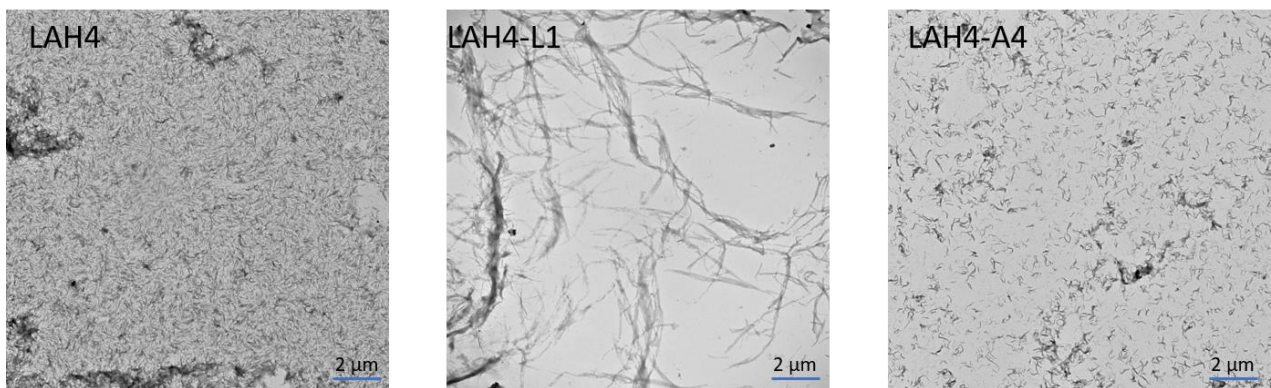

Figure 9: Microscopie à transmission électronique des trois peptides LAH4, LAH4-L1 et LAH4-A4 lorsqu'ils sont fibrillés. LAH4-L1 et LAH4-A4 dans du tampon phosphate 10 mM à pH 7.4 et LAH4-A4 dans du tampon phosphate 10 mM à pH 6,25. Sous agitation pendant 1 semaine.

La structure des fibres a été analysée par MET : LAH4-A4 tend à former de courtes structures de fibres non linéaires, LAH4 tend à former des fibres linéaires courtes et LAH4-L1 tend à se regrouper et à former des structures plus compactes et plus longues. Nous avons pu étudier les détails physico-chimiques et structuraux de ces trois fibres. En particulier en utilisant la spectroscopie RMN à l'état solide et la spectroscopie infrarouge à transformée de Fourier (IRTF), permettant de résoudre la structure secondaire des fibres. LAH4-A4 et LAH4-L1

s'auto-assemblent en présence de tampon phosphate de 10 mM à pH 7.4 et la structure secondaire des peptides dans les fibres est en hélice α. En revanche, les fibres LAH4 se forment en tampon phosphate à pH 6.2 près du pKa des histidines et les peptides adoptent une structure en feuillet β (Figure 10).

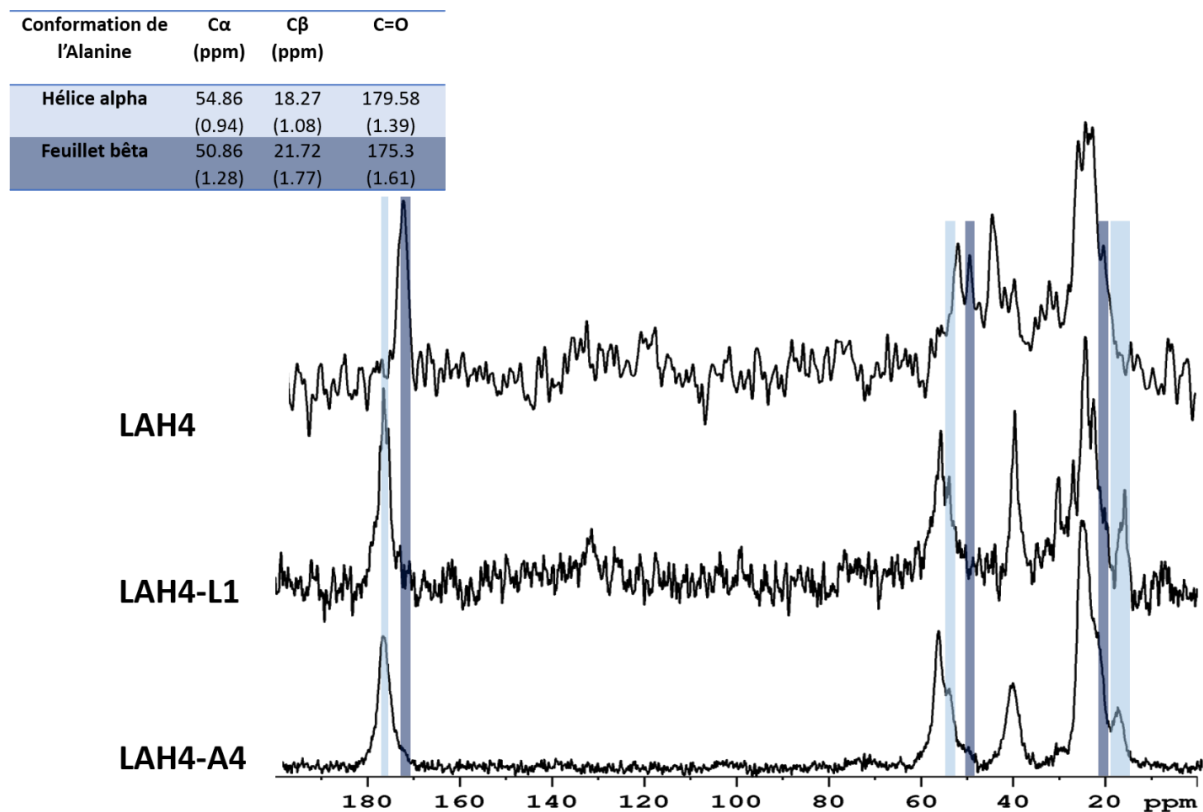| Conformation de l'Alanine	Cα (ppm)	Cβ (ppm)	C=O
Hélice alpha	54.86 (0.94)	18.27 (1.08)	179.58 (1.39)
Feuillet bêta	50.86 (1.28)	21.72 (1.77)	175.3 (1.61)

Figure 10: Spectres RMN à l'état solide des trois peptides LAH4, LAH4-L1 et LAH4-A4. Modification de structure de LAH4 comparée à LAH4-L1 et LAH4-A4 avec comme référence les déplacements chimiques de l'Alanine : bleu clair pour une conformation en hélice α et bleu foncé pour une conformation en feuillet β.

L'auto-assemblage des peptides est principalement lié à des interactions électrostatiques et hydrophobes. Il a été démontré que les modifications dans la séquence primaire pourraient influer sur la structure des fibres [33]. Cette modification structurale doit être directement liée à la position des histidines. En outre, le mécanisme d'auto-assemblage peut être différent, LAH4 a besoin d'un pH proche du pKa des histidines sinon il ne structure pas à pH 7.4 (0%). Il peut y avoir des distributions de charge entre les histidines des différentes molécules de peptide, se restructurant en adoptant un feuillet β. Tandis que LAH4-A4 est moins sensible à

la variation de pH avec un meilleurs pourcentage de fibrillation à pH 7.4, il peut y avoir association des peptides par des interactions hydrophobes permettant alors de maintenir leur assemblage dans une conformation en hélice α. Le positionnement des histidines dans la structure secondaire peut modifier l'auto-assemblage du peptide, résultant en deux conformations différentes : hélice α ou feuillet β (Figure 8).

De plus, les analyses préliminaires des activités antimicrobiennes et de transfection ont montré des différentes activités selon que le peptide soit en solution ou autoassemblé. Ces analyses ont montré une perte d'activité pour les peptides LAH4 lorsqu'ils sont auto-assemblés en feuillet β. La perte d'activité de transfection pour LAH4 peut s'expliquer par un blocage à différents stades du processus de transfection. Les peptides LAH4-L1 et LAH4-A4 ne favorisent pas mais ne modifient pas non plus l'activité antimicrobienne ou de transfection lorsqu'ils sont auto-assemblés sous forme de fibres en hélice α. Les activités de transduction doivent encore être testées pour savoir si les fibres ont plus d'activité que les peptides en solution.

Afin de mieux comprendre l'auto-assemblage de ces peptides et leurs différences, une première étude par spectroscopie RMN à l'état solide a été effectuée pour analyser la structure des fibres et tenter d'élucider leur mécanisme d'action. Dans un premier temps, nous nous sommes intéressés au peptide LAH4-A4. Cependant, la séquence étant KKALLHAALAHLLALAHHLLALLKKA et ne comportant que quatre acides aminés différents, il est donc plutôt difficile d'attribuer les déplacements chimiques et donc d'identifier chaque résidu en spectroscopie RMN à l'état solide. Une stratégie a donc été mise en place : marquer spécifiquement différents segments de la séquence (Figure 11). Nous avons synthétisé et purifié LAH4-A4 avec quatre acides aminés consécutifs entièrement marqués en ^{15}N et ^{13}C.

LAH4-A4	Séquence marquée en ^{15}N et ^{13}C (en rouge)
Échantillon 1	KKALLH**AALA**HLLALAHHLLALLKKA-NH2
Échantillon 2	KKALLHAALAHLLALAHHLL**ALLK**KA-NH2
Échantillon 3	K**KALL**HAALAHLLALAHHLLALLKKA-NH2
Échantillon 4	KKALLHAALAH**LLALA**HHLLALLKKA-NH2

Figure 11: Séquence de LAH4-A4 avec les différentes positions marquées en ^{15}N et ^{13}C en rouge

De la spectroscopie RMN en solution en présence de TFE afin que le peptide adopte une structure en hélice α avec les échantillons étiquetés en $^{13}C/^{15}N$ a été réalisée pour avoir le déplacement chimique de chaque acide aminé et la structure du LAH4-A4 en solution. Puis, la formation de fibres a été effectuée avec les conditions déterminées précédemment à partir des peptides étiquetés à différentes positions pour analyser la structure des fibres de LAH4-A4 par spectroscopie RMN à l'état solide (Figure 12).
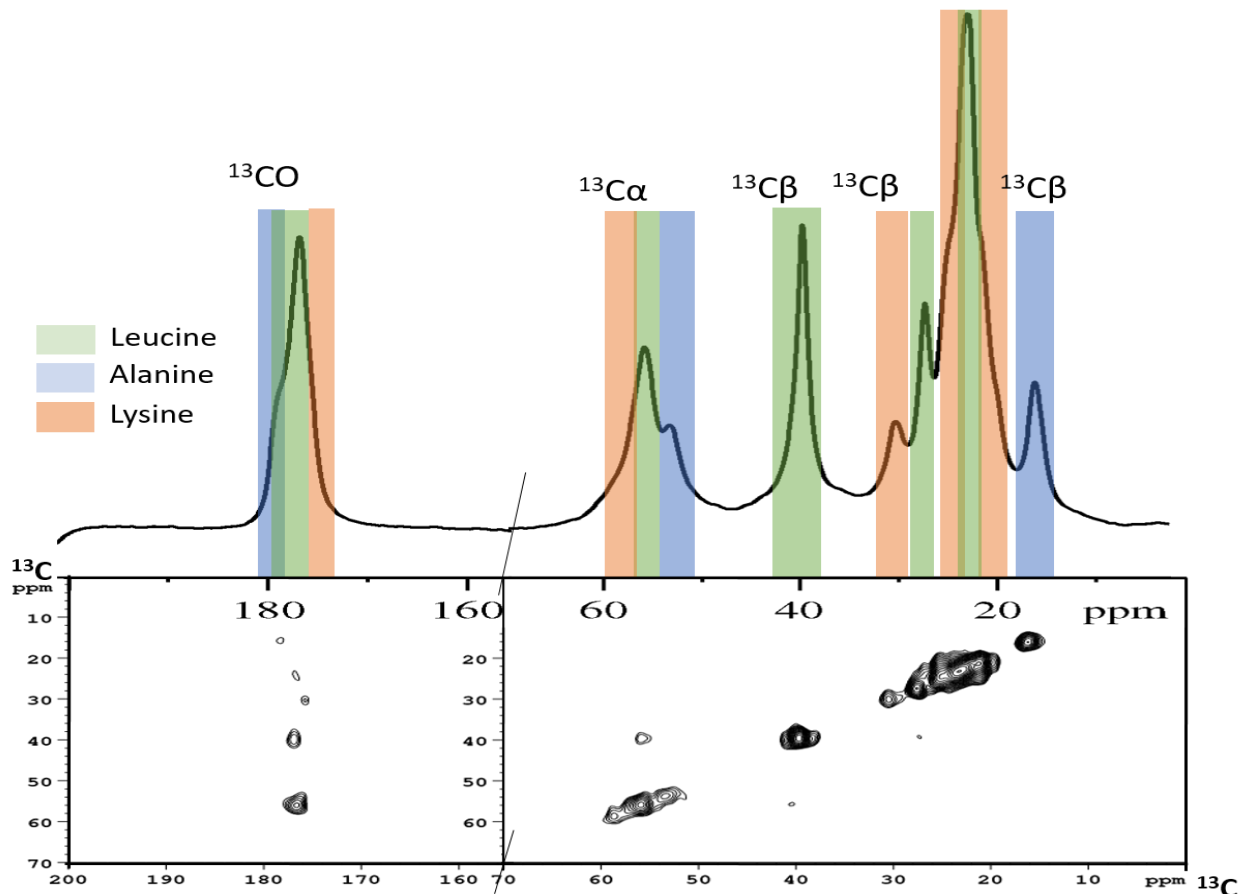
Figure 12: Spectre RMN à l'état solide caractéristique d'un échantillon marqué avec les déplacements supposés des différents acides animés lorsque le peptide est en hélice α. En orange la Lysine, en vert la Leucine et en bleu l'Alanine.

La comparaison entre la structure du peptide déterminé en solution et en fibre est effectuée. La structure du peptide LAH4-A4 en solution en présence de TFE permet au peptide d'adopter une structure en hélice α. Cette analyse RMN nous a permis d'assigner les différents changements chimiques d'acides aminés de LAH4-A4 dans ses conformations en hélice α. La modification de la structure secondaire peut être déterminée à l'aide des valeurs de déplacement chimique (TALOS+ et CSI). Les résultats trouvés pour ce peptide en solution ne sont pas si différents de ceux trouvés pour LAH4. En effet, dans la solution TFE, le peptide LAH4-A4 adopte une conformation en hélice α préférentielle pour la région L4-L23 mais ne prenant pas en compte les acides aminés aux extrémités (Figure 13 B). Dans les fibres, les extrémités font également partie de la structure en hélice α. Dans cette structure, le peptide est auto-assemblé et il y a un changement dans la mobilité des lysines (Figure 13 A). Ainsi,

nous avons été en mesure de différencier la structure peptidique quand il est en solution est sous forme de fibre (Figure 13).
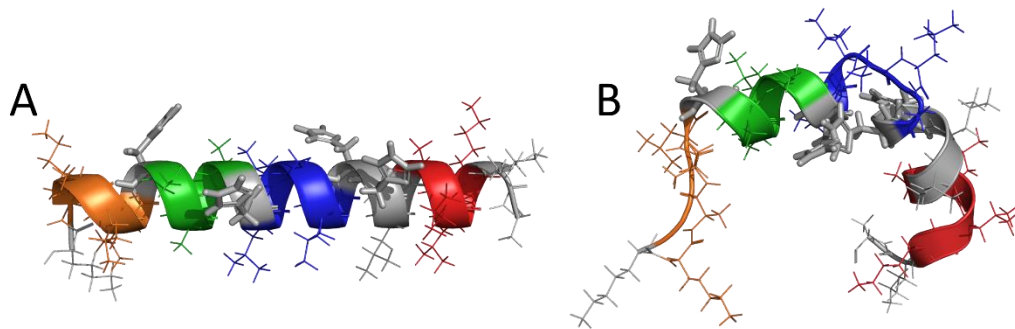

Figure 13: Structure de LAH4-A4 (VF-1) sous forme de fibre (A) ou sous forme monomère en solution (B) avec prévision TALOS+ pour les angles φ et ψ.

Après avoir attribuer les déplacements chimiques du peptide sous forme de fibre, des expériences de diffusion des rayons X aux petits et grands angles (SAXS et WAXS) ont été réalisées afin d'obtenir des distances de répétition du peptide dans les fibres.
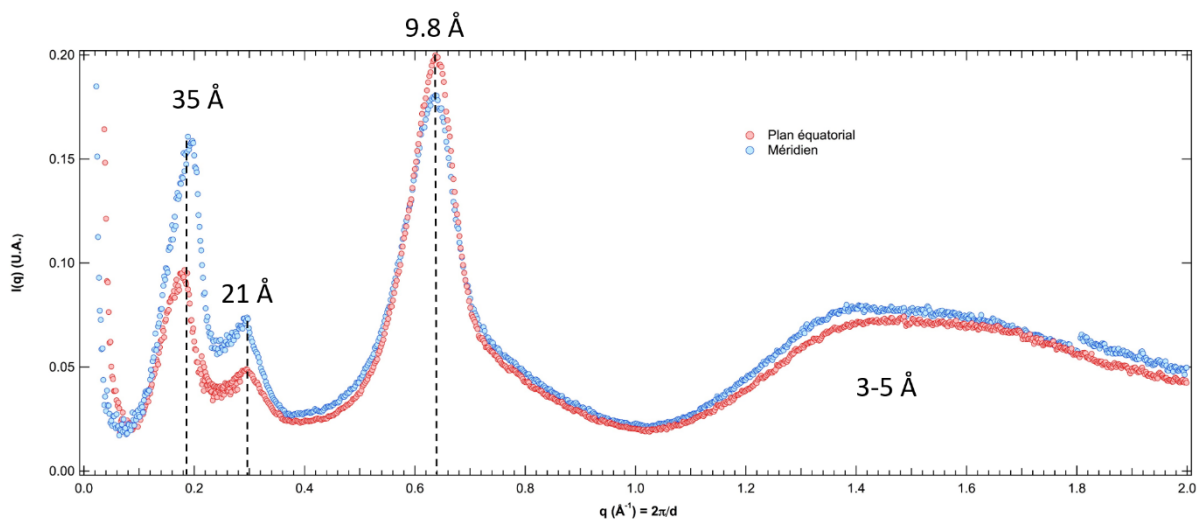

Figure 14: Les expériences SAXS et WAXS (SWAXS) avec des fibres de LAH4-A4 séchées. Les intensités suivants la direction équatoriale (rouge) et méridienne (bleu) selon le vecteur de diffusion q=2π/d.

Les résultats montrent des répétitions dans le plan méridien à 35 Å et 21 Å, dans le plan équatorial à 9,8 Å et la diffusion isotropique à 4-5 Å. Ces distances correspondent à une hélice α : 4-5 Å pour un pas d'hélice et 35 Å pour la longueur peptide lorsqu'il est en hélice α.

Cependant, les distances de 9,8 Å et 21 Å ne font pas partie des distances caractéristiques de peptides en hélice α. Par conséquent, ces distances peuvent être liées à des distances de répétition inter-fibre.

Afin d'obtenir plus de détails sur l'auto-assemblage des fibres LAH4-A4, des études de spectroscopie RMN à l'état solide sont en cours. Cette étude permettra d'identifier les contacts inter-fibre ainsi que les interactions intermoléculaires afin d'élucider la structure des fibres de LAH4-A4.

IX.3 Conclusion générale

Ce manuscrit est dédié aux peptides de la famille de LAH4 avec un intérêt particulier sur la façon dont les changements dans la séquence peuvent influencer leur structure ou l'auto-assemblage et / ou la modification dans leur activité.

Tout d'abord, deux séries de peptides LAH4-Ln et LAH4-An ont été étudiée en faisant varier l'angle hydrophile allant de 60° à 180°. Cette étude montre que, l'activité de libération de calcéine est corrélée avec l'angle hydrophile des peptides. En effet, une diminution du pourcentage de calcéine libérée a été observée lorsque les angles hydrophiles augmentent. Cette corrélation ne dépend pas de leurs propriétés physico-chimiques pour les peptides ayant un angle hydrophile de 60° à 140° pour les deux séries LAH4-An et LAH4-Ln. Pour les peptides ayant un angle hydrophile de 60° à 140°, ces variations sont probablement liées au degré de pénétration de la membrane selon l'angle hydrophile du peptide. Toutefois, pour les peptides aux grands angles hydrophiles (160° et 180°) il n'y a pas de corrélation entre l'activité de libération de calcéine et l'angle hydrophile, de plus ces peptides n'ont pas les mêmes propriétés physico-chimiques. Les interactions membranaires pour les deux séries LAH4-Ln et LAH4-An sont importantes pour expliquer la transduction, la transfection ou les activités antimicrobiennes. Les activités de transfection et antimicrobiennes ont montré la même tendance que l'activité de libération de calcéine, ce qui n'est pas le cas pour la transduction. Ces différentes activités peuvent être liées à leurs mécanismes d'action : alors que les activités de transfection et antimicrobiennes sont liées à la déstabilisation de la membrane, la transduction a besoin d'une fusion avec la membrane.

Afin de comprendre et d'augmenter l'activité de transfection, le peptide LAH4-A4 ayant déjà montré une forte activité de transfection en solution et ayant même montré la capacité de former des fibres dans le milieu utilisé lors des tests de transduction avec une augmentation de son activité de transduction. L'optimisation d'un protocole de fibrillation du peptide LAH4-A4 a été effectuée pour avoir des résultats plus reproductibles au fil du temps. Cette étude a permis de déterminer les paramètres essentiels pour obtenir des fibres plus stables et un meilleur rendement d'environ 70 %. Ces conditions bien définies sont les suivantes : la fibrillation se produit dans le tampon de phosphate de 10 mM à pH 7.4 sous agitation forte.

21

En outre, l'amélioration du protocole de fibrillation (par dialyse ou agitation) ne modifie pas la structure secondaire des fibres LAH4-A4. Cette étude a été étendue à LAH4 et LAH4-L1 pour étudier les corrélations entre les séquences peptidiques, l'auto-assemblage et les activités. Les protocoles de fibrillation pour les deux peptides ont été développés. Les fibrillations de LAH4-L1 et LAH4-A4 s'effectue dans les mêmes conditions à pH 7.4 tandis que le LAH4 développe des fibres dans le même tampon mais nécessite un pH inférieur vers 6,2. Le pH et le phosphate jouent un rôle essentiel dans la fibrillation de ces peptides. De plus, la structure des fibres par ssRMN et IRTF a été analysée, montrant que LAH4-A4 et LAH4-L1 forment des fibres en hélice α tandis que les fibres de LAH4 forme un feuillet β. Les assemblages supramoléculaires des peptides de la famille LAH4 peuvent être finement réglés en changeant la composition tampon (pH, sel, ions) ou par de modestes changements dans leur séquence. De plus, des tests de transfection et antimicrobiens ont été réalisés pour voir l'effet de ces peptides auto-assemblés sur ces activités. Dans leur état fibrillaire, les peptides LAH4-L1 et LAH4-A4 en hélice α restent actifs bien qu'à un niveau inférieur. En revanche, les fibres de LAH4 en feuillet β conduisent à la perte complète des activités antimicrobiennes et de transfection. Afin d'obtenir plus d'informations sur ces fibres et de mieux comprendre leur auto-assemblage, nous nous sommes consacrés à déterminer la structure des fibres LAH4-A4 par spectroscopie ssRMN.

En raison de la redondance élevée dans la composition d'acide aminé de LAH4-A4, la stratégie utilisée consistait à synthétiser les peptides LAH4-A4 avec des segments spécifiquement étiquetés en ^{15}N et ^{13}C à différentes positions dans la séquence peptidique, sur quatre résidus consécutifs. Dans cette étude, nous avons pu d'abord déterminer la structure du LAH4-A4 en solution et dans le peptide sous forme de fibres en structure hélice α. Cette étude nous a permis d'obtenir les déplacements chimiques des acides aminés de LAH4-A4 quand il est en solution ou sous forme de fibres. Le peptide en solution adopte une structure α hélicale entre L4 et L23. Les résidus aux extrémités, en particulier les lysines, ont tendance à ne pas participer à cette structure hélicale. Alors que le peptide sous forme de fibre modifie la flexibilité des chaînes latérales des lysines. En effet, les résidus K2 et K24 font partie de la structure en hélice α lorsque le peptide est sous forme de fibres. Il y a donc un changement dans la structure secondaire des extrémités du peptide lorsqu'il est en solution ou en

auto-assemblage. La perte d'activité de transfection peut être liée à ces modifications du peptide lorsqu'il est assemblé. La complexation du peptide avec l'ADN causée par des interactions électrostatiques entre les résidus de lysine et les groupements phosphate de l'ADN peut être empêchée. Des expériences SWAXS ont été réalisées pour obtenir des informations sur l'auto-assemblage des fibres. Cela nous a permis de trouver des distances caractéristiques d'une structure en hélice α à savoir 5,4 Å pour un pas d'hélice et 10 Å pour la distance peptidique-peptide ainsi que 35 Å correspondant à la longueur du peptide en structure d'hélice. Le pic à 21 Å ne correspond à aucune distance dans la structure en hélice α, cette distance est probablement liée à des répétitions dans la structure de la fibre. Afin de déterminer l'auto-assemblage peptidique puis d'acquérir une meilleure compréhension structurale de ces fibres, le travail de spectroscopie RMN à l'état solide est toujours en cours. La stratégie consiste à avoir des informations intermoléculaires en faisant fibriller ensemble deux peptides étiquetés différemment afin de rechercher des pics de corrélation inter peptidiques dans l'espace.

IX.4 Référence

1. T. C. B. Vogt and B. Bechinger. The interactions of histidine-containing amphipathic helical peptide antibiotics with lipid bilayers. *J. Biol. Chem.* **274**, 29115–29121 (1999).

2. A. Marquette, A. J. Mason and B. Bechinger. Aggregation and membrane permeabilizing properties of designed histidine-containing cationic linear peptide antibiotics. *J. Pept. Sci.* **14**, 488–495 (2008).

3. A. J. Mason, A. Martinez, C. Glaubitz, O. Danos, A. Kichler and B. Bechinger. The antibiotic and DNA-transfecting peptide LAH4 selectively associates with, and disorders, anionic lipids in mixed membranes. *FASEB J.* **20**, 320–322 (2006).

4. B. Bechinger. Towards membrane protein design: pH-sensitive topology of histidine-containing polypeptides. *J. Mol. Biol.* **263**, 768–775 (1996).

5. B. Bechinger. The structure, dynamics and orientation of antimicrobial peptides in membranes by multidimensional solid-state NMR spectroscopy. *Biochim. Biophys. Acta - Biomembr.* **1462**, 157–183 (1999).

6. J. Georgescu, V. H. O. Munhoz and B. Bechinger. NMR Structures of the histidine-rich peptide LAH4 in micellar environments: Membrane insertion, pH-dependent mode of antimicrobial action, and DNA transfection. *Biophys. J.* **99**, 2507–2515 (2010).

7. B. Bechinger, R. Kinder, M. Helmle, T. C. B. Vogt, U. Harzer and S. Schinzel. Peptide structural analysis by solid-state NMR spectroscopy. *Biopolym. - Pept. Sci. Sect.* **51**, 174–190 (1999).

8. N. Voievoda. Biophysical investigation of the membrane and nucleic acids interactions of the transfection peptide LAH4-L1. *Thesis* (2014).

9. A. Kichler, C. Leborgne, J. März, O. Danos and B. Bechinger. Histidine-rich amphipathic peptide antibiotics promote efficient delivery of DNA into mammalian cells. *Proc. Natl. Acad. Sci. U. S. A.* **100**, 1564–1568 (2003).

10. A. J. Mason, C. Gasnier, A. Kichler, G. Prévost, D. Aunis, M. H. Metz-Boutigue and B. Bechinger. Enhanced membrane disruption and antibiotic action against pathogenic bacteria by designed histidine-rich peptides at acidic pH. *Antimicrob. Agents Chemother.* **50**, 3305–3311 (2006).

11. Ü. Langel. Cell-Penetrating Peptides Methods and Protocols. *Cell-Penetrating Peptides* vol. 1324 177–190 (2015).

12. T. Lehto, K. Ezzat and Ü. Langel. Peptide nanoparticles for oligonucleotide delivery. *Prog. Mol. Biol. Transl. Sci.* **104**, 397–426 (2011).

13. E. Eiríksdóttir, K. Konate, Ü. Langel, G. Divita and S. Deshayes. Secondary structure of cell-penetrating peptides controls membrane interaction and insertion. *Biochim. Biophys. Acta - Biomembr.* **1798**, 1119–1128 (2010).

14. N. Nayerossadat, P. Ali and T. Maedeh. Viral and nonviral delivery systems for gene delivery. *Adv. Biomed. Res.* **1**, 1–11 (2012).

15. H. Yin, R. L. Kanasty, A. A. Eltoukhy, A. J. Vegas, J. R. Dorkin and D. G. Anderson. Non-viral vectors for gene-based therapy. *Nat. Rev. Genet.* **15**, 541–555 (2014).

16. A. Kichler, B. Bechinger and O. Danos. Des peptides cationiques antibactériens comme vecteurs de transfert de gènes. *Medecine/Sciences* **19**, 1046–69 (2003).

17. B. L. Davidson and X. O. Breakefield. Viral vectors for gene delivery to the nervous system. *Nat. Rev. Neurosci.* **4**, 353–364 (2003).

18. G. Moulay, C. Leborgne, A. J. Mason, C. Aisenbrey, A. Kichler and B. Bechinger. Histidine-rich designer peptides of the LAH4 family promote cell delivery of a multitude of cargo. *J. Pept. Sci.* **23**, 320–328 (2017).

19. N. Liu, B. Bechinger and R. Süss. The histidine-rich peptide LAH4-L1 strongly promotes PAMAM-mediated transfection at low nitrogen to phosphorus ratios in the presence of serum. *Sci. Rep.* **7**, 1–12 (2017).

20. S. Majdoul, A. K. Seye, A. Kichler, N. Holic, A. Galy, B. Bechinger and D. Fenard. Molecular determinants of vectofusin-1 and its derivatives for the enhancement of lentivirally mediated gene transfer into hematopoietic stem/progenitor cells. *J. Biol. Chem.* **291**, 2161–2169 (2016).

21. L. S. Vermeer, L. Hamon, A. Schirer, M. Schoup, J. Cosette, S. Majdoul, D. Pastré, D. Stockholm, N. Holic, P. Hellwig, A. Galy, D. Fenard and B. Bechinger. Vectofusin-1, a potent peptidic enhancer of viral gene transfer forms pH-dependent α-helical nanofibrils, concentrating viral particles. *Acta Biomater.* **64**, 259–268 (2017).

22. A. Kichler, A. J. Mason and B. Bechinger. Cationic amphipathic histidine-rich peptides for gene delivery. *Biochim. Biophys. Acta - Biomembr.* **1758**, 301–307 (2006).

23. D. Fenard, D. Ingrao, A. Seye, J. Buisset, S. Genries, S. Martin, A. Kichler and A. Galy. Vectofusin-1, a new viral entry enhancer, strongly promotes lentiviral transduction of human hematopoietic stem cells. *Mol. Ther. Nucleic Acids* **2**, 1–10 (2013).

24. C. Meier, T. Weil, F. Kirchhoff and J. Münch. Peptide nanofibrils as enhancers of retroviral gene transfer. *Wiley Interdiscip. Rev. Nanomedicine Nanobiotechnology* **6**, 438–451 (2014).

25. R. Gautier, D. Douguet, B. Antonny and G. Drin. HELIQUEST: a web server to screen sequences with specific α-helical properties. *Bioinformatics* **24**, 2101–2102 (2008).

26. M. Lointier, C. Aisenbrey, A. Marquette, J. H. Tan, A. Kichler and B. Bechinger. Membrane pore-formation correlates with the hydrophilic angle of histidine-rich amphipathic peptides with multiple biological activities. *Biochim. Biophys. Acta - Biomembr.* **1862**, 1–9 (2020).

27. N. Voievoda, T. Schulthess, B. Bechinger and J. Seelig. Thermodynamic and biophysical analysis of the membrane-association of a histidine-rich peptide with efficient antimicrobial and transfection activities. *J. Phys. Chem. B* **119**, 9678–9687 (2015).

28. N. Harmouche and B. Bechinger. Lipid-Mediated Interactions between the Antimicrobial Peptides Magainin 2 and PGLa in Bilayers. *Biophys. J.* **115**, 1033–1044 (2018).

29. D. Ingrao, S. Majdoul, A. K. Seye, A. Galy and D. Fenard. Concurrent measures of fusion and transduction efficiency of primary CD34+ cells with human immunodeficiency virus 1-based lentiviral vectors reveal different effects of transduction enhancers. *Hum. Gene Ther. Methods* **25**, 48–56 (2014).

30. B. Langlet-Bertin, C. Leborgne, D. Scherman, B. Bechinger, A. J. Mason and A. Kichler. Design and evaluation of histidine-rich amphipathic peptides for siRNA delivery. *Pharm. Res.* **27**, 1426–1436 (2010).

31. X. Tian, F. Sun, X. R. Zhou, S. Z. Luo and L. Chen. Role of peptide self-assembly in antimicrobial peptides. *J. Pept. Sci.* **21**, 530–539 (2015).

32. J. Wolf. Biophysical investigations of the LAH4 family peptides : enhancer of gene delivery, from peptide-peptide interactions to peptide-membrane interactions Biophysical investigations of the LAH4 family of peptides enhancer of gene delivery. *Thesis* (2019).

33. R. Gerbier, R. A. Perez, J. F. Margathe, A. Flahault, P. Couvineau, J. Gao, N. D. Mota, H. Dabire, B. Li, E. Ceraudo, A. H. Citharel, L. Esteoulle, C. Bisoo, M. Hibert, A. Berdeaux, X. Iturrioz, D. Bonnet and C. L. Cortes. Development of original metabolically stable apelin-17 analogs with diuretic and cardiovascular effects. *FASEB J.* **31**, 687–700 (2017)

LISTE DES PRESENTATIONS

Affiche : Justine Wolf, Louic Vermeer, Arnaud Marquette, <u>Morane Lointier</u>, Jesus Raya, Philippe Bertani, Dennis W. Juhl, Antoine Kichler, Martin Gotthard, Max Wittmann Regine Süss, Loic Amon, Anne Galy, David Fernard, Burkhard Bechinger **Peptide nanostructures with antimicrobial, transfection and transduction activities**. European Materials Research Society (E-MRS), Strasbourg, 19/06/2018.

Affiche : <u>Morane Lointier</u>, Tan Jia Hao, Arnaud Marquette, Burkhard Bechinger. **Structural and functional investigations of designed histidine-rich peptides used for nucleic acid transfection and lentiviral transduction**. International Conference on Medicinal Chemistry RICT, Strasbourg, 4-6/07/2018.

Affiche : <u>Morane Lointier</u>, Philippe Bertani, Dennis Wilkens Juhl, Burkard Bechinger. **Structural and functional investigations of histidine rich-peptides with potent cell penetrating, antimicrobial and lentiviral transduction activities.** Magnetism and Magnetic Resonance (MRM school), Strasbourg, 2-6/06/2019

Communication Orale : <u>Morane Lointier</u>, Tan Jia Hao, Arnaud Marquette, Burkhard Bechinger. **Structural and functional investigations of histidine rich-peptides with potent cell penetrating, antimicrobial and lentiviral transduction activities.** Journées de l'UMR 7177, Strasbourg, 29-30/10/2018

Communication Orale : <u>Morane Lointier</u>, Tan Jia Hao, Arnaud Marquette, Burkhard Bechinger. **Structural and functional investigations of histidine rich-peptides with potent cell penetrating, antimicrobial and lentiviral transduction activities.** International Conference of the Groupe d'Etudes Des Membranes (GEM) de la Société Française de Biophysique, Canne Mandelieu, 3-6/04/2019.

LISTE DES PUBLICATIONS

M. Lointier, C. Aisenbrey, A. Marquette, J. H. Tan, A. Kichler and B. Bechinger. **Membrane pore-formation correlates with the hydrophilic angle of histidine-rich amphipathic peptides with multiple biological activities**. *Biochimica et Biophysica Acta – Biomembranes.* **1862**, 183212 (2020). doi:10.1016/j.bbamem.2020.183212

D. W. Juhl, E. Glattard, M. Lointier, P. Bampilis, B. Bechinger. **The reversible non-covalent aggregation into fibers of PGLa and Magainin 2 preserves. Their antimicrobial activity and synergism**. *Frontiers in Cellular and Infection Microbiology.* **10**, (2020). doi:10.3389/fcimb.2020.526459

Remerciements

Après 26 ans d'étude voici enfin l'aboutissement d'un travail, et c'est avec émotion qu'une nouvelle page s'ouvre à moi.

Je tiens tout d'abord à remercier mon directeur de thèse Burkhard Bechinger, qui m'a donné l'opportunité de réaliser cette expérience aussi folle qu'éprouvante. Cette expérience avec les conversations que nous avons pu avoir m'ont permis de m'élever et grandir intellectuellement. Alors merci de m'avoir procuré un cadre afin de pouvoir réaliser ce travail.

Je tiens particulièrement à citer mes collèges qui ont dû me supporter jour après jour avec des idées aussi délirante que farfelue. Philipe, Jésus et Arnaud avec des pause-café à rallonge permettant de planifier les futures manipulations. Vous ne m'aurez plus dans vos pattes quand j'en aurais marre de travailler. Christopher qui m'a supporté… Il a subi !!! Tous mes délires, ma musique bruyante et mes pétages de plomb qui sont nombreux. Il a toujours été présent pour son aide et les conversations que l'on a pu avoir. Elise qui m'a inculqué une rigueur et qui à tout le temps été présente pour moi pour me soutenir. Voici la seconde thèse que tu as pu écrire. Alors Merci à vous tous pour votre bonne humeur et pour m'avoir aidé dans mon travail tout au long de ces trois ans.

J'ai également une pensée pour tous les anciens doctorants et post doctorants stagiaires qui sont passés dans le laboratoire durant ma thèse avec qui on a pu avoir des moments de vie au laboratoire, Maud, Kevin, Jian, Justine et Dennis. Ainsi que les nouveaux Jianquio, Ahmad, Kathakali, Adrien et particulièrement Romu qui va souffrir en reprenant le sujet.

Je voudrais aussi remercier le laboratoire de Peter Faller qui a été présent pour le prêt d'une HPLC et pour le soutien psychologique. Sans oublier les pauses midi où on a pu se fendre le haricot et les apéros labo. Alors merci à Peter, Laurent, Vincent, Angélique, Maxime, Thibault, Enrico, Barbara, Christophe…

Ma famille, A ma maman, cette femme extraordinaire qui m'a soutenu dans toutes les circonstances dans mes moments de doutes, de stress et j'en passe. Tu es celle qui as toujours cru en mes capacités et qui me tire toujours vers le haut à chaque moment de ma vie. Je te remercie pour ta patience, ta présence, ton exemple, ton amour, ta confiance… Mais surtout pour l'éducation que tu m'as inculquée. Laurent pour ta présence et ta bienveillance à mes

côtés. Mon père même s'il intervient durant la visioconférence et Sophie pour leur soutien, leur présence et les vacances. Mes frères Robin et Fabio que je ne vois pas souvent, mais qui sont toujours présents et aux moments passés avec eux que je chéris. Et à toute ma famille, mes cousins Agathe, Alexandre, Jules et Maëlle, les cousins Toulousain Pierre et Vincent avec toute leurs petites familles. A ma belle-famille d'Alsace qui m'a ouvert les bras : Monique pour nos projets de construction qui me permet de m'évader et Aurélie et Guillaume pour les folles soirées et les superbes cadeaux.

Comme un proverbe le dit « on ne choisit pas sa famille, mais on choisit ses amis », oui alors eux aussi, je tenais à les remercier, car ils en ont vu de toutes les couleurs avec moi.
À mes ami(e)s du sud, Cassy, Tessouille, Camillou, Sha, Antho et ma gitane pour vos encouragements, votre confiance en mes capacités, même si même moi, je n'y croyais pas (« je suis un bouquant ! ») vos délires, votre réconfort. Merci d'être vous et d'être présents à chaque moment de ma vie.
À la TEAM de Strasbourg qui permet de déconnecter et passer de bons moments ensemble : Nico, Magnum, Maxime, Ralaboulinette, Benji, Erika, Roro, JR, Nelly, Fischou, Alcane... Bertho, Raph qui m'ont supporté dans le même bâtiment et à toutes ces soirées où l'on est juste allé boire une bière. Flo, Léo pour votre soutien (putain Morane tu es conne !). Maman Ophélie, déjà de m'avoir convaincu de faire une thèse : « Ça, je ne sais pas si c'est positif ! ». À tous les Capichef, mais surtout Thibault (capichef en chef), Coco (boby) pour toutes nos soirées et nos pâtes perdues. La Team des thésards, car la rédaction, c'est plus qu'une passion. Au gang des vieilles loutres (Louloute et Julie) qui sont toujours présentes à me soutenir à Strasbourg dans les moments hauts en couleur comme dans les plus bas. On peut enfin faire péter les bubles !!!!

Et le meilleur pour la fin, Alex celui qui partage ma vie, celui à qui je me confie, celui qui prends soin de moi. Nul ne sait me comprendre mieux que toi, celui qui m'a supporté, m'a soutenu pendant toute la période de cette thèse et particulièrement pendant la période de rédaction, ça n'a pas dû être évidement.

À toutes les personnes même celle que je n'ai pas cité mais qui font partie de ma vie et qui sont présentes aux moments importants de ma vie.
C'est un truc de dingue, je ne peux pas mettre des mots sur ça. Je n'aurais jamais pensé qu'un jour j'en arriverais là.

Morane LOINTIER

Recherches structurales et

fonctionnelles sur les peptides riches en histidine

Résumé

La famille LAH4 comprend des dérivés de ce peptide, cationiques et capables de se structurer en hélice α amphipathique en fonction du pH de l'environnement. Ils interagissent et perturbent les membranes, sont utilisées pour diverses applications biologiques : antimicrobiennes, de transfection et de transduction. Le travail de cette thèse a pour but de comprendre la relation entre la similitude des séquences et la variété des activités biologiques. Il s'articule en trois parties : tout d'abord, l'étude de l'effet de la modification de la séquence sur deux séries « LAH4-An » et « LAH4-Ln » basées sur le changement de l'angle hydrophile ; puis l'étude des conditions de fibrillation de LAH4-A4, LAH4-L1 et LAH4 afin de mieux comprendre leurs auto-assemblages puisque la formation de fibres s'est montrée important pour la transduction. Et enfin, la détermination de la structure des fibres de LAH4-A4 puisqu'elle est essentielle pour comprendre leurs mécanismes d'action.

Mots clés : Hélice amphipathique ; Peptide antimicrobien ; Peptide pénétrant des cellules ; Angle hydrophile ; Activité antibactérienne, Transduction lentivirale ; Transfection ; Fibres ; Assemblage supramoléculaire.

Summary

The LAH4 family is composed of cationic peptides derived from LAH4, all able to structure into amphipathic α-helix depending on the pH of the environment. They interact and disrupt membranes, are used for various biological applications: antimicrobial, transfection and transduction. The work of this thesis deals with the understanding of the relationship between the sequence similarity and the variety of biological activities. It was divided into three parts : first, the study of sequence modification effect on the two series "LAH4-An" and "LAH4-Ln" based on the hydrophilic angle change; then, the study of fibrillation conditions of LAH4-A4, LAH4-L1 and LAH4 to better understand their self-assemblies since fibril formation has been important for transduction. And finally, the determination of the fibrils structure of LAH4-A4 since it is essential to understand their mechanisms of action.

Keywords : Amphipathic helix ; Antimicrobial peptide ; Cell penetrating peptide ; Hydrophilic angle ; Antibacterial activity , Lentiviral transduction ; Transfection ; Fibril ; Supramolecular assembly.